Neurocomputational and Data Mining Techniques to Decode Task Engagements through a Multimodal Approach

Thesis Submitted by

Swati Agrawal

In Partial Fulfillment of the Requirements for the Degree of

Doctor of Philosophy
(Applied Physics)

Under the Guidance of:

Dr. C. Vijayakumar
Scientist 'F'
NMR Research Centre,
INMAS, DRDO

Institute of Nuclear Medicine &
Allied Sciences, DRDO,
Lucknow Road, Timarpur,
Delhi-110054

Dr. Rinku Sharma
Professor,
Department of Applied Physics,
Delhi Technological University

Delhi Technological University,
Shahbad Daulatpur,
Main Bawana Road,
Delhi-110042

SWATI AGRAWAL

ORCID iD: 0000-0002-8268-1916

©DELHI TECHNOLOGICAL UNIVERSITY, DELHI, 2020, ALL RIGHTS RESERVED

"I dedicate this thesis to my family and my husband, Apurv, for their constant support, encouragement, and love."

Delhi Technological University

Shahbad Daulatpur, Main Bawana Road, Delhi

CERTIFICATE

This is to certify that the thesis titled "**Neurocomputational and Data Mining Techniques to Decode Task Engagements through a Multimodal Approach**" is being submitted by **Swati Agrawal** with registration number **2K16/PHD/AP/01** to the Delhi Technological University for the award of the Degree of Doctor of Philosophy in Applied Physics. The work embodied in this thesis is a record of bonafide research work carried out by me under the guidance of **Dr. Rinku Sharma** and **Dr. C Vijayakumar**. It is further certified that this work is original and has not been submitted in part or fully to any other University or Institute for the award of any degree or diploma.

Swati Agrawal
Candidate
Roll number:2K16/PHD/AP/01

This is to certify that the above statement made by the candidate is correct to the best of our knowledge.

Dr. C Vijayakumar
(Joint Supervisor)
Scientist 'F',
NMR Research Centre,
INMAS, DRDO

Dr. Rinku Sharma
(Supervisor)
Associate Professor,
Department of Applied Physics,
Delhi Technological University

Dr. A. Srinivas Rao
Head,
Department of Applied Physics,
Delhi Technological University

ACKNOWLEDGEMENTS

This thesis results from many experiences I have encountered at INMAS (DRDO) and DTU. Though it will not be enough to express my gratitude to all those who helped me, I would still like to thank the dozens of remarkable individuals I also wish to acknowledge.

First and foremost, I would like to express my sincere gratitude to my mentors, Dr. C. Vijayakumar and Dr. Rinku Sharma, for their continuous support of my Ph.D. study. Their immense knowledge, motivation, and patience have given me more power and spirit to excel in research writing. Without their assistance and dedicated involvement throughout the process, it would have never been accomplished.

Apart from my mentors, I am thankful to Prof. S.C. Sharma, Chairman DRC, Applied Physics, DTU, Prof. A. Srinivas Rao, Head of Department, Applied Physics, DTU, Prof. J.P. Saini, Honorable Vice-Chancellor, DTU, Dr. Maria D'Souza, Head of Department, NMR Research Centre, INMAS, DRDO, Dr. Subash Khushu, Scientist 'G' (Retd), INMAS, DRDO, and Dr. A.K. Mishra, Director, INMAS, DRDO for their support.

I would also like to thank the technical staff at INMAS, DRDO, and lab staff at the Department of Applied Physics, DTU. I would particularly like to thank Mr. Pawan Kumar, Mrs. Prabhjot Kaur, and Ms. Rubaina Khan of INMAS, DRDO, for supporting me to conduct the experiments with simultaneous EEG-fMRI setup.

I thank my fellow labmates, Ardaman Kaur, Priya Singh, and Abhishek Kumar, for the fun time we spent together and stimulating the discussions. I would also like to thank my friends and seniors from DTU, Abhishek Bhardwaj, Dr. Harpreet Kaur, Dr. Neha Gupta, Dr. Ajay Kumar, and Dr. Ravi Gupta, for their support, feedback and guidance. In addition, I would also like to thank those interns at INMAS for being a part of my experiment. I want to thank Himanshu Singh, who helped me arrange human volunteers for the experiments and experiment setup.

Finally, I must express my profound gratitude to my parents for supporting me spiritually throughout writing this thesis and my life. In the end, I am grateful to my brother Shashank Agrawal and my husband Apurv Vishnoi, who gave enough moral support, encouragement, motivation for achieving my objective without any obstacle in the way.

ABSTRACT

Decoding complex brain functioning is a longstanding challenge in cognitive neuroscience. Over the last few decades, several remarkable studies advanced the more profound understanding of brain mechanisms from temporal to spatial scale and local to global cortical communications. To decipher the mechanisms underlying various cognitive engagements needs such a system that can integrate human cognitive mechanisms to the vital knowledge of neuroscience. Thus, developing a multimodal approach capable of extracting the information and utilizing them for exploring the inner neurocognitive processes will contribute to a potential understanding of complex brain behavior.

In line with this approach, the simultaneous EEG-fMRI technique is a promising non-invasive data acquisition technique that exhibits highly complementary characteristics for studying a broad range of brain functions with millimeter spatial resolution and millisecond temporal resolution. However, the hemodynamical mechanisms of the task stimulus induce a complex relationship between neural activity and associated response. The researchers [1,2] have observed that neural activity's HRF (Hemodynamic Response Function) response is sluggish and spreads over time depending upon the intensity and duration of neural activity. Hence, there is a need to consider stimuli and voxel-specific hemodynamic delay and develop an algorithm to explore task-related neural mechanisms. Also, behavioral factors such as task familiarity, practice, current brain state, feedback, and intelligence level of individuals lead to significant changes in an individual's brain functioning and performance. A more profound understanding of these factors has been found essential while designing work to decode the complex neurocognitive mechanisms.

The central objective is to decipher the neuronal mechanisms underlying the distinct cognitive engagements by building on the strengths of the multimodal approach of neurocomputational and data mining techniques. For this purpose, this thesis develops a comprehensive understanding of cognitive aspects and subsequent modulations in neuronal mechanisms by combining the proposed and conventional

neurocomputational methods. The cognitive engagement of the target detection task is explored to understand the neurovascular coupling and task-related modulations using the integrated voxel-wise analysis of functional connectivity modulation with the neurovascular underpinning changes. For this purpose, a novel approach of reorganizing the blood oxygen level-dependent (BOLD) information has been proposed utilizing the HRF parameters. The findings are validated through a graph-theoretical approach at the selected regions. The study revealed the strong association of neurovascular underpinnings with the modulation of functional networks and the associated neuronal activity during task engagement. Further, to understand the in-depth knowledge of the factors affecting an individual's performance during task engagements, the role of feedback learning and fluid intelligence in the task are explored. Functional connectivity estimation and neurovascular approaches analyze feedback learning and its effect on subsequent task engagement. Our findings strengthened the associations of explicit frontal-parietal EEG cortical oscillations with the local and global neuronal engagements.

Another effort to explore the role of an individual's fluid intelligence is understanding the neural mechanisms of intelligence associated with feedback learning and subsequent memory retrieval of encoded objects. The study proposed a deep learning-based framework to classify encoded objects from distractors. Subsequently, neural mechanisms of multifrequency elicitations, which correlate with intelligence, are studied through the multifrequency interaction, EEG-informed-fMRI, and hemodynamical functional connectivity approaches. Finally, an attention-based LSTM deep-learning model is successfully employed to decipher these distinct EEG oscillations during encoded objects' memory retrieval and learning engagement. Thus, the study brings more insights into the multifrequency cortical engagement caused by frontal-parietal interaction of intelligence-associated feedback learning and memory retrieval of encoded objects.

Furthermore, decoding cognitive-task engagement from coarse EEG information is still challenging due to the underlying complex local and distant cortical neural elicitation and communication. This study proposes an attention-based deep learning framework that processes novel, optimized, quasi-stable frequency microstates as

input information. The frequency microstate was optimized using hemodynamic functional connectivity measures estimated using graph theory analysis. The local and distant cortical neural mechanisms associated with each optimized frequency microstates were analyzed using microstate-informed fMRI to use them as neural signatures of cognitive task engagement. The optimized, quasi-stable frequency microstates were used as input information to train and validate the attention-based Long Short-Term Memory (LSTM) architecture to classify the neural engagement of the target from the distractor cognitive tasks. The study demonstrates better classification results of complex cognitive task neural mechanisms, using an attention-based deep learning framework utilizing optimized quasi-stable frequency microstates.

LIST OF FIGURES

Figure No.			*Page No.*
Figure 1.1	**:**	Schematic diagram of brain signal detection mechanisms. EEG measures the electrical potential differences on the scalp that are generated by cortical neural activity. Neurons transmitting neurological signals across their synapses act as dipole sources. MEG detects the magnetic fields associated with such neuronal activation by SQUID sensors. fMRI measures the hemodynamic responses, particularly magnetic dynamics of protons (H+) related to neural activity; its technique is principally based on the detection of local BOLD signal contrast during neuronal activation. Using multiple arrays of optodes, NIRS characterizes changes in the intensity of attenuated near-infrared (IR) light (owing to scattering or absorption), resulting from changes in concentration between oxyhemoglobin (HbO2) and deoxyhemoglobin (Hb) during local neural activity. Adapted from [3].	2
Figure 1.2	**:**	Knowledge Discovery in databases.	6
Figure 1.3	**:**	Classification of data mining techniques.	6
Figure 1.4	**:**	Schematic diagram for BOLD response during task execution using mixed paradigm.	8
Figure 1.5	**:**	A schematic diagram of thesis framework.	11
Figure 2.1	**:**	Schematic illustration of experimental task paradigm: visual target detection task. Five trials with different target objects were used. Each trial consisted of sequence of images, representing collection of objects for 3000 ms followed by subject response.	27
Figure 2.2	**:**	Hemodynamically reorganized BOLD approach for estimation of modulation in functional networks and their neurovascular	

underpinnings during task engagement. BOLD, blood oxygen level dependent. 31

Figure 2.3 : Illustrations of DMN modulation during task engagement (deactivation: blue, activation: red): (A) target stimuli, (B) nontarget stimuli. AG, angular gyrus; CG, cingulate gyrus; DMN, default mode network; FMC, frontal medial cortex; FP, frontal pole; IC, Intracalcarine cortex; LG, lingual gyrus; LOC, lateral occipital cortex; PC, precuneus cortex; PCG, paracingulate gyrus; SFG, superior frontal gyrus. 34

Figure 2.4 : Illustrations of modulation in visual and frontal-parietal networks. 35

Figure 2.5 : Neurovascular underpinnings of target stimuli: (A) alpha reordered BOLD correlation (positive: red, negative: blue); (B) beta-reordered BOLD correlation (positive: red, negative: blue); and (C) gamma-reordered BOLD correlation positive: green and copper, negative: red and blue). IFG, inferior frontal gyrus; MFG, middle frontal gyrus; PHG, parahippocampal gyrus. 36

Figure 2.6 : Neurovascular underpinnings of nontarget stimuli: (A) alpha-reordered BOLD correlation (positive: red, negative: blue); (B) beta-reordered BOLD correlation (positive: red, negative: blue); and (C) gamma-reordered BOLD correlation (positive: red and pink, negative: green and blue). 38

Figure 2.7 : Graph theory analysis: (A) resting state, (B) target stimuli, and (C) nontarget stimuli (red: positive correlation, blue: negative correlation; for $p < 0.05$, FDR). FDR, false discovery rate; LPFC, lateral prefrontal cortex; MPFC, medial prefrontal cortex; PCC, posterior cingulate cortex. 39

Figure No. *Page No.*

Figure 3.1 : A sample experimental design of the feedback declarative memory task. The participants are asked to retrieve the previously memorized object during the retrieval phase of 3s. The study provides visual feedback after each stimulus for 2s during feedback learning, regarding the correctness of the answer to the volunteer's response. The volunteer's task is to detect, learn, and adjust to these changes. 57

Figure 3.2 : Methodological block diagram of the study. The schematic diagram demonstrates the analyses employed in this study. Using electrophysiology, the frequency extraction of the frontal and parietal EEG channels was done using time-frequency analysis, which was time-locked to the feedback and memory retrievals. Using neuroimaging, we explore the relationship of frontal-parietal regions with medial temporal lobe and subregions of basal ganglia. These interactions are analyzed using functional connectivity analysis for feedback and memory retrievals. Also, the direct relationship of the medial temporal lobe and subregions of basal ganglia with the feedback and memory retrievals was analyzed using functional connectivity analysis. Further, the EEG-informed-fMRI approach for both feedback and memory retrievals was employed to study the association of frontal-parietal EEG powers with medial temporal lobe and subregions of basal ganglia. For this, the neural correlates of concerned frequencies (delta, theta, lower-alpha, higher alpha, lower beta, and higher beta) and frontal-parietal EEG channels were evaluated using EEG-informed-fMRI approach for both feedback and memory retrievals and studied for medial temporal lobe and subregions of basal ganglia. 60

Figure No.			*Page No.*
Figure 3.3	**:**	Graphical illustration of functional connectivity of frontal-parietal regions with medial temporal lobe and subregions of basal ganglia. (a). feedback learning. (b). memory retrieval. Azure, indigo, brown and red circles represent frontal, parietal, medial temporal lobe, and basal ganglia, respectively. The significant connectivity among regions is depicted with red lines between nodes. MFG: Middle Frontal Gyrus, IFGOper: Inferior Frontal Gyrus Opercular, Forb: Frontal Orbital Cortex, SFG: Superior Frontal Gyrus, IFGtri: Inferior Frontal Gyrus Triangular, aSMG: Anterior Supramarginal Gyrus, SPL: Superior Parietal Lobule, pSMG: Posterior Supramarginal Gyrus, AG: Angular Gyrus, aPHG: Anterior Parahippocampal Gyrus, pPHG: Posterior Parahippocampal Gyrus, MedFC: Medial Frontal Cortex.	63
Figure 3.4	**:**	Graphical illustration of functional connectivity of medial temporal lobe with subregions of basal ganglia. (a). Feedback learning. (b). Memory retrieval. Brown and red circles represent medial temporal and subregions of basal ganglia, respectively. Red lines between nodes depict the significant connectivity among regions.	64
Figure 3.5	**:**	Associations of frontal electrophysiological powers (delta, theta, lower-alpha, higher alpha, lower beta, and higher beta) in the functioning of the medial temporal lobe (Parahippocampal Cortex & Amygdala) and basal ganglia (Caudate, Putamen & Nuclear Accumbens) during feedback learning and memory retrievals. (a) Voxel-based distribution. (b). Significant T-value based distribution. FB: Feedback learning, MR: Memory retrieval.	68

Figure No.			*Page No.*
Figure 3.6	**:**	Associations of parietal electrophysiological powers (delta, theta, lower-alpha, higher alpha, lower beta, and higher beta) in the functioning of the medial temporal lobe (Parahippocampal Cortex & Amygdala) and basal ganglia (Caudate, Putamen & Nuclear Accumbens) during feedback learning and memory retrievals. (a) Voxel-based distribution. (b). Significant T-value based distribution.	69
Figure 4.1	**:**	A sample experimental design of the feedback declarative memory task. The participants had to retrieve the previously encoded object in the task's retrieval phase within 3000 ms. Feedback (Right/Wrong) based on their performance was provided for 2000 ms after each stimulus during the feedback slide. The participant had to detect, learn, and adjust to these changes based on provided feedback during the task. Memory retrieval and feedback learning phases are demonstrated in the figure using blue and green blocks, respectively.	91
Figure 4.2	**:**	Schematic picture explains methodology employed in the study.	95
Figure 4.3	**:**	Time-frequency representation of the feedback learning and memory retrievals. The figure illustrates the grand average time-frequency plots of frequencies up to 50 Hz following feedback learning and memory retrieval blocks at frontal (F3, F4, Fz) and parietal (P3, P4, Pz) electrodes.	102
Figure 4.4	**:**	Correlation plot between intelligence and EEG power. The plot illustrates a significant correlation ($p<0.05$) between intelligence score (calculated from Raven Progressive Matrices, RPM Test) and relative EEG powers for feedback learning and memory retrieval phases.	104

Figure 4.5 : Multifrequency interactions between intelligence-associated EEG powers of feedback learning and subsequently engaged memory retrievals. Grey and green nodes represent EEG powers associated with the frontal and parietal channels, respectively. The flow's width is proportional to the correlation values at a significance level of $p<0.05$. The diagram illustrates the role of fluid intelligence in associating feedback learning to subsequent memory retrievals through multifrequency interactions of intelligence-correlated EEG powers. 105

Figure 4.6 : Neurovascular underpinnings of intelligence associated EEG powers of the feedback learning phase. SFG: Superior Frontal Gyrus, MFG: Medial Frontal Gyrus, IFG: Inferior Frontal Gyrus, PreCG: PreCentral Gyrus, PostCG: PostCentral Gyrus, SMG: Supramarginal Gyrus, AG: Angular Gyrus, LG: Lingual Gyrus, FP: Frontal Pole, SPL: Superior Parietal Lobule, FOrbC: Frontal Orbital Cortex, FMC: Frontal Medial Cortex, PC: Precuneus Cortex. Voxels in red to yellow and blue to aqua indicate a positive and negative correlation, respectively, for $p<0.05$. 108

Figure 4.7 : Neurovascular underpinnings of intelligence associated EEG powers of memory retrieval. Voxels in red to yellow and blue to aqua indicate a positive and negative correlation, respectively, for $p<0.05$. 109

Figure 4.8 : Neural sources of each cortical oscillation and their functional connectivity, estimated using graph theory analysis. The red circles represent the 'regions of interest' taken from neural sources of each cortical oscillatory power through EEG informed fMRI. Functional connectivity maps are represented

based on estimated graph theory parameters (cost and global efficiency) for feedback learning and memory retrieval phases at a significance level $p<0.05$. 110

Figure 4.9 : Performance comparison of the deep learning frameworks between attention-based LSTM (a-LSTM) and traditional LSTM. The graphical representation demonstrates the classification performance metrics (accuracy, precision, and recall) for both frameworks corresponding to three distinct task engagements (Memory retrieval (MR), feedback learning (FB), and distractors (D)). 113

Figure 5.1 : Schematic of task paradigm design. 141

Figure 5.2 : Methodological framework of the study. 144

Figure 5.3 : Schematic diagram of Attention-based LSTM deep learning framework adopted in the study. 'T' represents the temporal, sliding input sampling window size and is chosen between 180 to 750 ms/segment associated with the specific number of cells ranging from 4 to 16, based on the stability of transition probabilities of the optimized microstates. 147

Figure 5.4 : A topographical representation of frequency-microstates for the target, distractor, and fixation. 152

Figure 5.5 : Estimated metrics of frequency-microstates. The violin graph plots the mean occurrence of each frequency-microstates for each frequency band. The violin plot's green and red color shades reveal the correlation (positive and negative) of the number of occurrences of quasi-stable elicitation with the task's fMRI functional connectivity measures. The red star on violin plots specifies the significance ($p<0.01$). 153

Figure 5.6 : Significantly associated, optimized, frequency-microstates with graph-theoretical measures of a) Target, b) Distractor, and c) Fixation task engagement. Frequency microstates are labelled as anterior-posterior (AP), left-right (LR), left diagonal (LD), and right diagonal (RD). 154-156

Figure 5.7 : Neuro-vascular coupling of each significant, fMRI functional connectivity optimized frequency-microstates of every task. The Regions shown are neural correlates observed for every task. The neuro-vascular association of optimized frequency microstate with each region is drawn through the arrow next to it (Synchronization: Up green arrow, De-synchronization: Down Red arrow). The area colored black has no neurovascular association with any of the optimized frequency microstates. microstates. 157

Figure 5.8 : Comparison of performance of the deep learning frameworks. A. Accuracy, B. Precision, C. Recall. Each architecture was independently optimized with 4, 6, 8, 10, 12, 14, 15 and 16 LSTM input cells for temporal EEG sampling of 750, 500, 375, 300, 250, 214, 200 to 180 ms/segment, respectively. 158

Supplementary Figure 4.1: Bar graphs for graph theory-based functional connectivity during feedback and memory retrieval phases. The bar graph represents the correlation values of significant associations. 185

Supplementary Figure 4.2: Robust Pearson correlation of functional connectivity measures during feedback: a). Left frontal pole centric interaction and Right frontal pole-right ventral anterior insula interaction. b). Left frontal pole-right hippocampus-right accumbens centric interaction and Hippocampus-right anterior insula interaction. Green : +ve Correlation, Red: -ve correlation. 186

Supplementary Figure 4.3: Functional task network modulation of DMN, ECN, Motor, Limbic, and Visual network in post-feedback declarative memory task compared to pre-feedback. Connectivity shown in red to yellow and blue to aqua indicates activation and deactivation of networks, respectively. Further, modulation of graph theory parameters of post-feedback declarative memory task as compared to pre-feedback task engagement. The figure also illustrates the cluster size of the associated functional network modulations. 186

Supplementary Figure 4.4: Effect of prefrontal regions on subsequent task engagement. Nodes illustrated in similar color indicate a significant correlation between them at ($p<0.05$). Red : +ve Correlation , Blue: -ve correlation. Correlation maps illustrate the significant correlation values between the feedback region (x-axis) and the subsequent task-engaged region (y-axis). 187

Supplementary Figure 4.5: Effect of Striatum on subsequent task engagement. Nodes illustrated in similar color indicate a significant correlation between them at ($p<0.05$). Red : +ve Correlation, Blue: -ve correlation. Correlation maps illustrate the significant correlation values between the feedback region (x-axis) and the subsequent task-engaged region (y-axis**)** 187

LIST OF TABLES

Table No.			*Page No.*
Table 3.1	**:**	Functional Connectivity of Frontal Parietal-MTL-Basal Ganglia for feedback learning and memory retrieval significant. Non-significant values are highlighted as red. IFG Oper: Inferior Frontal Gyrus Pars opercularis ,SFG: Superior Frontal Gyrus, MFG: Medial Frontal Gyrus, SPL: Superior Parietal Lobule, AG: Angular Gyrus, IFGTri: Inferior Frontal Gyrus Pars triangularis, FOrb: Frontal Orbital Cortex, pSMG: Posterior Supramarginal Gyrus, aSMG: Anterior Supramarginal Gyrus, aPHG: Anterior Para hippocampal gyrus, pPHG: Posterior Para hippocampal gyrus	65
Table 3.2	**:**	Functional Connectivity of MTL & Basal Ganglia for feedback learning and memory retrieval. Non-significant values are highlighted as red.	66
Table 4.1	**:**	Studies that bring more insights in understanding fluid intelligence associates with learning and memory.	115
Table 5.1	**:**	Final Tuning parameter of LSTM model.	150

Supplementary Table 2.1. Comparison Results Between the Proposed Approach and Graph Theory. The results are summarized as modulations in functional connectivity of brain for visual target detection task from resting state, associated GLM activity with corresponding neurovascular underpinnings, for both stimuli using proposed approach. Every cluster is represented in the following order: [Type of correlation whether Activation (A) or Deactivation (D) (Laterality whether left (L) or right (R)]. Results of graph theory analysis are summarized as variation in measures with respect to resting state, and thus positive values denoted the increment, and negative values denoted the decrement in the variation ratio. BOLD, blood oxygen level

dependent; EEG, electroencephalography; GLM, general linear model; LP, lateral parietal; LPFC, lateral prefrontal cortex; LVC, lateral visual cortex; MPFC, medial prefrontal cortex; MVC, medial visual cortex; PCC, posterior cingulate cortex; PPC, posterior parietal cortex; PVC, primary visual cortex. 180-181

Supplementary Table 4.1: Neural Correlates of intelligence-correlated EEG powers for feedback learning phase. R, L and C represent laterality of EEG electrode, right, left and central, respectively. '+' and '-' denote positive and negative correlates of EEG powers. 182-183

Supplementary Table 4.2: Neural Correlates of intelligence-correlated EEG powers for memory retrieval phase. R, L and C represent laterality of EEG electrode, right, left and central, respectively. '+' and '-' denote positive and negative correlates of EEG powers. 184

LIST OF APPENDICES

Appendix No.	*Page No.*
Supplementary material for Chapter Two	180
Supplementary material for Chapter Four	182

LIST OF PUBLICATIONS

ARTICLES IN INTERNATIONAL REFEREED JOURNALS (3)

1. ***Swati Agrawal,*** *Vijayakumar Chinnadurai, Ardaman Kaur, Pawan Kumar, Prabhjot Kaur, Rinku Sharma, and Ajay Kumar Singh (2019).* ***Estimation of Functional Connectivity Modulations During Task Engagement and Their Neurovascular Underpinnings Through Hemodynamic Reorganization Method****. Brain Connectivity, 9(4), 341-355. https://doi.org/10.1089/brain.2018.0656*

   (Impact Factor: 5.263)

2. ***Swati Agrawal,*** *Rinku Sharma, Vijayakumar Chinnadurai (2021).* ***Functional connectivity between frontal/parietal regions and MTL-basal ganglia during feedback learning and declarative memory retrieval.*** *Journal of Biosciences, 46(3), 1-17. https://doi.org/10.1007/s12038-021-00194-y*

   (Impact Factor: 1.645)

3. ***Swati Agrawal,*** *Vijayakumar Chinnadurai & Rinku Sharma, (2022).* ***Hemodynamic functional connectivity optimization of frequency EEG microstates enables attention LSTM framework to classify distinct temporal cortical communications of different cognitive tasks****. Brain Informatics, 9(1), 1-17. https://link.springer.com/article/10.1186/s40708-022-00173-5*

   (Impact Factor: 6.385)

ARTICLES COMMUNICATED IN INTERNATIONAL JOURNALS

1. ***Swati Agrawal,*** *Vijayakumar Chinnadurai, Rinku Sharma.* ***Fluid intelligence association with feedback learning and subsequent memory retrieval: Deciphering neural mechanisms through multifrequency, EEG informed fMRI, functional connectivity approaches and classification through deep learning framework.***

INTERNATIONAL CONFERENCES (7) (Not included in the thesis)

1. ***Swati Agrawal**, C. Vijayakumar, Ardaman Kaur, Subash Khushu, Rinku Sharma, Suresh C. Sharma. 2017 **Assessment of Neural Correlates of target detection in Visual Search using Simultaneous EEG-FMRI and Resting EEG Technique**. Brain Modes, 2017.*

2. ***Swati Agrawal,** Vijayakumar C, Ardaman Kaur, Subash Khushu, Rinku Sharma, and Suresh Sharma.2018. **Hemodynamic reorganization approach to estimate the functional connectivity in task based functional MRI study**. Proc. Intl. Soc. Mag. Reson. Med. 26 (2018).2403. https://archive.ismrm.org/2018/2403.html*

3. *C. Vijayakumar, Sonali Fotedar, **Swati Agrawal**, Ardaman Kaur, Subash Khushu, Ajay Kumar Singh. **Deep Learning based Brain-Computer Interface system for automatic target detection using Electroencephalography data**.*

4. ***Kaur, A.**, Chinnadurai, V., Agrawal, S., Singh, H., Khushu, S., Kumar, P., Kaur, P.,Kumar, A., Chaujar, R., & Sharma., S. "**Assessment of Neural correlates of Engagement in a Situational Awareness Task using Simultaneous EEG-fMRI technique**,". International Committee on Military Medicine, pp. 216-217, November 19th-24th, 2017, Vigyan Bhawan, New Delhi, India.*

5. ***Kaur, A.**, Chinnadurai, V., Agrawal, S., Singh, H., Khushu, S., Singh, A. K., Chaujar, R., & Sharma., S. C. "**Assessment of Engagement and its neurovascular correlates in a Situational Awareness Task: An EEG Informed fMRI approach**,". Brain Modes, pp. 66-67, December 11th -14th, 2017, Savoy Suites, Manesar, Gurgaon, India.*

6. ***Kaur, A.**, Chinnadurai, V., Agrawal, S., Khushu, S., Chaujar, R., & Sharma., S. "**Assessment of neural correlates of cortical communication of Alpha/Gamma bands between frontal and parietal-occipital regions in Situational Awareness task as well as in resting-state: An EEG informed fMRI approach**,". Joint Annual Meeting ISMRMxviii ESMRMB, June 16th-21st, 2018, Paris Expo Porte de Versailles, Paris, France. http://archive.ismrm.org/2018/4514.html.*

7. ***Kaur, A.**, Chinnadurai, V., Agrawal, S., Khushu, S., Chaujar, R., & Sharma., S. "**Does Pre-task Resting state Absolute Alpha (PRAA) power and its Frontal Asymmetry Index (FAI) predict outcome of Situational Awareness task? Assessment through EEG informed fMRI approach**,". Joint Annual Meeting ISMRM-ESMRMB, June 16th-21st, 2018, Paris Expo Porte de Versailles, Paris, France. http://archive.ismrm.org/2018/4515.html.*

TABLE OF CONTENTS

Title	*Page No.*
Dedication	ii
Certificate	iii
Acknowledgments	iv
Abstract	vi
List of Figures	ix
List of Tables	xviii
List of Appendices	xx
List of Publications	xxi
Table of Contents	xxiv
Chapter 1: Introduction	**1**
1.1 Integration of brain mapping techniques is an optimum solution to 'neuroscience research'	1
1.1.1 EEG (Electroencephalography)	1
1.1.2 FMRI (Functional Magnetic Resonance Imaging)	2
1.2 Feature extraction	3
1.3 Multimodal integration of neurocomputational techniques with data mining techniques to explore task-engagements	5
1.4 Challenges in task-engagement exploration	7
1.5 Objectives of thesis	10
1.6 Thesis structure	14
1.7 References	18
Chapter 2: Evaluation of the Functional Networks and Neurovascular Underpinnings at Voxel-Level during Task-Engagement	**22**
2.1 Abstract	22
2.2 Introduction	23
2.3 Materials and methods	25
2.3.1 Participants and procedure	25
2.3.2 Task design	26

Title	*Page No.*
2.3.3 Data acquisition with simultaneous EEG-fMRI	26
2.3.4 Data pre-processing steps	27
2.3.4.1 Reorganization of BOLD information in task fMRI data: the proposed approach	27
2.3.4.2 Pre-processing of EEG data	29
2.3.5 Data analysis	30
2.3.5.1 Assessment of functional connectivity in task fMRI data	30
2.3.5.2 Assessment of functional connectivity in resting fMRI data	30
2.3.5.3 Selection of regions of interest (ROI)	31
2.3.5.4 Graph theory measures	32
2.3.5.5 Estimation of neurovascular underpinnings	32
2.4 Results	33
2.4.1 Task modulations in functional networks and neurovascular underpinnings	34
2.4.1.1 Target stimuli	34
2.4.1.2 Non-target stimuli	37
2.4.2 Graph theory analysis for the validation of modulation in functional networks	39
2.5 Discussion	40
2.5.1 Association of functional network modulation with neural correlates of the task	40
2.5.2 Functional inhibition in alpha band reflects the task relevant neuronal activity	41
2.5.3 Cross frequency of alpha/beta neurovascular underpinnings	42
2.5.4 Cross frequency coupling of alpha/gamma neurovascular underpinnings	42
2.5.5 Validation of proposed approach with graph theory analysis	43
2.6 Conclusion	44
References	46

Title	*Page No.*
Chapter 3: Analyzing the Effect of Performance Feedback on Subsequent Task Engagement by Assessing the Role of the Frontal-Parietal EEG Cortical Oscillations	**54**
3.1 Abstract	54
3.2 Introduction	55
3.3 Materials and methods	56
3.3.1 Participants and procedure	56
3.3.2 Task design	57
3.3.3 Data acquisition with simultaneous EEG-fMRI	58
3.3.4 Data pre-processing steps	68
3.3.4.1 Pre-processing of EEG data	68
3.3.4.2 Pre-processing of fMRI data	59
3.3.5 Data analysis	59
3.3.5.1 Time-frequency analysis	60
3.3.5.2 Functional connectivity analysis	61
3.3.5.3 Associations of frontal-parietal electrophysiological powers with feedback learning and memory retrieval: The EEG informed fMRI approach	61
3.4 Results	62
3.4.1 Association of frontal-parietal regions with medial temporal lobe (MTL) and basal ganglia: The functional connectivity analysis	62
3.4.2 Relationship of the medial temporal lobe (MTL) and basal ganglia: The functional connectivity analysis	66
3.4.3 Associations of EEG oscillations and medial temporal lobe (MTL): The EEG-informed-fMRI approach	67
3.4.3.1 Feedback learning	67
3.4.3.2 Memory retrieval	67
3.4.4 Associations of EEG oscillations with basal ganglia	69
3.4.4.1 Feedback learning	70

Title	*Page No.*
3.4.4.2 Memory retrieval	70
3.5 Discussion	71
3.5.1 Does the connectivity of MTL, and basal ganglia modulate for memory retrieval from feedback Learning	71
3.5.2 Does memory retrieval dissociate MTL and basal ganglia from frontal-parietal regions? .	72
3.6 Conclusion	74
References	76
Chapter 4: Association of Fluid Intelligence with Feedback Learning and Subsequent Task Engagement: Classification through Deep Learning Framework	**84**
4.1 Abstract	84
4.2 Introduction	85
4.2.1 Fluid intelligence, learning, and associated cortical neural oscillations	85
4.2.2 Declarative memory mechanisms and associated cortical neural oscillations	86
4.2.3 Recurrent deep learning approaches for classifying eeg information	87
4.2.4 Present study	88
4.3 Materials and methods	89
4.3.1 Participants and procedure	89
4.3.2 Behavioral task	90
4.3.3 Task design	90
4.3.4 Data acquisition with simultaneous EEG-fMRI	91
4.3.5 Pre-processing steps	92
4.3.5.1 MR and traditional artifact removal in EEG data	92
4.3.5.2 Artifact removal in fMRI data	94
4.3.6 Data analysis	94

Title	*Page No.*
4.3.6.1 Estimation of intelligence associated cortical oscillations during feedback learning and memory retrieval of encoded objects	94
4.3.6.2 Estimation of the effect of feedback learning on subsequently engaged memory retrieval through multifrequency interactions	97
4.3.6.3 Estimation of neural mechanisms of intelligence-correlated learning and memory retrieval of encoded objects	97
4.3.6.4 Classifying elicitation of intelligence-associated EEG oscillations during feedback learning and memory retrieval of encoded objects using attention-based LSTM model	99
4.4 Results	101
4.4.1 Association of fluid intelligence with EEG oscillations that elicits during learning and memory retrieval of encoded objects	102
4.4.1.1 The time-frequency analysis	102
4.4.1.2 Association of fluid intelligence	103
4.4.2 Effect of intelligence associated learning on subsequently engaged memory retrieval: Multi frequency interaction analysis	105
4.4.3 Neural mechanisms of intelligence-associated EEG oscillations that elicits during feedback learning and memory retrieval of encoded objects	106
4.4.3.1 EEG informed fMRI analysis	106
4.4.3.2 Hemodynamic functional connectivity analysis	109
4.4.4 Attention-based deep learning model	112
4.5 Discussion	114
4.5.1 Fronto-parietal cortical oscillations and their association with fluid intelligence	114
4.5.2 Intelligence-associated EEG oscillations of feedback-learning modulate subsequent memory retrieval	116
4.5.3 Fluid intelligence modulation on learning and memory retrieval: understanding of neuronal sources and their functional connectivity	117

Title	*Page No.*
4.5.4 Performance of proposed deep learning computation model	120
4.6 Significance of the study	120
4.7 Conclusion	121
References	123
Chapter 5: Hemodynamic functional connectivity optimization of frequency EEG microstates enables attention LSTM framework to classify distinct temporal cortical communications of different cognitive tasks	**137**
5.1 Abstract	137
5.2 Introduction	138
5.2.1 Decoding distant cortical communications from cortical EEG	138
5.2.2 Microstates and global cortical communication	139
5.2.3 Deep learning approaches for temporal EEG analysis	140
5.2.4 Present Study	140
5.3 Methods and materials	141
5.3.1 Participants and task design	141
5.3.2 Simultaneous EEG-fMRI acquisition and preprocessing	142
5.3.3 Estimation of frequency-microstates and their optimization with task's cortical communications	144
5.3.4 Attention-based LSTM model and validation	146
5.4 Results	150
5.4.1 Frontal-parietal- temporal regions interaction during task engagements	150
5.4.2 Hemodynamic functional connectivity optimization of quasi-stable frequency-microstates	151

Title	*Page No.*
5.4.3 Neurovascular analysis of optimized frequency microstates: EEG Informed fMRI analysis	152
5.4.4 Performance of Deep Attentional LSTM Model	157
5.5 Discussion	159
5.5.1 Association of distinct frequency microstates with each task's cortical functional connectivity	161
5.5.2 Performance of attention-based deep learning system in classifying time series quasi-stable cortical frequency EEG information	162
5.5.2.1 Temporal sampling window of quasi-stable frequency information optimizes the performance of deep learning architectures	162
5.5.2.2 Effect of attention mechanism with traditional LSTM architectures	162
5.6 Significance of the study	163
5.7 Conclusion	163
References	165
Chapter 6: Conclusions and Future Direction	**172**
6.1 Conclusions	172
6.2 Future directions	176
References	178
Appendices	**180**
Reprints of Journal Publications	

CHAPTER 1
INTRODUCTION

1.1 INTEGRATION OF BRAIN MAPPING TECHNIQUES IS AN OPTIMUM SOLUTION TO NEUROSCIENCE RESEARCH

Integration of distinct brain mapping techniques has been growing in recent years by improving the understanding of neuroscience research problems. It is the concept that integrates multiple brain mapping modalities to extract an in-depth understanding of the brain structure and functions. Integration of multiple modalities also eases the exploration of complex brain mechanisms by overcoming the limitations of individual modality. Modern neuroimaging techniques have resulted in non-invasive approaches for measuring brain activity, such as magnetoencephalography (MEG), electroencephalography (EEG), near-infrared spectroscopy (NIRS), single-photon emission computed tomography (SPECT), positron emission tomography (PET) and magnetic resonance imaging (MRI) broadly based on brain electrophysiology and hemodynamics/ metabolism. In recent years, depending on the technical feasibility of multi-modality integration, various modes of integration have been employed in the neuroscience research field, such as EEG-fMRI, NIRS-fMRI, PET-NIRS, PET-EEG, PET-MEG, EEG-NIRS. The simultaneous acquisition of EEG and fMRI data has received extensive attention in cognitive and clinical neurosciences. Integrating EEG and fMRI provides two different and outstanding electrophysiological and hemodynamic information associated with the neuronal activity at a level of millisecond and millimeter spatiotemporal resolution. A brief description of these modalities is demonstrated in Figure 1.1 and described as follows.

1.1.1 EEG (Electroencephalography)

The EEG signal represents the recorded neuronal activity on multiple electrodes on the scalp's surface at a macroscopic scale. It represents the summated electrical activity generated by postsynaptic potentials (excitatory and inhibitory), predominately reflecting the activity of cortical neurons arranged in layers in roughly the same orientation beneath the cortical surface. There exists no direct contribution of the deeper structures, such as the hippocampus, thalamus, or brainstem. EEG

measures the current flows generated due to synaptic excitations of the dendrites in the cerebral cortex. Large populations of active neurons can generate the electrical activity is recorded at the head surface. The electrical electrical activity is passed through the multiple deep layers, skull, and skin. After that, the electrical signals detected weakly are amplified. Transmission of electrical activity from multi-layered deep brain structure to the head surface causes volume conduction and poor spatial resolution. However, as the electrical activity propagates instantaneously to the recording electrodes at the head surface, it provides excellent timing information through the scalp potential. EEG has been a potent tool in neuroscience research due to the capability to measure the electrical activity of both the normal and abnormal brain with a higher temporal resolution.

1.1.2 fMRI (Functional Magnetic Resonance Imaging)

It is a non-invasive imaging technique that utilizes the metabolic and hemodynamic responses consequent to task-induced neuronal activity or the spontaneous activity of the resting brain [4,5].

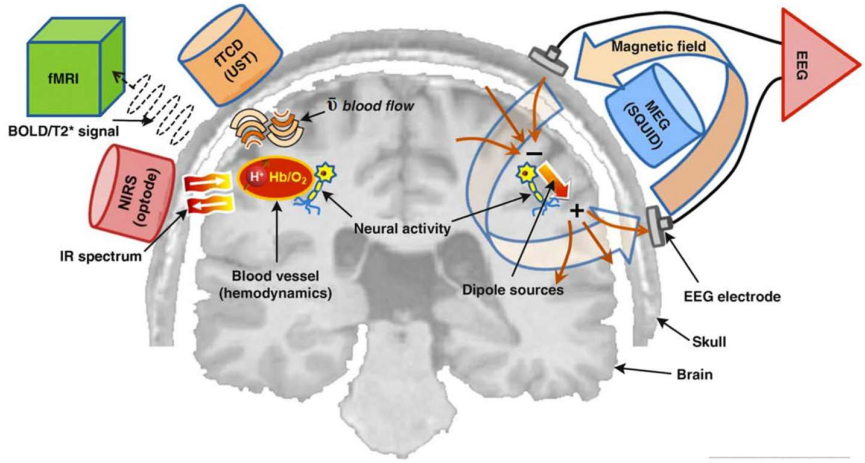

Figure 1.1: Schematic diagram of brain signal detection mechanisms. EEG measures the electrical potential differences on the scalp that are generated by cortical neural activity. Neurons transmitting neurological signals across their synapses act as dipole sources. MEG detects the magnetic fields associated with such neuronal activation by SQUID sensors. fMRI measures the hemodynamic responses, particularly magnetic dynamics of protons (H+) related to neural activity; its technique is principally based on the detection of local BOLD signal contrast during neuronal activation. Using multiple arrays of optodes, NIRS characterizes changes in the intensity of attenuated near-infrared (IR) light (owing to scattering or absorption), resulting from changes in concentration between oxyhemoglobin (HbO2) and deoxyhemoglobin (Hb) during local neural activity. **Adapted from** [3]

Blood oxygenation level-dependent signal (BOLD) contrast imaging is used in fMRI that results from magnetic field changes surrounding the red blood cells and it depends on the oxygenated hemoglobin. Increased neural activity stimulates the arterial cerebral blood flow (CBF) to meet the greater oxygen demand, resulting in the lower deoxy-Hb content and an increased BOLD signal. Thus, the BOLD signal is considered to constitute only an indirect measure of neuronal activity and relates inversely proportionate to the local content of deoxyhemoglobin [6]. Due to the intermediary processes of neurovascular coupling, the HRF response of neural activity to be sluggish and spreads over time depending upon the intensity and duration of neural activity. It typically rises after ~2 sec from the onset of task stimulus and reaches the peak at ~3 to 5 sec, and finally reaches the plateau after ~6 sec [4]. It depends on the paradigm, response amplitude and signal-to-noise ratio (SNR). Other modalities such as NIRS and MEG are also emerging and potential modalities in studying brain mechanisms. Further, complementary spatio-temporal features of multiple modalities have motivated the advancements towards integrating multiple brain mapping modalities irrespective of individual modality. Specifically, the integration of EEG and fMRI has gotten most of the attention. Several studies reveal that electrophysiological and hemodynamic/metabolic signals reflect distinct but closely coupled aspects of the underlying neural activity. Thus, the integration of fMRI with EEG data then provides a better understanding of underlying neural mechanisms. Many efforts have been made for simultaneous acquisition and data integration to achieve a promising integrated approach capable of millimeter spatial resolution and millisecond temporal resolution. However, the technical challenges for ensuring the identical sensory stimulation in the EEG and fMRI, simultaneous acquisition provide fundamental advantages over separate recording sessions for directly relating electrical and hemodynamic signals, thereby benefiting neurocomputing and neuroscience fields.

1.2 FEATURE EXTRACTION

Feature extraction is a crucial stage in EEG signal classification and is a task-relevant signal signifier while classifying the distinct brain states. However, their optimization is essential to improve the quality of cognitive performance evaluations, as it directly

impacts a classifier's performance [7]. Some commonly used EEG features, and the feature extractors used to acquire them, are discussed here.

ERP (Event-Related Potentials): Event-related potentials are small voltages generated in the brain structures in response to specific events or stimuli elicited by a wide variety of sensory, cognitive, or motor events [8]. Rather than understanding a continuous EEG recording, task-related or event-related modulation of brain activity is more informative. Therefore, event-related potentials are useful to study the brain response time-locked to the stimuli. Due to their high temporal precision, accuracy, and very little data processing, ERPs are preferred as the fastest and easiest approach for comparing ERPs across the two conditions or brain states. Although, information loss due to ERP averaging and lesser linkage with neurophysiological limit its exploration of interregional communications.

Time-Frequency Analysis: EEG data is a multidimensional signal that contains frequency as a prominent dimension. The EEG oscillations reflect fluctuations in the dendritic electrical activity of populations of neurons. Due to the neurophysiological mechanisms of neural oscillations, the analysis can extract neural mechanisms at synaptic, cellular, and systems-level of multiple spatial and temporal scales [9]. Also, it can answer more accurately the cognitive processes as well. The brain's rhythmic activity contains multiple frequencies simultaneously, where different cognitive processes seem to utilize different frequency ranges or conjunctions of frequency ranges. The brain rhythms have been grouped into bands defined by logarithmically increasing center frequencies and frequency widths. Brain rhythm frequency bands include delta (1– 4 Hz), theta (4 – 8 Hz), alpha (8 – 12 Hz), beta (15 – 30 Hz), lower gamma (30 – 80 Hz), and upper gamma (80 – 150 Hz). This analysis link EEG data to neurophysiological processes and patient groups.

Power Spectral Density (PSD): Power spectral density evaluates the distribution of power in an EEG signal over a range of EEG frequencies. It determines levels of brain activity in EEG recordings to assess the power of each frequency observed for resting and task-engaged states. PSD is calculated by taking Fourier Transform of the autocorrelation

and is useful in describing the frequency distribution of the signal and is extensively used to study the amount of signal power present in each frequency band.

Independent Component Analysis (ICA): Independent component analysis (ICA) is a blind source separation technique that decomposes the signal into a set of mutually independent components. It finds a set of maximally independent signals that mix linearly to produce the recorded data [10]. The EEG signal can be expressed as :

$$y(t) = A.x(t) + n(t)$$

Where $y(t) = \left(y_1(t), y_2(t), y_3(t), y_4(t), \ldots . y_p(t)\right)$ is p-channel EEG signal and $x(t) = \left(x_1(t), x_2(t), x_3(t), x_4(t), \ldots . x_p(t)\right)^T$ is a set of independent sources. The coefficients that describe the contribution of each source is defined by the mixing matrix $A = \left(a_1, a_2, a_3, a_4, \ldots . a_p\right)$.

Therefore, $x(t) = W.y(t) = A^{-1}.y(t)$, Where $\mathrm{W} = A^{-1}$ *is* e coefficients of W vector are computed by minimizing mutual information. Several algorithms have been developed for estimating these weight matrices, such as the INFOMAX, JADE, FastICA, etc. Due to the capability of extracting the information of independence, the ICA technique has also been an excellent tool for identifying artifacts originating from the sources independent of the EEG signal.

1.3 DATA MINING TECHNIQUES

Data mining approaches facilitate the neuroscience field to analyze the immense neural mechanism associated with the task-activation, lesion-deficit, and various clinical analyses. The availability of enormous heterogeneous data sets and the complexity of brain mechanisms motivate efficient developing methods for exploring deeper insights from distinct perspectives. Data mining approaches have been seen with the potential of extracting valuable and informative findings from massive information contained in brain mapping data sets. Also, retrieving high-level knowledge from low-level data is known as 'Knowledge Discovery in databases,'. It comprises several steps such as framing a hypothesis, data collection, pre-processing

of raw data, data transformation, extracting the necessary information as Data mining, and evaluation or interpretation of data (Figure 1.2).

Data mining algorithms can be classified into supervised learning (predictive models) or unsupervised learning (descriptive models). Descriptive modelling produces new and nontrivial information based on available data set to understand the patterns in large data sets by analyzing the system. The predictive data mining produces the model of the system described by the given data set to produce a model which can be expressed as an executable code and can perform classification, prediction, estimation, or other similar tasks. Some of the data mining methods are illustrated in Figure 1.3. By using various data mining algorithms, neuroscience research can transform the mounds of data into useful information for exploring the deeper insights of resting and task-evoked brain functions.

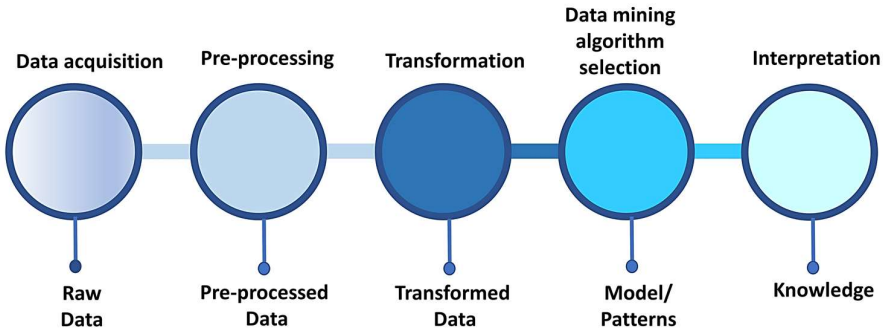

Figure 1.2: Knowledge Discovery in databases.

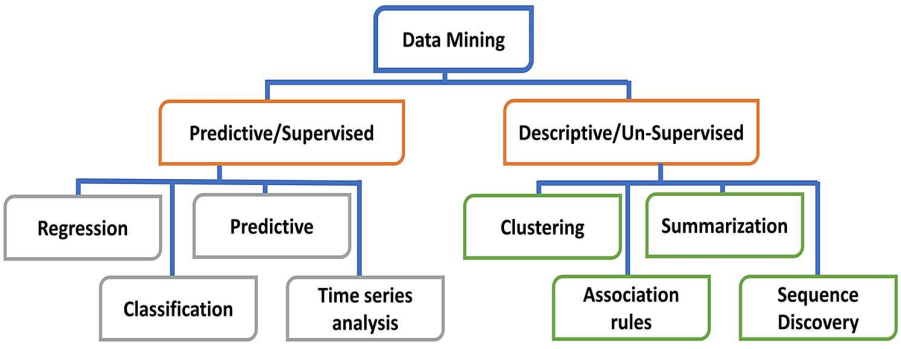

Figure 1.3: Classification of data mining techniques.

1.4 CHALLENGES IN TASK-ENGAGEMENT EXPLORATION

Existing theories fail to explain any aspect of that circumstance when the linkage between fMRI and EEG/MEG becomes invalid. Here, we will discuss a few critical issues while investigating the future developments in multimodal integration during task engagements.

BOLD response-related issue in understanding the neurovascular coupling and task-functional networks.

Functional brain networks exhibiting temporally coherent fluctuations have been traditionally studied to explore the resting state using the functional magnetic resonance imaging technique. However, their existence during cognitive task engagement still appears unclear for various tasks and various behavioral phenomena. For this, various voxel-level approaches have been used to estimate resting and task networks, such as ICA (independent component analysis) and DCM (dynamic causal modeling). The task-driven neuronal activity and associated modulations of functional network organization have substantial potential to reveal more insight into the functional dynamics of the brain.

The task stimulus-induced neuronal activity generally results in variations in the hemodynamic response and BOLD signals over time and space. The researchers [1,11] have observed that HRF response of neural activity to be sluggish and spread over time depending upon the intensity and duration of neural activity. It typically rises after ~2 sec from the onset of task stimulus and reaches the peak at ~3 to 5 sec, and finally reaches the plateau after ~6 sec [4]. Therefore, previous studies have designed the tasks with either block fMRI paradigm or simple event-related paradigms where a long empty block was acquired after stimulus block to allow the hemodynamic response to settle down.

However, when the task duration is shorter than hemodynamic delay, the BOLD response gets shifted to subsequent fMRI volume acquired later, as shown in Figure 1.4. This would lead to the erroneous estimation of task networks and neurovascular coupling. Further, this hemodynamic delay also varies concerning the type of tissue (voxel) and stimuli involved. Hence, there is a need to consider stimuli and voxel-

specific hemodynamic delay and develop an algorithm to understand the neurovascular coupling and task-based network connectivity.

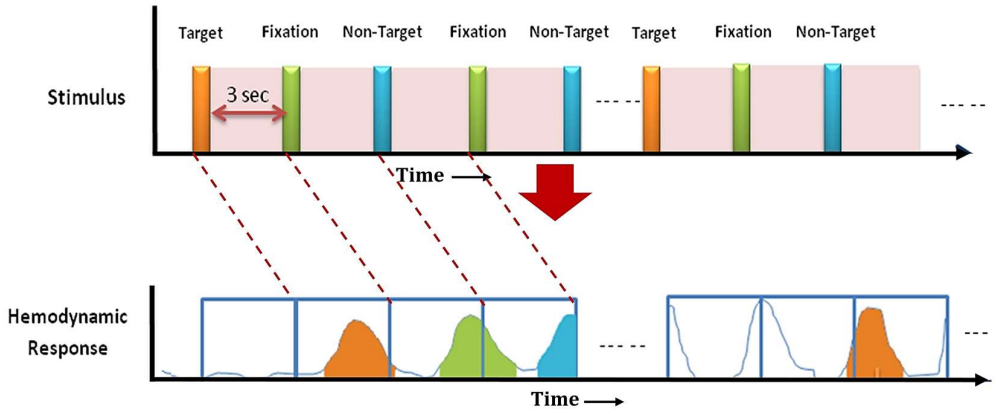

Figure 1.4: Schematic diagram for BOLD response during task execution using mixed paradigm.

Potential behavioral factors affect task engagement and associated neural mechanisms.

While exploring task engagement, the modulations in neuronal mechanisms are observed due to behavioral phenomena such as task familiarity, practice, current brain state, and intelligence level of individuals. These behavioral factors lead to significant changes in the brain functioning and the performance of an individual. Their effect on task engagement may bring a better and realistic understanding of the task and further modulations in functional mechanisms of the brain over the period. For instance, some influential behavioral phenomena might be helpful, such as performance feedback, which is information an individual receives concerning its evaluation through a rating mechanism during the task engagement. Another factor is fluid intelligence, which refers to perceiving relationships independent of previous specific practice or instruction concerning those relationships. The detailed description of these two factors are explained as follows:

Effect of performance feedback on subsequent task engagement

Motivation and learning associated with the feedback are observed facilitating the individual to adjust their behavior, improve the performance during subsequent task engagement [12], and behavior adaptations [13]. Further, memory is revealed as a

cognitive process that updates with experience, and learning is a process that contributes to the formation of these memories [14]. Specifically, performance feedback can motivate the desire to achieve a goal, such as receiving positive feedback or mastering a task and brings both informative and motivational aspects during task engagement to continue the current approach [15]. In contrast, the negative punishment feedback pauses the individual and encourages them to learn from their mistakes and reorganize their approach before the next task engagement [16]. There is hardly any study that has reported the modulation of functional connectivity measures during task engagement because of feedback learning and motivation. Thus, it needs to explore the influence of performance feedback in modulating the neuronal mechanisms associated with subsequently performed declarative memory retrieval tasks and the electrophysiological basis underlying these neuronal mechanisms.

Role of fluid intelligence in task engagements

Another constraint affecting the performance during task engagement is an individual's fluid intelligence. As per earlier studies, human adaptability to cognitive tasks is found responding to previously experienced actions and learning caused by associated performance feedback [17–19]. Several studies [20–23] link these learning abilities of individuals with their fluid intelligence, the individual's ability to reason, deduce, and solve problems. Further, Ricardo Primi [24] investigated the association of fluid intelligence with inter-individual differences and revealed the underlying correlated intelligence and learning mechanism. There is still an ambiguity in understanding the role of an individual's fluid intelligence while learning from performance feedback and subsequent task engagement. Thus, it needs to understand the association of fluid intelligence with feedback learning mechanisms and their effect on subsequent task engagement.

Development of neurocognitive-based task classification model

The human brain dynamically engages distinct neural populations between distant cortical regions, and their spatiotemporal oscillations often modulate systematically with behavioral and cognitive tasks. During such a neural engagement, the local

cortical circuitry performs a specific localized job, and global cortical communication involves information processing from different cortical, localized regions. Many research [25–27] acquired cortical EEG information simultaneously with fMRI imaging to understand functional connectivity, neural origins, and correlated brain states. However, decoding the neural basis of the distant cortical region's functional connectivity from spatially coarse-grained cortical EEG information is still challenging compared to the hemodynamic approaches based on task fMRI information. Thus, decoding the goal-directed task neural engagement and its association with several behavioral aspects focuses on developing many neural assistive/augmentative technologies. A unique and efficient algorithmic approach is needed to classify cortical EEG information associated with their local/global neural engagement caused by the cognitive task engagement.

1.5 OBJECTIVES OF THESIS

The central objective of is to examine and decipher distinct cognitive task engagements by building on the strengths of neurocomputational and data mining techniques. For this purpose, the thesis advances a comprehensive understanding by combining the proposed and conventional methods to explore distinct aspects of cognitive task engagements, associated neuronal mechanisms and develop a neurocognitive-based task classification model using the data mining technique. The schematic diagram for the thesis framework is demonstrated in Figure 1.5. The objectives include:

1. Understanding the neurovascular coupling through the hemodynamic reorganization by utilizing the hemodynamic response function characteristics. This is a fundamental step needed to understand the neurovascular coupling and functional networks during task engagements. For this, the HRF parameters are assessed and the BOLD activity is then reorganized utilizing the estimated parameters. The reorganized BOLD is used for further estimation of task's functional networks.

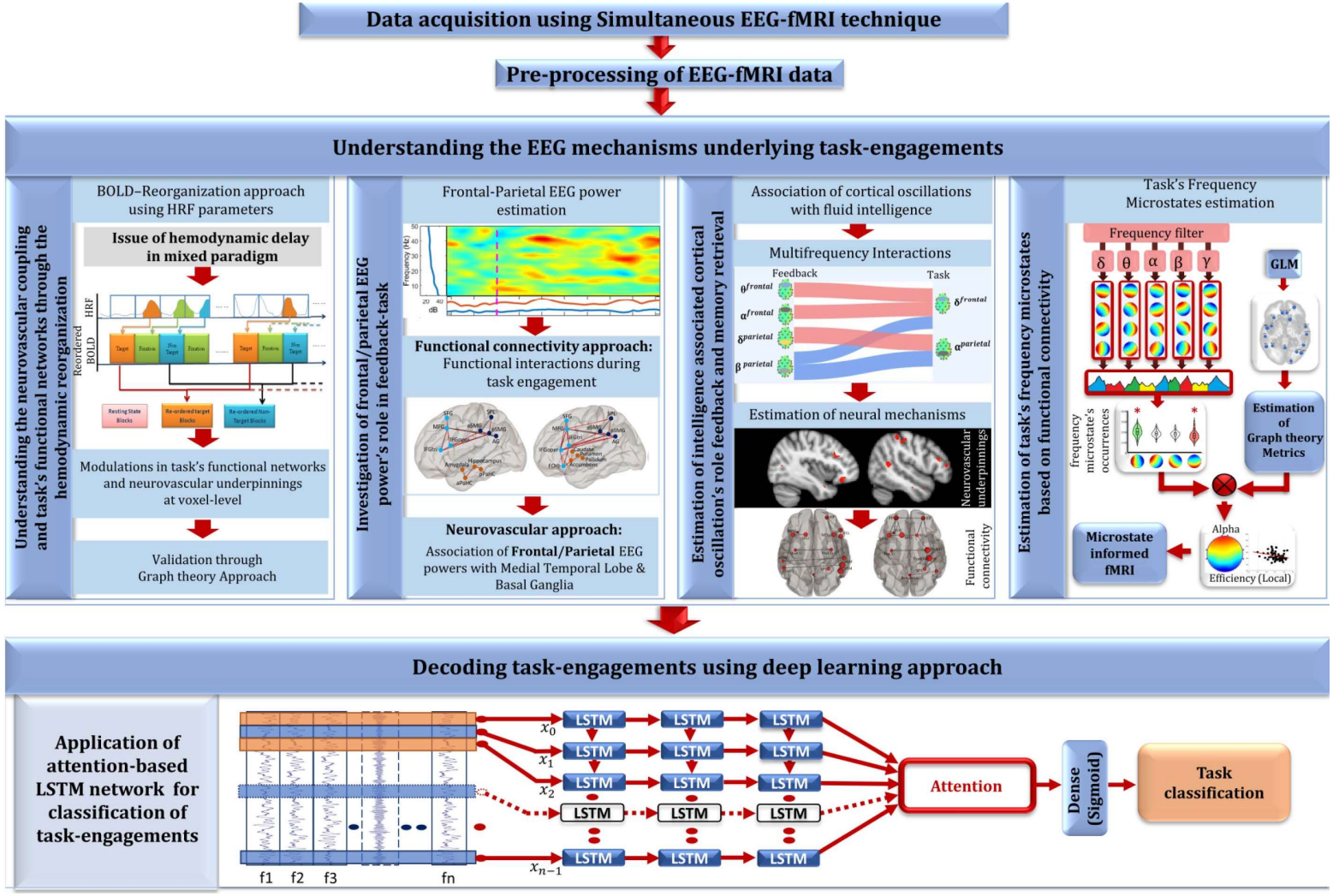

Figure 1.5: A schematic diagram of thesis framework.

2. Evaluating the effect of task engagement on the organization of functional networks and associated changes in their neurovascular underpinnings at voxel-level using simultaneous EEG-fMRI technique. This objective aims to understand task-related modulations through the integrated voxel-wise analysis of functional connectivity modulation with associated neurovascular underpinnings changes during visual target detection. A novel approach of reorganizing the blood oxygen level-dependent (BOLD) information has been proposed for this purpose, and results are validated through a graph-theoretical approach at the selected regions.

a. To design and develop the paradigm for target detection tasks in simultaneous EEG-fMRI setup.

b. To estimate the voxel-wise modulation of task-associated functional networks and associated changes in their neurovascular underpinnings.

c. To evaluate the performance of proposed approach against the traditional GLM approach.

3. Analyzing the effect of performance feedback on subsequent task engagement by assessing the role of the frontal-parietal EEG cortical oscillations in the functional interactions of feedback learning with subsequent declarative memory retrieval. This objective aims to understand how frontal-parietal regions contribute to declarative memory retrieval after feedback learning. This examines the association of frontal-parietal EEG powers with MTL and basal ganglia during feedback learning and memory retrieval using the functional connectivity approach. Afterward, feedback-related modulations are explored using the neurovascular approach to strengthen the associations of explicit associations frontal-parietal EEG powers with the bold activity of affected regions.

a. To design and develop the task paradigm of declarative memory retrieval in simultaneous EEG-fMRI setup.

b. To estimate the functional connectivity of frontal-parietal regions with MTL and sub-regions of basal ganglia during feedback learning and memory retrieval.

c. To assess the spectral contribution of frontal-parietal EEG powers in functional interactions by exploring the neurovascular underpinnings using the EEG-informed fMRI approach.

4. Associating fluid intelligence with feedback learning and subsequent task engagement by exploring multifrequency, EEG informed fMRI, functional connectivity approaches and classifying them using a deep learning framework.

This objective aims to understand the neural mechanisms of intelligence associated with feedback learning and subsequent memory retrieval of encoded objects and proposes a deep learning-based framework to classify them from distractors. For this purpose, the association of fluid intelligence (assessed through Raven Progressive Matrices) with the elicited cortical EEG oscillation is estimated. Subsequently, neural mechanisms underlying these intelligence-correlated multifrequency elicitations are studied through the multifrequency interaction, EEG-informed-fMRI, and hemodynamical functional connectivity approaches.

a. To identify the association of fluid intelligence with the EEG cortical oscillations of feedback learning and subsequent memory retrieval of encoded objects.

b. To examine the effect of feedback learning on subsequently engaged memory retrieval through multifrequency interactions and estimate the neural mechanisms of intelligence-correlated learning and memory retrieval of encoded objects.

c. Classifying elicitation of intelligence-associated EEG oscillations during feedback learning and memory retrieval of encoded objects using a deep learning framework.

5. Designing an integrated system for deciphering the distant cortical communication between distinct local neural engagement caused by the task engagement using hybrid- deep learning in multimodal integration approach.

This objective primarily assesses distant cortical interactions involving frontal-parietal and frontal-temporal functional connectivity elicitation during task engagement through cortical EEG information. The findings are validated through the task fMRI

functional connectivity and EEG informed fMRI estimations, finally classified the cortical EEG information through deep learning architectures.

a. To estimate the novel frequency microstates representing quasi-stable frequency patterns and their association with the distant cortical communication during task engagement.
b. To assess the neural mechanisms and functional connectivity from simultaneously acquired fMRI information.
c. To assess the association between fMRI functional connectivity with quasi-stable frequency-microstate's elicitations and validate their neural mechanisms through the EEG-informed fMRI.
d. To develop a hybrid deep learning framework for classifying the target detection task engagement using stacked temporal dynamics of the frequency microstate quasi-stable pattern.

1.6 THESIS STRUCTURE

The thesis is organized into six chapters to accommodate all the research objectives. The organization of this thesis is as follows.

Chapter-1 presents the multimodal integration approach as an optimum solution to neuroscience research and describes the need for multimodal integration. After that, the chapter progresses towards the basic principles of the neuroimaging techniques, their potential advantages, and drawbacks. Further, the possible solution 'multimodal integration' has been discussed that overcome the roadblocks of various neuroimaging techniques. The approach of data mining in extracting deeper insights is explained in brief. Then the chapter progresses to the challenges on the way to an exploration of task engagement using multimodal approach. Lastly, the thesis's overall structure and the importance of the research work presented are discussed.

Chapter-2 provides a brief description of modulations in functional networks for task engagement. The inadequacies in the voxel-wise analysis of functional networks lead the study to explore the complexity of HRF (Hemodynamic response function) over

the task engagement, which varies with types of task stimulus and regions of activity and might lead to the incorrect estimation of the functional network. To overcome these shortfalls and to understand the neurovascular coupling, our work develops a novel approach of reorganizing the blood oxygen level-dependent (BOLD) information based on the HRF characteristics. The proposed approach is then used to examine the voxel-wise modulations in the functional networks and neurovascular coupling while employing it for the visual target detection task. The results are then validated through a graph-theoretical approach at the selected regions and compared with modulations of neurovascular underpinnings using multimodal integration. The approach employs the complex behavior of HRF during task engagement and brings better insights into the neurovascular coupling and neuronal dynamics during visual target detection task engagement.

Further, extensive research revealed the significant modulations in the neuronal mechanisms underlying the cognitive task engagements; there are still many questions that require much more research to appreciate the performance of individuals during task engagement, externally or internally. Feedback associated with learning affects the individual's behavior and performance during subsequent task engagement through informative and motivational aspects. At first, the study investigated the role of EEG powers in the functional interactions of feedback learning and subsequent memory retrieval. Existing literature [28–30] explain the electrophysiology of positive-negative feedbacks, the affected regions, and subsequently, the behavior modulations. Several researchers [31–34] suggested engaging frontal and parietal brain regions during feedback and memory retrieval tasks, respectively. However, the contribution of frontal-parietal EEG powers to declarative memory retrieval after feedback learning remains less explored. Hence, the work explained in **Chapter 3** examines the association of frontal-parietal EEG powers with MTL and basal ganglia during feedback learning and memory retrieval using functional connectivity and neurovascular approach. Our findings reveal the modulation in functional connectivity of MTL and basal ganglia from feedback learning to memory retrieval due to the varying roles of basal ganglion sub-regions (putamen and pallidum). It also suggests that frontal-parietal regions dissociate from the MTL and the basal ganglia during

memory retrieval. The neurovascular approach and functional connectivity analysis prove that MTL-basal ganglia interactions during feedback and declarative memory tasks are associated distinctly with frontal-parietal EEG powers.

Further, in our work, EEG powers (frontal-parietal EEG powers) reflected a significant role in modulating the neuronal mechanism of feedback subsequent task engagement and task's functional networks, specifically declarative memory retrieval. Several studies have associated these learning abilities of individuals with their fluid intelligence, the individual's ability to reason, deduce, and solve problems. However, significantly less knowledge exists on how distinct cortical engagement is associated with fluid intelligence and relates to the learning and memory retrieval mechanisms. Hence, the present study aims to develop a deep learning-based computational model to decode the cortical EEG oscillations that associate individuals' fluid intelligence with their learning mechanisms during performance feedback and subsequent memory retrieval. Thus, **Chapter 4** comprises the work explaining the association of fluid intelligence with feedback learning and subsequent memory retrieval. For this purpose, multifrequency EEG analysis, associated neural mechanisms using EEG-informed-fMRI, and functional connectivity approaches have been employed. The role of an individual's fluid intelligence is explored by associating intelligence scores to the EEG powers of feedback learning and subsequent memory retrieval using robust correlation analysis. Further, these intelligence-associated frequency powers of memory retrieval and subsequent learning mechanisms are subjected to robust correlational analysis to understand their multifrequency cortical interaction across frontoparietal regions. Then, the study employed simultaneously acquired fMRI information to estimate the elicitation of distinct cortical communication between distant and distinct brain regions using graph-theoretical based hemodynamic functional connectivity analysis and EEG informed fMRI measures. Finally, an attention-based LSTM deep-learning model classified the deciphered distinct EEG oscillations that elicit encoded objects' learning and memory retrieval against the engagement of distractors. Further, it investigates the functional interactions underlying feedback learning and subsequent memory retrieval. The findings revealed the significant role of the left frontal pole and striatum in feedback learning and the

role of the striatum in modulating the prefrontal regions in memory retrieval. Further, feedback-related modulations are found supported by the task-related functional networks.

Further, decoding the goal-directed task neural engagement has primarily focused on developing many neural assistive/augmentative technologies. It has been observed that the human brain dynamically engages distinct neural populations between distant cortical regions, and their spatiotemporal oscillations often modulate systematically with behavioral and cognitive tasks. During such a neural engagement, the local cortical circuitry performs specific localized jobs, and global cortical communication involves information processing from different cortical, localized regions. However, decoding the neural basis of distant cortical region's functional connectivity, mainly involving frontal-parietal and frontal-temporal interactions from spatially coarse-grained cortical EEG information, is still a challenge compared to the hemodynamic approaches based on task fMRI information. Hence **Chapter 5** primarily aims to assess distant cortical interactions that involve frontal-parietal and frontal-temporal functional connectivity elicitation during task engagement through cortical EEG information. It further validates it through the task fMRI functional connectivity and EEG informed fMRI estimations and finally classifies them through attention based deep learning architectures.

Chapter-6 summarizes the overall research work illustrated in this thesis and the concrete conclusions drawn from the results presented in this dissertation. This chapter also discusses the future scope of the present work and how this work can be extended and used for further research.

REFERENCES

[1] A.L. Vazquez, E.R. Cohen, V. Gulani, L. Hernandez-Garcia, Y. Zheng, G.R. Lee, S.G. Kim, J.B. Grotberg, D.C. Noll, Vascular dynamics and BOLD fMRI: CBF level effects and analysis considerations, Neuroimage. 32 (2006) 1642–1655. https://doi.org/10.1016/j.neuroimage.2006.04.195.

[2] T.D. Wager, A. Vazquez, L. Hernandez, D.C. Noll, Accounting for nonlinear BOLD effects in fMRI: Parameter estimates and a model for prediction in rapid event-related studies, Neuroimage. 25 (2005) 206–218. https://doi.org/10.1016/j.neuroimage. 2004.11.008.

[3] B.K. Min, M.J. Marzelli, S.S. Yoo, Neuroimaging-based approaches in the brain-computer interface, Trends Biotechnol. 28 (2010) 552–560. https://doi.org/10. 1016/j.tibtech.2010.08.002.

[4] K.K. Kwong, J.W. Belliveau, D.A. Chesler, I.E. Goldberg, R.M. Weisskoff, B.P. Poncelet, D.N. Kennedy, B.E. Hoppel, M.S. Cohen, R. Turner, Dynamic magnetic resonance imaging of human brain activity during primary sensory stimulation., Proc. Natl. Acad. Sci. U. S. A. 89 (1992) 5675–9. https://doi.org/10.1073/PNAS.89.12.5675.

[5] P.A. Bandettini, E.C. Wong, R.S. Hinks, R.S. Tikofsky, J.S. Hyde, Time course EPI during task activation., Magn. Reson. Med. 25 (1992) 390–397.

[6] S. Ogawa, T.M. Lee, A.R. Kay, D.W. Tank, Brain magnetic resonance imaging with contrast dependent on blood oxygenation, Proc. Natl. Acad. Sci. U. S. A. 87 (1990) 9868–9872. https://doi.org/10.1073/pnas.87.24.9868.

[7] Z. Iscan, Z. Dokur, T. Demiralp, Classification of electroencephalogram signals with combined time and frequency features, Expert Syst. Appl. 38 (2011) 10499–10505. https://doi.org/10.1016/J.ESWA.2011.02.110.

[8] D.H.R. Blackwood, W.J. Muir, Cognitive brain potentials and their application, Br. J. Psychiatry. 157 (1990) 96–101. https://doi.org/10.1192/s0007125000291897.

[9] F. Varela, J.P. Lachaux, E. Rodriguez, J. Martinerie, The brainweb: Phase synchronization and large-scale integration, Nat. Rev. Neurosci. 2 (2001) 229–239. https://doi.org/10.1038/35067550.

[10] A.J. Bell, T.J. Sejnowski, An information-maximization approach to blind separation and blind deconvolution., Neural Comput. 7 (1995) 1129–1159. https://doi.org/ 10.1162/neco.1995.7.6.1129.

[11] T.D. Wager, M.C. Keller, S.C. Lacey, J. Jonides, Increased sensitivity in neuroimaging analyses using robust regression, Neuroimage. 26 (2005) 99–113. https://doi.org/10.1016/j.neuroimage.2005.01.011.

[12] T.H. Bailey, L.J. Phillips, The influence of motivation and adaptation on students' subjective well-being, meaning in life and academic performance, High. Educ. Res. Dev. 35 (2016) 201–216. https://doi.org/10.1080/07294360.2015.1087474.

[13] B. Krenn, S. Würth, A. Hergovich, The impact of feedback on goal setting and task performance: Testing the feedback intervention theory, Swiss J. Psychol. 72 (2013) 79–89. https://doi.org/10.1024/1421-0185/a000101.

[14] A.R. Preston, H. Eichenbaum, Interplay of hippocampus and prefrontal cortex in memory, Curr. Biol. 23 (2013) R764–R773. https://doi.org/10.1016/j.cub.2013.05.041.

[15] G. Li, S. Whiteson, W.B. Knox, H. Hung, Using informative behavior to increase engagement while learning from human reward, Auton. Agent. Multi. Agent. Syst. 30 (2016) 826–848. https://doi.org/10.1007/s10458-015-9308-2.

[16] C.B. Holroyd, M.G.H. Coles, The neural basis of human error processing: Reinforcement learning, dopamine, and the error-related negativity, Psychol. Rev. 109 (2002) 679–709. https://doi.org/10.1037/0033-295X.109.4.679.

[17] M. Köster, A. Haese, D. Czernochowski, Neuronal oscillations reveal the processes underlying intentional compared to incidental learning in children and young adults, PLoS One. 12 (2017). https://doi.org/10.1371/journal.pone.0182540.

[18] T.G. Popov, A. Carolus, D. Schubring, P. Popova, G.A. Miller, B.S. Rockstroh, Targeted training modifies oscillatory brain activity in schizophrenia patients, NeuroImage Clin. 7 (2015) 807–814. https://doi.org/10.1016/j.nicl.2015.03.010.

[19] B. Studer, S. Koeneke, J. Blum, L. Jäncke, The effects of practice distribution upon the regional oscillatory activity in visuomotor learning, Behav. Brain Funct. 6 (2010) 1–10. https://doi.org/10.1186/1744-9081-6-8.

[20] S. Jaarsveld, T. Lachmann, Intelligence and creativity in problem solving: The importance of test features in cognition research, Front. Psychol. 8 (2017) 1–12. https://doi.org/10.3389/fpsyg.2017.00134.

[21] D. Huepe, M. Roca, N. Salas, A. Canales-Johnson, Á.A. Rivera-Rei, L. Zamorano, A. Concepción, F. Manes, A. Ibañez, Fluid intelligence and psychosocial outcome: From logical problem solving to social adaptation, PLoS One. 6 (2011) 1–9. https://doi.org/10.1371/journal.pone.0024858.

[22] K. Fukuda, E. Vogel, U. Mayr, E. Awh, Quantity, not quality: The relationship between fluid intelligence and working memory capacity, Psychon. Bull. Rev. 17 (2010) 673–679. https://doi.org/10.3758/17.5.673.

[23] R. Primi, Complexity of geometric inductive reasoning tasks contribution to the understanding of fluid intelligence, Intelligence. 30 (2001) 41–70. https://doi.org/10.1016/S0160-2896(01)00067-8.

[24] R. Primi, M.E. Ferrão, L.S. Almeida, Fluid intelligence as a predictor of learning: A longitudinal multilevel approach applied to math, Learn. Individ. Differ. 20 (2010) 446–451. https://doi.org/10.1016/j.lindif.2010.05.001.

[25] H. Laufs, A. Kleinschmidt, A. Beyerle, E. Eger, A. Salek-haddadi, C. Preibisch, K. Krakow, EEG-correlated fMRI of human alpha activity, 19 (2003) 1463–1476. https://doi.org/10.1016/S1053-8119(03)00286-6.

[26] Mantini, Electrophysiological signature of brain resting state networks, Proc. Natl. Acad. Sci. U. S. A. 104 (2007) 13170–13175. papers://40c68295-5659-4035-8dff-71162e06882b/Paper/p3414.

[27] K.A. Kiehl, P.F. Liddle, Reproducibility of the hemodynamic response to auditory oddball stimuli: A six-week test-retest study, Hum. Brain Mapp. 18 (2003) 42–52. https://doi.org/10.1002/hbm.10074.

[28] J. Hattie, H. Timperley, The power of feedback, Rev. Educ. Res. 77 (2007) 81–112. https://doi.org/10.3102/003465430298487.

[29] W. Lee, J. Reeve, Self-determined, but not non-self-determined, motivation predicts activations in the anterior insular cortex: An fMRI study of personal agency, Soc. Cogn. Affect. Neurosci. 8 (2013) 538–545. https://doi.org/10.1093/scan/nss029.

[30] E. Tricomi, J.A. Fiez, Information content and reward processing in the human striatum during performance of a declarative memory task, Cogn. Affect. Behav. Neurosci. 12 (2012) 361–372. https://doi.org/10.3758/s13415-011-0077-3.

[31] C. Chang, Z. Liu, M.C. Chen, X. Liu, J.H. Duyn, EEG correlates of time-varying BOLD functional connectivity, Neuroimage. 72 (2013) 227–236. https://doi.org/10.1016/j.neuroimage.2013.01.049.

[32] K.R. Ridderinkhof, W.P.M. Van Den Wildenberg, S.J. Segalowitz, C.S. Carter, Neurocognitive mechanisms of cognitive control: The role of prefrontal cortex in action selection, response inhibition, performance monitoring, and reward-based learning, Brain Cogn. 56 (2004) 129–140. https://doi.org/10.1016/j.bandc.2004.09. 016.

[33] I. van de Vijver, K. Richard Ridderinkhof, M.X. Cohen, Frontal oscillatory dynamics predict feedback learning and action adjustment, J. Cogn. Neurosci. 23 (2011) 4106–4121. https://doi.org/10.1162/jocn_a_00110.

[34] A.D. Wagner, B.J. Shannon, I. Kahn, R.L. Buckner, Parietal lobe contributions to episodic memory retrieval, Trends Cogn. Sci. 9 (2005) 445–453. https://doi.org/10.1016/j.tics.2005.07.001.

CHAPTER 2

EVALUATION OF THE FUNCTIONAL NETWORKS AND NEUROVASCULAR UNDERPINNINGS AT VOXEL-LEVEL DURING TASK-ENGAGEMENT

This chapter is a marginally modified version of the research article published as Agrawal, S., Chinnadurai, V., Kaur, A., Kumar, P., Kaur, P., Sharma, R., & Kumar Singh, A. (2019). Estimation of Functional Connectivity Modulations During Task Engagement and Their Neurovascular Underpinnings Through Hemodynamic Reorganization Method. Brain connectivity, 9(4), 341-355. *https://doi.org/10.1089/brain.2018.0656*

2.1 ABSTRACT

This study proposes an approach to understand the effect of task engagement through integrated analysis of modulations in functional networks and associated changes in their neurovascular underpinnings at every voxel. For this purpose, a novel approach that brings reorganization in acquired task-functional magnetic resonance imaging information based on hemodynamic characteristics of every task stimulus is proposed and validated. At first, modulations in functional networks of visual target detection task were estimated at every voxel through proposed methodology. It revealed task stimulus dependency in the modulation of default mode network (DMN). The DMN modulated as task negative network (TNN) during target stimulus. On the contrary, it was not entirely TNN during nontarget stimulus. The frontal-parietal and visual networks modulated as task positive network during both task stimuli. Further, modulations of neurovascular underpinnings associated with engagement of task were estimated by correlating the hemodynamically reorganized task blood oxygen level dependent information with simultaneously acquired electroencephalography frequency powers. It revealed the strong association of neurovascular underpinnings with their modulation of functional networks and the associated neuronal activity during task engagement. Finally, graph theoretical parameters such as local, global efficiency and clustering coefficient were also measured at the specific regions for

validating the results of proposed method. Modulation observed in graph theory measures clearly validated the activation and deactivation of functional networks observed by the proposed method during task engagement. Thus, the voxel-wise estimation of task-related modulation of functional networks and associated neurovascular underpinnings through proposed technique provide better insights into neuronal mechanism involved during engagement in a task.

2.2 INTRODUCTION

Cognitive task and the associated neuronal activity modulate the functional connectivity of resting state networks. Estimation of the task induced modulations in resting state networks and associated neurovascular underpinnings can reveal more insight into the functional dynamics of the brain.

Many researchers have studied the task-related modulations of functional networks using neuroimaging techniques. Raichle and colleagues [1] have assessed the nature of intricate modulation in resting state network caused by the task, and proposed a baseline state for understanding network dynamics. Fox and colleagues [2] observed the anti-correlation between DMN and attention network during attention-demanding cognitive task. These anti-correlated networks such as DMN and attention networks were labeled as Task Negative Network (TNN) and Task Positive Network (TPN) respectively. Similarly, the anti-correlation of DMN was also observed with other TPNs such as visual and motor networks [3–10]. Subsequently, volume of research demonstrating the existence of different TPNs during various tasks [11,12] and their modulation from resting state [4,13–15].

On the other hand, many researchers [16–21] observed that the tasks such as autobiographic memory retrieval, self-generated thoughts, mind wandering and absence of the external goal-directed tasks revealed positive modulation of DMN, which thus makes the DMN as TPN.

However, [22] has cautioned the use of terminology such as TPN and TNN. Furthermore, it is argued that both networks could be simultaneously engaged during tasks. For example, DMN may be co-active as well as functionally coupled with

frontal-parietal control network during task. Many studies observed co-activation of these two networks, in particular, during problem-solving task [23], devising the plan to achieve personal goals [24] and working memory encoding and retrieval [25] tasks. Similarly, several studies have reported the co-activation of DMN with TPNs during many of the cognitive tasks [25–31]. Hence, the task related engagement of DMN and its modulation is still poorly understood. These ambiguities motivated us to study the task-related modulation of functional networks.

For this purpose, the present study presents the methodology which estimates the modulations of functional networks during task engagement and associated changes in neurovascular underpinnings at voxel level. The neurovascular underpinnings provide better understanding of task-related modulations. Many researchers [32–35] have revealed that neurovascular underpinnings during task have a strong interplay with the hemodynamical changes caused by neuronal activity. So, integrated analyses of modulation of functional networks and neurovascular underpinnings are capable of revealing more insight which will clarify the ambiguities associated with task-related neuronal dynamics. However, the existing functional connectivity measures such as graph theory and dynamic causal model are ROI based techniques and thus limits the possibility of analyzing task evoked modulations at the voxel level. This further limits their utility in comparing these observations with neurovascular underpinning modulations at every voxel. Hence, a method that estimates modulation of functional networks during task engagement and compares them with their neurovascular underpinnings at the voxel level would be helpful in addressing the ambiguities of associated task-related modulations.

Various voxel level approaches have been used to estimate task as well as resting network. Shine and colleagues [36] implemented ICA based analysis by calculating the temporal derivative of each component time course and estimated moment-to-moment functional coupling during visual hallucination tasks. Sambataro and colleagues [37] estimated dynamics during rest as well as in the cognitive task by using multivariate analysis and estimated brain voxels with independent component loadings across all intrinsic networks. Arbabshirani and colleagues [3] explored the use of spatial ICA in investigating functional connectivity during task to the network

level. Schlösser and colleagues [38] investigated the task-related effective connectivity using DCM analysis, where stroop task was used as event related paradigm. Rowe and colleagues [39] implemented DCM model and identified the changes in the effective connectivity in Parkinson's disease using finger tapping task. Although these methods reveal voxel wise modulations of functional networks, they are not capable of facilitating the integrated voxel wise analysis of modulations of functional networks and their associated changes in neurovascular underpinnings.

Hence, the present study aims to understand task related modulations through the integrated voxel wise analysis of functional connectivity modulation with their associated changes in neurovascular underpinnings during visual target detection task. A novel approach of reorganizing the BOLD information has been proposed for this purpose, and results are validated through graph theoretical approach at the selected regions. The reordered BOLD information was first subjected to the estimation of voxel wise modulation of DMN, frontal-parietal and visual networks associated with both target and non-target task stimuli. Further, these functional network modulations were compared with modulations of neurovascular underpinnings associated with target and non-target task engagement. The neurovascular underpinnings were estimated by correlating the proposed reorganized BOLD information with simultaneously acquired EEG frequency powers. Finally, task fMRI data was processed through the conventional general linear model to identify the significant neural correlates of both target and non-target stimuli and the results are compared with modulations of both functional network and neurovascular underpinnings.

2.3 MATERIALS AND METHODS

2.3.1 Participants and procedure

Twenty healthy right-handed volunteers [13 males and 7 females] aged between 20-32 years (mean age: 24 years) participated in this study. All participants gave informed consent following the presentation of the study. The exclusion criteria were comprised of any history of psychiatric and neurological disorder, head injury and use of medication affecting the cognitive performance. The vision of participants was corrected using MR-compatible lenses whenever required. The purpose of study was

explained to the participants before the experiment. The results from two of the volunteers were not considered due to extreme head motion and minimum criteria of corrected answers.

2.3.2 Task design

Participants performed the target detection task by visual search, through collections of colored geometric shapes shown in the slides. The task paradigm used during experiment has described in Figure 2.1. Volunteers were instructed to respond upon identification of target among the collection of objects by pressing the buttons. The collection of objects was changed every 3 seconds. After each object, a slide consisting of single cross in the center was shown as a fixation block for 3 seconds. Among the ninety-four blocks of objects shown, only 32 blocks had target objects embedded. Target and non-target blocks were mixed in random fashion to avoid prediction by volunteers. Stimuli were projected onto MR-compatible lenses fitted on head coil inside MR.

2.3.3 Data acquisition with Simultaneous EEG-fMRI

Data acquisition of both task and resting state fMRI were performed using a simultaneous EEG-fMRI technique. The MRI acquisition was performed using 3T Siemens Magnetom Skyra scanner.

The fMRI data were acquired using Eco Planer Imaging (EPI) sequence with TR =3000 ms; TE= 36 ms; voxel size =3.6*3.6*3.0 mm; matrix =64*64; FoV read = 230 mm; flip angle =90^{o}, 36 axial slices. The axial slices were acquired parallel to Anterior-Posterior (AC-PC) line in interleaving manner with slice thickness of 3.0 mm. The high-resolution structural images of the brain were acquired using T1 MPRAGE sequence with parameters, voxel size =1.0*1.0*1.0 mm; TR= 2000 ms; flip angle = 90 Degrees; FoV = 240 mm; matrix= 512*512; slice thickness = 1.0 mm, 160 axial slices. Prior to the task fMRI acquisition, resting state fMRI acquisition was carried out keeping TR =2000 ms, TE = 30 ms; voxel size =3.8.0*3.8*5.0 mm; matrix =64*64; FoV read = 240 mm; flip angle =90^{o} volumes=205. The axial slices were acquired parallel to Anterior-Posterior (AC-PC) line in interleaving manner with slice

thickness of 5.0 mm. During rest acquisition, volunteers were instructed to close their eyes but stay awake and remain as still as possible during acquisition.

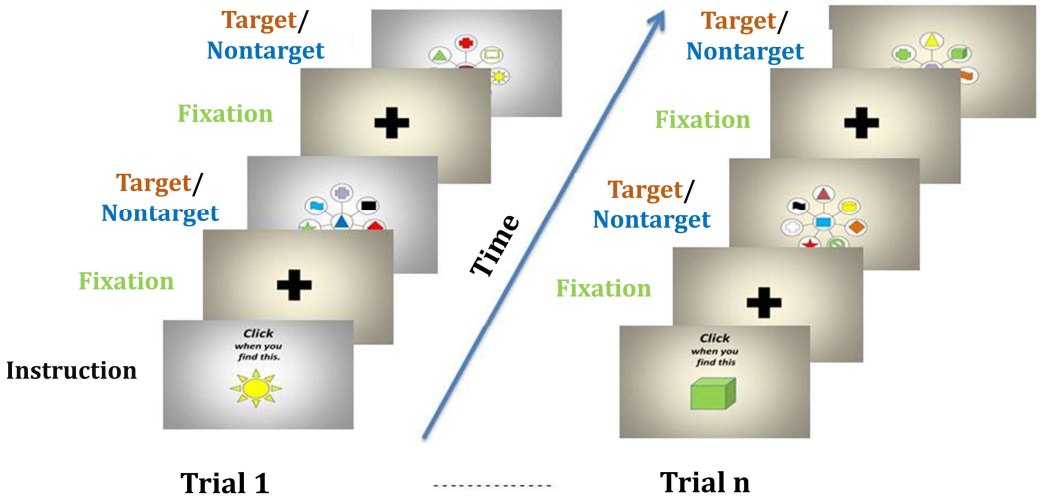

Figure 2.1: Schematic illustration of experimental task paradigm: visual target detection task. Five trials with different target objects were used. Each trial consisted of sequence of images, representing collection of objects for 3000 ms followed by subject response.

The EEG data of volunteers were acquired simultaneously during both resting and task fMRI using 32 channel MR compatible Brain Amp differential amplifier. The Ag/Agcl electrodes integrated in cap were positioned on scalp following 10-20 system with reference electrode in between Fz and Cz. The ground electrode was placed in between Cz and Pz. The ECG electrode was placed to measure the cardiac effect for the artifact corrections. The impedance of all the scalp electrodes was maintained below 5 kOhms. EEG data was acquired at 5 kHz sampling rate.

2.3.4 Data pre-processing steps

2.3.4.1 Reorganization of BOLD information in task fMRI data: The proposed approach

In the functional MRI, the task stimulus induces changes in the neuronal activity which results in variations in the hemodynamic response over space and time. This is observed in the changes of BOLD signals over the time. Although, there is no direct relationship between neuronal activities of task stimuli with the HRF parameters of evoked BOLD responses, Logothetis and colleagues [40] showed that these HRF parameters correlate

highly with post synaptic activity. In addition, various researchers [41,42] observed that HRF response of neural activity to be sluggish and spread over the time depends upon the intensity and duration of neural activity. It typically rises after ~2 sec from the onset of task stimulus and reaches the peak at around ~3 to 5 sec and finally reaches the plateau after ~6 sec [43]. However, this changes in BOLD activity various with types of task stimulus and regions of activity. In most of the fMRI connectivity models, this temporal BOLD information is directly used and convolved with standard HRF. But, the standard HRF function does not precisely explain the changes caused by the different stimulus and regions where neuronal activity occurs. The time the blood takes to travel from arteries to capillaries and draining veins during neuronal activity is different in different regions. This study quantifies this differential nature of BOLD activity and then uses it to reorganize the BOLD information (Figure 2.2). At first, quantification of changes in BOLD activity at every voxel caused by task stimulus is carried out by assessing their HRF parameters such as Amplitude (A), Time to Peak (TTP) and Width (W). Then, this information is used to reorganize the BOLD temporal data. The following section explains these operations in details for both target and non-target stimulus at every voxel.

At first, task fMRI data was preprocessed using SPM 12 for artifact removal. Then, the data was corrected for slice timing, realigned and registered to the MNI template space. The data was first motion corrected by applying rigid body transformation. All the images were then smoothed using Gaussian kernel of 5 mm. The preprocessed task fMRI dataset were subjected to the estimation of characteristics of hemodynamic response function (HRF) of every voxel associated with task stimulus. In this study, HRF parameters have estimated such as Amplitude (A), Time to Peak (TTP) and Width (W) as a potential measure of response, latency and duration of neuronal activity associated with each voxel and stimulus.

The brief methodology used for this purpose is shown in Fig. 2. The reconstructed task fMRI data $R(T)$ was measured as

$$R(T) = \{R_{r,c,s}(T)\} = \{Mean\{Y_{r,c,s}(t)\} \vee t_{earlier} < t < t_{later}\} \quad (1)$$

where r, c and s were the row, column and slice of voxel in the acquired task fMRI dataset $Y(T)$. $t_{earlier}$ and t_{later} were the earlier and later time point around Amplitude (A) of HRF function of the voxel located at given r, c and s. They were estimated [44] as,

$$t_{earlier} = \left\{Firstpoint\{t\} \vee t > TTP^{\mu}_{r,c,s} \wedge h^{\mu}_{r,c,s}(t) < A^{\mu}_{r,c,s}/2\right\} \quad (2)$$

$$t_{later} = \left\{Lastpoint\{t\} \vee t < TTP^{\mu}_{r,c,s} \wedge h^{\mu}_{r,c,s}(t) < A^{\mu}_{r,c,s}/2\right\} \quad (3)$$

where $h^{\mu}_{r,c,s}(t)$is the HRF function estimated for voxel located at (r, c, s) to the given specific stimuli μ. $TTP^{\mu}_{r,c,s}$ and $A^{\mu}_{r,c,s}$ are the Time to Peak and Amplitude measured from $h^{\mu}_{r,c,s}(t)$. The estimation of $TTP^{\mu}_{r,c,s}$ and $A^{\mu}_{r,c,s}$ were carried out by

$$TTP^{\mu}_{r,c,s} = min\left\{t \vee \frac{dh^{\mu}_{r,c,s}(t)}{dt} = 0 \wedge \frac{d^2h^{\mu}_{r,c,s}(t)}{dt^2} < 0\right\} \quad (4)$$

$$A^{\mu}_{r,c,s} = sign\left(\beta^{\mu}_{r,c,s}(1)\right)\sqrt{\left(\beta^{\mu}_{r,c,s}(1)\right)^2 + \left(\beta^{\mu}_{r,c,s}(2)\right)^2 + \left(\beta^{\mu}_{r,c,s}(3)\right)^2} \quad (5)$$

The $\beta^{\mu}_{r,c,s}(1)$,$\beta^{\mu}_{r,c,s}(2)$ and $\beta^{\mu}_{r,c,s}(3)$ are the regression coefficients parameters of the canonical HRF and its first and second order derivative terms. These are obtained by fitting the acquired task fMRI data with the general linear model using canonical HRF and its derivatives. The GLM through canonical HRF and its derivatives was carried out in SPM 12. Further, temporal filtering using high pass filtering cutoff of 100s was done to remove the low-frequency artifacts from the data.

2.3.4.2 Pre-processing of EEG data

The simultaneously acquired cortical EEG information of both resting and task were subjected to the following preprocessing procedures before estimations of modulations in neurovascular underpinnings during task engagement. The acquired EEG raw data was processed for MR related artifact correction using Brain Vision Analyzer, Brain product through adaptive artifact subtraction (AAS) method. The effect of pulse beats and cardio ballistic is removed using CB correction by using peak detection method. Subsequently, data were down sampled to 250 Hz and digital filtered between 0.5 and 100 Hz. Independent component analysis (ICA) was used for

the attenuation of ocular and the residual imaging artifacts using the filtered EEG recordings. These preprocessed EEG data were subsequently processed through EEGLAB, Mathworks for the estimation of EEG frequency powers.

2.3.5 Data analysis

2.3.5.1 Assessment of Functional Connectivity in task fMRI data

Reconstructed task fMRI data $R_{r,c,s}(T)$ subsequently subjected to MELODIC probabilistic ICA [45] of functional connectivity using FMRIB Software Library (FSL) version 5.0.9. Multi session temporal concatenation independent component analysis using variance normalized time courses and automatic dimensionality estimation were utilized in this process. The thresholds of maps were taken as 0.5 with structural image as a background image. Extraction of resting state networks across noise was done by masking the task networks for both stimuli with gray matter mask. Masked networks were then labeled and further, modulation in functional networks across DMN, FP and visual networks were carried out.

Besides the functional connectivity approach using ICA, task data was processed using general linear model using FSL FEAT with the effect of time and dispersion derivative by considering the different stimulus as conditions with one-sample t-test using the cluster threshold of $z = 2.56$ ($p<0.05$).

2.3.5.2 Assessment of Functional Connectivity in resting fMRI data

The preprocessing of resting fMRI data was performed using FMRIB Software Library (FSL) version 5.0.9. The data was first motion corrected using MCFLIRT by applying rigid body transformation. Further, slice time corrected images were imposed for extraction of non-brain matter using Brain Extraction Tool. Spatial Smoothening was done to remove the noise without affecting the valid activation in data and normalized by grand mean scaling at a value of 5 mm FWHM Gaussian kernel. Temporal filtering using high pass filtering cutoff of 100s was done to remove the low-frequency artifacts from the data. The preprocessed resting state data was then analyzed using MELODIC (FSL) for the characterization of resting state

networks by multiple concatenations across group data. Extraction of resting state networks across noise was done by masking the resting state networks with gray matter mask. Masked networks were then labeled and further, modulations in functional networks across DMN, FP and visual networks were carried out.

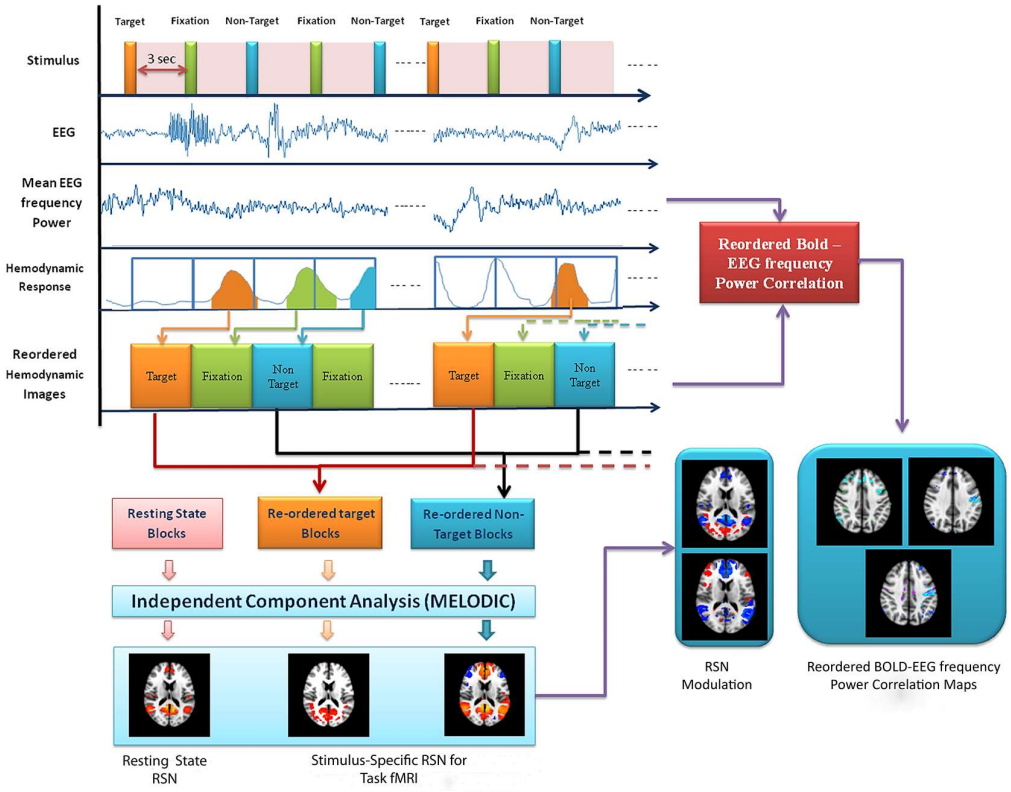

Figure 2.2: Hemodynamically reorganized BOLD approach for estimation of modulation in functional networks and their neurovascular underpinnings during task engagement. BOLD, blood oxygen level dependent.

2.3.5.3 Selection of Regions of interest (ROI)

The Study primarily focuses on assessing the modulation of functional network during task engagement and the associated changes in neurovascular underpinnings. For this purpose, the method based on reorganization of hemodynamic information is proposed and the modulations in DMN, frontal parietal and visual networks were estimated. The DMN revealed modulation in Medial Pre-Frontal Cortex (MPFC), Lateral Parietal (LP Right and Left) and Precuneus Cortex (PCC). Visual network has revealed high modulations in Medial Visual Cortex (MVC), Primary Visual Cortex (PVC) and Lateral Visual Cortex (LVC Right and Left). Finally, frontal-parietal

network has revealed significant modulations in lateral prefrontal cortex (LPFC Right and Left) and Posterior Parietal Cortex (PPC Right and Left). The detailed results are presented in results section. In order to validate these observations of proposed method, the modulations observed in these regions have been cross validated through graph theoretical approach. Hence, these regions are considered as regions of interest during the analysis of graph theoretical approach.

2.3.5.4 Graph Theory measures

The measures of graph theory were computed using functional connectivity (CONN) toolbox [46] implemented in MATLAB. In this ROI based analyses, temporal correlations for the resting state and task specific stimuli's BOLD signal time series were examined for the seed regions of DMN, frontal-parietal and visual networks for each subject. Functional connectivity maps of the all ROI's were further derived by Fisher's r-to-z transformation. For the group-level analysis, one-sample t-test was conducted to detect brain regions showing significant functional connectivity across participants. The group-level functional connectivity maps were further corrected for multiple comparisons using FDR-correction with a corrected threshold of $p < 0.05$. The graph theory parameters such as global efficiency, local efficiency, clustering coefficient and degree were then calculated for concerned ROIs.

2.3.5.5 Estimation of neurovascular underpinnings

The neurovascular underpinning brings better insight into the coupling between task induced neuronal activity and their hemodynamic information. This hemodynamic information as assessed by BOLD relies on parameters that affect neuronal activities such as cerebral blood flow, cerebral blood volume and metabolic consumption of oxygen.

In this study, the assessment of these neurovascular underpinning was carried out in two stages. At first, the mean EEG frequency powers pertaining to every stimulus block (both target and non-target stimuli) were estimated. For this purpose, artifact corrected EEG data of every stimulus block was band-pass filtered ranging from 1 Hz to 100 Hz. Then, they were subjected to the estimation of EEG time-locked frequency matrix (Ω) for both target and non-target stimuli as;

$$\Omega = \{\text{median}(\Omega(\text{i},\text{j}))|\ i = 1\ to\ N, j = 1{:}Nf\ \} \quad (6)$$

where $\Omega(\text{i},\text{j})$ is the median of j^{th} EEG frequency component of all the EEG channels pertaining to the i^{th} true positive stimuli block in the paradigm. N and Nf are total number true positive stimuli block and total number of frequency band respectively. In this study, Nf was kept four, which includes alpha (8 to 12 Hz), beta (12 to 30 Hz), Lower Gamma (30 to 50 Hz) and Upper Gamma (50 to 100 Hz) EEG powers. As mentioned in section 2.2, there were 32 target blocks and 62 non-target blocks in the task paradigm shown to the volunteers. Among these, only those blocks which were identified correctly as target and non-target by the volunteer were considered to estimate N for this purpose.

Then, hemodynamic parameters associated with every stimulus were quantified and used for reorganization of BOLD information as explained in the section 2.4. This reordered BOLD information ($R(i)$) pertaining to both target and non-target stimuli were correlated with EEG time-locked frequency matrix ($\boldsymbol{\Omega}$) data as follows,

$$\Gamma_{(r,c,s)}(j) = \{Correlation\ (R_{(r,c,s)}(i)\ , \Omega(\text{i},\text{j}))||\ i = 1\ to\ N, j = 1{:}Nf\ \} \quad (7)$$

where $\Gamma_{(r,c,s)}(j)$ is the correlation map pertaining to the jth frequency band. r, c and s are the row, column and slice of voxel. The correlation map (Γ) was estimated by Pearson's correlation for true positive target and non-target blocks independently for every volunteer. Finally, group analysis of estimated correlation maps of all the volunteers was performed using the one sample t-test.

2.4 RESULTS

The present study aims to understand the modulation of functional networks during task engagement and the associated changes in neurovascular underpinnings during visual target detection task. For this purpose, the hemodynamic based reorganization method is proposed and validated through graph theoretical approach at selected regions. The proposed method revealed task-related network modulations (Figure 2.3 & 2.4) and the associated neurovascular underpinnings (Figure 2.5 & 2.6) at every voxel. Supplementary Table 2.1 summarizes the modulations in networks and corresponding neurovascular underpinnings.

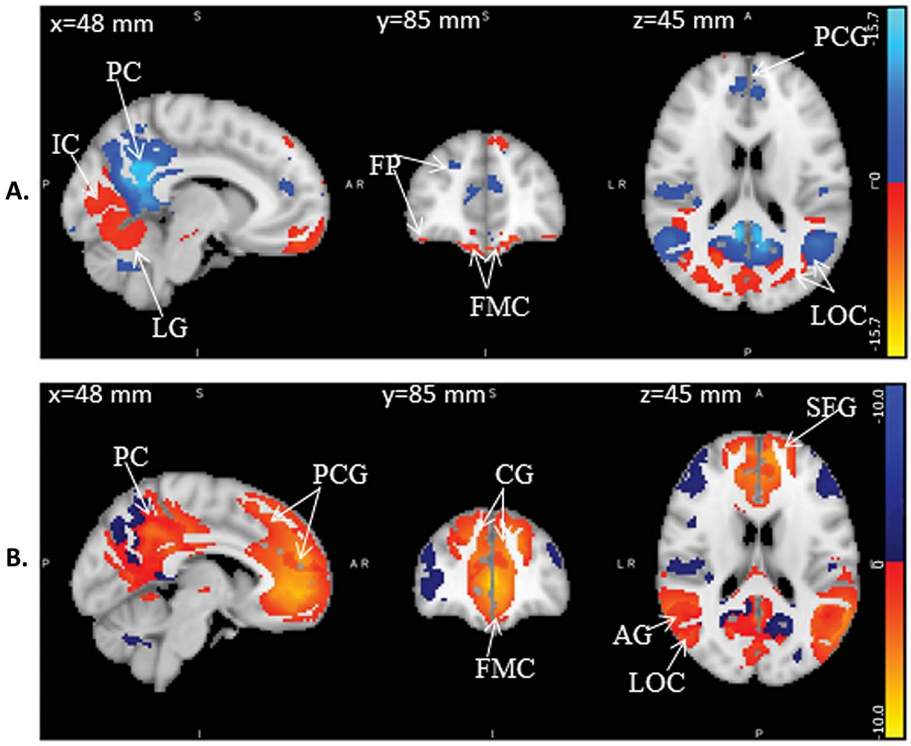

Figure 2.3: Illustrations of DMN modulation during task engagement (deactivation: blue, activation: red): (A) target stimuli, (B) nontarget stimuli. AG, angular gyrus; CG, cingulate gyrus; DMN, default mode network; FMC, frontal medial cortex; FP, frontal pole; IC, Intracalcarine cortex; LG, lingual gyrus; LOC, lateral occipital cortex; PC, precuneus cortex; PCG, paracingulate gyrus; SFG, superior frontal gyrus.

2.4.1 Task modulations in functional networks and neurovascular underpinnings

2.4.1.1 Target stimuli

Fig. 3A illustrates the modulations in DMN for the true positive target stimuli and regions are summarized in Supplementary Table 2.1. The regions cingulate gyrus, paracingulate gyrus, frontal medial cortex and parahippocampal gyrus which are part of Medial Pre-Frontal Cortex (MPFC) have revealed negative modulation in both hemispheres during target stimuli. Similarly, angular gyrus and middle temporal cortex which are part of Lateral Parietal (LP) cortex and PCC that belongs to precuneus cortex was also deactivated during target stimuli. However, in addition to the deactivation, some portion of frontal medial cortex and parahippocampal gyrus in the left hemisphere, part of MPFC were seen activated. From neurovascular underpinnings analyses, alpha and beta powers correlated negatively (Figure 2.5) with reordered BOLD in MPFC and LP. Similarly, gamma power was correlated negatively in LP and PCC.

Hence these negative modulations of DMN are accompanied by significant neuronal activation observed through GLM model in MPFC and LP. These observations explain the established hypothesis that DMN is a TNN during target.

The visual network has also presented (Figure 2.4) task-related modulation during target stimuli. The occipital pole, lingual gyrus that are part of PVC, and supracalcarine and intracalcarine cortex, the part of Medial Visual Cortex (MVC) deactivated during target stimuli.

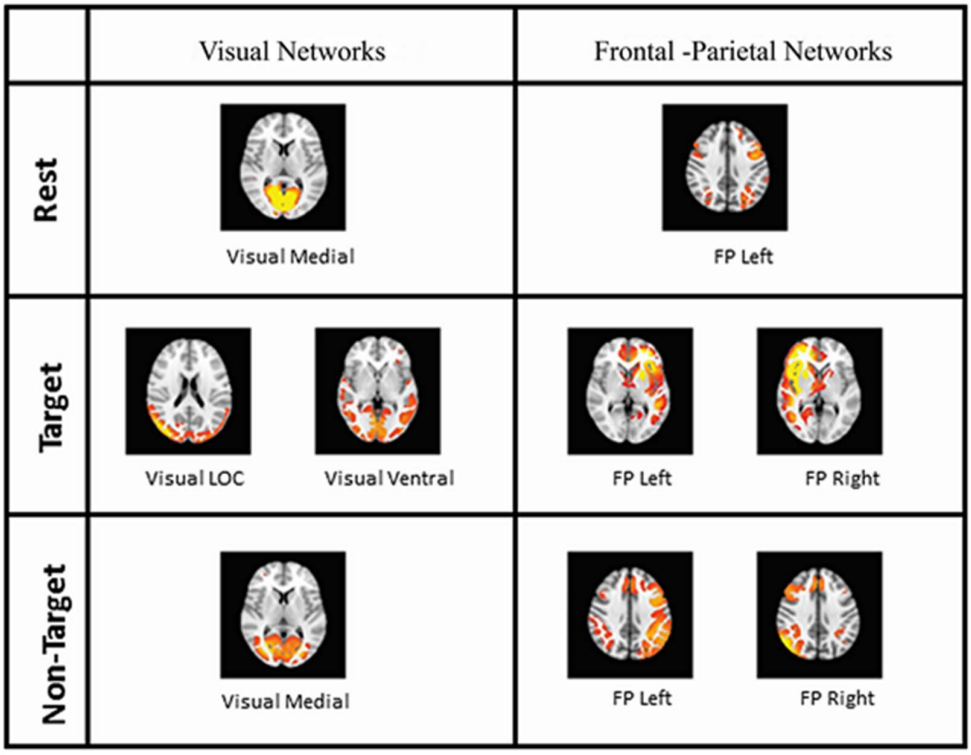

Figure 2.4: Illustrations of modulation in visual and frontal-parietal networks.

On the other hand, inferior lateral occipital cortex, part of Lateral Visual Cortex (LVC) was modulated positively. These modulations observed in the visual network are supported by significant neuronal activity observed through GLM model in visual cortex. Further it is also strengthened by the positive and negative correlation of alpha power observed in the deactivated and activated regions respectively. This association of negative correlation of alpha power and BOLD with activation in visual network regions justify the hypothesis that visual network as TPN during target stimuli.

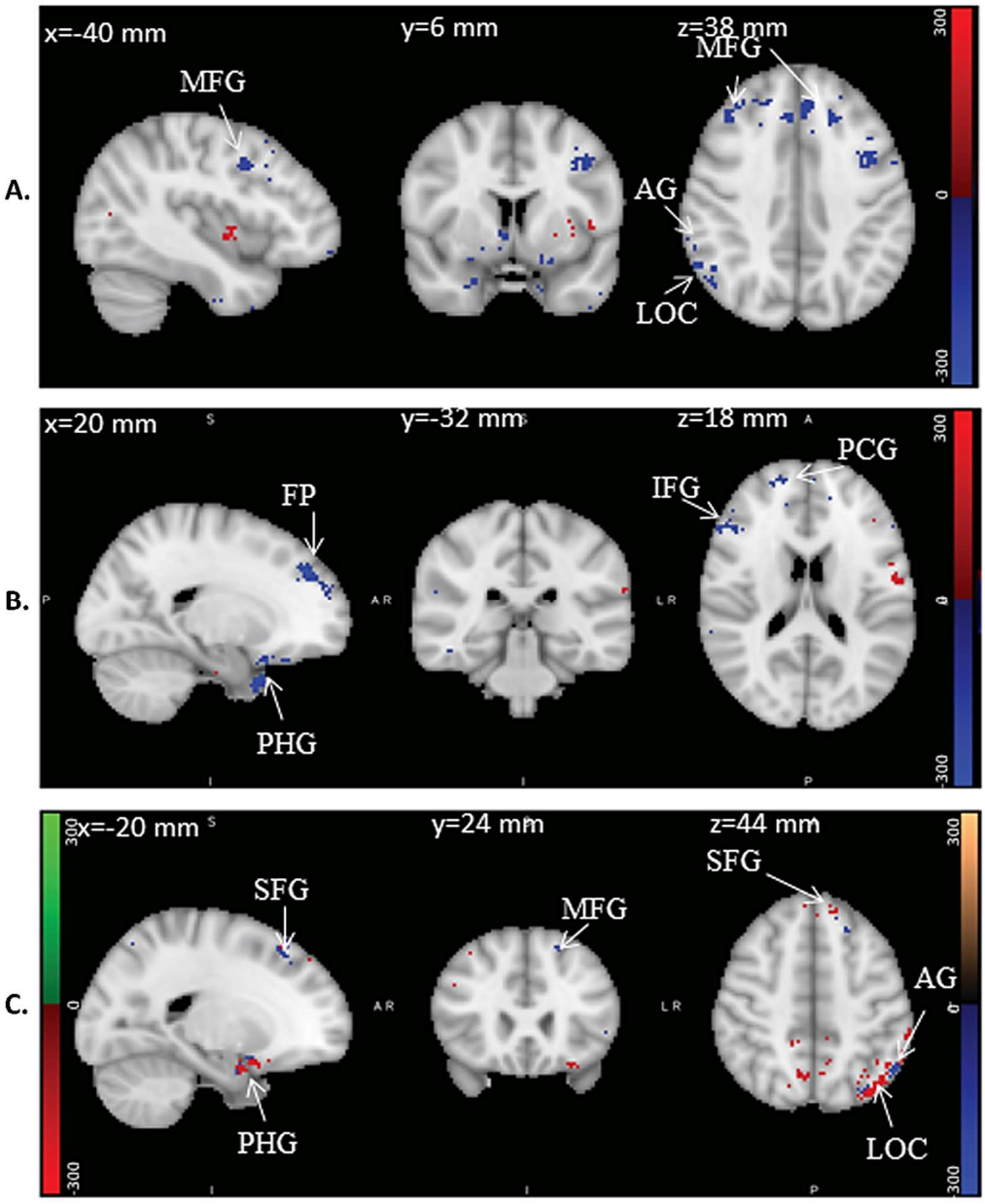

Figure 2.5: Neurovascular underpinnings of target stimuli: (A) alpha reordered BOLD correlation (positive: red, negative: blue); (B) beta-reordered BOLD correlation (positive: red, negative: blue); and (C) gamma-reordered BOLD correlation positive: green and copper, negative: red and blue). IFG, inferior frontal gyrus; MFG, middle frontal gyrus; PHG, parahippocampal gyrus.

In frontal-parietal network (Figure 2.4), positive modulation was observed in the inferior and middle frontal gyrus, part of lateral prefrontal cortex (LPFC). The similar trend was seen in angular gyrus and superior lateral occipital cortex, part of Posterior Parietal Cortex (PPC). Both LPFC and PPC revealed significant neuronal activity as

seen in GLM model. They also revealed negative correlation of alpha, beta and gamma powers with BOLD. This in turn supports the hypothesis that frontal-parietal network is a TPN during target stimuli.

2.4.1.2 Non-Target stimuli

Figure 2.3B illustrates the modulation observed in DMN for the true positive non-target stimuli and regions are tabulated in Supplementary Table 2.1. Bilateral activation of DMN was observed in MPFC, LP and PCC. However, some portion of PCC has revealed deactivations in the left hemisphere (Figure 2.6). On the other hand, none of the DMN modulations except in MPFC found associated with any statistically significant neuronal activity through GLM model. Similarly, there was no significant alpha correlation with BOLD was observed except in LP. The LP revealed negative correlation of alpha with BOLD. On the other hand, positive beta power correlation was seen in MPFC and LP. Gamma power correlated positively with reordered BOLD in PCC and LP and negatively in MPFC. These observations suggest that DMN is not completely manifesting as TNN during non-target stimuli.

The visual network revealed deactivations in MVC and PVC. On the other hand, bilateral activations were observed in LVC. All these modulations of visual network were accompanied by significant neuronal activity through GLM model. However, the deactivation of visual network in MVC and PVC were supported by positive correlation of beta power instead of alpha power. Negative alpha power correlation was found associated with activation observed in LVC. This clearly suggests that visual network is TPN during non-target stimuli. However, beta power correlated with BOLD during deactivation than alpha power. Further gamma power correlated negatively with BOLD in MVC, PVC and LVC.

In frontal-parietal network, bilateral activation was observed in LPFC and PPC. However, left LPFC and PPC have shown significant neuronal activity. In addition, the negative alpha correlation was observed in PPC. These results suggest that frontal-parietal network behaves as TPN during non-target stimuli. Gamma power showed negative correlation in PPC and the beta power correlated positively in LPFC.

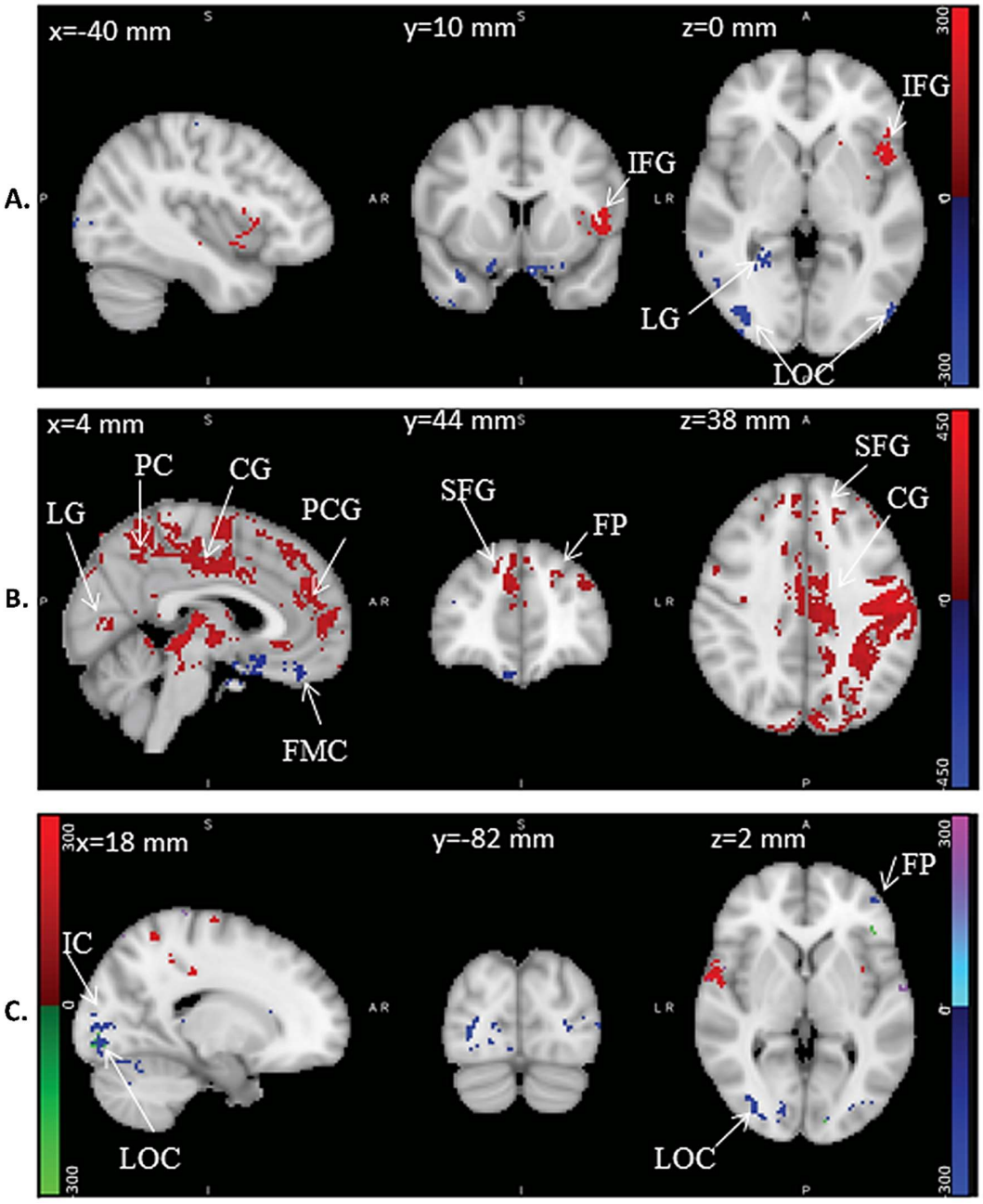

Figure 2.6: Neurovascular underpinnings of nontarget stimuli: (A) alpha-reordered BOLD correlation (positive: red, negative: blue); (B) beta-reordered BOLD correlation (positive: red, negative: blue); and (C) gamma-reordered BOLD correlation (positive: red and pink, negative: green and blue).

2.4.2 Graph theory analysis for the validation of modulation in functional networks

As explained in section 2.3.5.4, the graph theory was performed on the selected regions of interest for resting state, target and non-target stimuli independently and results are shown in Figure 2.7. The modulations of graph theory measures during task engagement are tabulated in Supplementary Table 2.1. The global efficiency, local efficiency, clustering coefficient and degree were estimated as graph theory measures in this study.

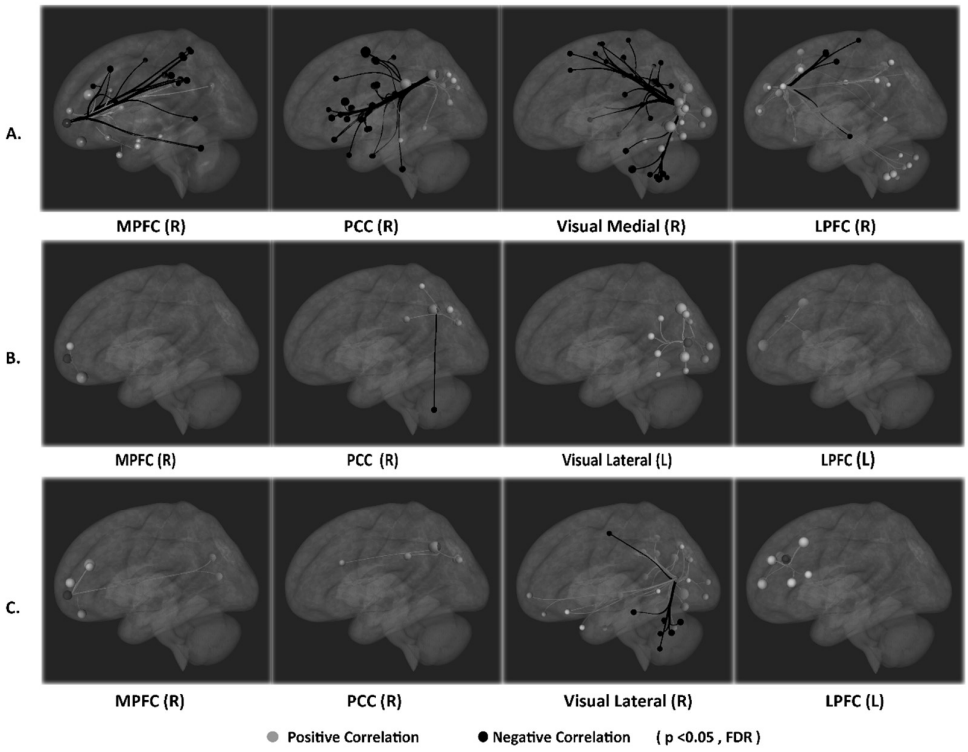

Figure 2.7: Graph theory analysis: (A) resting state, (B) target stimuli, and (C) nontarget stimuli (red: positive correlation, blue: negative correlation; for $p < 0.05$, FDR). FDR, false discovery rate; LPFC, lateral prefrontal cortex; MPFC, medial prefrontal cortex; PCC, posterior cingulate cortex.

The local efficiency and clustering coefficient revealed significant increase in all those regions where deactivation of DMN was observed. Similarly, global efficiency and degree has shown significant increase in MPFC and left LP. However, this trend was not seen in PCC. Graph theory measures of non-target stimuli revealed increase

in all DMN regions. In particular, the global efficiency observed in DMN during non-target stimuli is much higher than target stimuli. This justifies the absence of TNN trend in DMN modulation in non-target stimuli. Activation of TPN is associated with increase in global efficiency [47–49].

The TPN such as visual and frontal-parietal networks for both task stimuli revealed increase in graph theory measures. Local efficiency and clustering coefficient have shown more sensitivity towards the activation of network. Similarly, the deactivation observed in TPN has revealed decrease in graph theory measures, in particular local efficiency and clustering coefficient.

2.5 DISCUSSION

In this study, modulation of functional connectivity during the visual target detection task and their neurovascular underpinnings were estimated through hemodynamically reorganized BOLD method. Further, the results of the proposed method have been validated at specific regions through graph theory.

To date, several studies investigated the functional connectivity to explore the dynamic interaction of brain regions in resting state. Several researchers [3,50,51] have reported the modulation in functional connectivity and reorganization caused by tasks. However, our study presents a simple approach which enables to visualize task-related modulations of functional connectivity and associated changes in neurovascular underpinnings at the voxel level. The following sections present the observations concluded from the current study.

2.5.1 Association of functional network modulation with neural correlates of the task

Task induces the significant activation in engaged brain regions, which causes deactivations in DMN. Hence, DMN has always been referred as a TNN. However, in this study, DMN revealed dual nature of task-related modulation. During target stimuli, DMN modulated as TNN. On the other hand, it was not entirely TNN during non-target stimuli. This is possibly due to de-synchronization of the task neuronal

correlates with the DMN modulation during non-target stimuli. In specifics, deactivation of DMN was associated with significant neural activity estimated through GLM model was observed in most of the regions except PCC during target stimuli. But, this association was not observed during non-target stimuli. Hence, the results revealed the stimuli dependency of DMN modulation during task. Similar results were also observed by many researchers. Newton and colleagues [28,52] have reported the correlation between fluctuation in modulation of DMN during distinct cognitive tasks. Simony and colleagues [53] also reported the reconfiguration of DMN during narrative comprehension task. Mayor and colleagues [54] have observed DMN deactivation within parts of DMN region and concluded that they are dependent on specific characteristics of attention and working memory components of the task stimuli. This explains the dual nature of DMN modulation during both target and non-target stimuli.

Further, the visual and frontal-parietal networks are known as TPN as it reveals positive modulation during task engagement. Hence, TPN associates the activation of networks with significant neuronal activity caused by the task. This trend was clearly evident in modulation of visual and frontal-parietal network modulation during both target and non-target stimuli. These observations of the proposed method clearly establish the fundamental interplay between neuronal activity and modulations of task positive and negative networks.

2.5.2 Functional inhibition in alpha band reflects the task relevant neuronal activity

Several studies reported the inhibition of alpha band activity during the task engagement [32,33,35,55]. In the present study, negative correlation of alpha power with reordered BOLD reflects the inhibition of alpha power during task engagement.

In general, alpha inhibition is associated with significant neuronal activity at the region. Hence, deactivation in TNN as well as activation in TPN will be presenting the inhibition of alpha power at that region. In this study during target stimuli, alpha inhibition was observed in deactivated regions of DMN except in PCC. Similarly, activated regions of frontal-parietal and visual networks also revealed alpha

inhibition. Further, significant neuronal activity was also found in alpha-inhibited regions of DMN, frontal-parietal and visual networks. This is in consistent with the observation of [56,57], whose work suggested the active role of alpha band during cognitive task as an inhibitory control. However, during non-target stimuli alpha inhibition was only associated with activated regions of visual network. No such relationship between alpha inhibition and modulation in DMN and frontal-parietal network was observed during non-target stimuli.

Hence, the observed dissociation of alpha inhibition in DMN during non-target stimuli might be connected with its absence of TNN modulation. Moreover, the present study is inadequate to strongly conclude on this aspect of observed result. More focus into this dual nature of DMN modulation might bring intricate insight into the neuronal dynamics.

2.5.3 Cross frequency of Alpha/Beta neurovascular underpinnings

The decline in alpha/beta activity was found associated with drop in the synchrony of the underlying neural populations suggesting the task-related neuronal activity. The degree of de-synchronization is connected with enhanced neuronal activity quantitatively, and found reflected as augmented BOLD signal [58].

Results of proposed method have also revealed the de-synchronization of alpha and beta powers with their reordered BOLD in addition to their association with significant neuronal activity. For target stimuli, alpha/beta bands correlated negatively with reordered BOLD in MPFC, LP, LVC, LPFC and PPC. Further, these regions were also associated with significant neuronal activity estimated through GLM model. However, no such task-relevant de-synchronization was observed in alpha/beta powers with reordered BOLD for non-target stimuli.

2.5.4 Cross frequency coupling of Alpha/Gamma neurovascular underpinnings

Synchronized activity is the resultant of competition (via inhibition) and cooperation (via excitation) of individual or set of neurons or large neuronal assemblies. This results in

neuronal oscillations for different frequencies. This brought scientific community to observe the cross frequency coupling of low and high frequency [59–68].

In the present study, the proposed method reveals more insight into the synchronization of alpha/gamma bands and their correlation with reordered BOLD. Task-related de-synchronization of alpha/gamma power with reordered BOLD was observed for target stimuli in LP, LVC, LPFC and PPC, in addition to their significant neuronal activation. However, PCC exhibited de-synchronization of gamma power with reordered BOLD. For non-target stimuli, de-synchronization of both alpha/gamma powers with reordered BOLD was observed merely in visual regions PVC and LVC. However, synchronization of gamma power with reordered BOLD was observed LP, PCC and PPC.

These observations of the proposed method are supported by the observation of [34], that BOLD signal not necessarily needs to exhibit positive correlation with high-frequency and negatively with low-frequency neuronal activity. This relationship is also observed to be varying across other cortical areas pertaining to higher cognitive functions as well as based on task stimuli. The results of the present study support the same hypothesis.

2.5.5 Validation of proposed approach with Graph theory analysis

The modulations observed in graph theory measures clearly support and validated the proposed method's observations. Engagement of task influences both local and distant functional connectivity in the regions which are involved in performing the tasks. This is seen as activation in the TPN during task engagement in the regions where significant neuronal activity is observed [69]. However, the deactivation is generally associated with significant neuronal activity in the TNN [70]. Hence, regions which are deactivating in TNN and activating in TPN would increase both local connectivity as well as interaction with the distant regions [71]. This is observed through graph theory as positive modulation of local and global efficiency and clustering coefficients [72–74]. This trend is observed in the modulation of functional network as assessed by both proposed method and graph theory measures.

Earlier studies also found that, higher global efficiency of the network corresponds to fast global information communication, and local efficiency supports faster local information processing [75,76].

In this study, increase in local efficiency observed in the regions of task engagement was in line with present understanding of small worldness. Further, small worldness of functional networks demonstrates the task-related integration of brain regions. Dosenbach and colleagues [77] revealed the small-world features of the sub-network of the task-control system, analogous to the whole-brain network. Wang and colleagues [78] highlighted the higher functional connectivity and network efficiencies due to greater cognitive demand. Similarly, the insignificant variation of global efficiency observed in this study in most of the regions is in line with the observation of earlier studies [79]. Lin and colleagues [80] have observed dynamic alteration in DMN prior, during and post working memory task. In their study, the DMN has revealed high activation in the frontal regions during task, which in turn was observed as lower graph theory measures. This supports our observations of dual nature of DMN and its stimuli dependency. Thus, graph theory observations justify the modulations in functional connectivity as assessed by the proposed method.

2.6 CONCLUSION

In this study, the integrated analysis of modulations in functional networks and the associated changes in neurovascular underpinning were carried out through the proposed method at every voxel. The results of the proposed method were further validated with graph theoretical approach at the selected regions. The integrated analysis brought better insight of neuronal dynamics during task engagement. They are:

a. The deactivation and activation of DMN were specific to nature of task stimuli. In this study, DMN was TNN during target stimulus. However, it was not entirely TNN during non-target stimulus. On the other hand, frontal-parietal and visual networks remained as TPN during both target and non-target stimuli.

b. There exists a strong association of the deactivations/activation of DMN with its significant neuronal activity during task engagement. However, this association was not strictly seen for non-target stimulus.

c. The task-specific alpha inhibition and its association with significant neuronal activity and synchronization of visual and frontal-parietal network observed throughout the current study. However, de-synchronization of DMN was seen associated with these variations.

d. The association of de-synchronized alpha/beta activity with significant neuronal activity during task engagement is clearly observed in this study.

Thus, the proposed approach of integrated voxel wise analysis of modulation of functional networks and the associated changes in neurovascular underpinning was found useful and helps us in bringing better understanding of neuronal mechanisms during task engagement.

REFERENCES

[1] M.E. Raichle, A.M. MacLeod, A.Z. Snyder, W.J. Powers, D.A. Gusnard, G.L. Shulman, A default mode of brain function., Proc. Natl. Acad. Sci. U. S. A. 98 (2001) 676–82. https://doi.org/10.1073/pnas.98.2.676.

[2] M.D. Fox, A.Z. Snyder, J.L. Vincent, M. Corbetta, D.C. Van Essen, M.E. Raichle, From The Cover: The human brain is intrinsically organized into dynamic, anticorrelated functional networks, Proc. Natl. Acad. Sci. 102 (2005) 9673–9678. https://doi.org/10.1073/pnas.0504136102.

[3] M.R. Arbabshirani, M. Havlicek, K.A. Kiehl, G.D. Pearlson, V.D. Calhoun, Functional network connectivity during rest and task conditions: A comparative study, Hum. Brain Mapp. 34 (2013) 2959–2971. https://doi.org/10.1002/hbm.22118.

[4] V.D. Calhoun, K.A. Kiehl, G.D. Pearlson, Modulation of temporally coherent brain networks estimated using ICA at rest and during cognitive tasks, Hum. Brain Mapp. 29 (2008) 828–838. https://doi.org/10.1002/hbm.20581.

[5] X. Di, B.B. Biswal, Modulatory interactions between the default mode network and task positive networks in resting-state, PeerJ. 2 (2014) e367. https://doi.org/10.7717/peerj.367.

[6] R. Esposito, F. Cieri, P. Chiacchiaretta, N. Cera, M. Lauriola, M. Di Giannantonio, A. Tartaro, A. Ferretti, Modifications in resting state functional anticorrelation between default mode network and dorsal attention network: comparison among young adults, healthy elders and mild cognitive impairment patients, Brain Imaging Behav. 12 (2018) 127–141. https://doi.org/10.1007/s11682-017-9686-y.

[7] W. Gao, W. Lin, Frontal parietal control network regulates the anti-correlated default and dorsal attention networks, Hum. Brain Mapp. 33 (2012) 192–202. https://doi.org/10.1002/hbm.21204.

[8] A. Manelis, L.M. Reder, Effective connectivity among the working memory regions during preparation for and during performance of the n-back task, Front. Hum. Neurosci. 8 (2014) 1–11. https://doi.org/10.3389/fnhum.2014.00593.

[9] R. Sala-Llonch, C. Peña-Gómez, E.M. Arenaza-Urquijo, D. Vidal-Piñeiro, N. Bargalló, C. Junqué, D. Bartrés-Faz, Brain connectivity during resting state and subsequent working memory task predicts behavioural performance, Cortex. 48 (2012) 1187–1196. https://doi.org/10.1016/j.cortex.2011.07.006.

[10] S. Tommasin, D. Mascali, T. Gili, I. Eid Assan, M. Moraschi, M. Fratini, R.G. Wise, E.

Macaluso, S. Mangia, F. Giove, Task-Related Modulations of BOLD Low-Frequency Fluctuations within the Default Mode Network, Front. Phys. 5 (2017) 1–8. https://doi.org/10.3389/fphy.2017.00031.

[11] J. Binder, J. Frost, T. Hammeke, P.S.F. Bellgowan, S.M. Rao, R.W. Cox, Conceptual processing during the conscious resting state: A functional MRI study, J. Cogn. …. 11 (1999) 80–93. https://doi.org/10.1162/089892999563265.

[12] M.E. Raichle, D.A. Gusnard, Intrinsic brain activity sets the stage for expression of motivated behavior, J. Comp. Neurol. 493 (2005) 167–176. https://doi.org/10.1002/cne.20752.

[13] E.M. Gordon, M. Stollstorff, C.J. Vaidya, Using spatial multiple regression to identify intrinsic connectivity networks involved in working memory performance, HumBrain Mapp. 33 (2011) 10. https://doi.org/10.1002/hbm.21306.

[14] A. Newton, V. Morgan, Modulation of steady state functional connectivity in the default mode and working memory networks by cognitive load, Hum. Brain Mapp. 32 (2011) 1649–1659. https://doi.org/10.1002/hbm.21138.Modulation.

[15] S. Spadone, S. Della Penna, C. Sestieri, V. Betti, A. Tosoni, M.G. Perrucci, G.L. Romani, M. Corbetta, Dynamic reorganization of human resting-state networks during visuospatial attention, Proc. Natl. Acad. Sci. 112 (2015) 8112–8117. https://doi.org/10.1073/pnas.1415439112.

[16] J.R. Andrews-Hanna, J.S. Reidler, C. Huang, R.L. Buckner, Evidence for the Default Network's Role in Spontaneous Cognition, J. Neurophysiol. 104 (2010) 322–335. https://doi.org/10.1152/jn.00830.2009.

[17] R.L. Buckner, D.C. Carroll, Self-projection and the brain, Trends Cogn. Sci. 11 (2007) 49–57. https://doi.org/10.1016/j.tics.2006.11.004.

[18] M. De Luca, S. Smith, N. De Stefano, A. Federico, P.M. Matthews, Blood oxygenation level dependent contrast resting state networks are relevant to functional activity in the neocortical sensorimotor system, Exp. Brain Res. 167 (2005) 587–594. https://doi.org/10.1007/s00221-005-0059-1.

[19] X. Xu, H. Yuan, X. Lei, Activation and Connectivity within the Default Mode Network Contribute Independently to Future-Oriented Thought, Sci. Rep. 6 (2016) 1–10. https://doi.org/10.1038/srep21001.

[20] G. Bush, L.M. Shin, The Multi-Source Interference Task: An fMRI task that reliably activates the cingulo-frontal-parietal cognitive/attention network, Nat. Protoc. 1 (2006) 308–313. https://doi.org/10.1038/nprot.2006.48.

[21] T. Ino, R. Nakai, T. Azuma, T. Kimura, H. Fukuyama, Brain Activation During Autobiographical Memory Retrieval with Special Reference to Default Mode Network, Open Neuroimag. J. 5 (2011) 14–23. https://doi.org/10.2174/1874440001105010014.

[22] R. Nathan Spreng, The fallacy of a "task-negative" network, Front. Psychol. 3 (2012) 1–5. https://doi.org/10.3389/fpsyg.2012.00145.

[23] K.D. Gerlach, R.N. Spreng, A.W. Gilmore, D.L. Schacter, Solving future problems: Default network and executive activity associated with goal-directed mental simulations, Neuroimage. 55 (2011) 1816–1824. https://doi.org/10.1016/j.neuroimage. 2011.01.030.

[24] R.N. Spreng, W.D. Stevens, J.P. Chamberlain, A.W. Gilmore, D.L. Schacter, NeuroImage Default network activity , coupled with the frontoparietal control network , supports goal-directed cognition, Neuroimage. 53 (2010) 303–317. https://doi.org/10. 1016/j.neuroimage.2010.06.016.

[25] T. Piccoli, G. Valente, D.E.J. Linden, M. Re, F. Esposito, A.T. Sack, F. Di Salle, The Default Mode Network and the Working Memory Network Are Not Anti-Correlated during All Phases of a Working Memory Task, PLoS One. 10 (2015) e0123354. https://doi.org/10.1371/journal.pone.0123354.

[26] R.E. Beaty, M. Benedek, S. Barry Kaufman, P.J. Silvia, Default and Executive Network Coupling Supports Creative Idea Production, Sci. Rep. 5 (2015) 1–14. https://doi.org/ 10.1038/srep10964.

[27] H. Koshino, T. Minamoto, K. Yaoi, M. Osaka, N. Osaka, Coactivation of the default mode network regions and working memory network regions during task preparation, Sci. Rep. 4 (2014) 34–39. https://doi.org/10.1038/srep05954.

[28] A.T. Newton, V.L. Morgan, B.P. Rogers, J.C. Gore, Modulation of steady state functional connectivity in the default mode and working memory networks by cognitive load, Hum. Brain Mapp. 32 (2011) 1649–1659. https://doi.org/10.1002/hbm.21138.

[29] L.M. Vaina, A computational study of whole-brain connectivity in resting state and task fMRI, Med. Sci. Monit. 20 (2014) 1024–1042. https://doi.org/10.12659/MSM.891142.

[30] D. Vatansever, D.K. Menon, E.A. Stamatakis, Default mode contributions to automated information processing, Proc. Natl. Acad. Sci. (2017) 201710521. https://doi.org/10. 1073/pnas.1710521114.

[31] J.M. Walz, R.I. Goldman, M. Carapezza, J. Muraskin, T.R. Brown, P. Sajda, Simultaneous EEG-fMRI reveals a temporal cascade of task-related and default-mode activations during a simple target detection task, Neuroimage. 102 (2014) 229–239. https://doi.org/10.1016/j.neuroimage.2013.08.014.

[32] W. Klimesch, Alpha-band oscillations, attention, and controlled access to stored information, Trends Cogn. Sci. 16 (2012) 606–617. https://doi.org/10.1016/j.tics. 2012.10.007.

[33] A. Uusberg, H. Uibo, K. Kreegipuu, J. Allik, EEG alpha and cortical inhibition in affective attention, Int. J. Psychophysiol. 89 (2013) 26–36. https://doi.org/10.1016/j. ijpsycho.2013.04.020.

[34] J. Kujala, G. Sudre, J. Vartiainen, M. Liljeström, T. Mitchell, R. Salmelin, Multivariate analysis of correlation between electrophysiological and hemodynamic responses during cognitive processing, Neuroimage. 92 (2014) 207–216. https://doi.org/10.1016/j. neuroimage.2014.01.057.

[35] F. Esposito, A. Bertolino, T. Scarabino, V. Latorre, G. Blasi, T. Popolizio, G. Tedeschi, S. Cirillo, R. Goebel, F. Di Salle, Independent component model of the default-mode brain function: Assessing the impact of active thinking, Brain Res. Bull. 70 (2006) 263–269. https://doi.org/10.1016/j.brainresbull.2006.06.012.

[36] J.M. Shine, A.J. Muller, C. O'Callaghan, M. Hornberger, G.M. Halliday, S.J.G. Lewis, Abnormal connectivity between the default mode and the visual system underlies the manifestation of visual hallucinations in Parkinson's disease: A task-based fMRI study, Parkinsons. Dis. 1 (2015). https://doi.org/10.1038/npjparkd.2015.3.

[37] F. Sambataro, E. Visintin, N. Doerig, J. Brakowski, M.G. Holtforth, E. Seifritz, S. Spinelli, Altered dynamics of brain connectivity in major depressive disorder at-rest and during task performance, Psychiatry Res. - Neuroimaging. 259 (2017) 1–9. https://doi.org/10.1016/j.pscychresns.2016.11.001.

[38] R.G.M. Schlösser, G. Wagner, K. Koch, R. Dahnke, J.R. Reichenbach, H. Sauer, Fronto-cingulate effective connectivity in major depression: A study with fMRI and dynamic causal modeling, Neuroimage. 43 (2008) 645–655. https://doi.org/10.1016/j. neuroimage.2008.08.002.

[39] J.B. Rowe, L.E. Hughes, R.A. Barker, A.M. Owen, Dynamic causal modelling of effective connectivity from fMRI: Are results reproducible and sensitive to Parkinson's disease and its treatment?, Neuroimage. 52 (2010) 1015–1026. https://doi.org/10.1016/ j.neuroimage.2009.12.080.

[40] N.K. Logothetis, The underpinnings of the BOLD functional magnetic resonance imaging signal., J. Neurosci. 23 (2003) 3963–3971. https://doi.org/23/10/3963 [pii].

[41] A.L. Vazquez, E.R. Cohen, V. Gulani, L. Hernandez-Garcia, Y. Zheng, G.R. Lee, S.G. Kim, J.B. Grotberg, D.C. Noll, Vascular dynamics and BOLD fMRI: CBF level effects and analysis considerations, Neuroimage. 32 (2006) 1642–1655. https://doi.org/10.1016 /j.neuroimage.2006.04.195.

[42] T.D. Wager, A. Vazquez, L. Hernandez, D.C. Noll, Accounting for nonlinear BOLD effects in fMRI: Parameter estimates and a model for prediction in rapid event-related studies, Neuroimage. 25 (2005) 206–218. https://doi.org/10.1016/j.neuroimage. 2004.11.008.

[43] K.K. Kwong, J.W. Belliveau, D.A. Chesler, I.E. Goldberg, R.M. Weisskoff, B.P. Poncelet, D.N. Kennedy, B.E. Hoppel, M.S. Cohen, R. Turner, Dynamic magnetic resonance imaging of human brain activity during primary sensory stimulation., Proc. Natl. Acad. Sci. U. S. A. 89 (1992) 5675–9. https://doi.org/10.1073/PNAS.89.12.5675.

[44] M.A. Lindquist, J. Meng Loh, L.Y. Atlas, T.D. Wager, Modeling the hemodynamic response function in fMRI: efficiency, bias and mis-modeling., Neuroimage. 45 (2009) S187–S198. https://doi.org/10.1016/j.neuroimage.2008.10.065.

[45] C.F. Beckmann, S.M. Smith, Probabilistic Independent Component Analysis for Functional Magnetic Resonance Imaging, IEEE Trans. Med. Imaging. 23 (2004) 137–152. https://doi.org/10.1109/TMI.2003.822821.

[46] S. Whitfield-gabrieli, A. Nieto-castanon, Conn : A Functional Connectivity Toolbox for Correlated and Anticorrelated Brain Networks, 2 (2012). https://doi.org/10.1089/ brain.2012.0073.

[47] X. Ma, G. Jiang, S. Fu, J. Fang, Y. Wu, M. Liu, G. Xu, T. Wang, Enhanced network efficiency of functional brain networks in primary insomnia patients, Front. Psychiatry. 9 (2018) 1–11. https://doi.org/10.3389/fpsyt.2018.00046.

[48] M.W. Voss, C.N. Wong, P.L. Baniqued, J.H. Burdette, K.I. Erickson, R.S. Prakash, E. McAuley, P.J. Laurienti, A.F. Kramer, Aging brain from a network science perspective: Something to be positive about?, PLoS One. 8 (2013). https://doi.org/10.1371/ journal.pone.0078345.

[49] J. Hwang, M. Legarreta, C.E. Bueler, J. DiMuzio, E. McGlade, I.K. Lyoo, D. Yurgelun-Todd, Increased efficiency of brain connectivity networks in veterans with suicide attempts, NeuroImage Clin. 20 (2018) 318–326. https://doi.org/10.1016/j.nicl.2018. 04.021.

[50] C. Rosazza, L. Minati, F. Ghielmetti, M.L. Mandelli, M.G. Bruzzone, Functional connectivity during resting-state functional MR imaging: study of the correspondence between independent component analysis and region-of-interest-based methods., AJNR. Am. J. Neuroradiol. 33 (2012) 180–7. https://doi.org/10.3174/ajnr.A2733.

[51] M.N. Desalvo, L. Douw, S. Takaya, H. Liu, S.M. Stufflebeam, Task-dependent reorganization of functional connectivity networks during visual semantic decision making, Brain Behav. 4 (2014) 877–885. https://doi.org/10.1002/brb3.286.

[52] N. Wenderoth, F. Debaere, S. Sunaert, S.P. Swinnen, The role of anterior cingulate cortex and precuneus in the coordination of motor behaviour, Eur. J. Neurosci. 22 (2005) 235–246. https://doi.org/10.1111/j.1460-9568.2005.04176.x.

[53] E. Simony, C.J. Honey, J. Chen, O. Lositsky, Y. Yeshurun, A. Wiesel, U. Hasson, Dynamic reconfiguration of the default mode network during narrative comprehension, Nat. Commun. 7 (2016) 1–13. https://doi.org/10.1038/ncomms12141.

[54] J.S. Mayer, A. Roebroeck, K. Maurer, D.E.J. Linden, Specialization in the default mode: Task-induced brain deactivations dissociate between visual working memory and attention, Hum. Brain Mapp. 31 (2010) 126–139. https://doi.org/10.1002/hbm.20850.

[55] J.J. Foxe, A.C. Snyder, The role of alpha-band brain oscillations as a sensory suppression mechanism during selective attention, Front. Psychol. 2 (2011) 1–13. https://doi.org/10.3389/fpsyg.2011.00154.

[56] W. Klimesch, P. Sauseng, S. Hanslmayr, EEG alpha oscillations: The inhibition-timing hypothesis, Brain Res. Rev. 53 (2007) 63–88. https://doi.org/10.1016/j.brainresrev.2006.06.003.

[57] B.K. Min, H.J. Park, Task-related modulation of anterior theta and posterior alpha EEG reflects top-down preparation, BMC Neurosci. 11 (2010). https://doi.org/10.1186/1471-2202-11-79.

[58] H. Yuan, T. Liu, R. Szarkowski, C. Rios, J. Ashe, B. He, Negative covariation between task-related responses in alpha/beta-band activity and BOLD in human sensorimotor cortex: An EEG and fMRI study of motor imagery and movements, Neuroimage. 49 (2010) 2596–2606. https://doi.org/10.1016/j.neuroimage.2009.10.028.

[59] M. Bauer, M.-P. Stenner, K.J. Friston, R.J. Dolan, Attentional Modulation of Alpha/Beta and Gamma Oscillations Reflect Functionally Distinct Processes, J. Neurosci. 34 (2014) 16117–16125. https://doi.org/10.1523/JNEUROSCI.3474-13.2014.

[60] M. Bonnefond, O. Jensen, The role of gamma and alpha oscillations for blocking out distraction, Commun. Integr. Biol. 6 (2013) 20–22. https://doi.org/10.4161/cib.22702.

[61] M. Bonnefond, O. Jensen, Gamma activity coupled to alpha phase as a mechanism for top-down controlled gating, PLoS One. 10 (2015) 1–11. https://doi.org/10.1371/journal.pone.0128667.

[62] E.A. Buffalo, P. Fries, R. Landman, T.J. Buschman, R. Desimone, Laminar differences in gamma and alpha coherence in the ventral stream, Proc. Natl. Acad. Sci. 108 (2011) 11262–11267. https://doi.org/10.1073/pnas.1011284108.

[63] P. Fries, J.H. Reynolds, A.E. Rorie, R. Desimone, Modulation of oscillatory neuronal synchronization by selective visual attention, Science (80-.). 291 (2001) 1560–1563. https://doi.org/10.1126/science.1055465.

[64] D. Osipova, D. Hermes, O. Jensen, Gamma power is phase-locked to posterior alpha activity, PLoS One. 3 (2008) 1–7. https://doi.org/10.1371/journal.pone.0003990.

[65] F. Roux, P.J. Uhlhaas, Working memory and neural oscillations: Alpha-gamma versus theta-gamma codes for distinct WM information?, Trends Cogn. Sci. 18 (2014) 16–25. https://doi.org/10.1016/j.tics.2013.10.010.

[66] C. Poch, P. Campo, G.R. Barnes, Modulation of alpha and gamma oscillations related to retrospectively orienting attention within working memory, Eur. J. Neurosci. 40 (2014) 2399–2405. https://doi.org/10.1111/ejn.12589.

[67] T. van Kerkoerle, M.W. Self, B. Dagnino, M.-A. Gariel-Mathis, J. Poort, C. van der Togt, P.R. Roelfsema, Alpha and gamma oscillations characterize feedback and feedforward processing in monkey visual cortex, Proc. Natl. Acad. Sci. 111 (2014) 14332–14341. https://doi.org/10.1073/pnas.1402773111.

[68] B. Voytek, Shifts in gamma phase–amplitude coupling frequency from theta to alpha over posterior cortex during visual tasks, Front. Hum. Neurosci. 4 (2010) 1–9. https://doi.org/10.3389/fnhum.2010.00191.

[69] M.W. Cole, T. Ito, D.S. Bassett, D.H. Schultz, Activity flow over resting-state networks shapes cognitive task activations, Nat. Neurosci. 19 (2016) 1718–1726. https://doi.org/10.1038/nn.4406.

[70] H. Takeuchi, Y. Taki, H. Hashizume, Y. Sassa, T. Nagase, R. Nouchi, R. Kawashima, Failing to deactivate: The association between brain activity during a working memory task and creativity, Neuroimage. 55 (2011) 681–687. https://doi.org/10.1016/j.neuroimage.2010.11.052.

[71] J. Sepulcre, H. Liu, T. Talukdar, I. Martincorena, B.T. Thomas Yeo, R.L. Buckner, The organization of local and distant functional connectivity in the human brain, PLoS Comput. Biol. 6 (2010) 1–15. https://doi.org/10.1371/journal.pcbi.1000808.

[72] T. Bolt, J.S. Nomi, M. Rubinov, L.Q. Uddin, Correspondence between evoked and intrinsic functional brain network configurations, Hum. Brain Mapp. 38 (2017) 1992–2007. https://doi.org/10.1002/hbm.23500.

[73] H. Cao, M.M. Plichta, A. Schäfer, L. Haddad, O. Grimm, M. Schneider, C. Esslinger, P. Kirsch, A. Meyer-Lindenberg, H. Tost, Test-retest reliability of fMRI-based graph theoretical properties during working memory, emotion processing, and resting state, Neuroimage. 84 (2014) 888–900. https://doi.org/10.1016/j.neuroimage.2013.09.013.

[74] M.N. Moussa, C.D. Vechlekar, J.H. Burdette, M.R. Steen, C.E. Hugenschmidt, P.J. Laurienti, Changes in Cognitive State Alter Human Functional Brain Networks, Front. Hum. Neurosci. 5 (2011) 1–15. https://doi.org/10.3389/fnhum.2011.00083.

[75] O. Sporns, The human connectome: A complex network, Ann. N. Y. Acad. Sci. 1224 (2011) 109–125. https://doi.org/10.1111/j.1749-6632.2010.05888.x.

[76] G.S. Wig, Segregated Systems of Human Brain Networks, Trends Cogn. Sci. 21 (2017) 981–996. https://doi.org/10.1016/j.tics.2017.09.006.

[77] N.U.F. Dosenbach, D.A. Fair, F.M. Miezin, A.L. Cohen, K.K. Wenger, R.A.T. Dosenbach, M.D. Fox, A.Z. Snyder, J.L. Vincent, M.E. Raichle, B.L. Schlaggar, S.E. Petersen, Distinct brain networks for adaptive and stable task control in humans, Proc. Natl. Acad. Sci. 104 (2007) 11073–11078. https://doi.org/10.1073/pnas.0704320104.

[78] B. Wang, P. Li, D. Li, Y. Niu, T. Yan, T. Li, R. Cao, P. Yan, Y. Guo, W. Yang, Y. Ren, X. Li, F. Wang, T. Yan, J. Wu, H. Zhang, J. Xiang, Increased Functional Brain Network Efficiency During Audiovisual Temporal Asynchrony Integration Task in Aging, Front. Aging Neurosci. 10 (2018) 1–15. https://doi.org/10.3389/fnagi.2018.00316.

[79] R.L. Buckner, J. Sepulcre, T. Talukdar, F.M. Krienen, H. Liu, T. Hedden, J.R. Andrews-Hanna, R.A. Sperling, K.A. Johnson, Cortical Hubs Revealed by Intrinsic Functional Connectivity: Mapping, Assessment of Stability, and Relation to Alzheimer's Disease, J. Neurosci. 29 (2009) 1860–1873. https://doi.org/10.1523/JNEUROSCI.5062-08.2009.

[80] P. Lin, Y. Yang, J. Gao, N. De Pisapia, S. Ge, X. Wang, C.S. Zuo, J. Jonathan Levitt, C. Niu, Dynamic Default Mode Network across Different Brain States, Sci. Rep. 7 (2017) 1–13. https://doi.org/10.1038/srep46088.

CHAPTER 3

ANALYZING THE EFFECT OF PERFORMANCE FEEDBACK ON SUBSEQUENT TASK ENGAGEMENT BY ASSESSING THE ROLE OF THE FRONTAL-PARIETAL EEG CORTICAL OSCILLATIONS

This chapter is a marginally modified version of the research article published as Agrawal, S., Sharma, R., & Chinnadurai, V. (2021). Functional connectivity between frontal/parietal regions and MTL–basal ganglia during feedback learning and declarative memory retrieval. Journal of Biosciences, 46(3), 1-17. https://doi.org/10.1007/s12038-021-00194-y

3.1 ABSTRACT

Feedback assists the memory system in preserving the learnings from ongoing activities and updating it for future retrievals. Thus, the feedback coming from an individual's performance affects the behavior and, thereby, the performance. However, little is known regarding the interactions of learning and memory associated regions. Thus, we employ a combination of functional connectivity and neurovascular approach to explore the significance of these interactions. Our study comprises thirty-five volunteers who undergo a feedback declarative memory task using simultaneous EEG-fMRI data acquisition. Functional connectivity analysis showed that MTL and basal ganglia possess significant connectivity but differential relationships during feedback learning and memory retrieval. Specifically, Putamen and pallidum (sub-regions of basal ganglia) are the central hubs in these mechanisms. The neurovascular analysis reveals the increased correlation of frontal-alpha and theta powers with the bold activity of MTL during memory retrievals. The results also report the role of the frontal (and parietal) alpha-beta powers in de-synchronization (and synchronization) of the bold activity of caudate; and parietal-theta (frontal-higher-alpha) power in de-synchronization (and synchronization) of bold activity of right accumbens. Hence, the study demonstrates the significant role of the frontal-parietal EEG powers in MTL-basal ganglia relationships and neuronal adaptations during declarative memory retrieval.

3.2 INTRODUCTION

Memory is a cognitive process that updates with experience, and learning is a process that contributes to the formation of these memories [1]. In recent years, several electrophysiological and neuroimaging studies [2–5] have emerged to examine long-term memory systems, in particular declarative memory. These studies suggested the prominent role of the medial temporal lobe in declarative memory and revealed its interaction with the feedback learning associated regions, prefrontal cortex and basal ganglia [6–9]. Existing literature [10–12] explains the electrophysiology of positive-negative feedbacks, the affected regions, and subsequently, the behavior modulations. Several researchers [13–16] have also suggested that feedback associated learning and memory retrieval tasks engage frontal and parietal regions, respectively. However, the neuronal mechanisms remain less explored for understanding how frontal-parietal regions contribute to the declarative memory retrieval after feedback learning.

Several previous neuroimaging studies [17–19] have outlined a reward-based learning circuit restricted to midbrain dopaminergic structures, the striatum, the orbitofrontal cortex (OFC), and the medial frontal cortex (MFC). Also, the dorsolateral prefrontal cortex is found as a key component in regulating the reward circuit [17]. The EEG based studies [20–22] have emphasized the role of beta rhythmic activity and reported it for reward over frontal regions of the brain. A recent study [23] has revealed that the hippocampus also plays a role in reward-guided behavior. The same study suggested that the theta oscillations of OFC are critically important for reward-guided learning, and theta oscillations of the hippocampus drive them. Thus, all these studies indicate a critical role of oscillatory mechanisms in feedback-associated functions of the frontal brain.

Conventionally, the non-declarative memory is associated with the reward-driven mechanisms of the basal ganglia during reward-guided behavior [24–27]. A few recent studies [28–31] have highlighted the potential role of the basal ganglia in declarative memory tasks also. Thus, the interactions between MTL and basal ganglia help understand the mechanisms involved in learning and memory. A recent study [32] suggested that the MTL and the striatum (a subregion of basal ganglia) can play a dissociable role during learning. It also indicated that midbrain dopaminergic nuclei

and prefrontal cortex might mediate cooperation between the striatum and the MTL for learning. Several studies [33,34] have also suggested that the prefrontal cortex contributes to memory by cognitive/strategic control over memory retrieval. Another study [35] has revealed the role of the ventral parietal cortex (VPC) in episodic memory retrieval. Some other studies [15,36] also pointed out the role of the parietal cortex during memory retrieval. Thus, the role of frontal-parietal regions is crucial while understanding the MTL and basal ganglia's relationship. To the best of our knowledge, no study explores the role of frontal-parietal regions in this relationship through the neurovascular approach.

Hence, this study examines the association of frontal-parietal EEG powers with MTL and basal ganglia during feedback learning and memory retrieval using functional connectivity and neurovascular approach. First, we test the functional connectivity of frontal-parietal regions with MTL and sub-regions of basal ganglia for feedback learning and memory retrievals. We assess the electrophysiology and estimate the spectral distribution of these time-locked stimuli conditions. The time-locked frontal-parietal powers are then correlated to the bold signal of MTL and basal ganglia. Our research reveals the modulation in the functional connectivity of MTL and basal ganglia from feedback learning to memory retrieval due to the varying roles of basal ganglion sub-regions (putamen and pallidum). It also suggests that frontal-parietal regions dissociate with the MTL and the basal ganglia during memory retrieval. These feedback related modulations are then studied with the neurovascular approach, and results reveal the significant associations of explicit frontal-parietal EEG powers with the bold activity of affected regions.

3.3 MATERIALS AND METHODS

3.3.1 Participants and procedure

Thirty-five healthy right-handed volunteers (17 males and 18 females, aged 20-32 years, mean age: 24 years) participated in this experiment. All participants reported normal or corrected-to-normal vision and no history of psychiatric, neurological disorder, or was using any medication. The participants who took part in the study were not involved in the practice task before the experiment to avoid any prior

experiential bias. All participants gave written informed consent for the examination before the experiment. Ethical approval for the study was obtained from the local ethical committee.

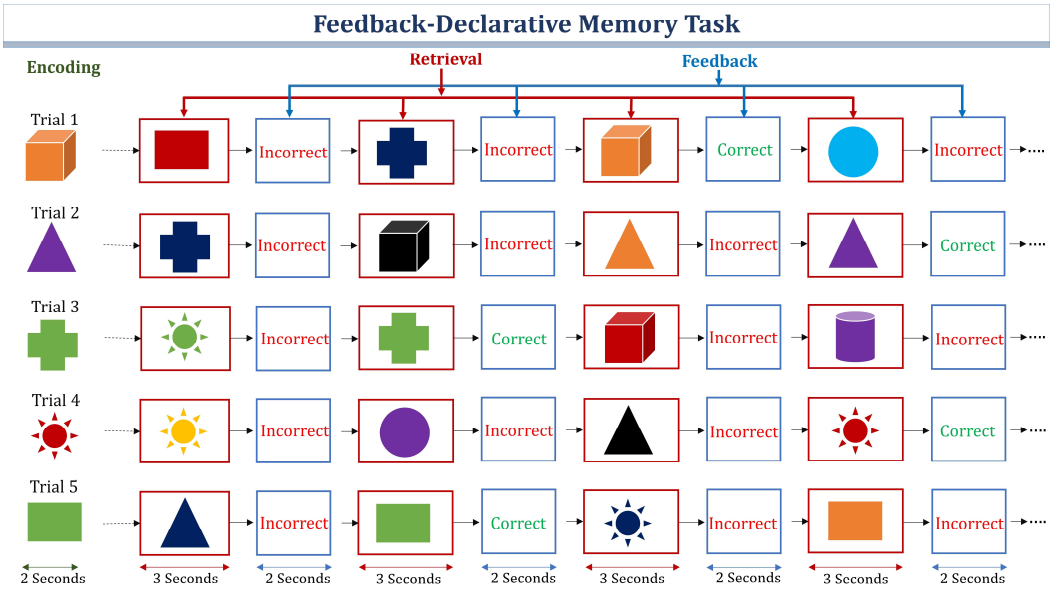

Figure 3.1: A sample experimental design of the feedback declarative memory task. The participants are asked to retrieve the previously memorized object during the retrieval phase of 3s. The study provides visual feedback after each stimulus for 2s during feedback learning, regarding the correctness of the answer to the volunteer's response. The volunteer's task is to detect, learn, and adjust to these changes.

3.3.2 Task design

During the experiment, we present a collection of simple geometrical figures such as a cube, circle, rectangle, and triangle filled with primary colors, to the participants. For the experiment, a stimulus is assigned as 'Target' object at the start of each trial for 3 seconds. During the presentation of 'Target' stimuli in the trial, the volunteer is asked to remember the shape and the color of the article. In the final phase of each trial, we present the volunteer with a collection of different geometric shapes for 3 seconds, one item at a time, and the volunteer is asked to retrieve the memorized target and respond upon recognition. There are five trials in total; each trial consists of 21 sub-trials. The experiment uses a mixed paradigm design composed of ninety-four stimuli distributed over five trials. Among the ninety-four stimuli slides, there are 32 slides of 'Target' object. We present a fixation block with a single cross in the center of the slide for 3 seconds after presenting each task stimulus.

3.3.3 Data acquisition with Simultaneous EEG-fMRI

The study provides visual feedback after each memory retrieval to assess its effect on their subsequent performance. The use of visual-feedback for 2 seconds offers the correctness of the volunteer's response after each stimulus and allows the volunteers to learn from their performance feedback. The volunteers were informed to avoid any motor response during feedback presentation. These task stimuli are projected onto MR compatible lenses fitted on the head coil inside MR. A sample task paradigm from the experiments is shown in Figure 3.1.

The study uses a simultaneous EEG-fMRI technique for data acquisition of declarative memory task. All images were acquired using a 3T Siemens Magnetom Skyra scanner. The scanner parameters were identical to those used in our previous study [37]. T2* weighted images were acquired using Eco Planar Imaging (EPI) sequence with TR =3000 ms; TE= 36 ms; voxel size =3.6*3.6*3.0 mm; matrix =64*64; FoV read = 230 mm; flip angle =90^{o}, 36 axial slices. The axial slices are acquired parallel to the Anterior-Posterior (AC-PC) line in an interleaving manner with a slice thickness of 3.0 mm. High-resolution T1-weighted structural images were acquired using T1 MPRAGE sequence with parameters, voxel size =1.0*1.0*1.0 mm; TR= 2000 ms; flip angle = 90^{o}; FoV = 240 mm; matrix= 512*512; slice thickness = 1.0 mm, 160 axial slices. The axial slices are acquired parallel to the Anterior-Posterior (AC-PC) line in an interleaving manner with a slice thickness of 5.0 mm.

Simultaneously, EEG data from 32 channel MR compatible Brain Amp differential amplifier is acquired at a 5 kHz sampling rate. EEG data were recorded from 32 Ag/AgCl scalp electrodes, distributed according to the 10-20 system with a reference electrode in between Fz and Cz. The ground electrode is placed between Cz and Pz. The ECG electrode is set to measure the cardiac effect for the artifact corrections. The impedance of all the scalp electrodes was maintained below 5 kohms.

3.3.4 Data pre-processing steps

3.3.4.1 Pre-processing of EEG data

We subject the acquired EEG data to the following pre-processing procedures. First, the EEG data is trimmed to a time-locked dataset. The study then uses the FMRIB

(EEGLAB) tool to remove MR related gradient artifacts, detect QRS complexes from an ECG channel, and to remove pulse ballistocardiograph artifacts from our time-locked EEG data. For the removal of MR artifact, FASTR (FMRI Artifact Slice Template Removal) aligns all the slice artifacts with correcting for any slight jitter in the exact location of the slice-timing events. It interpolates the data, and then shift each artifact until the correlation is maximized between data and a reference artifact (the first artifact in the data). The second stage of FASTR [38], computes an average template for the artifact, and subtract it from the center contaminated data by taking a moving-window average of slice artifacts. QRS detection uses combined adaptive thresholding [39] and the Teager energy operator [40], followed by a correction algorithm. This algorithm aligns all events and corrects for false positives and negatives. The removal of pulse artifacts uses QRS events to subtract an artifact template from the data, and here it is done by using an optimal basis set for the number of PCs 3. For carrying out the time-frequency analyses, the study uses the Harvard Automated Processing Pipeline for EEG (HAPPE) processes [41] by using filtering, artifact rejection, and re-referencing the contaminated EEG data. We then estimate EEG frequency powers from pre-processed EEG data using EEGLAB (MathWorks).

3.3.4.2 Pre-processing of fMRI data

All the fMRI artifact removal processing is carried out using standard artifact removal pipeline of Statistical Parametric Mapping (version: SPM 12). The following pre-processing is applied: realignment and slice time correction for minimizing the effect of head motion and slice acquisition delays, registration of functional scans to standard MNI template space, spatial smoothing using a Gaussian kernel (5mm FWHM). Statistical analyses were performed on the smoothed data with a high pass filter to remove low-frequency noise.

3.3.5 Data Analysis

The acquired task data is subsequently subjected to the data-analysis procedure, which is as the methodological block diagram of the study shown in Figure 3.2.

3.3.5.1 Time-Frequency analysis

Time-frequency analysis is performed by assessing event-related spectral perturbations (ERSP) using a complex-sinusoidal wavelet transform procedure as implemented in EEGLAB [42]. For this, we have extracted the stimulus-locked EEG data for feedback learning and memory retrievals associated with positive outcomes only for frontal (Fz, F3, F4) and Parietal (Pz, P3, P4) channels. The time-frequency analysis is performed using Morlet wavelets for 2 seconds epoch (-500 ms to 1500 ms post stimuli or feedback) and then subject the data for baseline correction (−500 to 0 ms) and group the data of all the trials corresponding to the same condition (feedback learning and memory retrievals). For the frequencies from 1 Hz to 35 Hz, the study compute mean-event-related changes in the spectral power for the epoch. The averaged oscillatory activity for the defined period is used to find the power of each frequency following feedback and memory retrieval. The study evaluates time-frequency curves using the data from all the participants and calculates mean ERSP.

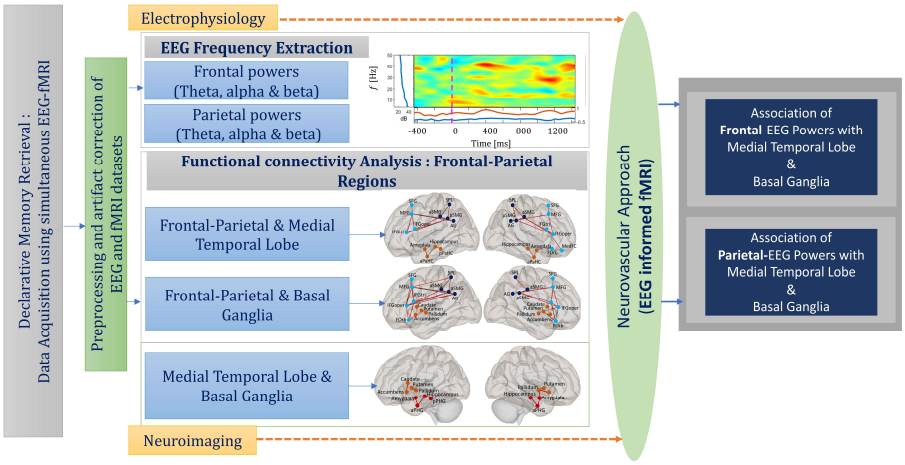

Figure 3.2: Methodological block diagram of the study. The schematic diagram demonstrates the analyses employed in this study. Using electrophysiology, the frequency extraction of the frontal and parietal EEG channels was done using time-frequency analysis, which was time-locked to the feedback and memory retrievals. Using neuroimaging, we explore the relationship of frontal-parietal regions with medial temporal lobe and subregions of basal ganglia. These interactions are analyzed using functional connectivity analysis for feedback and memory retrievals. Also, the direct relationship of the medial temporal lobe and subregions of basal ganglia associated with the feedback and memory retrievals was analyzed using functional connectivity analysis. Further, the EEG-informed-fMRI approach for both feedback and memory retrievals was employed to study the association of frontal-parietal EEG powers with medial temporal lobe and subregions of basal ganglia. For this, the neural correlates of concerned frequencies (delta, theta, lower-alpha, higher alpha, lower beta, and higher beta) and frontal-parietal EEG channels were evaluated using EEG-informed-fMRI approach for both feedback and memory retrievals and studied for medial temporal lobe and subregions of basal ganglia.

3.3.5.2 Functional connectivity analysis

The estimation of functional connectivity is carried out to understand the interactions of frontal-parietal regions with MTL and basal ganglia during feedback and memory retrievals. For this, the areas of interest are selected, and the connectivity is evaluated using graph theory during feedback learning and subsequent memory retrievals. Estimation of graph theory is done based on functional connectivity using the CONN toolbox [43]. Functional connectivity maps of all ROI's were further derived using Fisher's r-to-z transformation. The group-level functional connectivity maps were FDR-correction at $p < 0.05$.

3.3.5.3 Associations of frontal-parietal electrophysiological powers with feedback learning and memory retrieval: The EEG informed FMRI approach

We perform statistical analyses to explore the relationship of EEG powers with the hemodynamics during feedback and subsequent memory retrieval in the GLM framework. For this, we set up a GLM design matrix, consisted of frontal-parietal electrophysiological powers as the parametric modulators. First, we extract the time-locked (200-600 milliseconds) spectral powers from each feedback and memory retrieval block for each volunteer. The estimation is done for frontal (Fz, F3, F4), parietal (Pz, P3, P4) electrodes and bands of interest (i.e., from (1-4) for delta, (4–8) Hz for theta, (9–12) Hz for lower-alpha, (12-14) higher alpha, (15-21) Hz for lower beta and (22-35) for higher beta). Each power spectra are then normalized with respect to total power. Normalization of each power spectra in our study is done to minimize the effect of mixing of features associated with multiple volunteers and multiple epochs. We use relative EEG powers as EEG regressors during GLM analyses as parametric modulators in feedback learning and subsequent memory retrieval. For EEG-correlated fMRI analysis, GLMs are applied to the data of each subject at the first level. These EEG regressors are then subjected to a general linear model (GLM) along with the six realignment parameters for each run. We then model the fMRI BOLD responses using a canonical hemodynamic response function with temporal and dispersion derivatives. At the second level, one-sample t-tests are computed for all frequency bands, EEG-BOLD signal correlations are significant at a corrected cluster threshold of $p<0.05$. Subsequent analyses are based on the interactions of frontal-parietal powers with MTL and basal ganglia, which correlates outside these brain regions that are not analyzed.

3.4 RESULTS

Extensive electrophysiological and neuroimaging studies [19,44,45] have highlighted the association of frontal and parietal regions in learning and task adaptations. Our research explores the role of frontal-parietal EEG powers in a relationship of MTL and basal ganglia during the declarative memory task. The study also uses a functional connectivity approach to understand the relationship of frontal-parietal regions with MTL and basal ganglia. We then explore the role of frontal-parietal EEG powers during the feedback learning and memory retrievals, as shown in Supplementary Figure S1. Further, we investigate the relationship between neural activity and BOLD signal in simultaneously acquired EEG and fMRI data during a declarative memory task. The results reveal the significant relationships of frontal-parietal EEG powers with the MTL and sub-regions of the basal ganglia. The following sections present these results in detail.

3.4.1 Association of frontal-parietal regions with medial temporal lobe (MTL) and basal ganglia: The functional connectivity analysis

The functional connectivity analyses explore the interactions of frontal-parietal regions with the MTL and basal ganglia for feedback learning and memory retrieval. Figures 3.3a and 3.3b demonstrate the connectivity patterns of these interactions, and table 3.1 and 3.2 summarize the significant connectivity of these regions.

The study finds a significant connectivity of frontal-arietal regions for feedback learning and memory retrievals. However, there is a significant reduction in the functional connectivity of MFG-SPL, MFG-AG, IFG Oper-AG, IFG Oper-aSMG and IFG Oper-pSMG from feedback learning to memory retrieval at a significant level ($p<0.001$). The study also observes the modulation in the functional connectivity of frontal-parietal regions with the MTL from feedback to memory retrieval. First, there was a significant correlation of the frontal orbital cortex with the rest of the MTL structure during feedback learning (Forb-Amygdala: $r_{Left}=4.74$ & $r_{Right}=6.16$) for both hemispheres. The study observes non-significant correlation values during memory retrieval, indicating that the MTL structure dissociates with the rest of the frontal-parietal regions during memory retrieval.

Frontal-Parietal-Medial Temporal Lobe connectivity

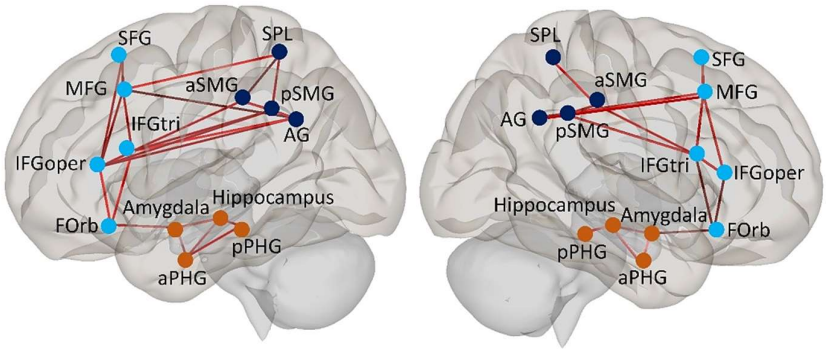

Functional Connectivity maps: Feedback Learning

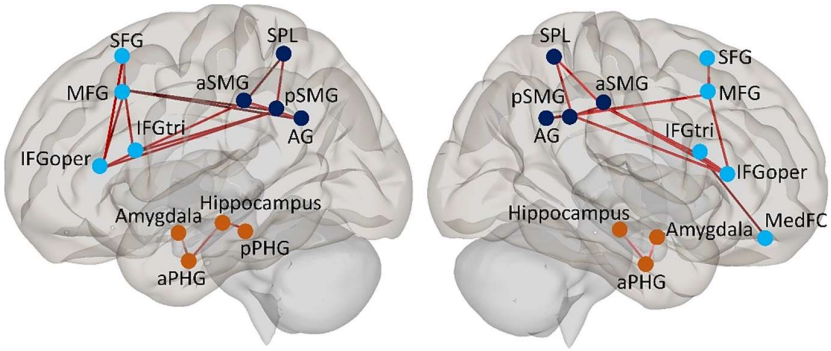

Functional Connectivity maps: Memory Retrieval

Frontal-Parietal- Basal Ganglia connectivity

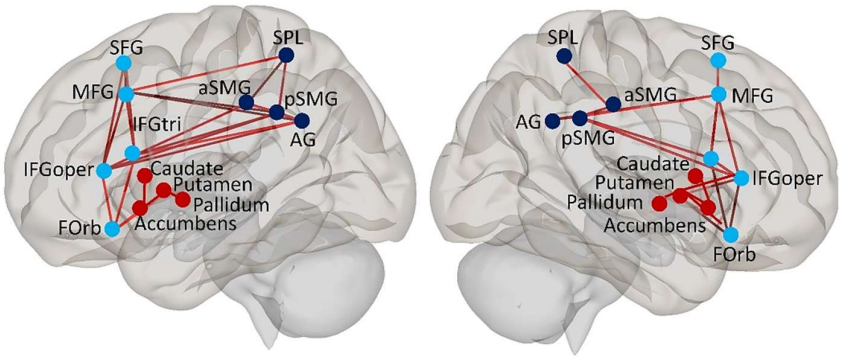

Functional Connectivity maps: Feedback Learning

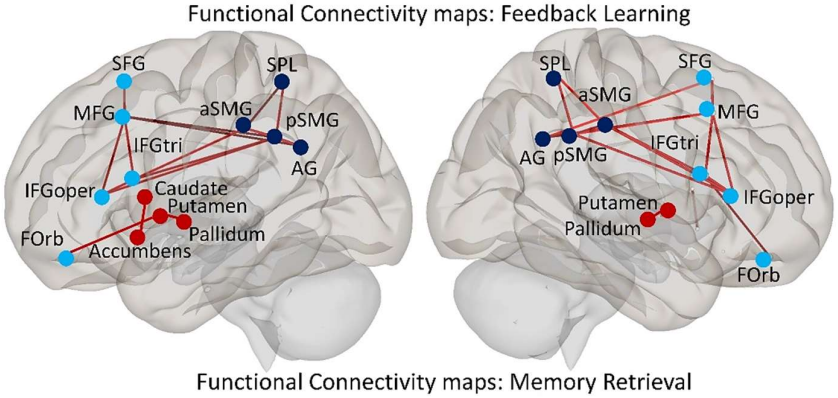

Functional Connectivity maps: Memory Retrieval

Figure 3.3: Graphical illustration of functional connectivity of frontal-parietal regions with medial temporal lobe and subregions of basal ganglia. (a). feedback learning. (b). memory retrieval. Azure, indigo, brown and red circles represent frontal, parietal, medial temporal lobe, and basal ganglia, respectively. The significant connectivity among regions is depicted with red lines between nodes. MFG: Middle Frontal Gyrus, IFGOper: Inferior Frontal Gyrus Opercular, Forb: Frontal Orbital Cortex, SFG: Superior Frontal Gyrus, IFGtri: Inferior Frontal Gyrus Triangular, aSMG: Anterior Supramarginal Gyrus, SPL: Superior Parietal Lobule, pSMG: Posterior Supramarginal Gyrus, AG: Angular Gyrus, aPHG: Anterior Parahippocampal Gyrus, pPHG: Posterior Parahippocampal Gyrus, MedFC: Medial Frontal Cortex.

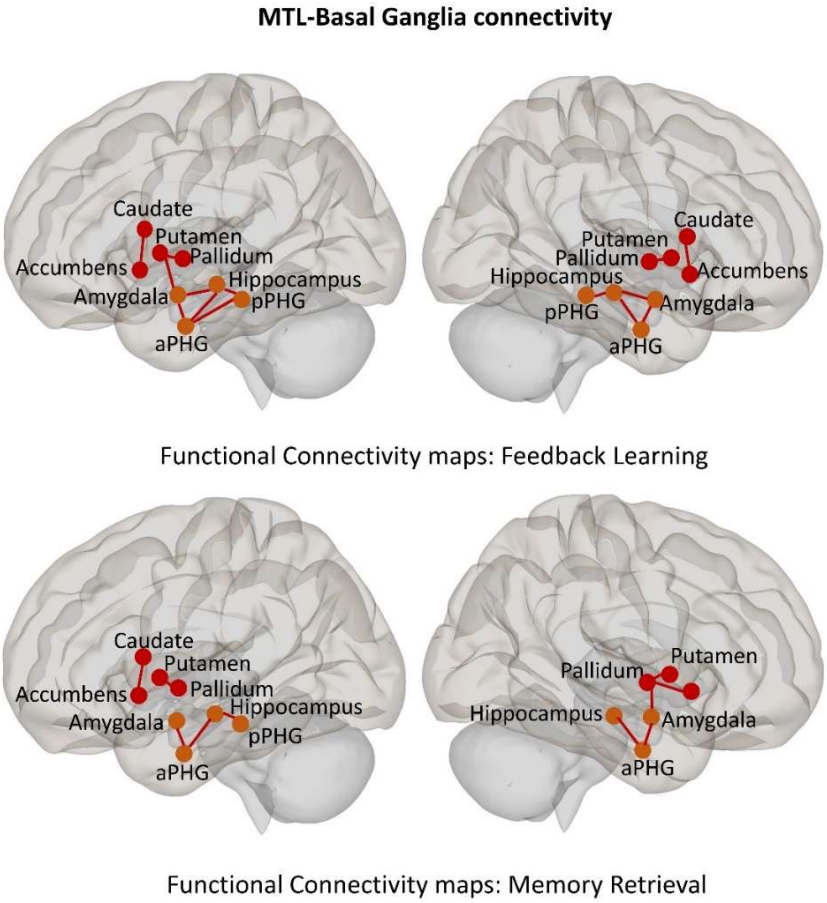

Figure 3.4: Graphical illustration of functional connectivity of medial temporal lobe with subregions of basal ganglia. (a). Feedback learning. (b). Memory retrieval. Brown and red circles represent medial temporal and subregions of basal ganglia, respectively. Red lines between nodes depict the significant connectivity among regions.

We find the significant interactions of the frontal cortex with sub-regions of the basal ganglia during feedback learning (Forb-Accumbens; Forb-Putamen). The correlation values (Forb-Accumbens: r_{Left}=3.95, r_{Right}=3.75; Accumbens-Caudate: r_{Left}=9.46, r_{Right}=6.01); Accumbens-Putamen: r_{Left}=4.42, r_{Right}=5.11) of functional connectivity analysis indicate that the accumbens plays a significant role in the relationship of the

frontal orbital cortex and the rest of the basal ganglia. The study also finds the significant correlations of inferior frontal gyrus with the sub-regions of the basal ganglia, specifically in the right hemisphere (IFG Oper-Putamen: r_{Right}=5.43). Yet, the study does not observe any correlation and reveals the absence of any connectivity of frontal regions with basal ganglia during memory retrieval, likewise the MTL. Thus, results suggest that the introduction of feedback might affect the functional connectivity of these regions.

Table 3.1: Functional Connectivity of Frontal Parietal-MTL-Basal Ganglia for feedback learning and memory retrieval significant. Non-significant values are highlighted as red. IFG Oper: Inferior Frontal Gyrus Pars opercularis ,SFG: Superior Frontal Gyrus, MFG: Medial Frontal Gyrus, SPL: Superior Parietal Lobule, AG: Angular Gyrus, IFGTri: Inferior Frontal Gyrus Pars triangularis, FOrb: Frontal Orbital Cortex, pSMG: Posterior Supramarginal Gyrus, aSMG: Anterior Supramarginal Gyrus, aPHG: Anterior Para hippocampal gyrus, pPHG: Posterior Para hippocampal gyrus.

1). Functional Connectivity of Frontal Parietal-MTL-Basal Ganglia								
	Feedback				Memory Retrieval			
Regions	Left Hemisphere		Right Hemisphere		Left Hemisphere		Right Hemisphere	
	T-value	p-value	T-value	p-value	T-value	p-value	T-value	p-value
SFG-IFG Oper	6.03	0.0001	-	-	4.09	0.0083	-	-
SFG-MFG	10.42	<0.0001	10.35	<0.0001	7.2	<0.0001	7.36	<0.0001
MFG-IFG Oper	10.57	<0.0001	8.09	<0.0001	6.73	<0.0001	4.3	0.0054
MFG-SPL	2.94	0.0284	-	-	-	-	-	-
MFG-AG	6	<0.0001	7.21	<0.0001	3.46	0.0293	5.29	0.0008
MFG-IFGTri	9.77	<0.0001	9.64	<0.0001	8.67	<0.0001	-	-
IFG Oper-Forb	6.51	<0.0001	6.14	<0.0001	-	-	-	-
IFG Oper-IFGTri	15.71	<0.0001	13.46	<0.0001	9.54	<0.0001	7.58	<0.0001
IFG Oper-AG	4.2	0.002	-	-	-	-	-	-
IFG Oper-pSMG	5.93	0.0001	3.93	0.0024	5.77	0.0003	3.73	0.0174
IFG Oper-aSMG	6.37	<0.0001	-	-	4.51	0.0036	3.61	0.0223
Forb-Amygdala	4.74	0.0005	6.16	0.0001	-	-	-	-
aSMG-pSMG	13.9	<0.0001	7.52	<0.0001	8.57	<0.0001	7.03	<0.0001
aSMG-SPL	7.49	<0.0001	8.94	<0.0001	6.25	0.0001	6.24	0.0001
pSMG-AG	14.46	<0.0001	15.61	<0.0001	11.17	<0.0001	10.92	<0.0001
Amygdala-Hippocampus	11.45	<0.0001	8.37	<0.0001	4.72	0.0026	4.07	0.0086
Amygdala- aPHG	11.46	<0.0001	13.4	<0.0001	5.16	0.001	7.21	<0.0001
Hippocampus- pPHG	12.41	<0.0001	10.26	<0.0001	5.82	0.0003	3.78	0.016
aPHG-pPHG	7.31	<0.0001	5.53	0.0002	3.34	0.0348	-	-
Forb-Accumbens	3.95	0.0092	3.75	0.0183	-	-	3.44	0.0298
Accumbens-Caudate	9.46	<0.0001	5.01	0.0008	5.97	0.0002	-	-
Accumbens-Putamen	4.42	0.0046	5.11	0.0008	-	-	-	-
Putamen-Pallidum	16.77	<0.0001	10.79	<0.0001	8.35	<0.0001	5.66	0.0003
Forb-Putamen	6.91	<0.0001	6.55	<0.0001	5.48	0.0005	3.32	0.0357
Hippocampus-aPHG	12.17	<0.0001	9.16	<0.0001	7.67	<0.0001	6.17	<0.0001
IFG Oper-Putamen	-	-	5.43	0.0001	-	-	-	-

Table 3.2: Functional Connectivity of MTL & Basal Ganglia for feedback learning and memory retrieval. Non-significant values are highlighted as red.

2). Functional Connectivity of MTL & Basal Ganglia								
	Feedback				Memory Retrieval			
Regions	**Left Hemisphere**		**Right Hemisphere**		**Left Hemisphere**		**Right Hemisphere**	
	T-value	p-value	T-value	p-value	T-value	p-value	T-value	p-value
Accumbens-Caudate	9.46	<0.0001	5.01	0.0008	5.97	0.0002	-	-
Putamen-Pallidum	16.77	<0.0001	10.79	<0.0001	8.35	<0.0001	5.66	0.0003
Amygdala- aPHG	11.46	<0.0001	13.4	<0.0001	5.16	0.001	7.21	<0.0001
Hippocampus-aPHG	12.17	<0.0001	9.16	<0.0001	7.67	<0.0001	6.17	<0.0001
Hippocampus- pPHG	12.41	<0.0001	10.26	<0.0001	5.82	0.0003	3.78	0.016
Putamen-Amygdala	5.86	<0.0001	5.26	0.0002	4.44	0.0041	-	-
Amygdala-Hippocampus	11.45	<0.0001	8.37	<0.0001	4.72	0.0026	4.07	0.0086
aPHG-pPHG	7.31	<0.0001	5.53	0.0002	3.34	0.0348	-	-

3.4.2 Relationship of the medial temporal lobe (MTL) and basal ganglia: The functional connectivity analysis

The results reveal the functional connectivity between MTL and basal ganglia during feedback and memory retrieval (Figure 3.4, Tables 3.1 & 3.2) at a significant level ($p<0.001$). The results show the significant correlation for feedback learning (Amygdala- aPHG, $r_{Left}=11.46$, $r_{Right}=13.4$; Putamen-Amygdala: $r_{Left}=5.86$, $r_{Right}=5.26$ and memory retrievals (Amygdala- aPHG, $r_{Left}=5.16$, $r_{Right}=7.21$; Putamen-Amygdala: non-significant). The significant correlation values (Accumbens-Caudate: $r_{Left}=9.46$, $r_{Right}=5.01$; Putamen-Pallidum: $r_{Left}=16.77$, $r_{Right}=10.79$) show the strong relationship of caudate-accumbens and putamen-pallidum throughout the feedback learning. Also, the study observes the modulation in these interactions during memory retrieval and reveals the correlation values (Accumbens-Caudate: $r_{Left}=5.97$; Putamen-Pallidum: $r_{Left}=8.35$, $r_{Right}=5.66$).

Hence, these results suggest that the MTL and the basal ganglia interact during task, and their functional relationship modulates from feedback to memory retrieval.

3.4.3 Associations of EEG oscillations and Medial Temporal Lobe (MTL): The EEG -informed- FMRI approach

Figures 3.5 demonstrates the association of frontal EEG powers (delta, theta, lower-alpha, higher alpha, lower beta, and higher beta) in the functioning of the MTL for feedback learning and memory retrievals.

3.4.3.1 Feedback Learning

The EEG-informed-fMRI results (Figures 3.5) report a positive relationship of frontocentral lower-beta and parietal-delta powers with the bold activity of anterior-para-hippocampal gyrus (aPHG) during feedback learning. We find that the bold activity of the posterior-para-hippocampal gyrus (pPHG) synchronizes with the frontal (lower-alpha, lower-beta) and parietal (theta, delta) EEG powers. The results also observe the pPHG as a negative correlate of parietal higher beta power. Thus, our study summarizes that frontal lower-beta power enhances the bold activity of aPHG, and combined effect of frontal alpha-beta, parietal theta powers enhances the bold activity of pPHG.

Further, our study finds the enhanced synchronization between frontal powers (lower-beta and delta) and the bold activity of the left amygdala in feedback learning. We also observe that the right amygdala positively associates with frontal-parietal delta power and negatively associates with parietal beta power. Thus, our study reveals that the bold activity of the amygdala enhances due to delta powers and reduce due to beta powers.

3.4.3.2 Memory Retrieval

The results (Figures 3.5) reveal that the frontal-theta and parietal-delta powers correlate with the bold activity of aPHG, and the frontocentral higher-beta power anticorrelate with the same. Results suggest that the frontal (higher-beta, delta) and the central-parietal powers (lower-beta, higher-alpha) synchronize with the bold activity of pPHG. Our study also observes the de-synchronization of the bold activity of pPHG, and it is due to the frontal (higher-alpha, lower-alpha, and theta) and parietal-higher alpha powers. Thus, we suggest that the hemodynamic synchronization of PHG occurs due to frontal EEG powers.

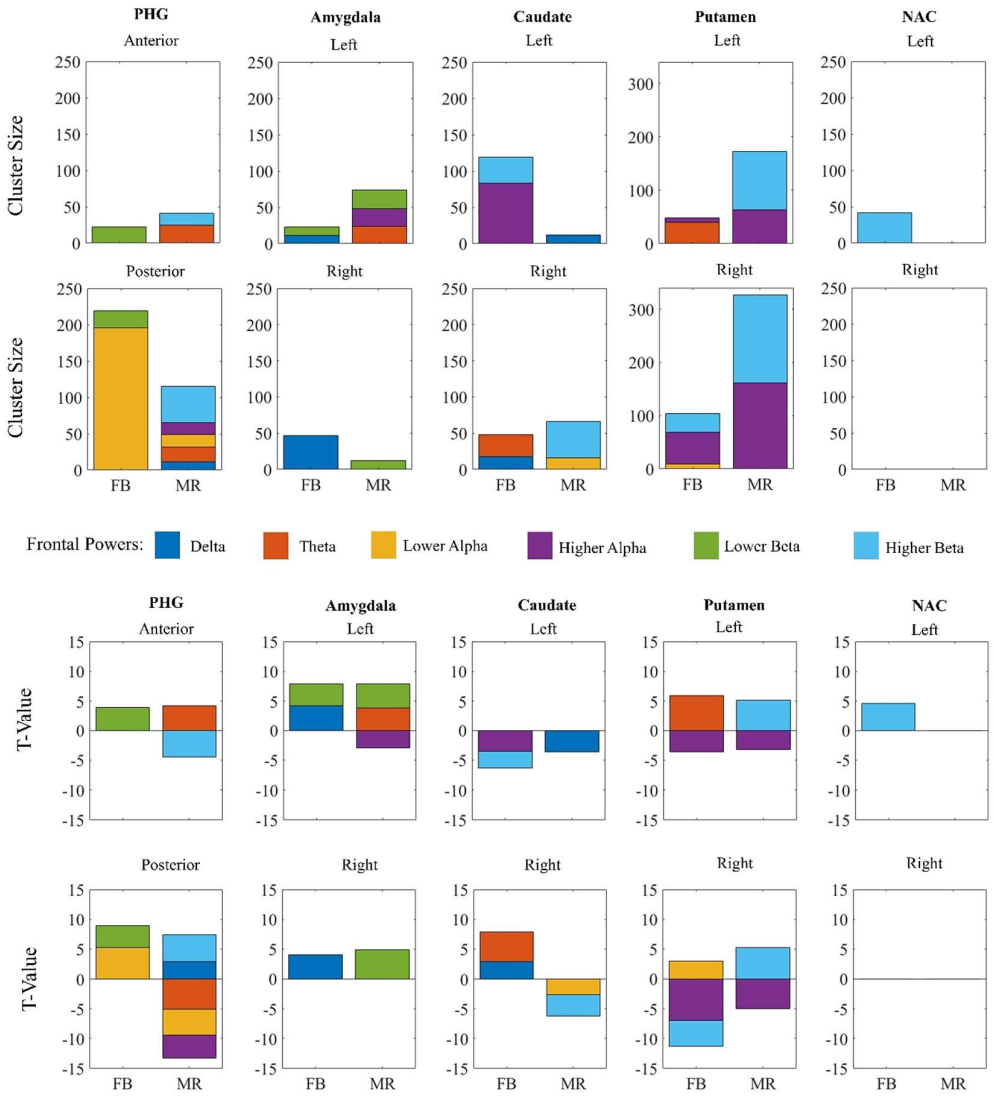

Figure 3.5: Associations of frontal electrophysiological powers (delta, theta, lower-alpha, higher alpha, lower beta, and higher beta) in the functioning of the medial temporal lobe (Parahippocampal Cortex & Amygdala) and basal ganglia (Caudate, Putamen & Nuclear Accumbens) during feedback learning and memory retrievals. (a) Voxel-based distribution. (b). Significant T-value based distribution. FB: Feedback learning, MR: Memory retrieval.

Further, there is a significant association of frontal EEG powers with the bold activity of the left-amygdala. The findings reveal that the bold activity of the left-amygdala synchronizes with lower-beta, theta powers, and de-synchronizes with the higher-alpha power. The study also observes the associations of the frontal-parietal beta powers with the right-amygdala. Thus, we find the enhancement in the bold activity of the amygdala, due to frontal-theta, higher alpha, and parietal beta powers.

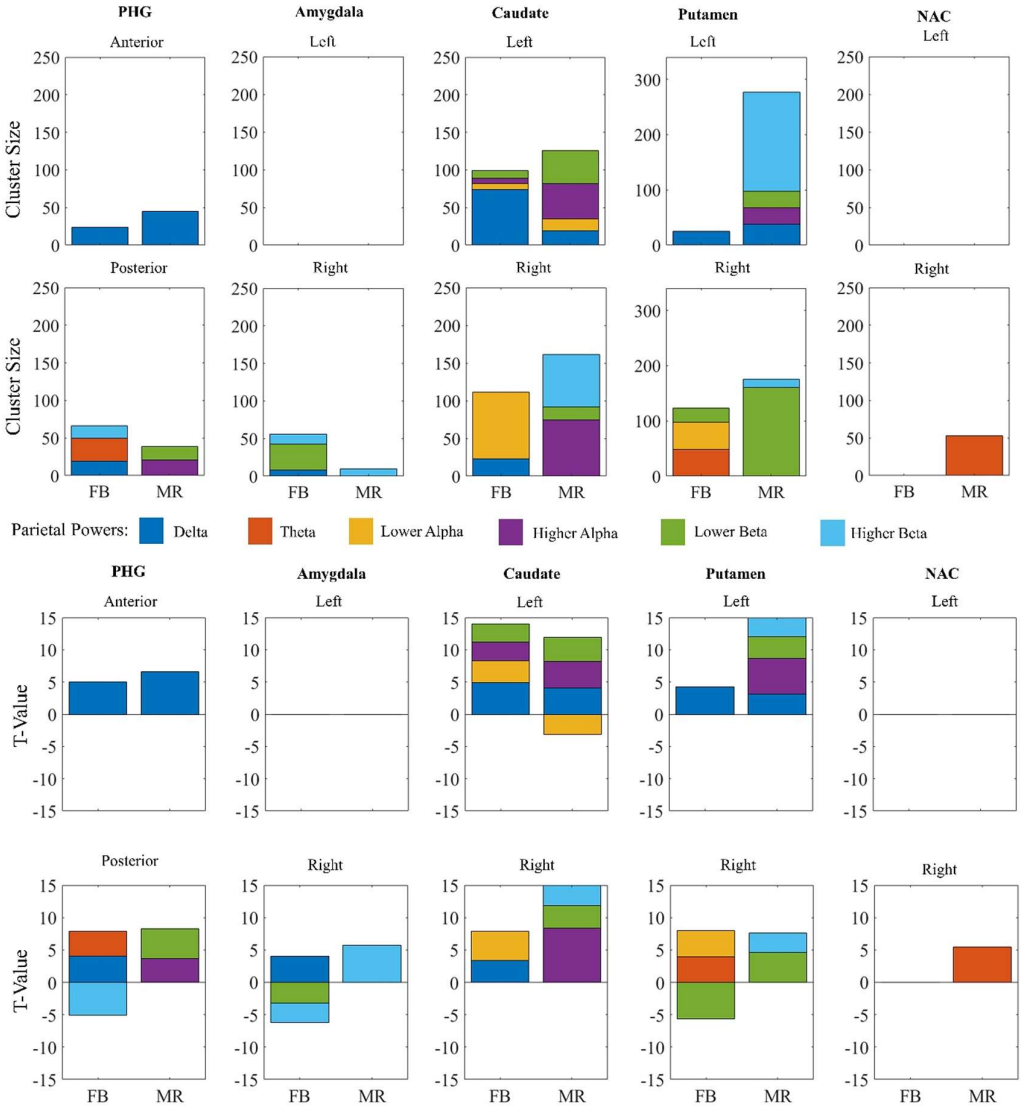

Figure 3.6: Associations of parietal electrophysiological powers (delta, theta, lower-alpha, higher alpha, lower beta, and higher beta) in the functioning of the medial temporal lobe (Parahippocampal Cortex & Amygdala) and basal ganglia (Caudate, Putamen & Nuclear Accumbens) during feedback learning and memory retrievals. (a) Voxel-based distribution. (b). Significant T-value based distribution.

3.4.4 Associations of EEG oscillations with Basal Ganglia

Figures 3.6 demonstrates the association of frontal EEG powers (delta, theta, lower-alpha, higher alpha, lower beta, and higher-beta) in the functioning of basal ganglia during feedback learning and memory retrievals.

3.4.4.1 Feedback Learning

Caudate: The study finds a significant role of the caudate in feedback learning such that parietal powers (lower-alpha, higher-alpha, lower-beta, delta) correlate with the left caudate. In specific, parietal-delta power reveal the most significant cluster. The frontal power (higher alpha, higher beta) anticorrelate with the bold activities of the left-caudate. The study also finds the role of the right caudate in feedback learning, and the results report a positive correlation of frontal (theta, delta) and parietal (lower-alpha, delta) powers with its bold activity. Thus, our result highlights the involvement of the caudate in feedback learning and associated EEG powers.

Putamen: The results explain that the frontal theta and parietal delta powers correlate with the bold activity of left putamen and the frontal higher alpha power anticorrelate with the same. We find the right putamen as a positive correlate of parietal-theta and frontal-parietal lower-alpha powers, and negative correlate of the frontal (higher alpha, higher beta) and the parietal lower beta powers. Thus, our results suggest the involvement of left and right putamen through theta and alpha powers.

Nuclear Accumbens: There is a significant association of frontocentral higher beta power in the modulation of the bold activity of left accumbens in feedback learning. The study does not find the right accumbens as any of the electrophysiological correlates. Thus, the role of frontocentral higher-beta power suggests an enhancement in the bold activity of left accumbens in feedback learning.

3.4.4.2 Memory Retrieval

Caudate: Our results emphasize the role of the caudate in declarative memory retrieval. In specific, parietal powers (higher alpha, lower beta, delta) synchronize and parietal alpha power desynchronizes the bold activity of left caudate. Similarly, we find the associations of parietal powers (higher-alpha, higher-beta, lower-beta) powers in synchronization and frontal powers (lower-alpha, higher-beta) in de-synchronization of the hemodynamic activity of right-caudate. Our study observes that the caudate engages in memory retrieval through an alpha-beta association such that bold activity, enhances through parietal powers and reduces through frontal powers.

Putamen: Our results signify the significant role of the putamen in memory retrieval and reveal the left putamen as a positive correlate of frontal higher-beta and parietal (higher alpha, beta, delta) powers. The study also observes the negative correlation of frontal (higher-alpha, lower-beta) and parietal (higher-alpha, lower-alpha, and theta) powers with the bold activity of left putamen. Similarly, it finds the engagement of the frontal-parietal higher-beta and parietal lower-beta powers in synchronization with the bold activity of the right putamen. Th study also see a de-synchronization of the bold activity of the same due to frontal-parietal alpha powers. Hence, these results confirm that the frontal-parietal higher-beta power and frontal higher-alpha power enhance the involvement of the putamen in memory retrieval.

Nuclear Accumbens: We find that parietal higher-alpha/theta correlates/anticorrelates with the bold activity of the right accumbens. However, the study does not observe any association of EEG powers with the left accumbens during memory retrievals.

3.5 DISCUSSION

The aim of study is to explore the relationship of frontal-parietal regions with MTL-basal ganglia during feedback learning and declarative memory retrieval. The role of the medial temporal lobe is widely observed in previous studies [2,46,47] of declarative memory engagement. The interactions of the MTL with the frontal cortex and the basal ganglia suggest that feedback affects their interaction dynamics and lead towards behavior adjustments [48–52]. In this study, the study investigates the effect of feedback and the role of frontal-parietal EEG spectral powers in the relationship of MTL and basal ganglia for memory retrieval. For this, we first check the functional connectivity of frontal-parietal regions with the MTL and basal ganglia using connectivity analysis. The study then explores the involvement of spectral powers in the feedback related learning and memory retrieval. We discuss all these findings in the following sections in detail.

3.5.1 Does the connectivity of MTL, and basal ganglia modulate for memory retrieval from feedback learning?

The functional interactions analysis reveals the significant functional connectivity of the putamen-pallidum and the caudate-accumbens during the task. In specific, we observe slightly unlike putamen-pallidum dynamics for feedback learning and

memory retrievals. The putamen plays a central role during feedback learning and the pallidum in memory retrieval. Our findings are found in line with these earlier neuroimaging studies [53], which suggest the crucial role of pallidum in learning or performing learned responses related to rewards. It has also seen that the reward pathway converges upon ventral pallidum, and this funneling of signals plays a unique role in generating major reward components [54]. However, earlier studies have highlighted the role of putamen in motivational processes [55]. Our study finds that the pallidum acknowledges for reward-based responses and interacts with MTL through putamen. There is a vital functional connectivity of the pallidum with the putamen and the MTL for memory retrieval. Yet, the pallidum plays a central role in the interaction between the putamen and MTL, which is different from feedback learning. The modulated dynamics of pallidum and putamen suggest that memory retrieval uses the pallidum as a central hub for performing a declarative memory retrieval by utilizing learned responses and getting motivated.

Several neuroimaging studies have highlighted the role of the prefrontal cortex in the interaction between MTL and sub-regions of the basal ganglia. It has also been suggested that the prefrontal cortex (PFC) may mediate the functional connectivity between the MTL and the striatum due to the executive control functions of the prefrontal cortex (PFC), which involves the scheduling and optimization of lower-level functions implemented in sub-cortical and posterior cortical regions [56–58]. We suggest the significant interactions of frontal-parietal EEG powers with MTL and basal ganglia during feedback and memory retrieval.

3.5.2 Does memory retrieval dissociate MTL and basal ganglia from frontal-parietal regions?

Our functional connectivity results demonstrate the significant interactions of frontal-parietal regions with MTL and basal ganglia during feedback learning. Further, the neurovascular results reveal that the synchronized bold activity of aPHG and pPHG with the frontocentral lower-beta/parietal-delta and frontal alpha-beta/parietal theta powers, respectively. Also, the study finds the bold activity of the left and right amygdala synchronized with the frontal lower beta/delta and frontal-parietal delta

powers. These findings imply the neurovascular relationship of frontal-parietal EEG powers in modulating the bold activity of MTL regions during the learning phase. These results collaborate with the results of several previous electrophysiological studies supporting the role of frontal-beta power in reward-related feedback and successful memory encoding [21,22,59–61]. Further, the significant increase of theta-power during successful memory encoding is found as a prominent marker of win-associated memory performance [62]. The role of the delta band is also revealed during positive mood memory formation [63]. Thus, our research suggests a significant role of frontal-parietal theta, delta, and lower-beta powers in the modulation of the bold activity of MTL during learning from positive feedback.

Similarly, the interactions of frontal-parietal regions with the basal ganglia during the learning phase reveal the significant functional association of the frontal orbital cortex and inferior frontal gyrus with the sub-regions of basal ganglia through accumbens. This finding is consistent with several neuroimaging studies, those have highlighted the role of basal ganglia in learning, such as category learning [64,65] and habit learning [66–68]. Later, an essential role of the basal ganglia in motivation [69,70] and decision making [71] is revealed. Several studies [72–74] have linked the reward-related feedback with the increased functional connectivity of the striatum with the prefrontal cortex. Moreover, a reward study [75] reported the elicitation of high beta power over the right prefrontal cortex in reward-related feedback stimuli. From our neurovascular results, the bold activity of caudate is found synchronized with the frontal-parietal alpha, parietal beta, parietal delta, and frontal theta powers. Also, the activity of Putamen is found synchronized with the frontal-parietal-theta, frontal-alpha powers, and left accumbens with the frontocentral higher-beta power. Thus, the findings mentioned above reveal the frontal-parietal alpha, beta, and theta powers as a significant cause of frontal-basal ganglia interactions during the learning phase.

However, the interactions between frontal-parietal and MTL regions modulate for memory retrieval from the learning phase. The results affirm the significant functional connectivity between frontal and parietal regions and distinct MTL regions, but no interactions of frontal-parietal with MTL regions. These observations suggest the functional dissociation between MTL and frontal regions. Yet, it is unknown that

which mechanism causes the functional dissociation of MTL from frontal-parietal regions. Thus, neurovascular underpinnings are explored, and results show the significant desynchronization of aPHG bold activity due to frontocentral higher beta and pPHG bold activity due to frontal-alpha-theta and parietal-higher alpha powers. Also, our study reveals the bold synchronization aPHG due to the combined effect of frontal theta, parietal delta, frontal-higher beta-delta, and parietal-lower beta-higher alpha powers. Further, the bold activity of the left amygdala synchronizes due to frontal-theta, lower beta powers, and de-synchronizes with frontal-higher alpha power. Our outcomes highlight the increased role of theta and alpha powers during memory retrieval. Consistent with these observations, a recent study [76] provides compelling evidence of binding the hippocampus, PFC, and striatum with the theta and alpha oscillations during successful recollection. However, earlier studies suggest that frontal theta power is a candidate mechanism by which emergent processes such as 'cognitive control' may be biophysically realized [77]. Hence, the neurovascular approach demonstrates the essential roles of frontal-alpha-theta powers underlying the functional dissociation of MTL from frontal-parietal regions during memory retrieval from learning phase. Further, memory retrieval reveals a significant dissociation in functional connectivity between basal ganglia and the frontal-parietal regions like the MTL. Yet, the study finds the significant functional connectivity of frontal-parietal regions and the sub-regions of basal ganglia individually. Our findings collaborate with the results of an earlier study [78] that notified the increased frontal-parietal synchrony during recognition memory. The dissociation of basal ganglia with frontal-parietal regions suggests the lack of functional interactions between two during memory retrieval.

3.6 CONCLUSION

The study used simultaneous EEG-fMRI to demonstrate the significant associations of frontal-parietal EEG powers with the hemodynamic activity of MTL and basal ganglia to brief feedback learning and declarative memory. The present study provides a novel evidence that frontal-parietal regions associate with MTL-basal ganglia in feedback learning and dissociate in memory retrieval. The modulated relationship highlights the functional role of the Putamen and the pallidum (sub-

regions of basal ganglia). The current work converges nicely with the studies implicating the major role of prefrontal cortex in the interactions of MTL-basal ganglia [79–81]. Our findings from functional connectivity and neurovascular approach provide evidence that interactions of MTL-basal ganglia during feedback and declarative memory task relies on the mechanism of the frontal-parietal EEG powers. The results reveal the significant modulation in the relationship of frontal-parietal EEG powers with the bold activity of MTL and suggest the enhanced role of frontal-alpha and theta powers during memory retrievals. The frontal-alpha-beta powers desynchronize, and the parietal-alpha-beta powers synchronize the bold activity of the caudate. Also, the parietal theta power significantly de-synchronize and frontal higher alpha power synchronizes the bold activity of right accumbens. Thus, our findings have important implication for understanding the major role of frontal and parietal EEG powers in feedback associated declarative memory retrieval.

REFERENCES

[1] A.R. Preston, H. Eichenbaum, Interplay of hippocampus and prefrontal cortex in memory, Curr. Biol. 23 (2013) R764–R773. https://doi.org/10.1016/j.cub.2013.05.041.

[2] I. Tendolkar, J. Arnold, K.M. Petersson, S. Weis, A. Brockhaus-Dumke, P. Van Eijndhoven, J. Buitelaar, G. Fernández, Contributions of the medial temporal lobe to declarative memory retrieval: Manipulating the amount of contextual retrieval, Learn. Mem. 15 (2008) 611–617. https://doi.org/10.1101/lm.916708.

[3] H. Eichenbaum, A.P. Yonelinas, C. Ranganath, The medial temporal lobe and recognition memory, Annu. Rev. Neurosci. 30 (2007) 123–152. https://doi.org/10.1146/annurev.neuro.30.051606.094328.

[4] A. de Vanssay-Maigne, M. Noulhiane, A.D. Devauchelle, S. Rodrigo, S. Baudoin-Chial, J.F. Meder, C. Oppenheim, C. Chiron, F. Chassoux, Modulation of encoding and retrieval by recollection and familiarity: Mapping the medial temporal lobe networks, Neuroimage. 58 (2011) 1131–1138. https://doi.org/10.1016/j.neuroimage.2011.06.086.

[5] J. Fell, E. Ludowig, B.P. Staresina, T. Wagner, T. Kranz, C.E. Elger, N. Axmacher, Medial temporal theta/alpha power enhancement precedes successful memory encoding: Evidence based on intracranial EEG, J. Neurosci. 31 (2011) 5392–5397. https://doi.org/10.1523/JNEUROSCI.3668-10.2011.

[6] S.L. Brincat, E.K. Miller, Frequency-specific hippocampal-prefrontal interactions during associative learning, Nat. Neurosci. 18 (2015) 576–581. https://doi.org/10.1038/nn.3954.

[7] M.X. Cohen, C.E. Elger, B. Weber, Amygdala tractography predicts functional connectivity and learning during feedback-guided decision-making, Neuroimage. 39 (2008) 1396–1407. https://doi.org/10.1016/j.neuroimage.2007.10.004.

[8] C.A. Seger, C.M. Cincotta, Dynamics of frontal, striatal, and hippocampal systems during rule learning, Cereb. Cortex. 16 (2006) 1546–1555. https://doi.org/10.1093/cercor/bhj092.

[9] R.T. Gerraty, J.Y. Davidow, G.E. Wimmer, I. Kahn, D. Shohamy, Transfer of learning relates to intrinsic connectivity between hippocampus, ventromedial prefrontal cortex, and large-scale networks, J. Neurosci. 34 (2014) 11297–11303. https://doi.org/10.1523/JNEUROSCI.0185-14.2014.

[10] E. Tricomi, J.A. Fiez, Information content and reward processing in the human striatum during performance of a declarative memory task, Cogn. Affect. Behav. Neurosci. 12 (2012) 361–372. https://doi.org/10.3758/s13415-011-0077-3.

[11] J. Hattie, H. Timperley, The power of feedback, Rev. Educ. Res. 77 (2007) 81–112. https://doi.org/10.3102/003465430298487.

[12] W. Lee, J. Reeve, Self-determined, but not non-self-determined, motivation predicts activations in the anterior insular cortex: An fMRI study of personal agency, Soc. Cogn. Affect. Neurosci. 8 (2013) 538–545. https://doi.org/10.1093/scan/nss029.

[13] I. van de Vijver, K. Richard Ridderinkhof, M.X. Cohen, Frontal oscillatory dynamics predict feedback learning and action adjustment, J. Cogn. Neurosci. 23 (2011) 4106–4121. https://doi.org/10.1162/jocn_a_00110.

[14] K.R. Ridderinkhof, W.P.M. Van Den Wildenberg, S.J. Segalowitz, C.S. Carter, Neurocognitive mechanisms of cognitive control: The role of prefrontal cortex in action selection, response inhibition, performance monitoring, and reward-based learning, Brain Cogn. 56 (2004) 129–140. https://doi.org/10.1016/j.bandc.2004.09.016.

[15] A.D. Wagner, B.J. Shannon, I. Kahn, R.L. Buckner, Parietal lobe contributions to episodic memory retrieval, Trends Cogn. Sci. 9 (2005) 445–453. https://doi.org/10.1016/j.tics.2005.07.001.

[16] L.J. Chang, T. Yarkoni, M.W. Khaw, A.G. Sanfey, Decoding the role of the insula in human cognition: Functional parcellation and large-scale reverse inference, Cereb. Cortex. 23 (2013) 739–749. https://doi.org/10.1093/cercor/bhs065.

[17] S.N. Haber, B. Knutson, The reward circuit: Linking primate anatomy and human imaging, Neuropsychopharmacology. 35 (2010) 4–26. https://doi.org/10.1038/npp.2009.129.

[18] T. V. Maia, Fear conditioning and social groups: Statistics, not genetics, Cogn. Sci. 33 (2009) 1232–1251. https://doi.org/10.1111/j.1551-6709.2009.01054.x.

[19] M.F.S. Rushworth, M.A.P. Noonan, E.D. Boorman, M.E. Walton, T.E. Behrens, Frontal Cortex and Reward-Guided Learning and Decision-Making, Neuron. 70 (2011) 1054–1069. https://doi.org/10.1016/j.neuron.2011.05.014.

[20] N. Doñamayor, J. Marco-Pallarés, M. Heldmann, M.A. Schoenfeld, T.F. Münte, Temporal dynamics of reward processing revealed by magnetoencephalography, Hum. Brain Mapp. 32 (2011) 2228–2240. https://doi.org/10.1002/hbm.21184.

[21] J. Marco-Pallares, D. Cucurell, T. Cunillera, R. García, A. Andrés-Pueyo, T.F. Münte, A. Rodríguez-Fornells, Human oscillatory activity associated to reward processing in a gambling task, Neuropsychologia. 46 (2008) 241–248. https://doi.org/ 10.1016/j.neuropsychologia.2007.07.016.

[22] M.X. Cohen, C.E. Elger, C. Ranganath, Reward expectation modulates feedback-related negativity and EEG spectra, Neuroimage. 35 (2007) 968–978. https://doi.org/10.1016/j.neuroimage.2006.11.056.

[23] E.B. Knudsen, J.D. Wallis, Closed-Loop Theta Stimulation in the Orbitofrontal Cortex Prevents Reward-Based Learning, Neuron. 106 (2020) 537-547.e4. https://doi.org/ 10.1016/j.neuron.2020.02.003.

[24] M.G. Packard, M. White, Q. Ha, Differential Effects of Fornix and Caudate Radial Maze Tasks : Evidence for Multiple Nucleus Lesions on Two Memory Systems, Science (80-.). (1989) 1465–1472.

[25] B.J. Knowlton, J.A. Mangels, L.R. Squire, A neostriatal habit learning system in humans, Science (80-.). 273 (1996) 1399–1402. https://doi.org/10.1126/ science. 273.5280.1399.

[26] N.J. Cohen, R.A. Poldrack, H. Eichenbaum, Memory for Items and Memory for Relations in the Procedural/Declarative Memory Framework, Memory. 5 (1997) 131–178. https://doi.org/10.1080/741941149.

[27] D. Shohamy, C.E. Myers, S. Grossman, J. Sage, M.A. Gluck, R.A. Poldrack, Cortico-striatal contributions to feedback-based learning: Converging data from neuroimaging and neuropsychology, Brain. 127 (2004) 851–859. https://doi.org/10.1093/brain/ awh100.

[28] D. Shohamy, R.A. Adcock, Dopamine and adaptive memory, Trends Cogn. Sci. 14 (2010) 464–472. https://doi.org/10.1016/j.tics.2010.08.002.

[29] M. Cohn, M. Moscovitch, P.S.R. Davidson, Double dissociation between familiarity and recollection in Parkinson's disease as a function of encoding tasks, Neuropsychologia. 48 (2010) 4142–4147. https://doi.org/10.1016/j.neuropsy chologia.2010.10.013.

[30] S. Han, S.A. Huettel, A. Raposo, R.A. Adcock, I.G. Dobbins, Functional significance of striatal responses during episodic decisions: Recovery or goal attainment?, J. Neurosci. 30 (2010) 4767–4775. https://doi.org/10.1523/JNEUROSCI.3077-09.2010.

[31] A.A. Moustafa, M.A. Gluck, Computational cognitive models of prefrontal-striatal-hippocampal interactions in Parkinson's disease and schizophrenia, Neural Networks. 24 (2011) 575–591. https://doi.org/10.1016/j.neunet.2011.02.006.

[32] M. Freedberg, A.C. Toader, E.M. Wassermann, J.L. Voss, Competitive and cooperative interactions between medial temporal and striatal learning systems, Neuropsychologia. 136 (2020) 107257. https://doi.org/10.1016/j.neuropsychologia.2019.107257.

[33] I.G. Dobbins, H. Foley, D.L. Schacter, A.D. Wagner, Executive Control during Episodic Retrieval, Neuron. 35 (2002) 989–996. https://doi.org/10.1016/s0896-6273(02)00858-9.

[34] D.R. Euston, A.J. Gruber, B.L. McNaughton, The Role of Medial Prefrontal Cortex in Memory and Decision Making, Neuron. 76 (2012) 1057–1070. https://doi.org/10.1016/j.neuron.2012.12.002.

[35] R. Cabeza, Role of parietal regions in episodic memory retrieval: The dual attentional processes hypothesis, Neuropsychologia. 46 (2008) 1813–1827. https://doi.org/10.1016/j.neuropsychologia.2008.03.019.

[36] B.A. Ally, J.S. Simons, J.D. McKeever, P. V. Peers, A.E. Budson, Parietal contributions to recollection: Electrophysiological evidence from aging and patients with parietal lesions, Neuropsychologia. 46 (2008) 1800–1812. https://doi.org/10.1016/j.neuropsychologia.2008.02.026.

[37] S. Agrawal, V. Chinnadurai, A. Kaur, P. Kumar, P. Kaur, R. Sharma, A. Kumar Singh, Estimation of Functional Connectivity Modulations during Task Engagement and Their Neurovascular Underpinnings Through Hemodynamic Reorganization Method, Brain Connect. 9 (2019) 341–355. https://doi.org/10.1089/brain.2018.0656.

[38] P.J. Allen, O. Josephs, R. Turner, A method for removing imaging artifact from continuous EEG recorded during functional MRI, Neuroimage. 12 (2000) 230–239. https://doi.org/10.1006/nimg.2000.0599.

[39] I.I. Christov, Real time electrocardiogram QRS detection using combined adaptive threshold, Biomed. Eng. Online. 3 (2004) 1–9. https://doi.org/10.1186/1475-925X-3-28.

[40] K.H. Kim, H.W. Yoon, H.W. Park, Improved ballistocardiac artifact removal from the electroencephalogram recorded in fMRI, J. Neurosci. Methods. 135 (2004) 193–203. https://doi.org/10.1016/j.jneumeth.2003.12.016.

[41] L.J. Gabard-Durnam, A.S.M. Leal, C.L. Wilkinson, A.R. Levin, The harvard automated processing pipeline for electroencephalography (HAPPE): Standardized processing software for developmental and high-artifact data, Front. Neurosci. 12 (2018) 1–24. https://doi.org/10.3389/fnins.2018.00097.

[42] A. Delorme, S. Makeig, EEGLAB: An open source toolbox for analysis of single-trial EEG dynamics including independent component analysis, J. Neurosci. Methods. 134 (2004) 9–21. https://doi.org/10.1016/j.jneumeth.2003.10.009.

[43] S. Whitfield-gabrieli, A. Nieto-castanon, Conn : A Functional Connectivity Toolbox for Correlated and Anticorrelated Brain Networks, 2 (2012). https://doi.org/10.1089/brain.2012.0073.

[44] J.R. Anderson, D. Byrne, J.M. Fincham, P. Gunn, Role of prefrontal and parietal cortices in associative learning, Cereb. Cortex. 18 (2008) 904–914. https://doi.org/10.1093/cercor/bhm123.

[45] B. Thürer, C. Stockinger, F. Putze, T. Schultz, T. Stein, Mechanisms within the parietal cortex correlate with the benefits of random practice in motor adaptation, Front. Hum. Neurosci. 11 (2017) 1–11. https://doi.org/10.3389/fnhum.2017.00403.

[46] L. Davachi, Item, context and relational episodic encoding in humans, Curr. Opin. Neurobiol. 16 (2006) 693–700. https://doi.org/10.1016/j.conb.2006.10.012.

[47] L.R. Squire, C.E.L. Stark, R.E. Clark, the Medial Temporal Lobe, Annu. Rev. Neurosci. 27 (2004) 279–306. https://doi.org/10.1146/annurev.neuro.27.070203. 144130.

[48] J.S. Simons, H.J. Spiers, Prefrontal and medial temporal lobe interactions in long-term memory, Nat. Rev. Neurosci. 4 (2003) 637–648. https://doi.org/10.1038/nrn1178.

[49] A.R. Preston, H. Eichenbaum, Interplay of hippocampus and prefrontal cortex in memory, Curr. Biol. 23 (2013) 1–21. https://doi.org/10.1016/j.cub.2013.05.041.

[50] N.D. Walsh, M.L. Phillips, Interacting outcome retrieval, anticipation, and feedback processes in the human brain, Cereb. Cortex. 20 (2010) 271–281. https://doi.org/10.1093/cercor/bhp098.

[51] A. Manuscript, Striatal contributions to declarative memory retrieval Jason, Bone. 23 (2008) 1–7. https://doi.org/10.1038/jid.2014.371.

[52] E. Tricomi, J.A. Fiez, Feedback signals in the caudate reflect goal achievement on a declarative memory task, Neuroimage. 41 (2008) 1154–1167. https://doi.org/10.1016/j.neuroimage.2008.02.066.

[53] M. Waraczynski, C. Demco, Lidocaine inactivation of the ventral pallidum affects responding for brain stimulation reward more than it affects the stimulation's reward value, Behav. Brain Res. 173 (2006) 288–298. https://doi.org/10.1016/j.bbr.2006.06.040.

[54] K.S. Smith, A.J. Tindell, J.W. Aldridge, K.C. Berridge, Ventral pallidum roles in reward and motivation, Behav. Brain Res. 196 (2009) 155–167. https://doi.org/10.1016/j.bbr.2008.09.038.

[55] W. Schultz, Multiple reward signals in the brain, Nat. Rev. Neurosci. 1 (2000) 199–207. https://doi.org/10.1038/35044563.

[56] R.A. Poldrack, P. Rodriguez, How do memory systems interact? Evidence from human classification learning, Neurobiol. Learn. Mem. 82 (2004) 324–332. https://doi.org/10.1016/j.nlm.2004.05.003.

[57] E.K. Miller, J.D. Cohen, An integrate theory of PFC function, Annu. Rev. Neurosci. 24 (2001) 167–202. https://doi.org/10.1146/annurev.neuro.24.1.167.

[58] D.A. Norman, T. Shallice, E-mmhhhhhmh, (n.d.).

[59] M.X. Cohen, K. Wilmes, I. van de Vijver, Cortical electrophysiological network dynamics of feedback learning, Trends Cogn. Sci. 15 (2011) 558–566. https://doi.org/10.1016/j.tics.2011.10.004.

[60] C.D.B. Luft, Learning from feedback: The neural mechanisms of feedback processing facilitating better performance, Behav. Brain Res. 261 (2014) 356–368. https://doi.org/10.1016/j.bbr.2013.12.043.

[61] N. Salari, M. Rose, Dissociation of the functional relevance of different pre-stimulus oscillatory activity for memory formation, Neuroimage. 125 (2016) 1013–1021. https://doi.org/10.1016/j.neuroimage.2015.10.037.

[62] M. Pu, R. Yu, Post-encoding frontal theta activity predicts incidental memory in the reward context, Neurobiol. Learn. Mem. 158 (2019) 14–23. https://doi.org/10.1016/j.nlm.2019.01.008.

[63] M. Gärtner, M. Bajbouj, Encoding-related EEG oscillations during memory formation are modulated by mood state, Soc. Cogn. Affect. Neurosci. 9 (2013) 1934–1941. https://doi.org/10.1093/scan/nst184.

[64] D. Shohamy, C.E. Myers, S. Onlaor, M.A. Gluck, Role of the basal ganglia in category learning: How do patients with Parkinson's disease learn?, Behav. Neurosci. 118 (2004) 676–686. https://doi.org/10.1037/0735-7044.118.4.676.

[65] D. Shohamy, C.E. Myers, J. Kalanithi, M.A. Gluck, Basal ganglia and dopamine contributions to probabilistic category learning, Neurosci. Biobehav. Rev. 32 (2008) 219–236. https://doi.org/10.1016/j.neubiorev.2007.07.008.

[66] F.G. Ashby, B.O. Turner, J.C. Horvitz, Cortical and basal ganglia contributions to habit learning and automaticity, Trends Cogn. Sci. 14 (2010) 208–215. https://doi.org/10.1016/j.tics.2010.02.001.

[67] C.A. Seger, B.J. Spiering, A critical review of habit learning and the basal ganglia, Front. Syst. Neurosci. 5 (2011) 1–9. https://doi.org/10.3389/fnsys.2011.00066.

[68] H.H. Yin, B.J. Knowlton, The role of the basal ganglia in habit formation, Nat. Rev. Neurosci. 7 (2006) 464–476. https://doi.org/10.1038/nrn1919.

[69] W. Schultz, Reward functions of the basal ganglia, J. Neural Transm. 123 (2016) 679–693. https://doi.org/10.1007/s00702-016-1510-0.

[70] C. Da Cunha, A. Gomez-A, C.D. Blaha, The role of the basal ganglia in motivated Behaviour, Rev. Neurosci. 23 (2012) 747–767. https://doi.org/10.1515/revneuro-2012-0063.

[71] F. Thibaut, Basal ganglia play a crucial role in decision making, Dialogues Clin. Neurosci. 18 (2016) 3.

[72] A. Pasupathy, E.K. Miller, Different time courses of learning-related activity in the prefrontal cortex and striatum, Nature. 433 (2005) 873–876. https://doi.org/10.1038/nature03287.

[73] M.J. Frank, E.D. Claus, Anatomy of a decision: Striato-orbitofrontal interactions in reinforcement learning, decision making, and reversal, Psychol. Rev. 113 (2006) 300–326. https://doi.org/10.1037/0033-295X.113.2.300.

[74] E. Camara, A. Rodriguez-Fornells, Z. Ye, T.F. Münte, Reward networks in the brain as captured by connectivity measures, Front. Neurosci. 3 (2009) 350–362. https://doi.org/10.3389/neuro.01.034.2009.

[75] A.H. Hosseini, C.B. Holroyd, Reward feedback stimuli elicit high-beta EEG oscillations in human dorsolateral prefrontal cortex, Sci. Rep. 5 (2015) 1–8. https://doi.org/10.1038/srep13021.

[76] N.A. Herweg, T. Apitz, G. Leicht, C. Mulert, L. Fuentemilla, N. Bunzeck, Theta-alpha oscillations bind the hippocampus, prefrontal cortex, and striatum during recollection: Evidence from simultaneous EEG–fMRI, J. Neurosci. 36 (2016) 3579–3587. https://doi.org/10.1523/JNEUROSCI.3629-15.2016.

[77] J.F. Cavanagh, M.J. Frank, Frontal theta as a mechanism for cognitive control, Trends Cogn. Sci. 18 (2014) 414–421. https://doi.org/10.1016/j.tics.2014.04.012.

[78] C. Summerfield, J.A. Mangels, Functional coupling between frontal and parietal lobes during recognition memory, Neuroreport. 16 (2005) 117–122. https://doi.org/10.1097/00001756-200502080-00008.

[79] C.A. Seger, E.K. Miller, Category learning in the brain, Annu. Rev. Neurosci. 33 (2010) 203–219. https://doi.org/10.1146/annurev.neuro.051508.135546.

[80] G.J. Peters, C.N. David, M.D. Marcus, D.M. Smith, The medial prefrontal cortex is critical for memory retrieval and resolving interference, Learn. Mem. 20 (2013) 201–209. https://doi.org/10.1101/lm.029249.112.

[81] M. Guitart-Masip, G.R. Barnes, A. Horner, M. Bauer, R.J. Dolan, E. Duzel, Synchronization of medial temporal lobe and prefrontal rhythms in human decision making, J. Neurosci. 33 (2013) 442–451. https://doi.org/10.1523/JNEUROSCI.2573-12.2013.

CHAPTER 4

ASSOCIATION OF FLUID INTELLIGENCE WITH FEEDBACK LEARNING AND SUBSEQUENT TASK ENGAGEMENT: CLASSIFICATION THROUGH DEEP LEARNING FRAMEWORK

4.1 ABSTRACT

Human adaptability to cognitive tasks is a long-standing challenge, and immensely associated with learning from previously experienced actions and retrieving them from memories. To decipher the neural mechanisms of individual's intelligence associated with feedback learning and subsequent memory retrieval, the study proposes an attention-based deep-learning framework. Thirty-five volunteers underwent declarative-memory based feedback-learning and memory retrieval tasks, and their simultaneous EEG-fMRI information was acquired. Then, robust correlation analysis estimated the association of fluid intelligence with the elicited cortical EEG oscillations. Subsequently, neural mechanisms insights are studied through the multi-frequency interaction, EEG-informed-fMRI and hemodynamical functional connectivity approaches utilizing the fMRI information. Finally, an attention-based LSTM deep-learning model is employed to decipher these distinct EEG oscillations during memory retrieval and learning engagement. LSTM and attention-based LSTM frameworks are independently trained to classify intelligence-correlated EEG oscillations. The results revealed significantly stronger correlation of fluid intelligence with frontal-alpha (r=0.40), frontal-theta (r=0.45), parietal-theta (r=0.49), parietal-beta (r=-0.42) and parietal-delta (r=-0.45) oscillation during feedback learning, and frontal-delta (r=-0.44) and parietal-alpha (r=0.44) oscillations during memory retrieval phase. Further, the multi-frequency interaction revealed a significant influence of frontal-theta, frontal-alpha, parietal-delta, and parietal-beta oscillations elicited during feedback learning on the subsequently engaged memory retrieval's cortical oscillations. EEG-informed fMRI and functional-connectivity results revealed strong frontal-parietal engagement. The proposed attention-based LSTM framework classified these identified EEG engagements of feedback learning and memory retrieval with classification accuracy (memory retrieval: 87%, feedback learning:

83%) against the traditional LSTM model (memory retrieval: 85%, feedback learning: 82%). In conclusion, the multi-frequency cortical engagement caused by frontal-parietal interaction of intelligence associated feedback learning and memory retrieval successfully employed the attention-based LSTM framework for classifying them.

4.2 INTRODUCTION

Developing a computational framework that decodes human adaptability to cognitive tasks is a long-standing challenge in computational neuroscience, functional neuroimaging, and physiology. Deciphering unique cortical EEG oscillations and their mutual interaction that explains neural mechanisms associated with the individual's adaptation to the cognitive tasks plays a significant role in realizing this framework. Human adaptation to any job is immensely associated with learning from previously experienced actions and retrieving them from memories. Further, several studies [1–3] have also observed a strong association of individuals' learning abilities with their fluid intelligence deduce, and solve problems. Hence, deciphering the cortical EEG oscillations that associate a person's fluid intelligence with their learning and memory mechanisms will be immensely useful in developing this next-generation, high-order cognitive brain-computer interface. However, significantly less knowledge exists on how distinct cortical engagement is associated with fluid intelligence and relates to the learning and memory retrieval mechanisms. Hence, the present study aims to develop a deep learning-based computational model to decode the cortical EEG oscillations that associate individuals' fluid intelligence with their learning mechanisms during performance feedback and subsequent memory retrieval.

4.2.1 Fluid Intelligence, learning, and associated cortical neural oscillations

Many researchers have recently observed fluid intelligence as a strong predictor of learning capacity and memory retrievals [3–5]. Further, there is ample evidence that fluid intelligence is an essential aspect of intelligence, reflecting the brain's elementary information processing in solving new and unfamiliar problems [6,7]. In addition, several studies [8–11] have observed the influence of fluid intelligence on working memory mechanisms and their improvement after working memory training [12,13]. Primi and

colleagues [3] investigated the association of fluid intelligence with inter-individual differences and revealed the underlying correlated intelligence and learning mechanism. Mainly, P300, the ERP signature of information processing that arises from distant cortical communication emanating from frontoparietal regions of the brain, was investigated [14] for individual variation in intelligence, cognitive information processing, and working memory. Roslan and colleagues [15] studied the role of EEG delta and beta neural oscillations as neural signatures for fluid intelligence as assessed by the RAVEN psychological test. The results revealed significantly higher cortical communications through the delta band and higher prefrontal brain's localized processing through the beta band than the resting state. In addition, the engagement of the fluid intelligence test significantly elevates theta–gamma coupling in frontal brain areas due to the elevated local neural processing [16].

4.2.2 Declarative Memory mechanisms and associated cortical neural oscillations

Declarative memory, a type of explicit long-term memory, plays an essential role in recollecting facts, events, and experiences consciously and seen engaged in memory processes [17,18]. Neuroimaging studies strongly support the medial temporal lobe (MTL) role in declarative memory retrieval tasks [19–21]. Several studies [22,23] provided new insight into the MTL-prefrontal interactions to integrate new memories into pre-existing knowledge during declarative memory. Generally, declarative memory learning happens quickly with very few presentations of the stimulus. This process depends on explicit knowledge, conscious awareness, and implicit knowledge of the stimulus [24–26]. Therefore, retrieving previously encoded memory is not generally known to engage higher-order cognitive functional regions such as prefrontal and medial frontal brain regions. In addition to analyzing the neuronal engagement subprocesses, time-frequency analysis using EEG information has proven helpful in understanding cortical communications of distant brain regions during various cognitive tasks. Perhaps the most consistently reported oscillatory component elicited during memory retrieval is theta band activity [27–30]. A recent study [31] provides compelling evidence of binding the hippocampus, PFC, and striatum with the theta and alpha oscillations during successful recollection.

Further, many investigations revealed the role of theta and gamma oscillations during encoding and retrieval across multiple forms of memory and brain regions [32]. Specifically, theta-gamma coupling elicitates after successful memory recall [33] and gamma power increment across the medial temporal lobe observed during memory encoding [34]. Analogous to enhancing theta/gamma powers at medial temporal and frontal sites, gamma boost in occipital and parietal regions was also observed for subsequently remembered items [35]. Further efforts to understand the role of feedback learning during memory task engagement, electrophysiological studies [36–39] have suggested the role of beta power in reward-related feedback over frontal regions of the brain and successful memory encoding. Neuroimaging studies [40–43] on learning from feedback has also revealed the recruitment of multiple brain regions, such as the medial temporal lobe, limbic, striatum, and frontal cortex. EEG informed fMRI brings more insight into the functional origin of EEG powers. It brings insights into the association of synchronization/desynchronization of BOLD signals with modulation in EEG frequency oscillation. However, despite these works, neural mechanisms and multifrequency cortical communication associated with fluid intelligence and their modulation during learning and subsequent memory retrieval is not fully understood.

4.2.3 Recurrent deep learning approaches for classifying EEG information

Recurrent Neural networks (RNN) have been better in extracting time and frequency domain features from the EEG signals for decoding the high-dimensional EEG information. Their capability to model time-series sequential data depending on the previous information permits explaining the task engagements and associated cognitive mechanisms. However, the traditional RNN system suffers with vanishing/exploding gradient problems. The Long Short-Term Memory (LSTM) architecture alleviates the vanishing gradient problem due to longer dependencies. These LSTM layers have reflected the ability to selectively remember important information for a more extended period in sequence prediction. The LSTM model has also been used by exploiting a wide range of features extracted prior to classification. It has been seen that there exists a significant increase in seizure prediction performance [44]. Further, the rhythm-specific multi-channel convolutional neural

network (CNN) based approach for automated emotion recognition using multi-channel EEG signals is used by utilizing the frequency domain features for automated emotion recognition applications [45], and EEG-channel correlation based emotion recognition model [46]. Similarly, [47] utilized LSTM recurrent neural networks, extracted time-frequency domain features of EEG signals and obtained improved classification performance. Several studies [48–54] revealed the usage of deep learning based approaches for EEG classification and established the role of EEG signals for better performance, detection and prediction. The attention mechanism was introduced [55] to highlight the more informative feature, give higher weights to the corresponding original feature sequence, and improve deep learning performance. Further, the hybrid attention-LSTM architecture [56–66] observed significantly improved efficiency and performance accuracy in several recent EEG studies.

4.2.4 Present Study

The present work aims to understand neural mechanisms and distinct cortical oscillations associated with fluid intelligence, learning and memory retrieval through EEG multifrequency interaction, hemodynamic functional connectivity, and EEG informed fMRI measures. The EEG informed fMRI and hemodynamic functional connectivity approaches bring more neuro mechanisms insights and functional interactions of the cortical regions [67–69]. During the experiments, participants engaged in three distinct phases, they are the memory encoding phase (memorizing the specific sets of objects), memory retrieval (retrieving earlier encoded objects from many other object collections) and performance feedback learning phase (informs about the correctness of their earlier memory retrieval engagement). As the study aims to understand how neural mechanisms associated with fluid intelligence influence individuals' learning and memory retrieval, it first acquired simultaneous EEG-fMRI information during the engagement of memory encoding, retrieval, and feedback learning phases and subject to the estimation of significant elicitation of frontoparietal EEG oscillations between 200-600 milliseconds since memory retrieval and subsequent learning mechanism's onset and their correlates with the individual's fluid intelligence measured through Raven Progressive Matrices test. Further, these intelligence-associated frequency powers of memory retrieval and subsequent

learning mechanisms are subjected to robust correlational analysis to understand their multifrequency cortical interaction across frontoparietal regions. Then, the study employed simultaneously acquired fMRI information to estimate the elicitation of distinct cortical communication between distant and distinct brain regions using graph-theoretical based hemodynamic functional connectivity analysis and EEG informed fMRI measures.

Finally, an attention-based LSTM deep-learning model classified the deciphered distinct EEG oscillations that elicit encoded objects' learning and memory retrieval against the engagement of distractors. For this purpose, two different deep learning architectures (traditional LSTM and attention-based LSTM networks) are independently trained to classify the engagement of memory retrieval and feedback learning. The intelligence-correlated EEG oscillations were passed as input to the respective input cells of the first LSTM layer. Both LSTM and attention-based LSTM deeply layered architectures possessed three stacked LSTM layers. The attention layers are coupled with the final LSTM layer in the attention-based LSTM network. The performance of both deep learning architectures is measured using metrics such as precision, accuracy, and recall. Finally, the proposed deep learning architecture is validated by employing a 10-fold cross-validation approach.

4.3 MATERIALS AND METHODS

4.3.1 Participants and procedure

In the experiment, a total of thirty-five healthy right-handed volunteers (17 males and 18 females, aged 20-32 years, mean age: 24 years) underwent a feedback declarative memory task experiment. None of the volunteers had any history of psychiatric, neurological disorders or was using any medication. The participants who took part in the study were not involved in any training session before the experiment and learnt tasks during the investigation without prior experience. All participants gave written informed consent. The experiment strictly followed the World Medical Association (Declaration of Helsinki), and the local ethical committee approved all measurements. The vision of participants was corrected using MR-compatible lenses whenever required.

4.3.2 Behavioral Task

As the present aims to understand the influence of individuals fluid intelligence on their feedback learning and memory retrieval, it employed the Raven Progressive Matrices (RPM) test [70], which studies the influence of genetic and environmental aspects on intelligence by measuring the brain's non-verbal, abstract, and cognitive functioning. The test is presented to volunteer in its standardized format, comprises five sets (A to E) of 12 items each, with objects within a set becoming increasingly complex, requiring the ever-greater cognitive capacity to encode and analyze information. All items are in black ink on a white background. A series of pictures are linked together by a specific dependency, and one figure is missing in that series. The job is to establish the pattern linking all the figures in one, indicating the desired form among the proposed options and the answer gap among six other figures. The questions and answers are all completely non-verbal.

4.3.3 Task design

As used in several previous studies, the present study employs a declarative memory task paradigm [71], where participants engaged in three distinct phases. They are the memory encoding phase (memorizing the specific sets of objects), memory retrieval (retrieving earlier encoded objects from many other object collections) and performance feedback learning phase (informs about the correctness of their earlier memory retrieval engagement). During the encoding phase, the collections of simple geometrical shapes like square, circle, rectangle, triangle, primary colours with images of basic objects like a book, table, cup, and car were presented to the volunteers. Each trial started with presenting fifty stimuli in a randomly intermixed manner for 60 seconds. During the presentation of stimuli in the encoding phase, the volunteers were instructed for 'no motor response' and memorized the objects and images for retrieval in the subsequent memory retrieval task. The retrieval session is done after 10 minutes of the encoding session.

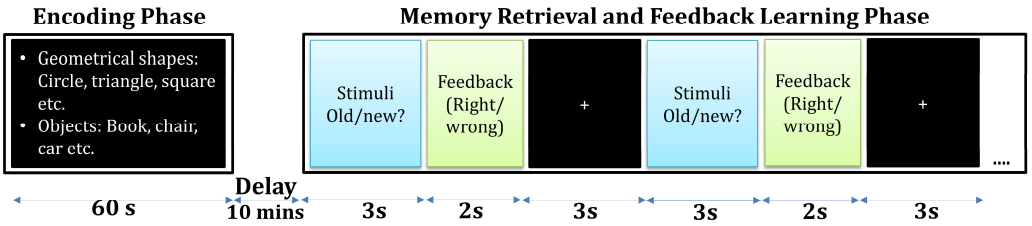

Figure 4.1: A sample experimental design of the feedback declarative memory task. The participants had to retrieve the previously encoded object in the task's retrieval phase within 3000 ms. Feedback (Right/Wrong) based on their performance was provided for 2000 ms after each stimulus during the feedback slide. The participant had to detect, learn, and adjust to these changes based on provided feedback during the task. Memory retrieval and feedback learning phases are demonstrated in the figure using blue and green blocks, respectively.

Figure 4.1 shows the task paradigm used in the experiments. The retrieval phase consisted of a recall task, where we presented the slides consisting of previously shown stimuli intermixed with new geometrical shapes and objects (distractor) to volunteer one item at a time for 3 seconds. The volunteer's task was to retrieve the memorized (encoded earlier) stimuli and respond upon recognition with a right thumb button press. Once the volunteer responded to the memory retrieval question, visual performance feedback (Right/Wrong) was given for 2 seconds during the feedback block. The performance feedback indicates the correctness of their memory retrieval response and allows the volunteers to learn from it. We also notify all the volunteers to avoid any motor response during feedback. In the study, visual feedback is given after each memory retrieval to assess its effect on their performance [72]. A fixation block was presented with a single cross in the center for 3 seconds after each feedback block. The study uses a mixed paradigm design composed of five trials consisting of different encoding and retrieval phases, with each trial consists of 21 sub-trials of memory retrievals. Among the stimuli slides presented in the experiment, 32 slides presented the geometrical shapes as stimuli and the rest as simple objects. All these task stimuli were projected onto MR compatible lenses fitted on the head coil inside MR.

4.3.4 Data acquisition with Simultaneous EEG-fMRI

The EEG data possess a much higher temporal resolution but heavily lags in spatial resolutions. On the other hand, fMRI data possess superior special resolution but lags in temporal resolutions. Hence, the integrated simultaneously acquired EEG-fMRI

information possesses both higher spatial and temporal resolutions. Hence, the present study employed multi-model data acquisition, simultaneous EEG-fMRI data acquisition to understand the neural mechanisms associated with fluid intelligence, learning, and memory retrieval. MR compatible 32-channel Brain Amp system with a cap containing 32 Ag/AgCl non-magnetic electrodes acquired EEG signal in 3T Siemens Magnetom Skyra scanner (Siemens, Erlangen). A dedicated electrode for referencing is placed close to the Cz position, between Fz and Cz, and the ground electrode is placed between Cz and Pz. One additional electrode for electrocardiogram (ECG) recording is placed on the volunteer's back. The impedance of all scalp electrodes was below five kOhms throughout the data acquisition, and EEG signals were recorded at a sampling rate of 5 kHz.

The functional images were acquired using Eco Planar Imaging (EPI) sequence with TR =3000 ms; TE= 36 ms; voxel size =3.6*3.6*3.0 mm; matrix =64*64; FoV read = 230 mm; flip angle =90^{o}, 36 axial slices. The axial slices are acquired parallel to the Anterior-Posterior (AC-PC) line in an interleaving manner with a slice thickness of 3.0 mm. The start of each trial synchronized with the acquisition of the functional MRI acquisition. The high-resolution structural images of the brain are acquired using T1 MPRAGE sequence with parameters, voxel size =1.0*1.0*1.0 mm; TR= 2000 ms; flip angle = 90^{o}; FoV = 240 mm; matrix= 512*512; slice thickness = 1.0 mm, 160 axial slices. The axial slices are acquired parallel to the Anterior-Posterior (AC-PC) line in an interleaving manner with a slice thickness of 5.0 mm.

4.3.5 Pre-processing steps

4.3.5.1 MR and traditional artifact removal in EEG data

The EEG data acquired simultaneously inside the MRI scanner is pre-processed using FMRIB (EEGLAB) plugin to remove MR-related gradient artifacts and cardio ballistic artifacts. For this, MR artifact removal used FASTR (FMRI Artifact Slice Template Removal) tool [73,74]. It aligned all the slice artifacts to correct any slight jitter in the slice-timing events' exact location, interpolated the data, and then shifted each artifact until the correlation between data and a reference artifact (the first artifact in the data) was maximized. The second stage of FASTR [75] computed an

average template for the artifact and then subtracted it from the centre contaminated data by taking a moving window average of slice artifacts. QRS detection used combined adaptive thresholding [76] and the Teager energy operator [77], followed by a correction algorithm. This algorithm aligned all events and corrected for false positives and negatives. The removal of pulse artifacts used QRS events to subtract an artifact template from the data using an optimal basis set for the number of PCs 3.

Subsequently, the study employed the Harvard Automated Processing Pipeline for EEG (HAPPE) [78] processes to conduct noise-free time-frequency analyses using EEGLAB (MathWorks). HAPPE is designed for data with high levels of an artifact or concise recording length, and it integrates with the EEGLAB functions. The MR and CB artifact corrected EEG data are subjected to the 0.1 Hz high pass and 57 Hz low pass filtering. Further, all the EEG channels were selected for ICA decomposition. The electrical noise from EEG is then removed using the Clean Line program through the multi-taper regression approach implemented in EEGLAB. The bad channels were identified by evaluating the normed joint probability of the average log power of all the selected channels and removed for the probability of more than three standard deviations from the mean for further analyses. A wavelet-enhanced ICA (W-ICA) approach removed the eye and muscle-generated artifacts, high-amplitude artifacts, and signal discontinuities from EEG data. This approach of W-ICA followed by ICA improved the resulting ICA decomposition of the EEG data [79].

Further, a machine-learning algorithm MARA (Multiple Artifact Rejection Algorithm) [80] evaluated the ICA-derived components for automated component rejection. MARA algorithm assigned the component a probability as the percent of artifact contamination estimated to be in the component and automatically rejects any components with artifact probabilities greater than 0.5. Further, artifact rejected data is segmented based on event markers. The artifact-corrected data were subsequently re-referenced to the common average reference and band-pass filtered from 1 Hz to 48 Hz ((1-4) Hz for delta, (4–8) Hz for theta, (9–14) Hz for an alpha, (15-35) Hz for beta and (35-48) Hz for gamma)). The filtered data of all the participants are then segregated specific to the feedback learning, memory retrievals, and distractor blocks.

4.3.5.2 Artifact removal in fMRI data

All subject task fMRI data are pre-processed using the standard artifact removal pipeline of Statistical Parametric Mapping (SPM 12): slice-time correction, realignment, co-registration, normalization, and smoothing. The slice-time correction was performed on slice-timing differences due to slice acquisition delays and spatially realigned. Movement parameters are assessed for each participant, and participants are excluded if head movement exceeds 3 mm, followed by registering the functional scans to standard MNI template space. The pre-processed images are subjected for spatially smoothing with 5*5*5 mm full width half maximum Gaussian kernel.

4.3.6 Data Analysis

The present work employs an attention-LSTM based deep-learning model to decode the cortical EEG oscillations that associate individuals' fluid intelligence with their learning mechanisms during performance feedback and subsequent memory retrieval. For this purpose, individuals' fluid intelligence is subjected to the robust correlation analysis with the spectrally-decomposed multiple EEG powers of feedback learning and subsequent memory retrieval. The role of fluid intelligence in associating feedback learning and subsequent memory retrieval phases is then estimated by multifrequency correlational analysis using a robust correlation approach. Identified intelligence correlated-EEG powers are subjected to the EEG-informed fMRI and functional connectivity analyses to estimate their local and global neural engagements. Finally, these intelligence-correlated EEG powers are used as input to train and test the attention-based Deep-learning system. Figure 4.2 explains these processes in detail. The following section will elaborate on each one of these steps in detail.

4.3.6.1 Estimating the association of intelligence with cortical oscillations during feedback learning and memory retrieval of encoded objects

The study used a specifically designed processing pipeline to identify the task's multifrequency EEG information associated with the individual's fluid intelligence. It extracts the task's timing information using time-frequency analysis, uses that for subsequent spectral composition analysis followed by the robust correlation analysis between multiple EEG powers and fluid intelligence scores. The following sections explain each one of the steps in detail.

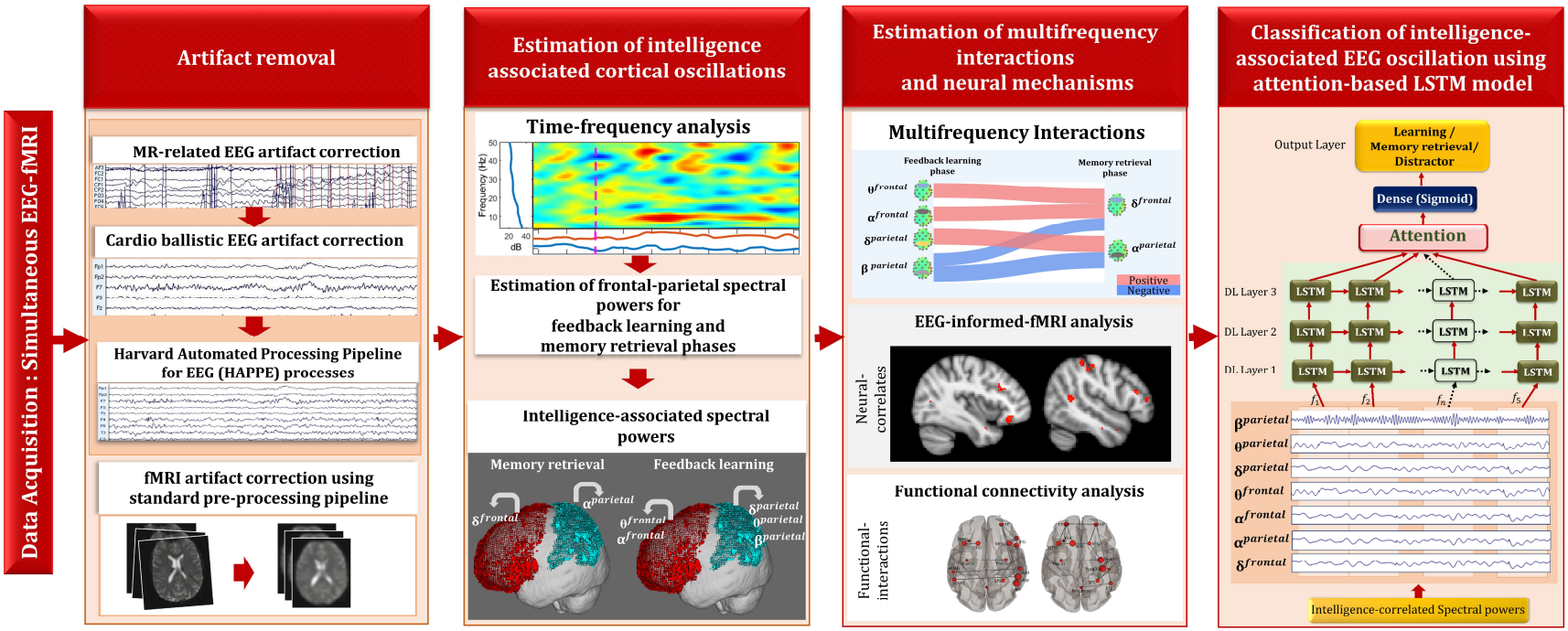

Figure 4.2: Schematic picture explains methodology employed in the study.

Time-Frequency analysis

The study assesses the spectral EEG activity corresponding to the declarative memory task's memory retrieval and feedback learning phases. It estimates event-related spectral perturbations (ERSP) implemented in EEGLAB [81]. The time-frequency analysis is performed using Morlet wavelets for the epoch of 2 seconds (-500 ms to 1500 ms post retrieval/feedback). For this, all trials corresponding to the memory retrieval are subjected to the baseline correction (−500 to 0 ms) and then grouped. The study computes mean event-related changes in the epoch's spectral power for the studied frequencies (1-4 Hz: delta, 4–8Hz: theta, 9–14 Hz: alpha, 15-35 Hz: beta, 36-48Hz: gamma) for frontal (Fz, F3, F4) and parietal (Pz, P3, P4) channels with a bootstrap significance level of $p < 0.01$. The study evaluates time-frequency curves for all the participants and calculates mean ERSP. The averaged oscillatory activity of feedback and memory retrieval for the defined period is used to identify each frequency's power distribution over the temporal scale for further spectral decomposition.

Robust correlation analysis

The study aims to understand the neural mechanisms on how intelligence associates with feedback learning and memory retrieval and then aims to employ the deep learning approaches to classify them from the rest of the distractors. Hence, it first employs robust correlation analysis [82] to identify the distinct cortical oscillations that elicit during feedback learning and memory retrieval and significantly correlates with individual intelligence scores, measured from Raven's Progressive Matrices Test. The selection of most discriminative features in a study [83] from the segmented time–frequency plane have shown an average classification accuracy and capable of handling inter-subject variability while constructing brain–computer interfaces. For this purpose, based on the time-frequency observations, the cortical EEG oscillations elicited between 200-600 milliseconds, post-feedback/memory retrieval is extracted, and their frequency information was passed on for robust correlation analysis with fluid intelligence scores as mentioned below.

$$\Gamma_{I,R} = \{\text{Robust Correlation } \left(I(i), R_{(r)}(i)\right);\ i = 1 \text{ to } n, r = 1{:}\, m\} \quad (1)$$

$$\Gamma_{I,FB} = \{\text{Robust Correlation } \left(I(i)\,, FB_{(r)}(i)\right);\ i = 1 \text{ to } n, r = 1{:}\, m\} \quad (2)$$

Here, $\Gamma_{I,FB}, \Gamma_{I,R}$ are the correlation maps of feedback and memory retrieval phase, respectively, and $I(i)$ is the intelligence score of i^{th} volunteers. $R_{(r)}(i)$ and $FB_{(r)}$ are frequency measures of the i^{th} volunteer's memory retrieval and feedback block, respectively. The m and n are numbers of frequency powers (delta, theta, alpha, beta, gamma) and the number of volunteers, respectively.

4.3.6.2 Multifrequency interaction analysis for estimating the effect of feedback learning on subsequent memory retrieval

Every learning process leaves an impact on the subsequently engaged task, particularly the memory retrieval mechanism. In the present study, modulation on the memory retrieval mechanism caused by the earlier learning is estimated by associating the multifrequency elicitation of the learning phase with the subsequent memory retrieval mechanisms. For this purpose, intelligence correlated EEG powers are extracted for the duration of 200-600 ms of feedback learning/memory retrieval phases and then subjected to robust correlation analysis.

$$\Gamma_{FB,MR} = \{\text{Robust Correlation } \left(FB_{(EEG_Power)}(i)\,, MR_{(EEG_Power)}(i)\right);\ i = 1 \text{ to } n\} \quad (3)$$

where $\Gamma_{FB,MR}$ are the correlation map, $FB_{(EEG_Power)}(i)$ is the intelligence-correlated EEG power of the feedback learning phase and $MR_{(EEG_Power)}(i)$is the intelligence-correlated EEG power of the i^{th} volunteer's memory retrieval phase. The n is the number of volunteers.

4.3.6.3 Neural mechanisms underlying intelligence-correlated cortical oscillations

Further, the present study estimates the neural mechanisms associated with the multifrequency elicitations during the learning and memory retrieval phase through EEG-informed fMRI and graph theory-based functional connectivity approaches. The following sections explain each one of the steps in detail.

EEG Informed fMRI analysis: Neural sources of intelligence-correlated EEG powers

The study carried out the regional inferences, neural sources of intelligence-correlated EEG powers through the EEG-informed-fMRI approach. First, separate EEG regressors are segregated and normalized from the observed frequency bands (intelligence-associated). Normalized EEG powers as regressors are introduced as parametric modulators in the GLM design matrix for feedback learning and memory retrievals. In the GLM framework, we model BOLD responses (associated with feedback learning and memory retrievals) by a canonical HRF with temporal and dispersion derivatives. In first-level analysis, the EEG regressors and the six realignment parameters for each run are subjected to a general linear model (GLM). Subsequently, these first-level contrast images are subjected to group-level random-effects analysis using a robust regression toolbox [84]. The robust regression toolbox uses robust iteratively reweighted least squares (IRLS) to identify and down-weight potential outliers that can cause an increase in false positives and false negatives. Effects are reported as significant for fMRI analyses using at the $p(FDR)<0.05$ at cluster level.

Hemodynamic functional connectivity: Functional interactions among intelligence-correlated EEG power's neural sources

The hemodynamic functional connectivity estimation better analyses local and global functional neural interaction mechanisms underlying the intelligence-correlated EEG powers. For this, the analysis utilizes EEG-informed-fMRI estimated neural correlates by selecting them as 'regions of interest' (ROI) and evaluates the graph theory-based functional connectivity measures using the CONN toolbox [85]. The Graph theory analysis has been employed in several functional connectivity studies to map the brain's connectivity patterns using local and global interactions [86–89]. In our work, all the selected ROIs from each neural correlate were determined as a seed ROI, one at a time. It takes the seed's BOLD time course signal to reference correlations and finds any correlation with other ROIs' BOLD time course signal. For ROI-to-ROI analysis, a threshold of $p \leq 0.001$ was used for bidirectional explorations of connectivity (i.e., positive and negative associations). The functional connectivity

maps ('ROI to ROI') of all ROI's were derived using Fisher's r-to-z transformation. The group-level functional connectivity maps were FDR corrected for multiple comparisons ($p < 0.05$). The ROI-to-ROI analysis has also been used for many other functional connectivity studies [90]. Further, graph theory measures (global efficiency and cost) were estimated for each ROI and threshold at p-FDR<0.05 in a two-sided analysis using the CONN toolbox.

4.3.6.4 Classifying elicitations of intelligence-associated EEG oscillations using attention-based LSTM model

The present study's core focus is developing deep-learning-based computational models to classify the engagement of intelligence-associated learning and memory retrieval from distractors. For this, a feature vector consisting of intelligence-correlated normalized EEG powers belonging to every task engagement is formed and further utilized as input information to train deep learning-based models to classify each of those task engagements.

The attention-based deep learning model for classification:

Our work used an attention-based Long Short-Term Memory (LSTM) model to classify the cortical elicitations of feedback learning and memory retrieval associated with fluid intelligence. LSTM is a recurrent neural network proposed by [91] to learn sequential features in time series data. Recently, it has been successfully employed for classifying time-dependent bio-signal, together with EEG information [92,93]. For further improvements, attention-mechanism [55] has been proposed and integrated with the LSTM networks. This integrated framework is found more suited for the classification of time-dependent EEG signals. The following subsection describes the architecture of an LSTM cell and the attention mechanism used in this study.

LSTM Architecture

LSTM addresses the vanishing and exploding gradient problems by learning both long- and short-term dependencies. It consists of interconnected cells that retain memory information to evaluate the output by processing the input data. The input information flows through the input (i_t) and the forget gate (f_t) initially. It also

enables the network to keep or erase the earlier memory information (C_{t-1}) or update them with currently learned information (C_t). Further, each cell's result is modulated by an output gate (o_t), which lets the cell compute its output based on the updated information. The function of LSTM cell architecture is presented as:

$$i_t = \sigma(W_i \,.\, [h_{t-1}, x_t] + b_i) \tag{4}$$

$$f_t = \sigma(W_f \,.\, [h_{t-1}, x_t] + b_f) \tag{5}$$

$$C_t = f_t * C_{t-1} + i_t * \tanh(W_c \,.\, [h_{t-1}, x_t] + b_c) \tag{6}$$

$$o_t = \sigma(W_o \,.\, [h_{t-1}, x_t] + b_o) \tag{7}$$

$$h_t = o_t * \tanh(C_t) \tag{8}$$

where $\sigma(x) = \frac{1}{1+e^{-x}}$, $\tanh(x) = \frac{2}{1+e^{-2x}} - 1$. h_t, C_{t-1} and x_t are the hidden states, cell state and input passed to the architecture at step t. W_f, W_i, W_c, W_o are the weights, and b_f, b_i, b_c, b_o are the biases.

Attention mechanism:

Attention-mechanism integrated with LSTM concentrates on the most discriminative information and subsequently improves the ability of LSTM in EEG time series analysis. For achieving it, hidden output states are multiplied with the trainable weights and capture more discriminative task-related features. It can be expressed as:

$$h_i = \text{LSTM}(s_i), i \in [1, L] \tag{9}$$

where, h_i denotes the i^{th} LSTM cell's output hidden state vector corresponding to the i^{th} input, and L is the number of cells in each recurrent layer of the LSTM network. Further, the attention mechanism is defined as follows:

$$u_i = \tanh(W_s h_i + b_s) , \tag{10}$$

$$\alpha_i = \frac{exp(u_i)}{\sum_j exp(u_j)} , \tag{11}$$

$$v = \sum_i \alpha_i \, h_i \tag{12}$$

here vector v is the attention layer's output, and W_s and b_s are trainable parameters.

Utilizing the benefits of the attention-based LSTM framework, our study employed three deep learning layers in attention-based LSTM architecture. The final LSTM layer was followed by an attention layer, succeeded by a fully connected layer having a sigmoid activation function to predict the probability of each task engagement (feedback learning, memory retrieval, and distractors).

Validation approach

For validating the performance of the proposed deep learning model, the study used a 10-fold cross-validation approach. No overlap is reflected at each fold for the training and testing segments. Further, performance metrics are derived by True Positive (TP), True Negative (TN), False Negative (FN), and False Positive (FP). They were defined as:

$$\text{Accuracy} = \frac{(TP+TN)}{(TP+TN+FP+FN)},$$

$$\text{Precision} = \frac{(TP)}{(TP+FP)}, \text{ and } \text{Recall} = \frac{(TP)}{(TP+FN)}.$$

Where True Positive (TP) refers to the number of correctly classified samples in a specific class, False Negative (FN) refers to the number of samples belonging to a specific class which was misclassified as in other classes as and False Positive (FP) refers to the number of samples misclassified as in a specific class when they belong to other classes.

4.4 RESULTS

The present study aims to decode the cortical EEG oscillations that associate individuals' fluid intelligence with their learning during performance feedback and subsequent memory retrieval of encoded objects. For this purpose, the study employed a multi-modal approach that includes a multifrequency correlation analysis, EEG informed fMRI, and hemodynamic functional connectivity analysis to decipher the neural oscillations that elicit during feedback learning and memory retrieval mechanisms and associates with the individual intelligence. Subsequently, these intelligence-correlated EEG oscillations are passed as input in a hybrid, attention-based Long Short Time Memory framework to classify the cortical EEG oscillations that associate individuals' fluid intelligence with their learning and subsequent

memory retrieval of encoded objects from distractors. The following section explains the results of each of the above steps in detail.

4.4.1 Association of fluid intelligence with EEG oscillations that elicits during learning and memory retrieval of encoded objects

4.4.1.1 The time-frequency analysis

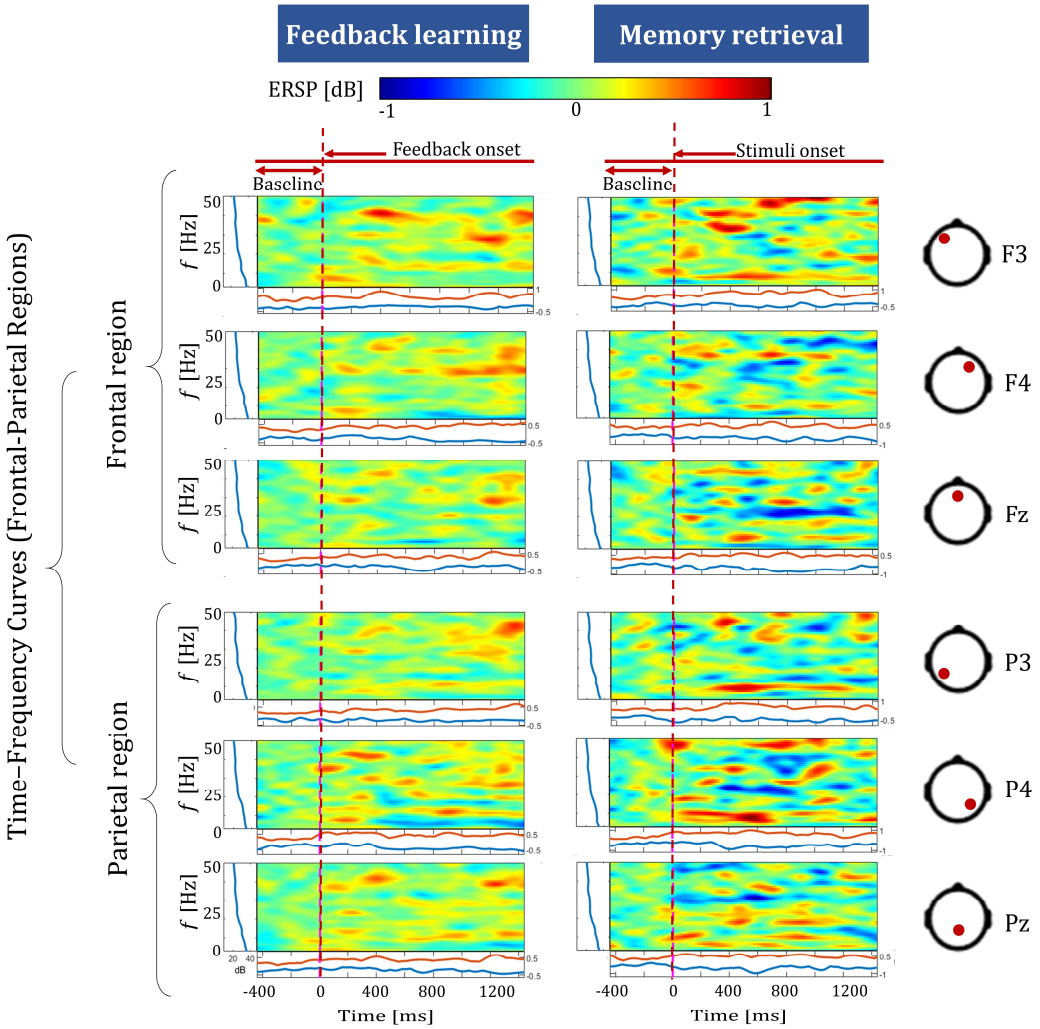

Figure 4.3: Time-frequency representation of the feedback learning and memory retrievals. The figure illustrates the grand average time-frequency plots of frequencies up to 50 Hz following feedback learning and memory retrieval blocks at frontal (F3, F4, Fz) and parietal (P3, P4, Pz) electrodes.

The study presents the time-locked (-500 to 1500 ms) EEG power spectra (1-48 Hz) for feedback and memory retrieval phases at frontal/parietal electrodes in Figure 4.3. The following sections present these results in detail.

Feedback learning phase

The EEG power spectra maps (Figure 4.3) illustrate the significant beta power after feedback onset at frontal-parietal electrodes (F3, F4, Fz, and Pz) for a 200 to 600 ms window. The study finds the feedback-associated frontal beta power, as observed in many previous studies [38,94]. The study also finds significant alpha at the frontal electrode (Fz) and theta power at the frontal-parietal (Fz, P3, Pz) in the same time window. The study also observes a decrease in delta power at the parietal electrode (Pz) for a 200 to 600 ms window.

Memory retrieval Phase

Figure 4.3 depicts event-related desynchronization in delta power at frontal (F3 and F4) and beta power at frontal-parietal (F3, F4, P4, and Pz) after memory retrieval onset (200 and 600 ms). The study observes theta power synchronization at frontal-parietal (F3, F4, P4, and Pz) and alpha powers at parietal electrodes (P3, Pz) in the same time window. Decrement of frontal-parietal beta and increment of theta powers has been associated with successful memory retrieval in various previous studies [95,96]. Some previous studies [97–99] observed the higher alpha activity for an increase in memory load.

4.4.1.2 Association of Fluid Intelligence

Figure 4.4 demonstrates the significant results of robust correlation analysis conducted between fluid intelligence and EEG powers of feedback learning and memory retrieval. For feedback learning phase, the study finds positive correlation between fluid intelligence scores and frontal alpha ($r= 0.40$, $p<0.05$), frontal theta ($r= 0.45$, $p<0.05$) and parietal theta powers ($r= 0.49$, $p<0.05$). However, the study shows a negative correlation between intelligence scores and parietal delta ($r=-0.45$, $p<0.05$), parietal beta ($r=-0.42$, $p<0.05$) powers of feedback.

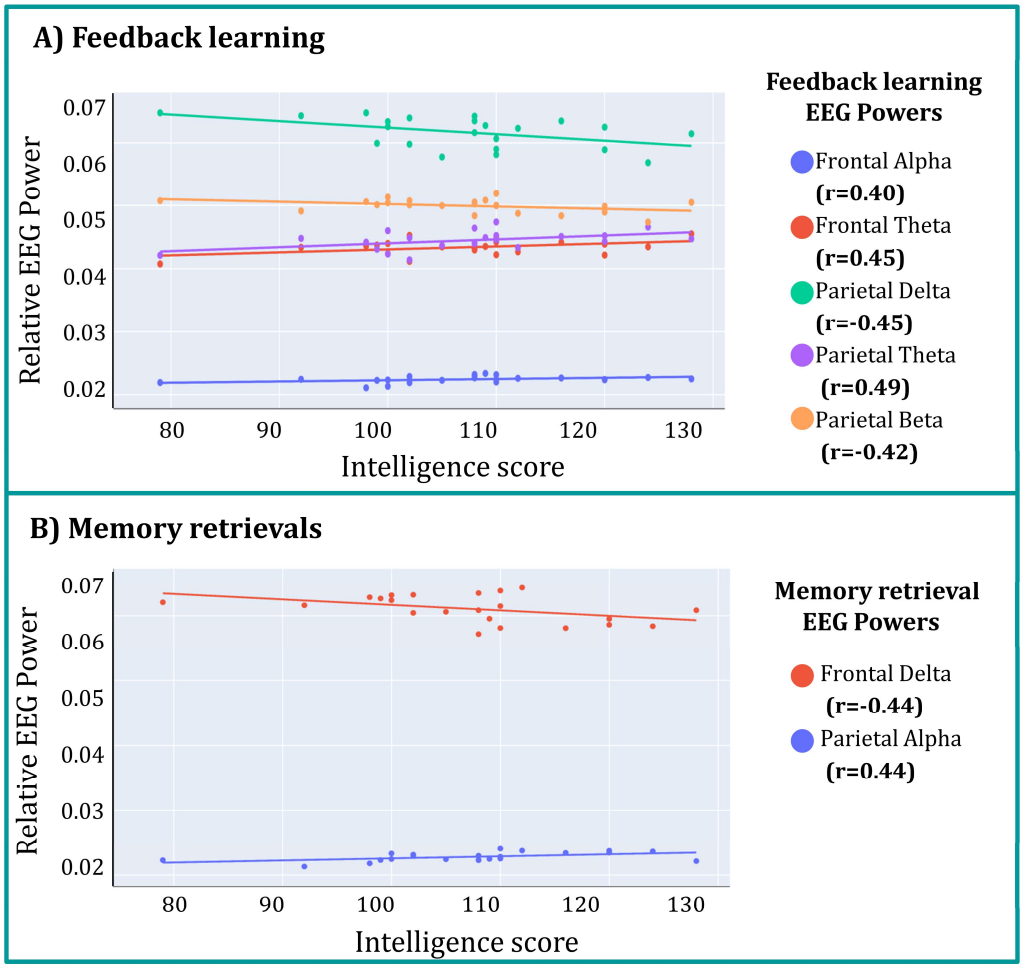

Figure 4.4: Correlation plot between intelligence and EEG power. The plot illustrates a significant correlation ($p<0.05$) between intelligence score (calculated from Raven Progressive Matrices, RPM Test) and relative EEG powers for feedback learning and memory retrieval phases.

The correlation results for the memory retrieval phase reveal a positive correlation between fluid intelligence and parietal alpha power ($r=0.44$, $p<0.05$), a negative with frontal delta power ($r=-0.44$, $p<0.05$). All above findings suggest the significant association of fluid intelligence with the frontal-parietal EEG powers of feedback learning and subsequent memory retrievals. The following sections will explore intelligence's role in associating learning with subsequent memory retrieval through multifrequency interactions. Subsequently, the neural mechanisms associated with these intelligence-correlated EEG powers will be explored and analyzed.

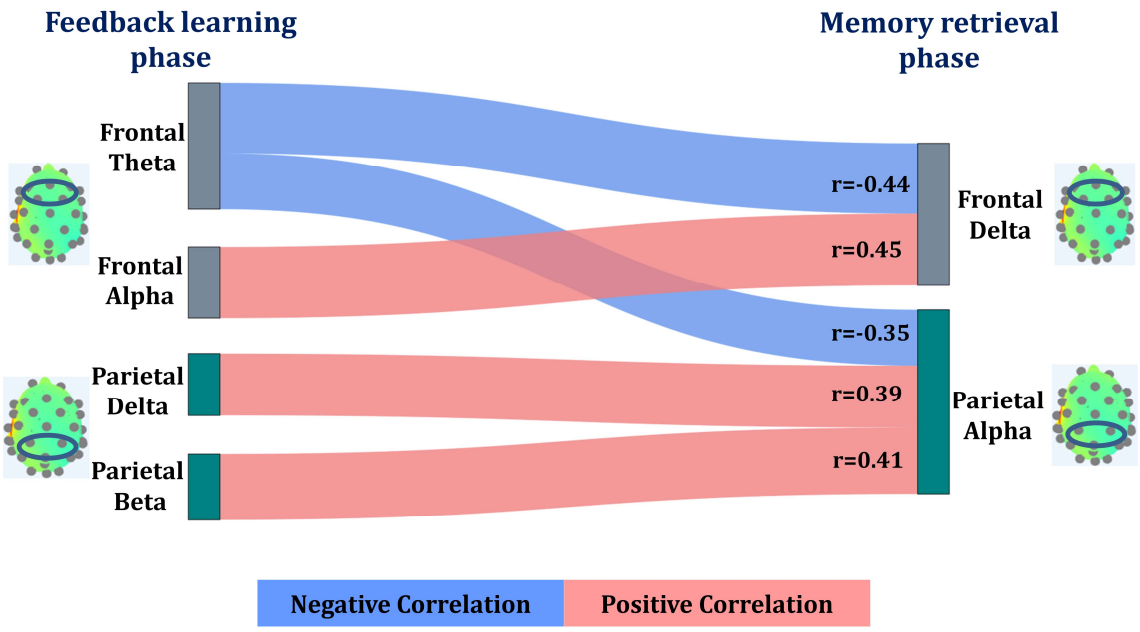

Figure 4.5: Multifrequency interactions between intelligence-associated EEG powers of feedback learning and subsequently engaged memory retrievals. Grey and green nodes represent EEG powers associated with the frontal and parietal channels, respectively. The flow's width is proportional to the correlation values at a significance level of $p<0.05$. The diagram illustrates the role of fluid intelligence in associating feedback learning to subsequent memory retrievals through multifrequency interactions of intelligence-correlated EEG powers.

4.4.2 Effect of intelligence and learning on subsequently engaged memory retrieval: Multifrequency interaction analysis

The findings of the robust correlation approach suggest a significant role of feedback learning in modulating the subsequent memory retrievals through the multifrequency interactions of intelligence-correlated EEG powers and illustrated in Figure 4.5. Specifically, the frontal delta power of memory retrieval is negatively correlated with the frontal theta (r=-0.44) and positively correlated with frontal alpha (r=0.45) of the feedback learning phase. Further, our interaction results emphasize that the parietal alpha power of memory retrieval positively correlates with the combined effect of parietal delta (r=0.39) and beta (r=0.41) and negatively with the frontal theta (r=-0.39) power of feedback, significantly. The role of frontal theta power has been suggested during the need for cognitive control in previous work [100]. It provided evidence that mid-frontal theta band activities for cognitive control. Hence, these findings reveal the

significant association of fluid intelligence in associating feedback learning to the subsequent memory retrieval oscillatory mechanisms.

4.4.3 Neural mechanisms underlying the intelligence-associated cortical oscillations

An in-depth understanding of neural mechanisms associated with the cortical oscillation used as neural signals in deep learning approaches facilitates better architectures design in neurocomputing. The present study aims to decipher one such multifrequency neural signal to classify encoded objects' intelligence-associated learning and memory retrieval mechanisms. However, few studies have presented how the distant cortical regions communicate during these cognitive engagements. Hence, the present study employs multi-model analysis that includes EEG-informed-fMRI and hemodynamic functional connectivity analysis to understand better the interaction among distinct and distant cortical regions involved during the feedback learning and memory retrieval of encoded objects. Additionally, supplementary figures (S:4.2 to S:4.6) demonstrate task-engaged functional connectivity during feedback learning and subsequent modulations in functional networks and the role of pre-frontal/striatum regions in modulating feedback-subsequent brain mechanisms.

4.4.3.1 EEG Informed fMRI analysis

Figures 4.6 and 4.7 and supplementary tables 4.1 and 4.2 present the EEG-informed-fMRI analysis results that explain the neurovascular insights of intelligence associated with EEG oscillations that elicit during the feedback learning and memory retrieval of encoded objects. In general, hemodynamic response, the BOLD signal in the frontal cortical regions synchronized with all the intelligence correlated cortical oscillations (frontal delta, frontal alpha, and parietal beta) elicited during the feedback phase. On the other hand, a large section of the parietal region's hemodynamic response is significantly desynchronized with the same intelligence correlated cortical oscillations. Similar frontal neuro-vascular synchronization and parietal neuro-vascular desynchronization are observed in the cortical oscillation associated with intelligence elicited during memory retrieval of encoded objects. The following

sections present a clear picture of the regions which revealed the above neurovascular synchronization/desynchronization.

Frontal and Parietal theta oscillation's neurovascular mechanisms during the feedback phase

Theta power elicited during the feedback phase significantly correlated positively with the BOLD signal in frontal cortical regions, particularly inferior ,middle and superior frontal gyrus (IFG,MFG,SFG), frontal pole (FP), frontal orbital cortex (FOC). On the other hand, frontal theta power correlates negatively with the BOLD of lingual gyrus (LG), precentral gyrus (PreCG), postcentral gyrus (PostCG), precuneus cortex (PC), and superior parietal lobule (SPL). Further, left-lateralized parietal theta power correlates positively with the BOLD signal of the frontal (MFG, IFG, FP) and some parietal regions (PreCG and POC).

Frontal alpha oscillation's neurovascular mechanisms during the feedback phase:

Our findings reveal that the frontal alpha of feedback correlates positively with frontal-parietal areas' BOLD activity. Specifically, a positive correlation is found for the BOLD signal of the MFG, SFG, IFG, FOC, SPL, AG, and supramarginal gyrus (SMG). However, frontal alpha power negatively correlates with the BOLD signal of FP and PC.

Parietal beta oscillation's neurovascular mechanisms during the feedback phase:

The parietal beta power positively correlates with the bold signal of the frontal (MFG, SFG, FP, and FOC) and parietal regions (PostCG, SMG, AG, and PC). Hence, our findings reveal the synchronization of the parietal beta power of feedback with the frontal-parietal region's BOLD activity.

Frontal delta and parietal alpha oscillation's neurovascular mechanisms during memory retrieval

The findings reveal the positive correlation of frontal delta power and BOLD signal of the FP, IFG, medial frontal cortex (FMC), PC, and negative correlation with the BOLD signal of MFG,

PostCG, and SPL. Further, EEG-informed-fMRI results reveal that lateralized parietal alpha power positively correlates with frontal regions' BOLD activity (SFG, FP, FMC) except MFG. Negative correlations are observed for parietal regions (PreCG, PC) except the SMG. Thus, results demonstrate that the frontal delta power and parietal alpha power of the memory retrieval phase positively correlate with the BOLD of frontal regions and negatively correlate with the parietal areas.

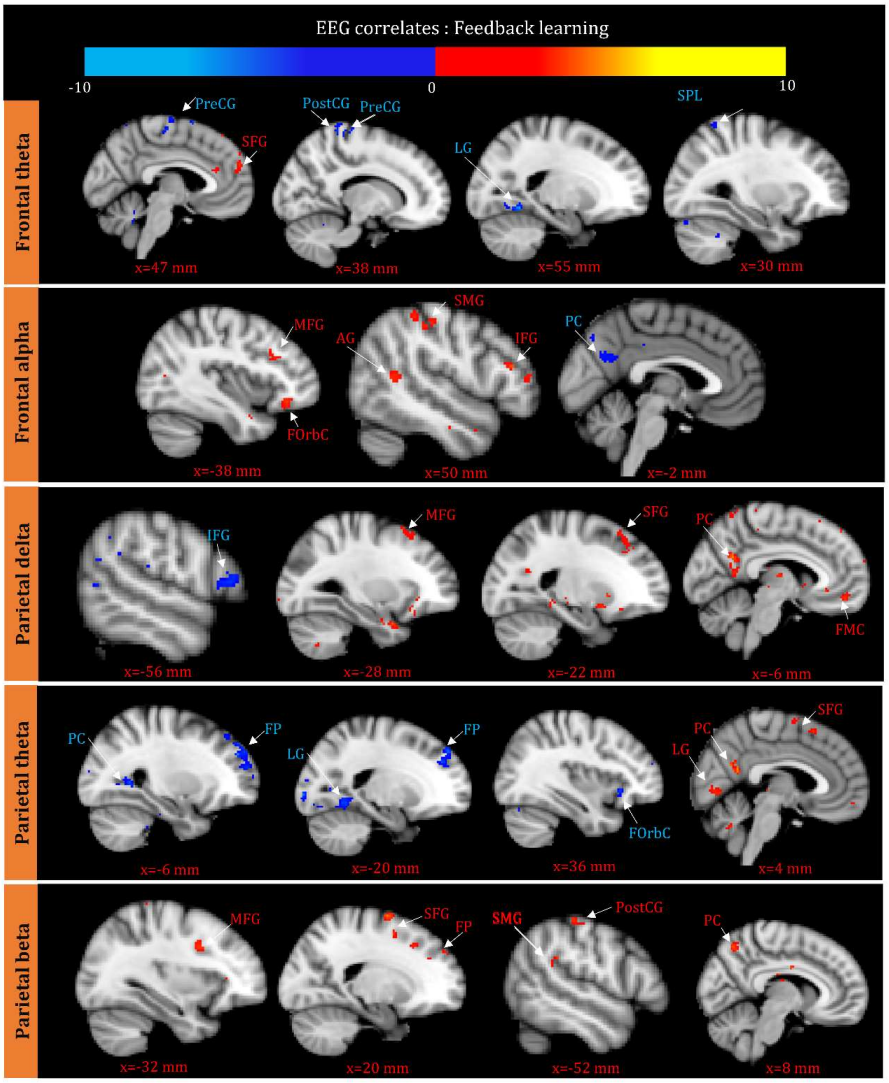

Figure 4.6: Neurovascular underpinnings of intelligence associated EEG powers of the feedback learning phase. SFG: Superior Frontal Gyrus, MFG: Medial Frontal Gyrus, IFG: Inferior Frontal Gyrus, PreCG: PreCentral Gyrus, PostCG: PostCentral Gyrus, SMG: Supramarginal Gyrus, AG: Angular Gyrus, LG: Lingual Gyrus, FP: Frontal Pole, SPL: Superior Parietal Lobule, FOrbC: Frontal Orbital Cortex, FMC: Frontal Medial Cortex, PC: Precuneus Cortex. Voxels in red to yellow and blue to aqua indicate a positive and negative correlation, respectively, for $p<0.05$.

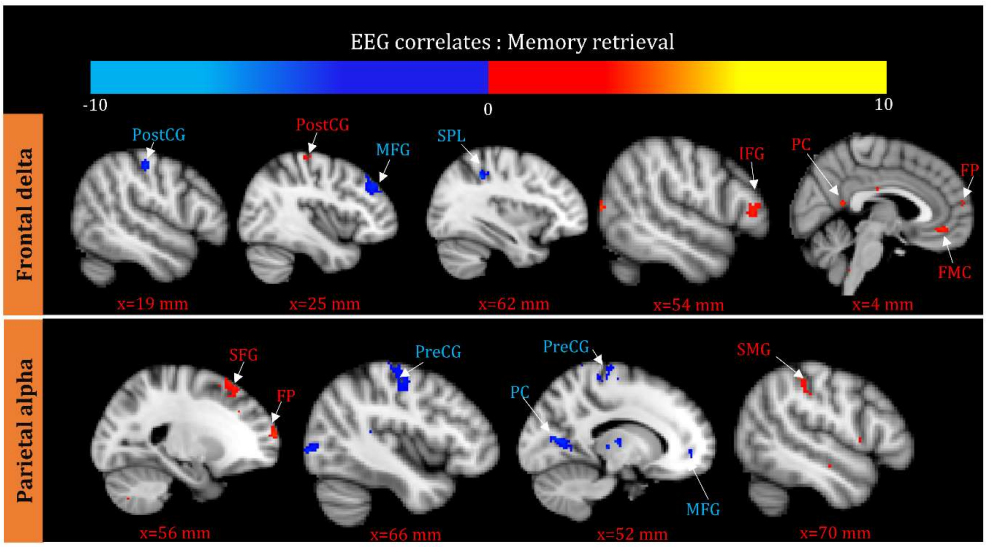

Figure 4.7: Neurovascular underpinnings of intelligence associated EEG powers of memory retrieval. Voxels in red to yellow and blue to aqua indicate a positive and negative correlation, respectively, for $p<0.05$.

4.4.3.2 Hemodynamic Functional Connectivity analysis

The neural mechanisms associated with the cortical EEG oscillations are better understood by clearly establishing their neural sources and functional interaction. The EEG informed fMRI results presented a clear picture of every neural source that caused the cortical EEG oscillation that associated an individual's intelligence with learning and memory retrieval. On the other hand, the functional connectivity analysis explains cortical communication between these neural sources. Figures 4.8 and supplementary figure 4.1 present hemodynamic functional connectivity analysis results and are explained in detail in the following section.

Feedback learning phase:

Our functional connectivity results show strong functional interactions of frontal and parietal regions during the feedback phase. Specifically, significant connectivity is observed for frontal theta power between the FP and AG (r=7.73), MFG and PreCG (r=4.58), MFG and POC (r=-6.61), FOC, and PC (r=-5.1), FOC and AG (r=-4.73), where r denotes correlation coefficient. The graph theory results (Figure 4.8 & supplementary figure) reveal the greater global efficiency and cost for the MFG, PreCG, and FP.

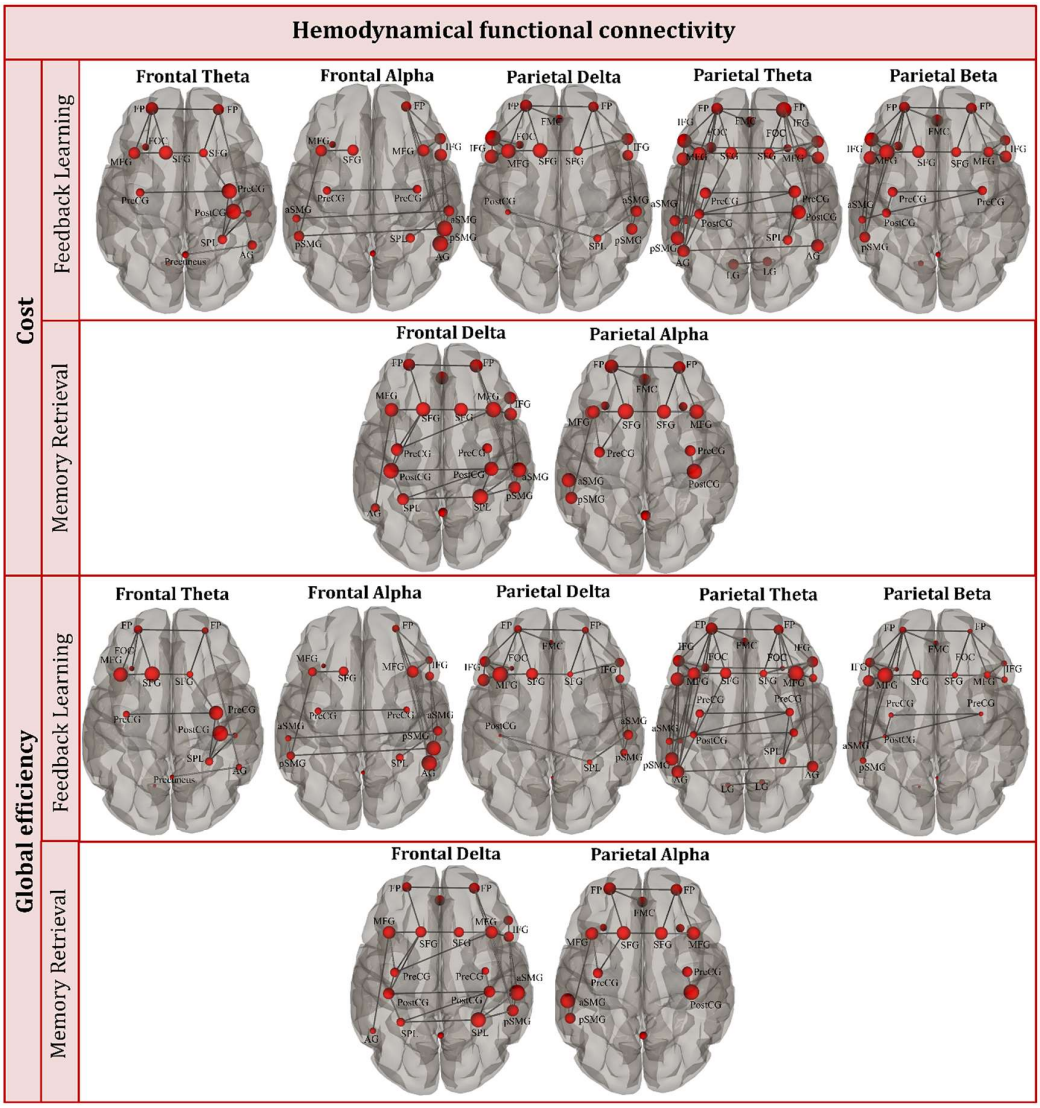

Figure 4.8: Neural sources of each cortical oscillation and their functional connectivity, estimated using graph theory analysis. The red circles represent the 'regions of interest' taken from neural sources of each cortical oscillatory power through EEG informed fMRI. Functional connectivity maps are represented based on estimated graph theory parameters (cost and global efficiency) for feedback learning and memory retrieval phases at a significance level $p<0.05$.

The higher value of these regions' graph theory parameters reflects integrative information processing [101]. Further, the functional connectivity for frontal alpha power finds significant correlations between MFG and posterior SMG (r=9.32), FP and posterior SMG (r=8.31), FP and AG (r=7.73), IFG and PC (r=-7.71). The graph theory results (Figure 4.8 & supplementary figure) reveal the greater global efficiency

and cost values for the AG, MFG, posterior SMG, SFG, and IFG. It is observed that the regions of higher graph theory parameters are also found to be significantly correlated in ROI-to-ROI connectivity. These findings indicate the lead role of these specific regions for frontal alpha-associated functional connectivity.

For parietal delta power, functional interactions show significant correlations of the FP (r=8.31), IFG (r=6.74), SFG (r=4.88), and FMC (r=-5.24) with posterior SMG, IFG with PC (r=-7.61). The graph theory results reveal the greater global efficiency and cost for the MFG, IFG, SFG, and posterior SMG. The study observes greater connectivity among frontal regions in specific. However, the posterior SMG is regarded as a central hub for frontal-parietal interactions. Subsequently, the parietal theta-associated functional connectivity finds significant correlations of the FP with AG (r=7.73) and PreCG (r=-4.26), MFG with posterior SMG (r=9.32) and AG (r=6.0), IFG with PreCG (r=4.78). The graph theory results reveal greater global efficiency and cost values for the MFG, IFG, SFG, FP, AG, and posterior SMG. For parietal beta power, the functional connectivity results find significant correlations of the MFG with posterior SMG (r=9.32) and PreCG (r=4.58), IFG with PC (r=-7.61), and anterior SMG (r=6.37). The graph theory findings reveal the greater global efficiency and cost for the MFG, IFG, SFG, posterior SMG, and PreCG. These frontal-parietal regions' higher graph theory parameters confirm the effective connectivity and more excellent integrated cognitive processing of frontal-parietal areas during feedback.

Similarly, graph theory analysis reveals a significantly lesser interaction of frontal-parietal regions. However, it observes higher graph theoretical measures for the PostCG, anterior SMG, SFG, and MFG.

Memory retrieval phase

The results for frontal delta power of memory retrieval find the significant functional connectivity of MFG (r=6.19) and IFG (r=4.55) with posterior SMG, MFG with SPL (r=4.63), and parietal interactions (PostCG with SPL (r=7.83) and anterior SMG (r=7.73)). The graph theory results highlight the greater global efficiency and cost values for the MFG, SPL, and SMG. Further, the parietal alpha-associated functional

connectivity does not find any interaction between the frontal and parietal regions. However, the study observes frontal-frontal (such as SFG and MFG (r=7.36), MFG and FP (r=4.93), and parietal-parietal (PreCG and PostCG (r=7.65)) interactions.

4.4.4 Attention-based deep learning model

In the present work, all the seven intelligence-correlated EEG powers having significant association with the task's neural mechanisms are further utilized as input information to train attention-based LSTM models. The study involved thirty-five volunteers while performing the feedback learning and subsequent memory retrieval task. The task paradigm consisted of 34 blocks of memory retrieval, 34 blocks of feedback learning, and 132 distractors blocks. More distractors are included to avoid the expectancy aspect of cognitive engagement. However, only 34 blocks of distractors were randomly chosen during model training to keep the sample size from each stimulus equal. Hence, each volunteer will have a 102 blocks dataset for every spectral power of feedback learning/memory retrieval and distractors. In each block, the data between 200ms to 600ms (400ms) is considered to estimate spectral powers. As the EEG data acquisition is carried out with 5000 samples/second, 2000 datapoints elicited in the 400ms of selected time block is considered for further processing. Hence, in total, 2,04,000 (2000 datapoints/block x 102 blocks) data points from every volunteer data set are selected for further processing. The pre-processed EEG data of the complete thirty-five volunteer set (71,40,000x 31) is initially subjected to seven intelligence correlated spectral power estimations resulting in feature vectors used for training, testing and validation.

Fine-tuning of performance during LSTM training

Both deep learning architectures (LSTM and attention-based LSTM) are trained with all the seven features passed to the input cells (5 nodes) of the first LSTM layer. The deep layered architecture employed in this study possessed three stacked layers, and the final LSTM layer was integrated with an attention layer. Subsequently, a fully connected layer (sigmoid activation function) to predict task engagement from the input is connected with the attention layer. The optimization of the deep LSTM network involved the tuning process of training epoch numbers, hidden layer size,

dropout rate, recurrent depth, and batch size. These parameters were applied after each LSTM layer and optimized with the weight matrix L2 regularisation coefficient. Finally, hyper-parameter such as learning rate was tuned for the stochastic Adam optimizer. Tuning leads the final optimized values such as hidden layer size of 128, training epoch numbers as 3000, rate dropout for input layer as 0, for 1st LSTM layer as 0.2, for 2nd LSTM layer as 0.1, for 3rd LSTM layer as 0.2, recurrent depth of 3 and learning rate of 0.001. Validation of the proposed deep learning architecture is performed by employing a 10-fold cross-validation approach. The performance metrics such as precision, accuracy, and recall are estimated.

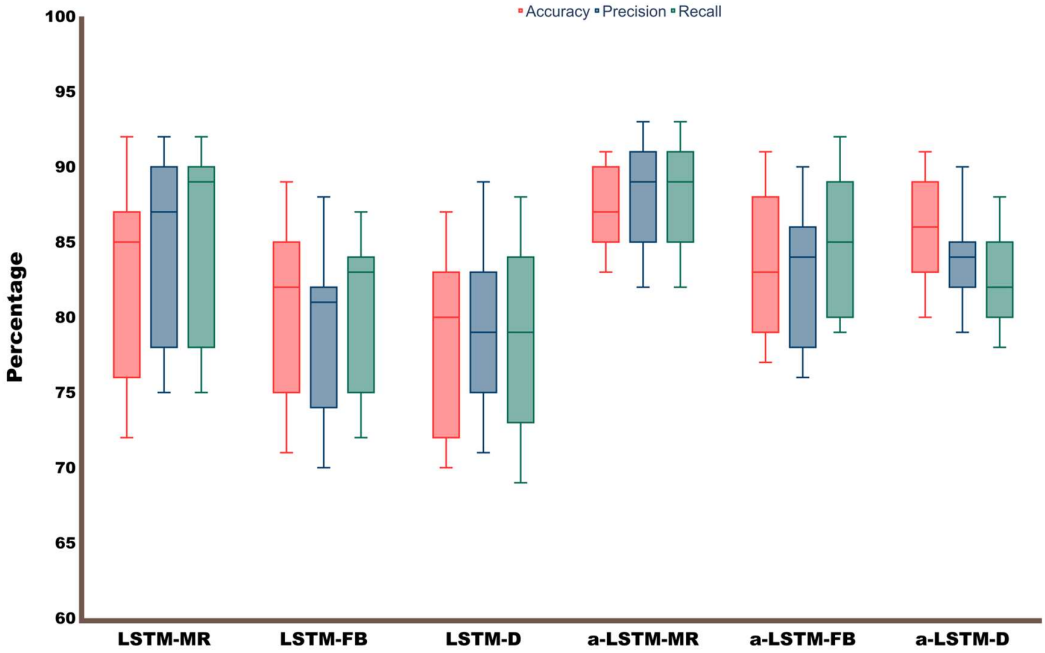

Figure 4.9: Performance comparison of the deep learning frameworks between attention-based LSTM (a-LSTM) and traditional LSTM. The graphical representation demonstrates the classification performance metrics (accuracy, precision, and recall) for both frameworks corresponding to three distinct task engagements (Memory retrieval (MR), feedback learning (FB), and distractors (D)).

Performance

The hybrid deep learning architecture design allows it to apply the attention layer that finds meaningful patterns using LSTM by overcoming the fixed-length input sequences. Our procedure evaluates the feature vectors that comprise the intelligence-correlated EEG powers of feedback learning and memory retrieval. Figure 4.9 offers a visual comparison in the performance metrics, precision, accuracy, and recall of both deep learning models

trained using (LSTM and attention-LSTM) using all the seven features. The LSTM combined with attention appears to perform significantly better for all three task engagements (Memory retrieval (MR), feedback learning (FB), and distractors (D)) in three of the performance metrics. In this regard, the proposed attention-based LSTM architecture has proven to enhance the performance of the models.

4.5 DISCUSSION

The present study aims to decide the distinct cortical oscillations that associate fluid intelligence with learning and memory retrieval of the encoded objects and understand their neural mechanisms through multifrequency, EEG informed fMRI, and hemodynamic functional connectivity analysis. It further employs the decoded distinct cortical EEG oscillations to develop a hybrid attention-LSTM based deep-learning model to classify the cortical EEG oscillations that associate individuals' fluid intelligence with their learning and subsequent memory retrieval mechanisms. The following section discusses the observations of the study in detail.

4.5.1 Fronto-Parietal cortical oscillations and their association with fluid intelligence

One of the core observations of this study is identifying the cortical oscillations associated with fluid intelligence during the engagement of learning and subsequent memory retrieval process. The present study observed strong engagement of frontal theta, alpha, and parietal delta, theta, and beta oscillations associated with fluid intelligence during the feedback learning process. On the other hand, frontal delta and parietal alpha, associated with fluid intelligence during the subsequent memory retrieval process. In general, the present study observed significant engagement of frontoparietal neuronal oscillations to be closely associated with distinct cognitive states' cognitive processes of fluid intelligence.

As listed in Table 4.1, many studies have studied the association of fluid intelligence with learning mechanisms and are intended to test the relationship between frontoparietal cortical activation and intelligence during task engagements. Specifically, learning is an essential factor in examining fluid intelligence's role, which establishes the strong relationship of higher fluid intelligence with the greater event-related desynchronization of parietal alpha activity [1].

Table 4.1: Studies that bring more insights in understanding fluid intelligence associates with learning and memory.

Study	Technique	Analysis	Cognitive Process	Observations
[105]	fMRI	Functional connectivity	Working Memory	Enhanced FC within and between DMN, CEN, and SN by feedback training, associated with the insula, correlated with behavioural improvements.
[14]	EEG	ERP	Visual oddball task	Association of higher RAPM with higher centro-parietal EEG activity. Amplitude/latency of parietal-P3 is positively/negatively correlated with learning and memory abilities.
[1]	EEG	Correlation between Fluid Intelligence and ERS-ERD	Working memory (Geometric Analogy Task)	More significant right-hemispheric parieto-occipital alpha activity during complex tasks.
[106]	fMRI	GLM	Procedural Memory	A more significant activity of hippocampus inferior frontal gyrus, middle/superior temporal lobe, inferior/superior parietal during successful retrieval after feedback.
[107]	Behavioral	Statistical	Declarative memory	Better performance after learning and consolidation of declarative memory during the nonverbal task.
[108]	EEG	ERP	Working memory (Tactile)	Significant differences in P300 and P400/N400 amplitude for complex positive/negative feedback trials, Learning leads to progressive changes in ERP of frontal, central, and posterior sites.
[109]	Behavioral	Statistical	Working memory	Performance feedback augments Practice-related improvements.
[110]	EEG	Spectral	Declarative memory	Positive correlation between signed reward prediction error and theta power, the negative correlation for alpha and high beta powers.
[111]	Behavioral	Statistical	Working Memory (Visuospatial)	Greater intentional learning for physical to observational practice.
[102]	EEG	ERP, ERS	Working memory	Stronger anti-correlation of theta-ERS with fluid intelligence; and association of alpha-ERD with fluid intelligence.
[112]	Behavioral	Statistical	Declarative memory	The critical role of declarative memory in the learning of a second language other than native.
[113]	EEG-fMRI	Spectral, EEG informed fMRI, Functional connectivity	Declarative memory	Modulated neuro-vascular mechanisms of frontal-parietal EEG powers from feedback learning to memory retrieval.

Luo and colleagues [102] revealed the varied level of frontocentral and parietal theta power for low-ability groups from the high-ability group and suggested the use of theta power to assess an individual's intelligence. The role of multifrequency interaction between slow and fast brain rhythms in high-order cognition through the delta-gamma phase-amplitude coupling is identified as a neurophysiological substrate of fluid intelligence [103]. Further, Preusse and colleagues [104] investigated the impact of fluid intelligence on neural efficiency by conducting an fMRI study on fluid intelligence tasks. It revealed the association of high fluid intelligence with the greater activation of parietal-occipital regions than average fluid intelligence and lower activation in frontal brain regions, indicating more efficient processing.

Similarly, other studies have explained the differences in neural efficiency with variation in fluid intelligence level [114,115]. Together, frontal-parietal alpha and theta oscillations, their modulation with intelligence level and neural origins, suggest fluid intelligence's clear picture through the electrophysiological and neuronal dynamics.

4.5.2 Intelligence-associated EEG oscillations of feedback-learning modulate subsequent memory retrieval

The findings of multifrequency interactions reveal the significant relationship between EEG oscillations of feedback-learning associated with fluid intelligence and subsequent memory retrievals. Specifically, the study reveals the modulation of the frontal delta power of memory retrieval caused by intelligence-associated frontal theta and alpha powers of feedback learning. The role of these feedback's EEG oscillations in modulating the subsequent memory retrieval supports the study that suggested the elicitations of frontal theta power during feedback processing and subsequent behavioral adaptations [100]. Alpha oscillations have been observed as a biomarker of relaxed wakefulness [116], frontal-alpha-synchronization during resting state, internal mental processing [117], and alpha-desynchronization for cognitive demands and attention [118] and semantic memory retrievals [29,119–123]. This understanding supports the current study's findings that intelligence-correlated EEG powers, frontal theta, and alpha oscillations of feedback learning inversely modulate the memory retrieval's delta power.

Further, the memory retrieval's parietal alpha power is found modulating with the combined effect of frontal theta and parietal delta-beta oscillations of feedback learning. The emerging evidence suggests the occurrence of posterior-alpha oscillations during high internal processing demands such as visual perception [124], in contrast to the well-established frontal-alpha oscillations. The association of retrieval's parietal alpha power with feedback's frontal theta and parietal delta powers is consistent with an earlier study [125] that links low-frequency (delta and theta) oscillations with motivational and emotional processes. The theta range is also known to be crucial neuronal oscillations for the memory processes [126–128]. Moreover, many feedback studies [38,129] have demonstrated the association of frontal-parietal beta oscillations during reward-related feedback explicitly by positive performance feedback [130]. All these studies support the present study's observations that multifrequency oscillations elicit during feedback learning modulates subsequently engaged memory retrieval and its associated cortical oscillations.

4.5.3 Association of fluid intelligence with learning and memory retrieval: Understanding the neural sources and their functional connectivity

The elicitation of EEG cortical oscillations is a powerful mechanism in analyzing the local and global neural engagement caused by cognitive task engagement. Specifically, distant cortical and long-range coordination emerges as the lower EEG frequency oscillation [131], and local neural systems are observed as high-frequency dynamics in EEG cortical oscillations . The association of cortical oscillations with neural engagements can be better studied by understanding the neural sources and functional interaction associated with these low and high-frequency cortical oscillations. The parietal-frontal integration theory of intelligence [132] suggests that fluid intelligence associates with the frontal and parietal brain regions' engagement (supramarginal and angular gyrus, superior parietal cortex, superior, middle, inferior frontal gyrus, and prefrontal cortex). Several other studies [133–135] also observed the recruitment of frontal-parietal brain regions during fluid intelligence demanding cognitive tasks. Therefore, the neural mechanisms of intelligence-associated EEG oscillation of feedback learning, and subsequent memory retrieval are examined with EEG-informed-fMRI and functional connectivity approaches and understood from the perspective of multifrequency interactions. The following sections discuss them exclusively.

Our findings suggest a substantial contribution of frontal theta power in the feedback learning process. In specific, it reveals synchronization of feedback's frontal theta power with the BOLD signal of frontal regions (inferior, middle and superior frontal gyrus, frontal pole, frontal orbital cortex), a few parietal regions (parietal operculum cortex, angular gyrus), and it's desynchronization with the BOLD signal of lingual gyrus, precentral gyrus, postcentral gyrus, precuneus cortex, and superior parietal lobule. The greater values of graph theory measures (global efficiency and cost) for frontal regions and lesser values for parietal areas validated these findings. In general, enhanced global efficiency and cost values are the markers for significantly interacting distant brain regions during higher cognitive demands [136–138]. Theta power elicitation during the feedback learning process is also highlighted in an earlier study [139]. This suggested association with the BOLD signal of the medial prefrontal cortex with theta elicitation. Further, the memory processes [31,140,141] have also been associated with theta power elicitation and revealed their association with the BOLD signal of the hippocampus, medial temporal lobe, and prefrontal regions in specific.

Further, frontal alpha power of feedback learning reflected in-synchronization with the BOLD signal of frontal-parietal regions (inferior, middle and superior frontal gyrus, frontal orbital cortex, superior parietal lobule, angular and supramarginal gyrus). The alpha-BOLD synchronization observed for frontal regions is better explainable with the associated graph theory measures. The lesser values of global efficiency and cost for frontal regions show weak global interaction among frontal regions. However, greater global efficiency and cost values for parietal regions suggest the greater integrating tendency of parietal regions for frontal alpha power [142]. The parietal beta power of feedback learning is found in synchronization with the BOLD signal of frontal-parietal regions (middle frontal gyrus, superior frontal gyrus, frontal pole, and frontal operculum postcentral gyrus, supramarginal gyrus, angular gyrus, and precuneus cortex). The role of beta power in learning from feedback is consistent with those feedback studies [36,143–147], which highlight the occurrence of beta oscillations during reward processing and its association with feedback, learning, and subsequent cognitive adjustment and the brain's frontal-parietal neural generators.

Neuronal mechanisms associated with memory retrievals

Memory retrieval's frontal delta power is found desynchronizing the BOLD signal of frontal (frontal pole, superior frontal gyrus, frontal operculum cortex) regions and parietal (postcentral gyrus, precentral gyrus, superior parietal lobule) regions except for the middle frontal gyrus. However, the study finds significant associations of the middle frontal gyrus with the superior parietal lobule-posterior supramarginal gyrus. Subsequently, graph theory measures indicated greater global efficiency/cost values for the middle frontal gyrus, superior parietal lobule, and posterior supramarginal gyrus. Initially, delta oscillations were identified for their role in functional cortical deafferentation or inhibition of the sensory differences that interfere with internal concentration [148]. Later, their role is revealed in detecting motivationally salient stimuli and feedback-related motivational processes [125,149].

Further, the parietal alpha power is observed desynchronizing the BOLD signal of frontal (superior frontal gyrus, frontal pole, medial frontal cortex, middle frontal gyrus) and parietal (precentral gyrus, precuneus cortex) regions. The graph theory results showed higher global efficiency and cost of frontal regions (frontal pole, superior, middle frontal gyrus, medial frontal cortex) and precentral gyrus. No functional interactions between frontal and parietal regions are found, suggesting the dissociation of frontal and parietal regions during memory retrieval. The dissociation of frontal regions from parietal regions during memory retrieval is consistent with several connectivity studies [150,151], which suggested the segregation of lateral and medial parietal-temporal pathways during memory retrieval. Together, the findings support the association of intelligence-associated parietal alpha power with the functional dissociation of frontal from parietal regions after learning from feedback. Hence, these observations from EEG informed fMRI, and hemodynamic functional connectivity clearly explains neural mechanisms and distinct cortical oscillations associated with fluid intelligence, learning, and memory retrieval. These identified distinct EEG oscillations during encoded objects' memory retrieval and learning engagement against the engagement of other distractor engagements are sub sequentially used in a deep learning computational model.

4.5.4 Performance of proposed deep learning computation model

The study focuses on decoding distinct cortical EEG oscillations that associate individuals' fluid intelligence with their learning mechanisms during performance feedback and subsequent memory retrieval. The assessment of cortical EEG information is done on the most informative EEG information (between 200ms to 600ms) extracted from the time-frequency analysis. This specific extraction has been considered for better information capturing and subsequently for improving the classification accuracy of the proposed system.

The classification of feedback learning and memory retrieval mechanisms performed using two different deep learning architectures consisting of LSTM and attention-based LSTM algorithms revealed comparable accuracy, precision, and recall rate. The performance of both deep learning architectures justified the critical selection of EEG powers from feedback learning and memory retrieval phases based on their association with an individual's fluid intelligence. The proposed method is classified better by training the system to assess neurocognitive knowledge underlying the intelligence's role in task engagements. The attention mechanisms further improved the system's performance by combining the effect of attention phenomena with the LSTM architecture. The attention mechanism allows the deep learning architecture to dynamically emphasize the task-relevant neural information in the time series sequence of EEG data and give less attention to other irrelevant information. The performance improvement of the attention-based LSTM system can be seen precisely in Figure 4.9. The plots suggest that the attention mechanism is optimum for extracting the most relevant task neural features and improves the LSTM's performance compared to independent LSTM.

4.6 SIGNIFICANCE OF THE STUDY

Despite extensive works in understanding fluid intelligence and its association with feedback learning, no work employs any computational model to identify multifrequency cortical elicitations associated with fluid intelligence and their modulation during learning and subsequent memory retrieval. Furthermore, most deep learning studies in brain computer interfaces are restricted to classification algorithms

based on their event-related potentials and cortical oscillations to classify sensory-motor neural signals such as sensory-motor rhythm (SMR), P300, Slow cortical potential (SCP), and Motor related cortical potential (MRCP). To the best of our knowledge, these studies have not considered individuals' learning capabilities and their effects on subsequent task engagements. Our present work further brings more insights in understanding neural mechanisms and distinct cortical oscillations associated with fluid intelligence, learning, and memory retrieval through EEG multifrequency interaction, hemodynamic functional connectivity, and EEG-informed-fMRI measures. Further, it brings more insights into the attention mechanism's ability to improvise LSTM deep learning architectures and classify cognitive task engagement based on the optimized neural signatures. To our current knowledge, the present study is one of the few works that employs simultaneous EEG-fMRI information to optimize the neural signatures for improvising the performance of deep learning architectures.

4.7 CONCLUSION

This study proposes a deep-learning-based computational model to classify the engagement of feedback learning and subsequent memory retrieval of encoded objects from distractors. For this purpose, the study deciphers the association of intelligence with EEG cortical oscillations during feedback learning and memory retrieval of encoded objects. It further brings more insights into their neural mechanisms through multifrequency analysis, EEG-informed-fMRI, and hemodynamical functional connectivity approaches. The results revealed a significantly stronger correlation of fluid intelligence with frontal-alpha, frontal-theta, parietal-theta, parietal-beta and parietal-delta powers during feedback learning, and frontal-delta and parietal-alpha powers during subsequently engaged memory retrieval phase. Further, the multifrequency interaction revealed a significant influence of frontal-theta, frontal-alpha, parietal-delta, and parietal-beta oscillations elicited during feedback learning on the subsequently engaged memory retrieval's cortical oscillations, particularly on frontal-delta, parietal-alpha elicitations.

The neural mechanisms associated with the multifrequency elicitations were assessed through EEG-informed fMRI and graph theory-based functional connectivity approaches. Their results revealed strong frontal-parietal engagement and, in particular, the frontal theta, alpha and a parietal beta of feedback learning synchronize with the BOLD oscillations of frontal-parietal regions. On the other hand, frontal delta and parietal alpha oscillations elicited during the memory retrieval phase desynchronized to the BOLD signal of frontal-parietal regions. The functional connectivity and graph theory approaches validated the association of frontal delta power with frontal-parietal integration, parietal alpha power with the functional dissociation of frontal regions from parietal regions. Further, the study classified the engagement of feedback learning and memory retrieval of encoded objects from distractors based on the deciphered cortical oscillations using attention-based LSTM networks. The performance of the proposed architecture revealed that the integration of LSTM with the attention mechanism significantly improves the performance of our proposed deep learning model. Hence, our study proposes a promising direction in deciphering the cortical oscillations associated with fluid intelligence and their role in associating feedback learning and subsequent memory retrieval mechanisms and further employing a deep learning-based framework to classify them from distractors.

REFERENCES

[1] A. Dix, I. Wartenburger, E. van der Meer, The role of fluid intelligence and learning in analogical reasoning: How to become neurally efficient?, Neurobiol. Learn. Mem. 134 (2016) 236–247. https://doi.org/10.1016/j.nlm.2016.07.019.

[2] M. Filičková, I. Ropovik, M. Bobaková, I. Kovalčíková, The relationship between fluid intelligence and learning potential: Is there an interaction with attentional control?, J. Pedagog. 6 (2015) 25–41. https://doi.org/10.1515/jped-2015-0002.

[3] R. Primi, M.E. Ferrão, L.S. Almeida, Fluid intelligence as a predictor of learning: A longitudinal multilevel approach applied to math, Learn. Individ. Differ. 20 (2010) 446–451. https://doi.org/10.1016/j.lindif.2010.05.001.

[4] T. Wang, X. Ren, K. Schweizer, Learning and retrieval processes predict fluid intelligence over and above working memory, Intelligence. 61 (2017) 29–36. https://doi.org/10.1016/j.intell.2016.12.005.

[5] E. Chan, S.E. MacPherson, M. Bozzali, T. Shallice, L. Cipolotti, The influence of fluid intelligence, executive functions and premorbid intelligence on memory in frontal patients, Front. Psychol. 9 (2018) 1–10. https://doi.org/10.3389/fpsyg. 2018.00926.

[6] R.B. Cattell, Theory of fluid and crystallized intelligence: A critical experiment, J. Educ. Psychol. 54 (1963) 1–22. https://doi.org/10.1037/h0046743.

[7] J.L. Horn, R.B. Cattell, Refinement and test of the theory of fluid and crystallized general intelligences, J. Educ. Psychol. 57 (1966) 253–270. https://doi.org/10.1037 /h0023816.

[8] P.M.J. Engel de Abreu, A.R.A. Conway, S.E. Gathercole, Working memory and fluid intelligence in young children, Intelligence. 38 (2010) 552–561. https://doi.org/10. 1016/j.intell.2010.07.003.

[9] A. Cochrane, V. Simmering, C. Shawn Green, Fluid intelligence is related to capacity in memory as well as attention: Evidence from middle childhood and adulthood, PLoS One. 14 (2019) 1–24. https://doi.org/10.1371/journal.pone.0221353.

[10] T.A. Salthouse, J.E. Pink, Why is working memory related to fluid intelligence?, Psychon. Bull. Rev. 15 (2008) 364–371. https://doi.org/10.3758/PBR.15.2.364.

[11] N. Unsworth, K. Fukuda, E. Awh, E.K. Vogel, Working memory and fluid intelligence: Capacity, attention control, and secondary memory retrieval, Cogn. Psychol. 71 (2014) 1–26. https://doi.org/10.1016/j.cogpsych.2014.01.003.

[12] J. Au, E. Sheehan, N. Tsai, G.J. Duncan, M. Buschkuehl, S.M. Jaeggi, Improving fluid intelligence with training on working memory: a meta-analysis, Psychon. Bull. Rev. 22 (2015) 366–377. https://doi.org/10.3758/s13423-014-0699-x.

[13] S.M. Jaeggi, M. Buschkuehl, J. Jonides, W.J. Perrig, Improving fluid intelligence with training on working memory, 105 (2008) 6829–6833.

[14] H.U. Amin, A.S. Malik, N. Kamel, W.T. Chooi, M. Hussain, P300 correlates with learning & memory abilities and fluid intelligence, J. Neuroeng. Rehabil. 12 (2015) 1–14. https://doi.org/10.1186/s12984-015-0077-6.

[15] N.S. Roslan, H.U. Amin, L.I. Izhar, M.N.M. Saad, S. Sivapalan, Role of EEG delta and beta oscillations during problem solving tasks, Int. Conf. Intell. Adv. Syst. ICIAS 2016. (2017) 2–5. https://doi.org/10.1109/ICIAS.2016.7824138.

[16] A. Pahor, N. Jaušovec, Theta-gamma cross-frequency coupling relates to the level of human intelligence, Intelligence. 46 (2014) 283–290. https://doi.org/10.1016/j.intell. 2014.06.007.

[17] I.G.D. Lila Davachi, Declarative Memory, J. Invest. Dermatol. 135 (2015) 612–615. https://doi.org/10.1038/jid.2014.371.

[18] L.R. Squire, A.J.O. Dede, Conscious and unconscious memory systems, Cold Spring Harb. Perspect. Med. 5 (2015). https://doi.org/10.1101/cshperspect.a021667.

[19] P.J. Bayley, L.R. Squire, The medial temporal lobe and declarative memory, Int. Congr. Ser. 1250 (2003) 245–259. https://doi.org/10.1016/s0531-5131(03)00192-4.

[20] L.R. Squire, C.E.L. Stark, R.E. Clark, the Medial Temporal Lobe, Annu. Rev. Neurosci. 27 (2004) 279–306. https://doi.org/10.1146/annurev.neuro.27.070203. 144130.

[21] I. Tendolkar, J. Arnold, K.M. Petersson, S. Weis, A. Brockhaus-Dumke, P. Van Eijndhoven, J. Buitelaar, G. Fernández, Contributions of the medial temporal lobe to declarative memory retrieval: Manipulating the amount of contextual retrieval, Learn. Mem. 15 (2008) 611–617. https://doi.org/10.1101/lm.916708.

[22] A.R. Preston, H. Eichenbaum, Interplay of hippocampus and prefrontal cortex in memory, Curr. Biol. 23 (2013) R764–R773. https://doi.org/10.1016/j.cub.2013. 05.041.

[23] J.S. Simons, H.J. Spiers, Prefrontal and medial temporal lobe interactions in long-term memory, Nat. Rev. Neurosci. 4 (2003) 637–648. https://doi.org/ 10.1038/nrn1178.

[24] M.M. Chun, Contextual cueing of visual attention, Trends Cogn. Sci. 4 (2000) 170–178. https://doi.org/10.1016/S1364-6613(00)01476-5.

[25] K. Henke, A model for memory systems based on processing modes rather than consciousness, Nat. Rev. Neurosci. 11 (2010) 523–532. https://doi.org/10.1038/nrn 2850.

[26] H.E. Schendan, M.M. Searl, R.J. Melrose, C.E. Stern, An fMRI study of the role of the medial temporal lobe in implicit and explicit sequence learning, Neuron. 37 (2003) 1013–1025. https://doi.org/10.1016/S0896-6273(03)00123-5.

[27] G. Buzsáki, E.I. Moser, Memory, navigation and theta rhythm in the hippocampal-entorhinal system, Nat. Neurosci. 16 (2013) 130–138. https://doi.org/10.1038/ nn.3304.

[28] W. Klimesch, Memory processes, brain oscillations and EEG synchronization, Int. J. Psychophysiol. 24 (1996) 61–100. https://doi.org/10.1016/S0167-8760(96)00057-8.

[29] W. Klimesch, EEG alpha and theta oscillations reflect cognitive and memory performance: a rKlimesch, W. (1999). EEG alpha and theta oscillations reflect cognitive and memory performance: a review and analysis. Brain Research Reviews, 29(2-3), 169–195. doi:10.1016/S016, Brain Res. Rev. 29 (1999) 169–195. https://doi.org/10.1016/S0165-0173(98)00056-3.

[30] B. Pastötter, K.H.T. Bäuml, Distinct slow and fast cortical theta dynamics in episodic memory retrieval, Neuroimage. 94 (2014) 155–161. https://doi.org/10.1016/j. neuroimage.2014.03.002.

[31] N.A. Herweg, T. Apitz, G. Leicht, C. Mulert, L. Fuentemilla, N. Bunzeck, Theta-alpha oscillations bind the hippocampus, prefrontal cortex, and striatum during recollection: Evidence from simultaneous EEG–fMRI, J. Neurosci. 36 (2016) 3579–3587. https://doi.org/10.1523/JNEUROSCI.3629-15.2016.

[32] E. Nyhus, T. Curran, Functional role of gamma and theta oscillations in episodic memory, Neurosci. Biobehav. Rev. 34 (2010) 1023–1035. https://doi.org/10.1016/j. neubiorev.2009.12.014.

[33] J. Fell, P. Klaver, H. Elfadil, C. Schaller, C.E. Elger, G. Fernández, Rhinal-hippocampal theta coherence during declarative memory formation: Interaction with gamma synchronization?, Eur. J. Neurosci. 17 (2003) 1082–1088. https://doi.org/10.1046/j.1460-9568.2003.02522.x.

[34] P.B. Sederberg, A. Schulze-Bonhage, J.R. Madsen, E.B. Bromfield, D.C. McCarthy, A. Brandt, M.S. Tully, M.J. Kahana, Hippocampal and neocortical gamma oscillations predict memory formation in humans, Cereb. Cortex. 17 (2007) 1190–1196. https://doi.org/10.1093/cercor/bhl030.

[35] P.B. Sederberg, M.J. Kahana, M.W. Howard, E.J. Donner, J.R. Madsen, Theta and Gamma Oscillations during Encoding Predict Subsequent Recall, J. Neurosci. 23 (2003) 10809–10814. https://doi.org/10.1523/jneurosci.23-34-10809.2003.

[36] M.X. Cohen, C.E. Elger, C. Ranganath, Reward expectation modulates feedback-related negativity and EEG spectra, Neuroimage. 35 (2007) 968–978. https://doi.org/10.1016/j.neuroimage.2006.11.056.

[37] M.X. Cohen, Error-related medial frontal theta activity predicts cingulate-related structural connectivity, Neuroimage. 55 (2011) 1373–1383. https://doi.org/10.1016/j .neuroimage.2010.12.072.

[38] J. Marco-Pallares, D. Cucurell, T. Cunillera, R. García, A. Andrés-Pueyo, T.F. Münte, A. Rodríguez-Fornells, Human oscillatory activity associated to reward processing in a gambling task, Neuropsychologia. 46 (2008) 241–248. https://doi.org/10.1016/j.neuropsychologia.2007.07.016.

[39] N. Salari, M. Rose, Dissociation of the functional relevance of different pre-stimulus oscillatory activity for memory formation, Neuroimage. 125 (2016) 1013–1021. https://doi.org/10.1016/j.neuroimage.2015.10.037.

[40] E. Camara, A. Rodriguez-Fornells, Z. Ye, T.F. Münte, Reward networks in the brain as captured by connectivity measures, Front. Neurosci. 3 (2009) 350–362. https://doi.org/10.3389/neuro.01.034.2009.

[41] M. Goldhacker, K. Rosengarth, T. Plank, M.W. Greenlee, The effect of feedback on performance and brain activation during perceptual learning, Vision Res. 99 (2014) 99–110. https://doi.org/10.1016/j.visres.2013.11.010.

[42] Y. Jiang, S. Il Kim, M. Bong, Effects of reward contingencies on brain activation during feedback processing, Front. Hum. Neurosci. 8 (2014) 1–9. https://doi.org/10.3389/fnhum.2014.00656.

[43] E. Tricomi, S. DePasque, The role of feedback in learning and motivation, Adv. Motiv. Achiev. 19 (2016) 175–202. https://doi.org/10.1108/S0749-74232016000001 9015.

[44] K. Tsiouris, V.C. Pezoulas, M. Zervakis, S. Konitsiotis, D.D. Koutsouris, D.I. Fotiadis, A Long Short-Term Memory deep learning network for the prediction of epileptic seizures using EEG signals, Comput. Biol. Med. 99 (2018) 24–37. https://doi.org/10.1016/j.compbiomed.2018.05.019.

[45] D. Maheshwari, S.K. Ghosh, R.K. Tripathy, M. Sharma, U.R. Acharya, Automated accurate emotion recognition system using rhythm-specific deep convolutional neural network technique with multi-channel EEG signals, Comput. Biol. Med. 134 (2021). https://doi.org/10.1016/j.compbiomed.2021.104428.

[46] M.R. Islam, M.M. Islam, M.M. Rahman, C. Mondal, S.K. Singha, M. Ahmad, A. Awal, M.S. Islam, M.A. Moni, EEG Channel Correlation Based Model for Emotion Recognition, Comput. Biol. Med. 136 (2021) 104757. https://doi.org/10.1016/j.compbiomed. 2021.104757.

[47] N. Michielli, U.R. Acharya, F. Molinari, Cascaded LSTM recurrent neural network for automated sleep stage classification using single-channel EEG signals, Comput. Biol. Med. 106 (2019) 71–81. https://doi.org/10.1016/j.compbiomed.2019.01.013.

[48] S. Muhammad Usman, S. Khalid, S. Bashir, A deep learning based ensemble learning method for epileptic seizure prediction, Comput. Biol. Med. 136 (2021) 104710. https://doi.org/10.1016/j.compbiomed.2021.104710.

[49] X. Hu, S. Yuan, F. Xu, Y. Leng, K. Yuan, Q. Yuan, Scalp EEG classification using deep Bi-LSTM network for seizure detection, Comput. Biol. Med. 124 (2020) 103919. https://doi.org/10.1016/j.compbiomed.2020.103919.

[50] R. San-Segundo, M. Gil-Martín, L.F. D'Haro-Enríquez, J.M. Pardo, Classification of epileptic EEG recordings using signal transforms and convolutional neural networks, Comput. Biol. Med. 109 (2019) 148–158. https://doi.org/10.1016/j.compbiomed. 2019.04.031.

[51] Ö. Yildirim, A novel wavelet sequences based on deep bidirectional LSTM network model for ECG signal classification, Comput. Biol. Med. 96 (2018) 189–202. https://doi.org/10.1016/j.compbiomed.2018.03.016.

[52] P. Khan, Y. Khan, S. Kumar, M.S. Khan, A.H. Gandomi, HVD-LSTM based recognition of epileptic seizures and normal human activity, Comput. Biol. Med. 136 (2021) 104684. https://doi.org/10.1016/j.compbiomed.2021.104684.

[53] U.R. Acharya, S.L. Oh, Y. Hagiwara, J.H. Tan, H. Adeli, Deep convolutional neural network for the automated detection and diagnosis of seizure using EEG signals, Comput. Biol. Med. 100 (2018) 270–278. https://doi.org/10.1016/j.compbiomed. 2017.09.017.

[54] Z. Abbasvandi, A.M. Nasrabadi, A self-organized recurrent neural network for estimating the effective connectivity and its application to EEG data, Elsevier Ltd, 2019. https://doi.org/10.1016/j.compbiomed.2019.05.012.

[55] et al Vaswani, A., Attention Is All You Need, IEEE Ind. Appl. Mag. 8 (2017) 8–15. https://doi.org/10.1109/2943.974352.

[56] M. Jiang, J. Gu, Y. Li, B. Wei, J. Zhang, Z. Wang, L. Xia, HADLN: Hybrid Attention-Based Deep Learning Network for Automated Arrhythmia Classification, Front. Physiol. 12 (2021). https://doi.org/10.3389/fphys.2021.683025.

[57] Y. Jin, D. Wu, W. Guo, Attention-based LSTM with filter mechanism for entity relation classification, Symmetry (Basel). 12 (2020) 1–16. https://doi.org/10.3390/ sym12101729.

[58] Neeraj, V. Singhal, J. Mathew, R.K. Behera, Detection of alcoholism using EEG signals and a CNN-LSTM-ATTN network, Comput. Biol. Med. 138 (2021) 104940. https://doi.org/10.1016/J.COMPBIOMED.2021.104940.

[59] F. Karim, S. Majumdar, H. Darabi, S. Harford, Multivariate LSTM-FCNs for time series classification, Neural Networks. 116 (2019) 237–245. https://doi.org/10.1016/j.neunet.2019.04.014.

[60] Y. Kim, A. Choi, Eeg-based emotion classification using long short-term memory network with attention mechanism, Sensors (Switzerland). 20 (2020) 1–22. https://doi.org/10.3390/s20236727.

[61] M. Rashid, N. Sulaiman, A. P. P. Abdul Majeed, R.M. Musa, A.F. Ahmad, B.S. Bari, S. Khatun, Current Status, Challenges, and Possible Solutions of EEG-Based Brain-Computer Interface: A Comprehensive Review, Front. Neurorobot. 14 (2020) 1–35. https://doi.org/10.3389/fnbot.2020.00025.

[62] Y. Xie, R. Liang, Z. Liang, C. Huang, C. Zou, B. Schuller, Speech Emotion Classification Using Attention-Based LSTM, IEEE/ACM Trans. Audio Speech Lang. Process. 27 (2019) 1675–1685. https://doi.org/10.1109/TASLP.2019.2925934.

[63] Q. Yao, R. Wang, X. Fan, J. Liu, Y. Li, Multi-class Arrhythmia detection from 12-lead varied-length ECG using Attention-based Time-Incremental Convolutional Neural Network, Inf. Fusion. 53 (2020) 174–182. https://doi.org/10.1016/j.inffus.2019.06.024.

[64] J. Zhang, A. Liu, M. Gao, X. Chen, X. Zhang, X. Chen, ECG-based multi-class arrhythmia detection using spatio-temporal attention-based convolutional recurrent neural network, Artif. Intell. Med. 106 (2020) 101856. https://doi.org/10.1016/j.artmed.2020.101856.

[65] L. Zhang, G. Zhu, L. Mei, P. Shen, S.A.A. Shah, M. Bennamoun, Attention in convolutional LSTM for gesture recognition, Adv. Neural Inf. Process. Syst. 2018-Decem (2018) 1953–1962.

[66] X. Zheng, W. Chen, An Attention-based Bi-LSTM Method for Visual Object Classification via EEG, Biomed. Signal Process. Control. 63 (2021) 102174. https://doi.org/10.1016/j.bspc.2020.102174.

[67] S. Agrawal, V. Chinnadurai, A. Kaur, P. Kumar, P. Kaur, R. Sharma, A. Kumar Singh, Estimation of Functional Connectivity Modulations during Task Engagement and Their Neurovascular Underpinnings Through Hemodynamic Reorganization Method, Brain Connect. 9 (2019) 341–355. https://doi.org/10.1089/brain.2018.0656.

[68] A. Kaur, V. Chinnadurai, R. Chaujar, Microstates-based resting frontal alpha asymmetry approach for understanding affect and approach/withdrawal behavior, Sci. Rep. 10 (2020) 1–25. https://doi.org/10.1038/s41598-020-61119-7.

[69] A. Kaur, R. Chaujar, V. Chinnadurai, Effects of Neural Mechanisms of Pretask Resting EEG Alpha Information on Situational Awareness: A Functional Connectivity Approach, Hum. Factors. 62 (2020) 1150–1170. https://doi.org/10.1177/0018720819869129.

[70] J. Raven, T. Nature, The Raven Progressive Matrices Tests : Their Theoretical Basis and Measurement Model Chapter 1 The Raven Progressive Matrices Tests : Their Theoretical Basis and Measurement Model, J. Behav. Med. 35 (2016) 500–508.

[71] A.H. Javadi, J.C. Glen, S. Halkiopoulos, M. Schulz, H.J. Spiers, Oscillatory reinstatement enhances declarative memory, J. Neurosci. 37 (2017) 9939–9944. https://doi.org/10.1523/JNEUROSCI.0265-17.2017.

[72] A.N. Kluger, A. DeNisi, The effects of feedback interventions on performance: A historical review, a meta-analysis, and a preliminary feedback intervention theory, Psychol. Bull. 119 (1996) 254–284. https://doi.org/10.1037/0033-2909.119.2.254.

[73] G.D. Iannetti, R.K. Niazy, R.G. Wise, P. Jezzard, J.C.W. Brooks, L. Zambreanu, W. Vennart, P.M. Matthews, I. Tracey, Simultaneous recording of laser-evoked brain potentials and continuous, high-field functional magnetic resonance imaging in humans, Neuroimage. 28 (2005) 708–719. https://doi.org/10.1016/j.neuroimage.2005.06.060.

[74] R.K. Niazy, C.F. Beckmann, G.D. Iannetti, J.M. Brady, S.M. Smith, Removal of FMRI environment artifacts from EEG data using optimal basis sets, Neuroimage. 28 (2005) 720–737. https://doi.org/10.1016/j.neuroimage.2005.06.067.

[75] P.J. Allen, O. Josephs, R. Turner, A method for removing imaging artifact from continuous EEG recorded during functional MRI, Neuroimage. 12 (2000) 230–239. https://doi.org/10.1006/nimg.2000.0599.

[76] I.I. Christov, Real time electrocardiogram QRS detection using combined adaptive threshold, Biomed. Eng. Online. 3 (2004) 1–9. https://doi.org/10.1186/1475-925X-3-28.

[77] K.H. Kim, H.W. Yoon, H.W. Park, Improved ballistocardiac artifact removal from the electroencephalogram recorded in fMRI, J. Neurosci. Methods. 135 (2004) 193–203. https://doi.org/10.1016/j.jneumeth.2003.12.016.

[78] L.J. Gabard-Durnam, A.S.M. Leal, C.L. Wilkinson, A.R. Levin, The harvard automated processing pipeline for electroencephalography (HAPPE): Standardized processing software for developmental and high-artifact data, Front. Neurosci. 12 (2018) 1–24. https://doi.org/10.3389/fnins.2018.00097.

[79] R.Y. You, Z. Chen, Blind source separation of multichannel electroencephalogram based on wavelet transform and ICA, Chinese Phys. 14 (2005) 2176–2180. https://doi.org/10.1088/1009-1963/14/11/006.

[80] I. Winkler, S. Haufe, M. Tangermann, Automatic Classification of Artifactual ICA-Components for Artifact Removal in EEG Signals, Behav. Brain Funct. 7 (2011) 1–15. https://doi.org/10.1186/1744-9081-7-30.

[81] A. Delorme, S. Makeig, EEGLAB: An open source toolbox for analysis of single-trial EEG dynamics including independent component analysis, J. Neurosci. Methods. 134 (2004) 9–21. https://doi.org/10.1016/j.jneumeth.2003.10.009.

[82] C.R. Pernet, R. Wilcox, G.A. Rousselet, Robust correlation analyses: False positive and power validation using a new open source matlab toolbox, Front. Psychol. 3 (2013) 1–18. https://doi.org/10.3389/fpsyg.2012.00606.

[83] N.F. Ince, A.H. Tewfik, S. Arica, Extraction subject-specific motor imagery time-frequency patterns for single trial EEG classification, Comput. Biol. Med. 37 (2007) 499–508. https://doi.org/10.1016/j.compbiomed.2006.08.014.

[84] T.D. Wager, M.C. Keller, S.C. Lacey, J. Jonides, Increased sensitivity in neuroimaging analyses using robust regression, Neuroimage. 26 (2005) 99–113. https://doi.org/10.1016/j.neuroimage.2005.01.011.

[85] S. Whitfield-Gabrieli, A. Nieto-castanon, CONN – fMRI functional connectivity toolbox v14, (2014).

[86] F. V. Farahani, W. Karwowski, N.R. Lighthall, Application of graph theory for identifying connectivity patterns in human brain networks: A systematic review, Front. Neurosci. 13 (2019) 1–27. https://doi.org/10.3389/fnins.2019.00585.

[87] J. Sepulcre, H. Liu, T. Talukdar, I. Martincorena, B.T. Thomas Yeo, R.L. Buckner, The organization of local and distant functional connectivity in the human brain, PLoS Comput. Biol. 6 (2010) 1–15. https://doi.org/10.1371/journal.pcbi.1000808.

[88] Y. Li, X. Rui, S. Li, F. Pu, Investigation of global and local network properties of music perception with culturally different styles of music $, Comput. Biol. Med. 54 (2014) 37–43. https://doi.org/10.1016/j.compbiomed.2014.08.017.

[89] L. Abrishami Shokooh, D.H. Toffa, P. Pouliot, F. Lesage, D.K. Nguyen, Identification of global and local states during seizures using quantitative functional connectivity and recurrence plot analysis, Comput. Biol. Med. 122 (2020) 103858. https://doi.org/10.1016/j.compbiomed.2020.103858.

[90] A. Fornito, A. Zalesky, M. Breakspear, The connectomics of brain disorders, Nat. Rev. Neurosci. 16 (2015) 159–172. https://doi.org/10.1038/nrn3901.

[91] S. Hochreiter, Long Short-Term Memory, 1780 (1997) 1735–1780.

[92] P. Nagabushanam, S. Thomas George, S. Radha, EEG signal classification using LSTM and improved neural network algorithms, Soft Comput. 24 (2020) 9981–10003. https://doi.org/10.1007/s00500-019-04515-0.

[93] P. Wang, A. Jiang, X. Liu, J. Shang, L. Zhang, LSTM-based EEG classification in motor imagery tasks, IEEE Trans. Neural Syst. Rehabil. Eng. 26 (2018) 2086–2095. https://doi.org/10.1109/TNSRE.2018.2876129.

[94] A. Hajihosseini, C.B. Holroyd, Reward feedback stimuli elicit high-beta EEG oscillations in human dorsolateral prefrontal cortex, (2015) 1–7. https://doi.org/ 10.1038/srep13021.

[95] W. Klimesch, M. Doppelmayr, W. Stadler, D. Pöllhuber, P. Sauseng, D. Röhm, Episodic retrieval is reflected by a process specific increase in human electroencephalographic theta activity, Neurosci. Lett. 302 (2001) 49–52. https://doi.org/10.1016/S0304-3940(01)01656-1.

[96] F. Meconi, S. Anderl-Straub, H. Raum, M. Landgrebe, B. Langguth, K.H.T. Bäuml, S. Hanslmayr, Aberrant prefrontal beta oscillations predict episodic memory encoding deficits in schizophrenia, NeuroImage Clin. 12 (2016) 499–505. https://doi.org/10.1016/j.nicl.2016.08.017.

[97] A.M. Tuladhar, N. Ter Huurne, J.M. Schoffelen, E. Maris, R. Oostenveld, O. Jensen, Parieto-occipital sources account for the increase in alpha activity with working memory load, Hum. Brain Mapp. 28 (2007) 785–792. https://doi.org/10.1002 /hbm.20306.

[98] O. Jensen, P. Goel, N. Kopell, M. Pohja, R. Hari, B. Ermentrout, On the human sensorimotor-cortex beta rhythm: Sources and modeling, Neuroimage. 26 (2005) 347–355. https://doi.org/10.1016/j.neuroimage.2005.02.008.

[99] M. Karrasch, C.M. Krause, M. Laine, A.H. Lang, M. Lehto, Event-related desynchronization and synchronization during an auditory lexical matching task, Electroencephalogr. Clin. Neurophysiol. 107 (1998) 112–121. https://doi.org/10. 1016/S0013-4694(98)00047-9.

[100] J.F. Cavanagh, M.J. Frank, Frontal theta as a mechanism for cognitive control, Trends Cogn. Sci. 18 (2014) 414–421. https://doi.org/10.1016/j.tics.2014.04.012.

[101] O. Sporns, J.D. Zwi, Sporns2004, Neuroinformatics. 2 (2004) 145–162.

[102] W. Luo, R. Zhou, Can Working Memory Task-Related EEG Biomarkers Measure Fluid Intelligence and Predict Academic Achievement in Healthy Children?, Front. Behav. Neurosci. 14 (2020) 1–14. https://doi.org/10.3389/fnbeh.2020.00002.

[103] A. Gągol, M. Magnuski, B. Kroczek, P. Kałamała, M. Ociepka, E. Santarnecchi, A. Chuderski, Delta-gamma coupling as a potential neurophysiological mechanism of fluid intelligence, Intelligence. 66 (2018) 54–63. https://doi.org/10.1016/j.intell .2017.11.003.

[104] F. Preusse, van der M. Elke, G. Deshpande, F. Krueger, I. Wartenburger, Fluid Intelligence Allows Flexible Recruitment of the Parieto-Frontal Network in Analogical Reasoning, Front. Hum. Neurosci. 5 (2011) 1–14. https://doi.org/ 10.3389/fnhum.2011.00022.

[105] Q. Zhang, G. Zhang, L. Yao, X. Zhao, Impact of real-time fMRI working memory feedback training on the interactions between three core brain networks, Front. Behav. Neurosci. 9 (2015) 1–9. https://doi.org/10.3389/fnbeh.2015.00244.

[106] C. Wiklund-hörnqvist, M. Andersson, B. Jonsson, L. Nyberg, Neural activations associated with feedback and retrieval success, Npj Sci. Learn. (2017) 1–7. https://doi.org/10.1038/s41539-017-0013-6.

[107] Á. Lukács, F. Kemény, J.A.G. Lum, M.T. Ullman, Learning and overnight retention in declarative memory in specific language impairment, PLoS One. 12 (2017) 1–23. https://doi.org/10.1371/journal.pone.0169474.

[108] P. Gui, J. Li, Y. Ku, L. Li, X. Li, X. Zhou, M. Bodner, F.A. Lenz, X.W. Dong, L. Wang, Y. Di Zhou, Neural correlates of feedback processing in visuo-tactile crossmodal paired-associate learning, Front. Hum. Neurosci. 12 (2018) 1–14. https://doi.org/10.3389/fnhum.2018.00266.

[109] K.C.S. Adam, E.K. Vogel, Improvements to visual working memory performance with practice and feedback, PLoS One. 13 (2018) 1–22. https://doi.org/ 10.1371/journal.pone.0203279.

[110] K. Ergo, E. De Loof, C. Janssens, T. Verguts, Oscillatory signatures of reward prediction errors in declarative learning, Neuroimage. 186 (2019) 137–145. https://doi.org/10.1016/j.neuroimage.2018.10.083.

[111] D. Apšvalka, E.S. Cross, R. Ramsey, Fluid intelligence and working memory support dissociable aspects of learning by physical but not observational practice, Cognition. 190 (2019) 170–183. https://doi.org/10.1016/j.cognition.2019.04.015.

[112] K. Sengottuvel, A. Vasudevamurthy, M.T. Ullman, F.S. Earle, Learning and Consolidation of Declarative Memory in Good and Poor Readers of English as a Second Language, Front. Psychol. 11 (2020) 1–8. https://doi.org/10.3389/fpsyg.2020.00715.

[113] S. Agrawal, R. Sharma, V. Chinnadurai, Functional connectivity between frontal/parietal regions and MTL–basal ganglia during feedback learning and declarative memory retrieval, J. Biosci. 46 (2021). https://doi.org/10.1007/s12038-021-00194-y.

[114] B. Rypma, J.S. Berger, V. Prabhakaran, B. Martin Bly, D.Y. Kimberg, B.B. Biswal, M. D'Esposito, Neural correlates of cognitive efficiency, Neuroimage. 33 (2006) 969–979. https://doi.org/10.1016/j.neuroimage.2006.05.065.

[115] N. Jaušovec, K. Jaušovec, Differences in induced brain activity during the performance of learning and working-memory tasks related to intelligence, Brain Cogn. 54 (2004) 65–74. https://doi.org/10.1016/S0278-2626(03)00263-X.

[116] H. Laufs, A. Kleinschmidt, A. Beyerle, E. Eger, A. Salek-haddadi, C. Preibisch, K. Krakow, EEG-correlated fMRI of human alpha activity, 19 (2003) 1463–1476. https://doi.org/10.1016/S1053-8119(03)00286-6.

[117] M. Benedek, S. Bergner, T. Könen, A. Fink, A.C. Neubauer, EEG alpha synchronization is related to top-down processing in convergent and divergent thinking, Neuropsychologia. 49 (2011) 3505–3511. https://doi.org/10.1016/j.neuropsychologia.2011.09.004.

[118] W. Klimesch, M. Doppelmayr, H. Russegger, T. Pachinger, J. Schwaiger, Induced alpha band power changes in the human EEG and attention, Neurosci. Lett. 244 (1998) 73–76. https://doi.org/10.1016/S0304-3940(98)00122-0.

[119] W. Klimesch, H. Schimke, J. Schwaiger, Episodic and semantic memory: an analysis in the EEG theta and alpha band, Electroencephalogr. Clin. Neurophysiol. 91 (1994) 428–441. https://doi.org/10.1016/0013-4694(94)90164-3.

[120] W. Klimesch, P. Sauseng, S. Hanslmayr, EEG alpha oscillations: The inhibition-timing hypothesis, Brain Res. Rev. 53 (2007) 63–88. https://doi.org/10.1016/j.brainresrev.2006.06.003.

[121] J. Harper, S.M. Malone, W.G. Iacono, Theta- and delta-band EEG network dynamics during a novelty oddball task, Psychophysiology. 54 (2017). https://doi.org/10.1111/psyp.12906.

[122] C. Babiloni, C. Miniussi, F. Babiloni, F. Carducci, F. Cincotti, C. Del Percio, G. Sirello, C. Fracassi, A.C. Nobre, P.M. Rossini, Sub-second "temporal attention" modulates alpha rhythms. A high-resolution EEG study, Cogn. Brain Res. 19 (2004) 259–268. https://doi.org/10.1016/j.cogbrainres.2003.12.010.

[123] C.M. Krause, T. Åström, M. Karrasch, M. Laine, L. Sillanmäki, Cortical activation related to auditory semantic matching of concrete versus abstract words, Clin. Neurophysiol. 110 (1999) 1371–1377. https://doi.org/10.1016/S1388-2457(99)00093-0.

[124] R.F. Helfrich, M. Huang, G. Wilson, R.T. Knight, Prefrontal cortex modulates posterior alpha oscillations during top-down guided visual perception, Proc. Natl. Acad. Sci. U. S. A. 114 (2017) 9457–9462. https://doi.org/10.1073/pnas.1705965114.

[125] G.G. Knyazev, EEG delta oscillations as a correlate of basic homeostatic and motivational processes, Neurosci. Biobehav. Rev. 36 (2012) 677–695. https://doi.org/10.1016/j.neubiorev.2011.10.002.

[126] W. Klimesch, M. Doppelmayr, H. Schimke, B. Ripper, Theta synchronization and alpha desynchronization in a memory task, Psychophysiology. 34 (1997) 169–176. https://doi.org/10.1111/j.1469-8986.1997.tb02128.x.

[127] J. Jacobs, G. Hwang, T. Curran, M.J. Kahana, EEG oscillations and recognition memory: Theta correlates of memory retrieval and decision making, Neuroimage. 32 (2006) 978–987. https://doi.org/10.1016/j.neuroimage.2006.02.018.

[128] N.A. Herweg, E.A. Solomon, M.J. Kahana, Theta Oscillations in Human Memory, Trends Cogn. Sci. 24 (2020) 208–227. https://doi.org/10.1016/j.tics.2019.12.006.

[129] A. HajiHosseini, C.A. Hutcherson, C.B. Holroyd, Beta oscillations following performance feedback predict subsequent recall of task-relevant information, Sci. Rep. 10 (2020) 1–8. https://doi.org/10.1038/s41598-020-72128-x.

[130] J. Marco-Pallarés, T.F. Münte, A. Rodríguez-Fornells, The role of high-frequency oscillatory activity in reward processing and learning, Neurosci. Biobehav. Rev. 49 (2015) 1–7. https://doi.org/10.1016/j.neubiorev.2014.11.014.

[131] G. Buzsáki, Rhythms of the Brain, 2009. https://doi.org/10.1093/acprof:oso/9780195301069.001.0001.

[132] R.E. Jung, R.J. Haier, The Parieto-Frontal Integration Theory (P-FIT) of intelligence: Converging neuroimaging evidence, Behav. Brain Sci. 30 (2007) 135–154. https://doi.org/10.1017/S0140525X07001185.

[133] J.R. Gray, C.F. Chabris, T.S. Braver, Neural mechanisms of general fluid, (2003) 1–7. https://doi.org/10.1038/nn1014.

[134] A. Woolgar, A. Parr, R. Cusack, R. Thompson, I. Nimmo-smith, T. Torralva, M. Roca, N. Antoun, F. Manes, J. Duncan, M. Posner, A. Woolgar, A. Parra, R. Cusack, R. Thompson, M. Rocab, N. Antounc, F. Manesb, J. Duncan, I. Nimmo-smith, T. Torralvab, Fluid intelligence loss linked to restricted regions of damage within frontal and parietal cortex, 107 (2015) 14899–14902. https://doi.org/10.1073/pnas.

[135] K.H. Lee, Y.Y. Choi, J.R. Gray, S.H. Cho, J.H. Chae, S. Lee, K. Kim, Neural correlates of superior intelligence: Stronger recruitment of posterior parietal cortex, Neuroimage. 29 (2006) 578–586. https://doi.org/10.1016/j.neuroimage.2005.07.036.

[136] M.N. Moussa, C.D. Vechlekar, J.H. Burdette, M.R. Steen, C.E. Hugenschmidt, P.J. Laurienti, Changes in Cognitive State Alter Human Functional Brain Networks, Front. Hum. Neurosci. 5 (2011) 1–15. https://doi.org/10.3389/fnhum.2011.00083.

[137] H. Cao, M.M. Plichta, A. Schäfer, L. Haddad, O. Grimm, M. Schneider, C. Esslinger, P. Kirsch, A. Meyer-Lindenberg, H. Tost, Test-retest reliability of fMRI-based graph theoretical properties during working memory, emotion processing, and resting state, Neuroimage. 84 (2014) 888–900. https://doi.org/10.1016/j.neuroimage.2013.09.013.

[138] T. Bolt, J.S. Nomi, M. Rubinov, L.Q. Uddin, Correspondence between evoked and intrinsic functional brain network configurations, Hum. Brain Mapp. 38 (2017) 1992–2007. https://doi.org/10.1002/hbm.23500.

[139] E. Mas-Herrero, J. Marco-Pallarés, Theta oscillations integrate functionally segregated sub-regions of the medial prefrontal cortex, Neuroimage. 143 (2016) 166–174. https://doi.org/10.1016/j.neuroimage.2016.08.024.

[140] A.R. Backus, J.M. Schoffelen, S. Szebényi, S. Hanslmayr, C.F. Doeller, Hippocampal-prefrontal theta oscillations support memory integration, Curr. Biol. 26 (2016) 450–457. https://doi.org/10.1016/j.cub.2015.12.048.

[141] M.E. Hasselmo, C. Bodelón, B.P. Wyble, A proposed function for hippocampal theta rhythm: Separate phases of encoding and retrieval enhance reversal of prior learning, Neural Comput. 14 (2002) 793–817. https://doi.org/10.1162/089976602317318965.

[142] E. Bullmore, O. Sporns, The economy of brain network organization, Nat. Rev. Neurosci. 13 (2012) 336–349. https://doi.org/10.1038/nrn3214.

[143] Z. Yaple, M. Martinez-Saito, N. Novikov, D. Altukhov, A. Shestakova, V. Klucharev, Power of Feedback-Induced Beta Oscillations Reflect Omission of Rewards: Evidence From an EEG Gambling Study, Front. Neurosci. 12 (2018) 1–11. https://doi.org/10.3389/fnins.2018.00776.

[144] M.X. Cohen, K. Wilmes, I. van de Vijver, Cortical electrophysiological network dynamics of feedback learning, Trends Cogn. Sci. 15 (2011) 558–566. https://doi.org/10.1016/j.tics.2011.10.004.

[145] C.D.B. Luft, Learning from feedback: The neural mechanisms of feedback processing facilitating better performance, Behav. Brain Res. 261 (2014) 356–368. https://doi.org/10.1016/j.bbr.2013.12.043.

[146] A.H. Hosseini, C.B. Holroyd, Reward feedback stimuli elicit high-beta EEG oscillations in human dorsolateral prefrontal cortex, Sci. Rep. 5 (2015) 1–8. https://doi.org/10.1038/srep13021.

[147] I. van de Vijver, K. Richard Ridderinkhof, M.X. Cohen, Frontal oscillatory dynamics predict feedback learning and action adjustment, J. Cogn. Neurosci. 23 (2011) 4106–4121. https://doi.org/10.1162/jocn_a_00110.

[148] T. Harmony, The functional significance of delta oscillations in cognitive processing, Front. Integr. Neurosci. 7 (2013) 1–10. https://doi.org/10.3389/fnint.2013.00083.

[149] D.J.L.G. Schutter, G.G. Knyazev, Cross-frequency coupling of brain oscillations in studying motivation and emotion, Motiv. Emot. 36 (2012) 46–54. https://doi.org/10.1007/s11031-011-9237-6.

[150] E. Takahashi, K. Ohki, D.S. Kim, Dissociated pathways for successful memory retrieval from the human parietal cortex: Anatomical and functional connectivity analyses, Cereb. Cortex. 18 (2008) 1771–1778. https://doi.org/10.1093/cercor/bhm204.

[151] D.I. Donaldson, M.E. Wheeler, S.E. Petersen, Remember the source: Dissociating frontal and parietal contributions to episodic memory, J. Cogn. Neurosci. 22 (2010) 377–391. https://doi.org/10.1162/jocn.2009.21242.

CHAPTER 5

HEMODYNAMIC FUNCTIONAL CONNECTIVITY OPTIMIZATION OF FREQUENCY EEG MICROSTATES ENABLES ATTENTION LSTM FRAMEWORK TO CLASSIFY DISTINCT TEMPORAL CORTICAL COMMUNICATIONS OF DIFFERENT COGNITIVE TASKS

This chapter is a marginally modified version of the research article published as Agrawal, S., Chinnadurai, V., & Sharma, R. (2022). Hemodynamic functional connectivity optimization of frequency EEG microstates enables attention LSTM framework to classify distinct temporal cortical communications of different cognitive tasks. Brain Informatics, 9(1), 1-17.

5.1 ABSTRACT

Temporal analysis of global cortical communication of cognitive tasks in coarse EEG information is still challenging due to the underlying complex neural mechanisms. This study proposes an attention-based time-series deep learning framework that processes fMRI functional connectivity optimized quasi-stable frequency microstates for classifying distinct temporal cortical communications of the cognitive task. Seventy volunteers were subjected to visual target detection tasks, and their electroencephalogram (EEG) and functional MRI (fMRI) were acquired simultaneously. At first, the acquired EEG information was preprocessed and bandpass to delta, theta, alpha, beta, and gamma bands and then subjected to quasi-stable frequency-microstate estimation. Subsequently, time-series elicitation of each frequency microstates is optimized with graph theory measures of simultaneously eliciting fMRI functional connectivity between frontal, parietal, and temporal cortices. The distinct neural mechanisms associated with each optimized frequency-microstate were analyzed using microstate-informed fMRI. Finally, these optimized, quasi-stable frequency microstates were employed to train and validate the attention-based Long Short-Term Memory (LSTM) time-series architecture for classifying distinct temporal cortical communications of the target from other cognitive tasks. The temporal,

sliding input sampling windows were chosen between 180 to 750 ms/segment based on the stability of transition probabilities of the optimized microstates. The results revealed twelve distinct frequency microstates capable of deciphering target detections' temporal cortical communications from other task engagements. Particularly, fMRI functional connectivity measures of target engagement were observed significantly correlated with the right-diagonal delta (r=0.31), anterior-posterior theta (r=0.35), left-right theta (r=-0.32), alpha (r=-0.31) microstates. Further, neuro-vascular information of microstate-informed fMRI analysis revealed the association of delta/theta and alpha/beta microstates with cortical communications and local neural processing, respectively. The classification accuracies of the attention-based LSTM were higher than the traditional LSTM architectures, particularly the frameworks that sampled the EEG data with a temporal width of 300 ms/segment. In conclusion, the study demonstrates reliable temporal classifications of global cortical communication of distinct tasks using an attention-based LSTM utilizing fMRI functional connectivity optimized quasi-stable frequency microstates.

5.2. INTRODUCTION

5.2.1 Decoding distant cortical communications from cortical EEG

The human brain dynamically engages distinct neural populations between distant brain regions, and their spatiotemporal oscillations often modulate systematically with behavioural and cognitive tasks. The synchrony or lack thereof between remote brain regions brings effective global brain communication, functional connectivity for information processing. Many researchers [1–3] employed simultaneous EEG information acquired with fMRI imaging to understand these functional connectivities, neural origins, and correlated brain states. These researches revealed that the elicitation of local neural systems is observed as high-frequency dynamics in EEG cortical oscillations. Cortical high-frequency gamma oscillation mainly explains local high-level neural information and positively correlates with the fMRI BOLD strength. Further, the distant cortical and long-range coordination emerges as the lower EEG cortical frequency oscillation [4]. The alpha and beta power modulate the BOLD response's latency and strength to gamma power changes [5]. Many researchers [6–8] have recently observed multi-frequency cortical EEG interaction

explaining hemodynamic task elicitation better than single EEG power information. JC Pang et al (Pang and Robinson, 2018) revealed that the inverse correlation of alpha and BOLD originates from high- and low-frequency components of the same underlying neural engagement caused by modulation in corticothalamic and intra-thalamic feedback. Despite these clear insights of distinct global and local neural processing associated with every task engagement, decoding their temporal dynamics computationally from spatially coarse-grained cortical times-series EEG information is still challenging.

5.2.2 Microstates and global cortical communication

Microstates are the cluster centres of EEG information and are unique in every cognitive task engagement in healthy and disease populations. Every microstate topography is associated with a "quasi-stable" functional state (Gschwind et al. 2016; Michel and Koenig, 2018), explaining the brain's specific neural interaction. These quasi-stable patterns span around 100 ms and are the most robust approach to bringing distant functional communication in cortical EEG information. Many researchers [12,13] observed that the time course of microstate metrics, when correlated with the fMRI BOLD signal, reveals functional networks similar to the resting-state networks. Further, the microstate dynamics are observed to measure transitions between global cortical communications characterized by specific local neural alpha inhibitions [14–17]. The traditional microstate estimation employs the EEG frequency range [18,19] of 2-20Hz. Hence, their time-series dynamics are primarily influenced by the cortical alpha inhibitory/excitatory modulations [20]. However, the cognitive task engagement's distant and local cortical communication manifests through other EEG rhythms [21,22]. Thus, the task-induced modulation of cortical communication and associated local neural engagement is manifested as a combination of different frequencies [23]. More recently, the beta-band and the coverage feature of the EEG microstate analysis have been revealed as the essential features for classifying epilepsy and PNES patients with reasonably high accuracy and precision [24].

5.2.3 Deep learning approaches for temporal EEG analysis

The EEG time-series information is higher-dimensional, and the cognitive information is spread across its timelines. Hence, the feature information derived from a single time point of EEG time series data is inadequate to explain any cognitive process. Thus, Recurrent Neural networks (RNN) perform better in extracting sequential information embedded in higher dimensional EEG time-series information. However, the traditional RNN system suffers in learning long-term dynamics due to vanishing/exploding gradient problems. Long Short-Term Memory (LSTM) architecture addresses this exploding gradient obstacle by learning both long- and short-term dependencies. Recently, the attention mechanism has been introduced [25] to improve the performance of deep learning models; it highlights the more informative feature and subsequently gives higher weights to the corresponding original feature sequence. It has been embedded with the LSTM architecture in several EEG studies [26–32] by effectively selecting the feature information and observed with significantly improved efficiency and performance accuracy of deep learning systems.

5.2.4 Present Study

The present study proposes an attention-based LSTM computational model that employs optimized frequency microstates to decipher the distant cortical communication of visual target detection tasks. The temporal dynamics of the frequency microstate metrics are correlated with fMRI hemodynamic functional connectivity measures to optimize the cortical EEG quasi-stable frequency patterns with the task's local/global brain communication. The hemodynamic functional connectivity is assessed by employing the graph-theoretical analysis on simultaneously acquired fMRI information. The significantly correlated frequency microstates are further subjected to the robust correlation analysis to understand their multi-frequency coupling elicited during intercortical interaction during the task engagement. The local and global neural mechanisms underlying these frequency quasi-stable microstates were further estimated through EEG-informed-fMRI analysis. Finally, a hybrid deep learning framework consisting of LSTM with an attention mechanism is employed to classify the target detection task engagement

from the temporal dynamics of these optimized frequency microstate quasi-stable patterns. The performance metrics such as precision, accuracy, and recall are estimated for all deep learning architectures and validated using a 10-fold cross-validation approach.

5.3. Methods and materials

5.3.1 Participants and task design

Seventy healthy right-handed volunteers (30 males and 40 females; mean age: 23 years; age range, 20-32 years) were selected from the academic environment. All participants gave written informed consent and did not have psychiatric or neurological disorders or medication. The experiment was conducted following the World Medical Association (Declaration of Helsinki), and the local ethical committee approved all measurements. The vision of participants was corrected using MR-compatible lenses whenever required.

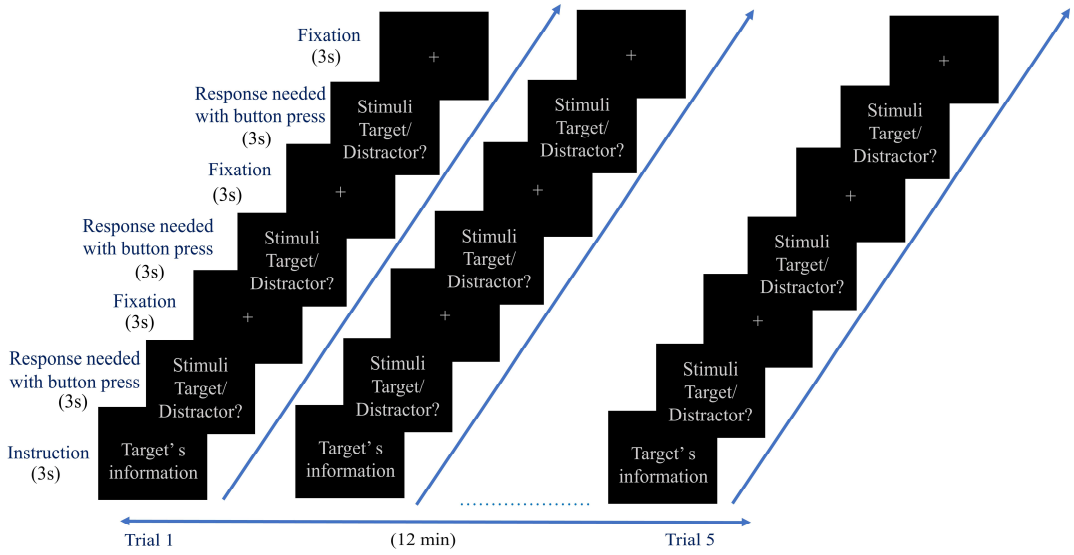

Figure 5.1: Schematic of task paradigm design.

These participants underwent the task paradigm (Figure 5.1) designed to perform three tasks. They are target detection, distractor detection, and fixation identification. For this purpose, the multiple distinct shapes (squares, circles, stars, and triangles) with primary colours (experimental conditions, stimuli) were shown at the beginning (called 'Targets stimulus'). Then volunteers were sequentially shown a single

stimulus, one at a time, and asked whether it was part of earlier displayed target stimuli collections. The volunteer must click the right thumb button whenever he identifies the target stimulus. Only 30 percent of stimuli were selected from earlier displayed stimuli, the targets, and randomly distributed among the "Distractor Stimulus." The correct identification of the target stimulus invokes the elicitation of distinct neural mechanisms compared to the identification of distractors. Each sequential stimulus was presented for the duration of 3000 milliseconds. The paradigm consisted of five trials. Each trial started with a different target stimuli collection, and 105 single stimuli were subsequently presented for target/distractor identification. Among 105 stimuli, only 32 were target stimuli and presented randomly. A fixation stimulus followed each stimulus; a single black-coloured cross in the slide's centre was presented for 3 seconds. These task stimuli are projected onto MR-compatible lenses fitted on the head coil inside MRI.

5.3.2 Simultaneous EEG-fMRI acquisition and preprocessing

In the present study, simultaneous EEG-fMRI data acquisition is carried out using a 3T Siemens Magnetom Skyra scanner (Siemens, Erlangen) and MR-compatible 32-channel Brain Amp system with an EEG cap. EEG signals are recorded at a sampling rate of 5 kHz, and the impedance of all scalp electrodes is maintained below five kOhms throughout the recording. The fMRI were acquired using Eco Planar Imaging (EPI) sequence with TR =3000 ms; TE= 36 ms; voxel size =3.6*3.6*3.0 mm; matrix =64*64; FoV read = 230 mm; flip angle =90^{o}, 36 axial slices. The axial slices are acquired parallel to the Anterior-Posterior (AC-PC) line in an interleaving manner with a slice thickness of 3.0 mm. The high-resolution structural images of the brain are acquired using T1 MPRAGE sequence with parameters, voxel size =1.0*1.0*1.0 mm; TR= 2000 ms; flip angle = 90^{o}; FoV = 240 mm; matrix= 512*512; slice thickness = 1.0 mm, 160 axial slices. The axial slices are acquired parallel to the Anterior-Posterior (AC-PC) line in an interleaving manner with a slice thickness of 5.0 mm.

EEG data acquired simultaneously inside the MRI scanner is initially subjected to the FMRIB plugin of EEGLAB to remove the MRI-related artifacts such as gradient switching and cardio ballistic artifacts. The gradient artifact removal process

employed FASTR (FMRI Artifact Slice Template Removal) tool [33,34]. It aligned all the artifact slices to correct any slight jitter in the exact location of the slice-timing events, interpolating and shifting each artifact until the correlation was maximized between data and a reference artifact (the first artifact in the data). The second stage of FASTR [35] computed an average template for the cardio ballistic artifact. It subtracted this template from the centre contaminated data by taking a moving window average of slice artifacts. QRS detection utilizes combined adaptive thresholding [36] and the Teager energy operator [37], followed by a correction algorithm to detect heartbeats robustly for false positives and negatives and remove the pulse artifacts by using an optimal basis set for the number of PCs 3.

Further, Harvard Automated Processing Pipeline (HAPPE) [38] is employed for noise-free time-frequency analyses using EEGLAB (MathWorks). MR and CB artifact corrected EEG data are subjected to the 0.1 Hz high pass and 57 Hz low pass filtering followed by ICA decomposition using all the EEG channels. The electrical noise is removed using the Clean Line program (Mullen, 2012) through the multi-taper regression approach implemented in EEGLAB. The bad channels are identified by evaluating the normed joint probability of the average log power of all the selected channels and removed for the probability of more than three standard deviations from the mean for further analyses. A wavelet-enhanced ICA (W-ICA) approach removes eye and muscle-generated artifacts, high-amplitude artifacts, and signal discontinuities from EEG data. This approach of W-ICA followed by ICA improves the resulting ICA decomposition of the EEG data [39]. A machine-learning algorithm MARA (Multiple Artifact Rejection Algorithm) [40] evaluates the ICA-derived components for automated component rejection for artifact probabilities greater than 0.5.

Further, artifact rejected data is segmented based on event markers. The artifact-corrected datasets were subsequently downsampled to 250Hz and re-referenced to the common average reference and bandpass filtered from 1 Hz to 48 Hz ((1-4) Hz for delta, (4–8) Hz for theta, (9–14) Hz for an alpha, (15-35) Hz for beta and (35-48) Hz for gamma)). Finally, all the participants' artifact corrected data are then segregated specific to the target, distractor, and fixation blocks. Further, simultaneously- acquired fMRI data is preprocessed using Statistical Parametric Mapping version 12. The information is corrected for slice-timing differences, spatially realigned, and excluded

if movement exceeds 3 mm. It follows by registering the functional scans to standard MNI template space. Further, artifact-corrected images are subjected to spatially smoothing with a 5*5*5 mm full-width half-maximum Gaussian kernel.

5.3.3 Estimation of frequency-microstates and their optimization with task's cortical communications

The present study develops a computational framework that classifies distinct task engagement's temporal global cortical communication through unique temporal EEG quasi-stable information that decodes the neural basis of the distant cortical communications. Figure 5.2 explains these processes in detail. The following section will elaborate on each one of these steps in detail.

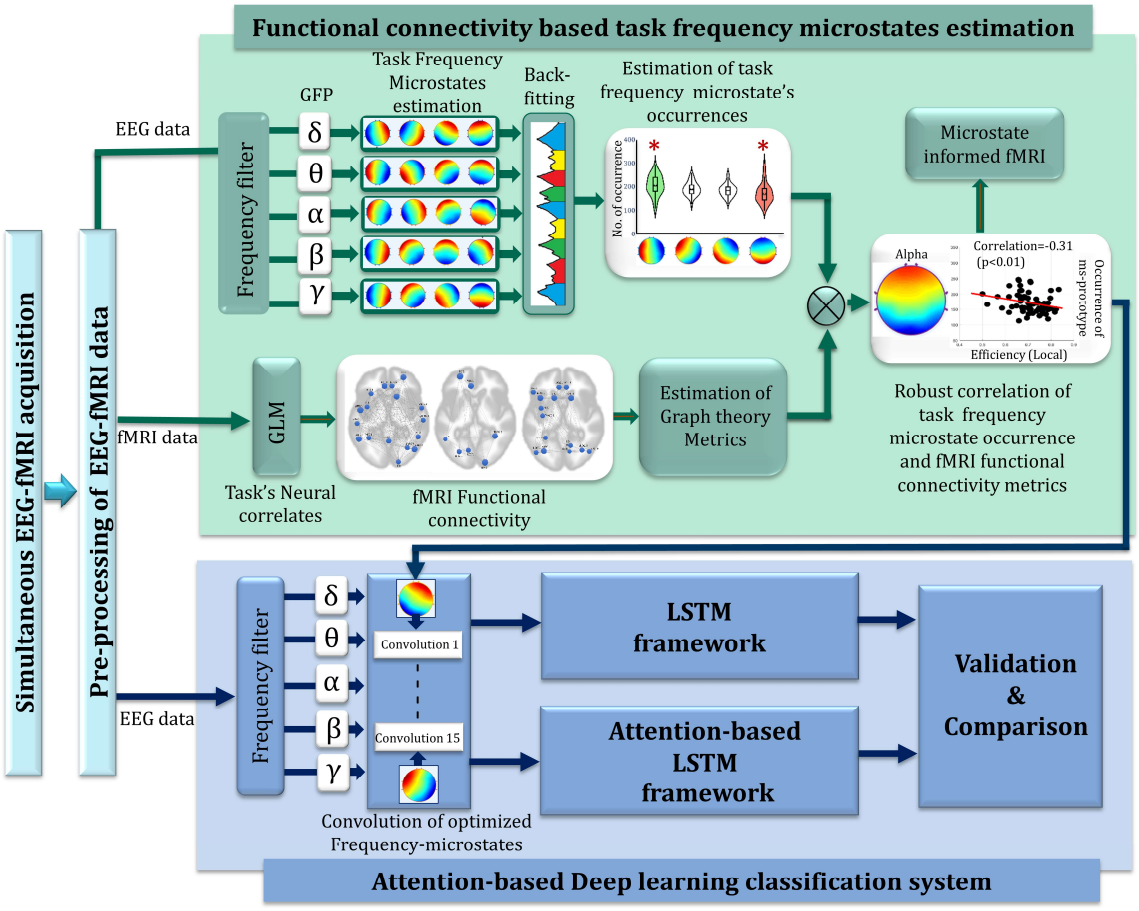

Figure 5.2: Methodological framework of the study.

At first, artifact-corrected EEG data is bandpass filtered to segregate it into frequency-band limited data comprising of (1-4) Hz for delta, (4–8) Hz for theta, (9–14) Hz for an alpha, (15-35) Hz for beta and (35-48) Hz for gamma. Then, each frequency information's Global Field Power (GFP) is computed and subjected to the modified K-means clustering algorithm [41] to identify every frequency-microstate topographic prototype. A detailed description of this estimation is given in supplementary section S1. Then, each frequency-microstate prototype is back fitted in every individual's data and estimated re-expressed sequences of microstate classes. Finally, statistics about the sequence of microstate classes, such as their frequency of occurrence or average duration, are calculated. This quasi-stable frequency-microstate patterns elicitation information is subsequently mapped with global functional connectivity of each task engagement assessed from simultaneously-acquired fMRI information.

Simultaneously, the task's neural sources are identified from simultaneously-acquired fMRI information employing the General Linear Model-based (GLM) analysis. At the subject level analysis, BOLD responses of each task engagement (target, distractor, and fixation) are modelled by a canonical hemodynamic response function with temporal and dispersion derivatives with six realignment parameters for each run. In second-level GLM modelling, group average maps were computed using one-sample t-tests, cluster corrected ($p<0.05$) across subjects. Subsequently, the second-level GLM model results for every task engagement are passed as Regions of Interest (ROI) to graph theory analysis to estimate the global/local functional connectivity [42]. A detailed description of this estimation is given in the supplementary file section S2. Finally, the graph theory metrics such as global and local efficiency of the functionally connected regions are estimated for each subject, and the ROI-to-ROI connectivity matrix is thresholded at p-FDR<0.05 in a two-sided analysis.

Finally, these tasks' global cortical communications information estimated from fMRI graph theoretical measures are utilized to optimize and identify the relevant cortical quasi-stable frequency EEG elicitations that correspond to the task engagement. For this purpose, the number of occurrences of each delta, theta, alpha, beta, and gamma EEG-microstates of every individual during task engagements (target, distractor, and fixation) is subjected to the robust correlation with global functional connectivities metrics measured from the simultaneously measured fMRI information. This study

further validated these significantly correlating frequency-microstates by subjecting them to the EEG-informed fMRI analysis [43,44] and studying their neural mechanisms. Since the frequency microstates that correlate with fMRI functional connectivity metrics are different for target, distractor, and fixation, three separate EEG-informed fMRI models were constructed for every task engagement. A detailed description of this estimation is given in the supplementary file section S3.

5.3.4 Attention-based LSTM model and validation

This study aims to develop an attention-based LSTM framework to classify the global cortical communication (estimated using fMRI functional connectivity optimized frequency quasi-stable oscillations) associated with global brain communications. For this purpose, each frequency-microstate strongly associated with fMRI functional connectivity measures was correlated with every individual preprocessed EEG information. Then, the feature vector consisting of the correlation value for each quasi-stable frequency microstates belonging to every task engagement is formed and used as a training, testing, and validation dataset for the attention-based LSTM deep learning model. The attention-based LSTM model employed in this study is illustrated in Figure 5.3.

LSTM has been a popular recurrent neural network for learning sequential features in time series data and classifying EEG information [45,46]. However, the standard LSTM is incapable of detecting important parts for classification. The attention mechanism is recently conceptualized [25] and integrated with the LSTM framework to overcome this issue. The attention mechanism improves the ability of LSTM by concentrating on time fragments with the most discriminative information in EEG time series. It helps to classify the data that involves remembering and aggregating feature embeddings in time-series information [47]. A detailed description of the LSTM model and attention mechanism is explained below.

The LSTM architecture consists of interconnected cells that hold the memory information through which the input data is processed to evaluate the output results. The cells have a common cell state, keeping long-term dependencies along the entire

LSTM chain of cells. In LSTM, input information flow is controlled by the input gate (i_t) and forget gate (f_t) and allows the network to decide whether to forget the previous state (C_{t-1}) or update the current state (C_t) with new information. Further, each cell's result is modulated by an output gate (o_t), which lets the cell compute its output based on the updated information. The function of LSTM cell architecture is calculated as:

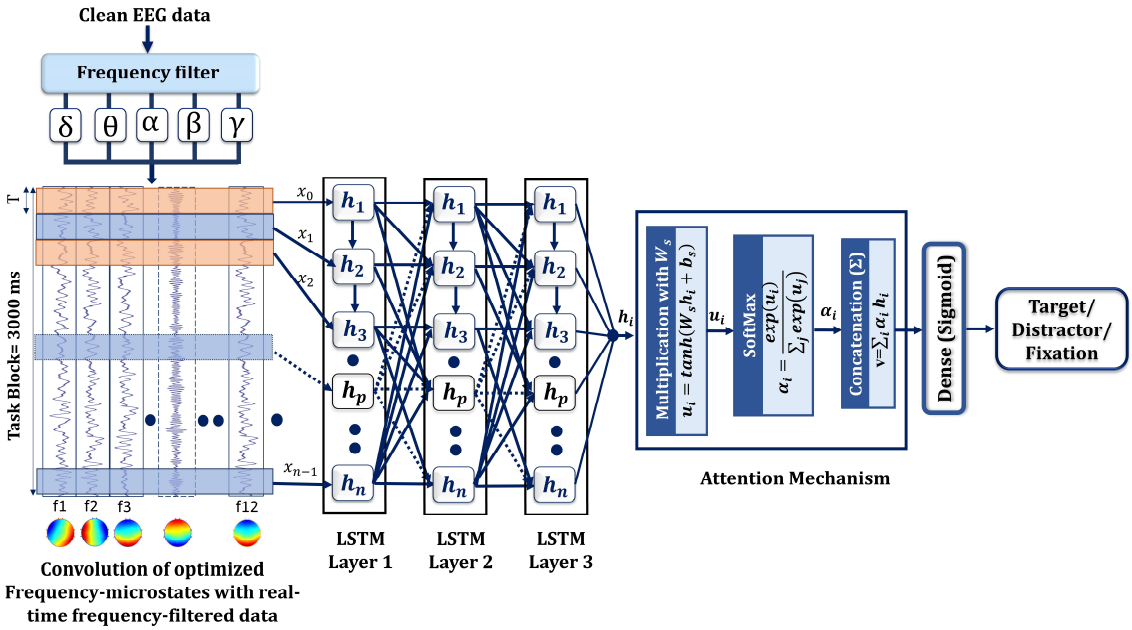

Figure 5.3: Schematic diagram of Attention-based LSTM deep learning framework adopted in the study. 'T' represents the temporal, sliding input sampling window size and is chosen between 180 to 750 ms/segment associated with the specific number of cells ranging from 4 to 16, based on the stability of transition probabilities of the optimized microstates.

$$i_t = \sigma(W_i \,.\, [h_{t-1}, x_t] + b_i) \quad .(1)$$

$$f_t = \sigma(W_f \,.\, [h_{t-1}, x_t] + b_f) \quad .(2)$$

$$C_t = f_t * C_{t-1} + i_t * \tanh(W_c \,.\, [h_{t-1}, x_t] + b_c) \quad .(3)$$

$$o_t = \sigma(W_o \,.\, [h_{t-1}, x_t] + b_o) \quad .(4)$$

$$h_t = o_t * \tanh(C_t) \quad .(5)$$

where $\sigma(x) = \frac{1}{1+e^{-x}}$, $\tanh(x) = \frac{2}{1+e^{-2x}} - 1$. . h_t, C_{t-1} and x_t are the hidden state, cell state and input passed to the architecture at time step t. W_f, W_i, W_c,W_o are the weights, and b_f, b_i, b_c, and b_o are the biases.

Attention mechanism:

The core concept of the attention mechanism is to simulate the human attention mechanism to improve the performance of deep learning [48] by utilizing the weighting parameters of the elements in the input sequence to generate the output sequence. It is carried out by multiplying the hidden output states by trainable weights, capturing more discriminative task-related features, and can be expressed as:

$$h_i = \mathrm{LSTM}(s_i), i \in [1, L] \quad .(6)$$

where h_i is the output hidden state vector for the i^{th} LSTM cell corresponding to the i_{th} input, and L is the number of cells in each recurrent layer of the LSTM network. To capture the importance of each hidden state, the attention mechanism is defined as follows:

$$u_i = \tanh(W_s h_i + b_s), \quad .(7)$$

$$\alpha_i = \frac{exp(u_i)}{\sum_j exp(u_j)}, \quad .(8)$$

$$v = \sum_i \alpha_i h_i \quad .(9)$$

where vector v is the attention layer's output, and Ws and bs are trainable parameters. This study uses all twelve quasi-stable frequency microstates (correlated with task engagement's neural mechanisms) as input information to train attention-based LSTM models. As mentioned in the methods, seventy volunteers participated in the study and performed target identification, distractor identification, and fixation (rest). Each paradigm involved 32 blocks of the target, 62 blocks of the distractor, and 94 blocks of fixation. More distractors and fixation are needed to avoid the expectancy aspect of cognitive engagement. For this, 32-channel EEG is employed to acquire the data with a 5k sampling rate and subsampled to 250 Hz during preprocessing. Each task engagement block was carried out for 3 seconds; 750 feature vectors were staggered for every task block. The 32nd channel data is ECG, hence not included for processing. Accordingly, each volunteer will have a 750 x 31 dataset at every block. Equal numbers, 32 blocks from each target, distractor, and fixation are

selected for training. Selecting distractor and fixation from many blocks is done randomly to avoid training bias. Hence, each volunteer had selected data with a size of 72,000x31 (24000x31 for every task engagement). The preprocessed EEG data of the complete seventy volunteer set (50,40,000 x 31) is initially subjected to the correlation with all the twelve significant frequency microstates, resulting in feature vectors with the size of 50,40,000 x 12. Each feature vector consists of the correlation value for each one of the quasi-stable frequency microstate information belonging to every task engagement is formed. The feature vectors are combined across task blocks, and distinct segregation of input feature vectors belonging to every task block was explored. For this, the study independently employed different attention-based LSTM architectures in input layers with 4 to 16-LSTM cells. This enabled analyzing the effect of temporal, sliding sampling window width on the performance of deep learning architectures. As every task stimulus last for 3 seconds, choosing different deep learning architectures with LSTM nodes of 4 to 16 allowed the EEG sliding temporal window to be 750 ms to 180 ms. The final LSTM layer was ensued by an attention layer, which was succeeded by a fully connected layer with a sigmoid activation function to predict the probability of each task engagement. Finally, to estimate the efficacy of attention mechanisms in the original LSTM system, all attention-based LSTM architectures were compared with their attention counterpart. The tuning parameters were applied after each LSTM layer and optimized the weight matrix L2 regularization coefficient of each LSTM layer for optimization. Finally, hyper-parameter such as learning rate was tuned for the stochastic Adam optimizer. The final optimized tuned parameter that performed better is tabulated in table 5.1.

Validation:

Finally, the attention-based LSTM architecture is validated by employing a 10-fold cross-validation approach with no overlap of training and testing segments. True Positive (TP), True Negative (TN), False Negative (FN), and False Positive (FP) were used to calculate the performance metrics. They are formulated as Precision = TP/(TP+FP), Accuracy = (TP+TN)/(TP+TN+FP+FN) and Recall = TP/(TP+FN).

Hyperparameters	Tuned parameters
Hidden layer size	256
Batch size	64
Training epoch numbers	1000
Rate dropout	Input Layer: 0, 1st LSTM Layer: 0.2, 2nd LSTM Layer: 0.1,3rd LSTM Layer: 0.2
Recurrent depth	3
Learning rate	0.001

Table 5.1: Final Tuning parameter of LSTM model.

5.4. Results

The present study presents the time series computational frameworks that classify different task engagement based on temporal modulation of distant brain communications through optimized frequency EEG microstates. The frequency EEG microstates were optimized by associating them with simultaneously eliciting distant hemodynamic functional connectivity measures. Further, the study explored the EEG-informed fMRI approach employed to understand the insights into the neuronal mechanisms related to frequency microstates that correlate with global task communications. The following sections present the results of each of the above steps in detail.

5.4.1 Frontal-parietal- temporal regions interaction during task engagements

The neural sources associated with each task engagement are assessed through fMRI GLM models with the double-sided t-test of $p<0.5$, FDR corrected. The results suggest that target engagement enhanced the hemodynamic response in the frontal [frontal orbital cortex (FOC), frontal pole (FP), superior frontal gyrus (SFG)], parietal [angular gyrus (AG), Precuneus cortex (PC)], and temporal [Inferior and middle temporal Gyrus (ITG, MTG)] cortices. Further, it involves significant engagement of the cingulate gyrus (CG), lateral occipital cortex, occipital pole (OP), paracingulate gyrus, and insular cortex (IC) regions. The neural correlates of distractor and fixation

have also revealed significantly different intercortical engagement. The detailed list of neural correlates of each task engagement is tabulated in Supplementary Table (ST.1).

This distinct inter-cortical communication during each task engagement is further supported by the graph theoretical functional connectivity metrics such as global (GE) and local efficiency (LE). The target engagement significantly engaged inter and intra-cortical communication at frontal cortex (FP [GE:0.893, LE:0.89], FOC [GE: 0.886, LE:0.89], and SFG [GE:0.886, LE:0.894]), parietal cortex (left AG [GE:0.872, LE:0.893], right AG [GE:0.9, LE:0.887], PC [GE:0.87, LE:0.894]) and temporal cortical regions (ITG [GE: 0.88, LE: 0.889], MTG [GE:0.889, LE: 0.891], temporal occipital fusiform cortex (TOFC) [GE:0.88, LE:0.89]) at $p < 0.05$ with FDR correction. Functional connectivity elicitation remained distinct for the target detection task and had minimal overlap with other task engagement. Notably, frontoparietal and frontotemporal interaction engagement were distinct for target, distractor, and fixation engagement. The detailed information on graph-theoretical measures estimated for each task engagement is given in supplementary section S2.

5.4.2 Hemodynamic functional connectivity optimization of quasi-stable frequency-microstates

Frequency microstates estimation revealed four dominant microstates for every EEG frequency band of each task engagement. Figure 5.4 illustrates spatial topographical patterns of frequency-microstate topography associated with every task engagement. Further, figure 5.5 presents the mean number of occurrences of all frequency microstates and highlights twelve specific frequency microstates whose number of occurrences is robustly correlated (+ve correlation: green, -ve correlation: red) with the fMRI functional connectivity measures. The detailed correlation information of frequency microstates with graph-theoretical measures of every task engagement is illustrated in figure 5.6. In this study, based on the microstate's green colour band direction, they are labelled as anterior-posterior (AP), left-right (LR), left diagonal (LD), and right diagonal (RD) microstate prototypes. For example, the delta microstate with a green band travelling between anterior-posterior is called the "anterior-posterior delta microstate." During target engagement, the number of

occurrences of right diagonal delta-microstate positively correlates with the global efficiency of fMRI functional connectivity measures. On the other hand, the local efficiency of fMRI connectivity measures correlates negatively with both left-right theta and alpha microstate occurrences and positively with anterior-posterior theta microstate.

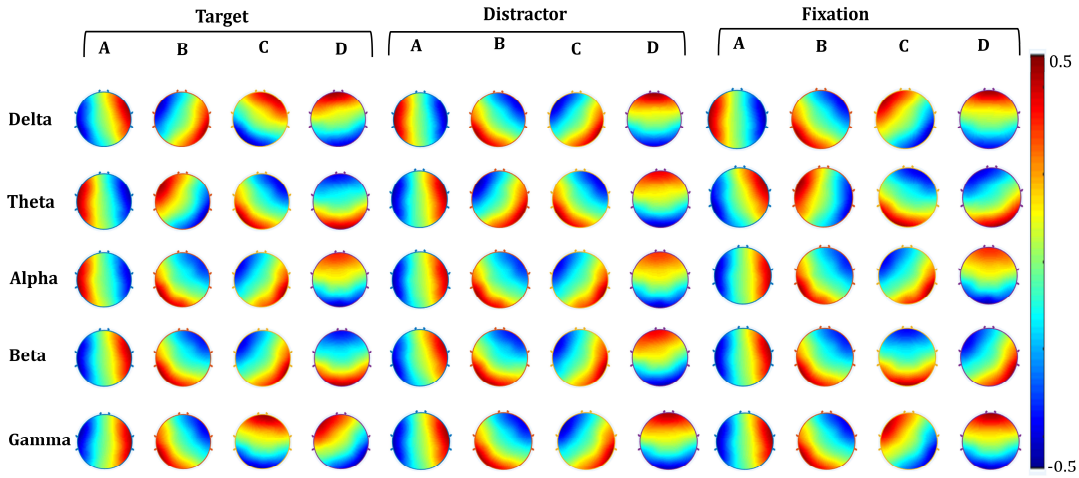

Figure 5.4: A topographical representation of frequency-microstates for the target, distractor, and fixation.

5.4.3 Neurovascular analysis of optimized frequency microstates: EEG Informed fMRI analysis

Engagement of task generally elicits local neural clustering (high-frequency quasi-stable oscillations) at distinct brain regions, responsible for efficient local information processing, together with distant cortical intercommunication to facilitate global communication (low-frequency quasi-stable oscillations). The neuro-vascular analysis through EEG-informed fMRI explains these insights through synchronizing neural information (optimized quasi-stable EEG oscillations) with hemodynamic information (vascular) elicited from a specific task engagement. For this purpose, each of twelve optimized frequency microstates is processed in independent EEG-informed fMRI models, which modelled each microstate as separate regressors ($p<0.01$, FDR corrected) to estimate their neuro-vascular information. Supplementary figures

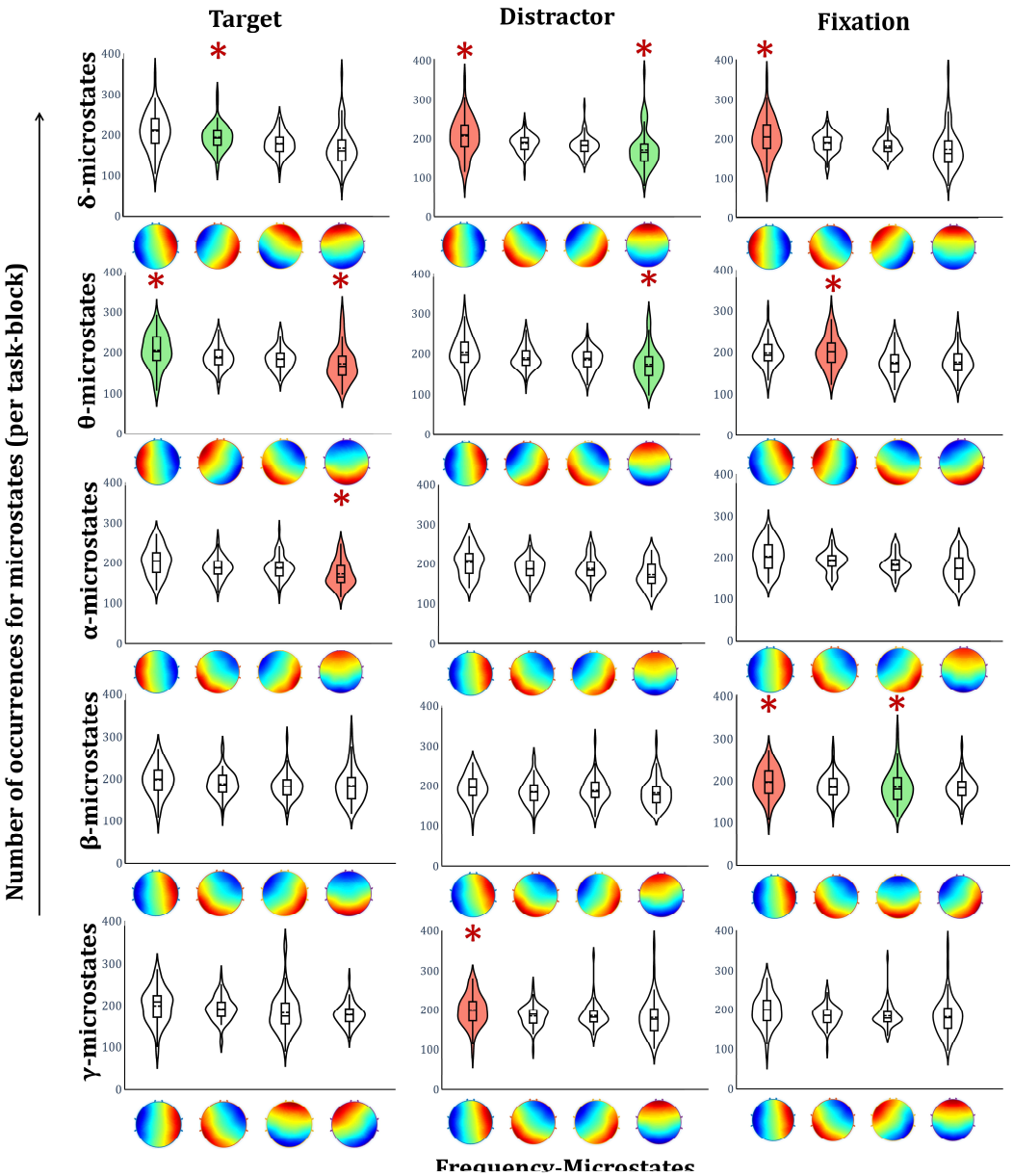

Figure 5.5: Estimated metrics of frequency-microstates. The violin graph plots the mean occurrence of each frequency-microstates for each frequency band. The violin plot's green and red colour shades reveal the correlation (positive and negative) of the number of occurrences of quasi-stable elicitation with the task's fMRI functional connectivity measures. The red star on violin plots specifies the significance ($p<0.01$).

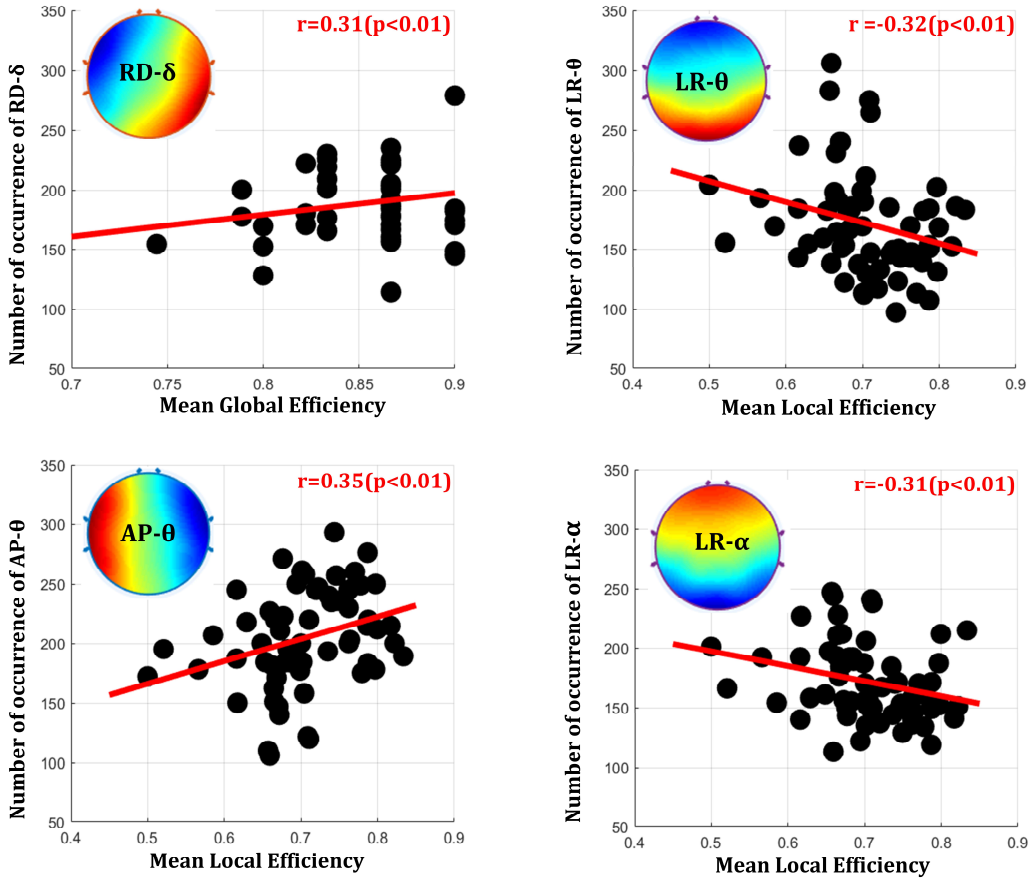

5.6(a): Target-engagement

(SF.1(a-c)) show neuro-vascular information of each twelve optimized microstates.

Figure 5.7 shows the neuro-vascular coupling of each significant frequency-microstate at the neural correlates of the respective task engagement and the associated functional connectivity. Target engagement elucidated the right-diagonal delta-microstate synchronously with the BOLD response in the frontal cortex. Further, anterior-posterior and left-right theta-microstates are found to synchronize with the BOLD response of frontal, temporal, parietal, and occipital regions except for right-lateralized SFG and AG. The role of theta-microstate in BOLD-synchronization of these regions characterizes its significant association with target engagement. The alpha-microstate is observed to de-synchronise with the parietal, PCG's BOLD

response, and synchronise with the frontal, occipital region during target engagement. Our findings also reveal the effects of multiple frequencies on specific brain regions, such that the BOLD response of FP, PCG, SFG, IC, PC, and AG are modulated with delta, theta, and alpha-microstates. Specifically, the study observes the de-synchronization of alpha-microstate with the delta and theta microstates such as PCG, SFG, PC, and synchronization between delta and theta microstates as IC and FP. Hence, the relationships mentioned above reveal that the multi-frequency interactions modulate the BOLD response of task-engaged brain regions.

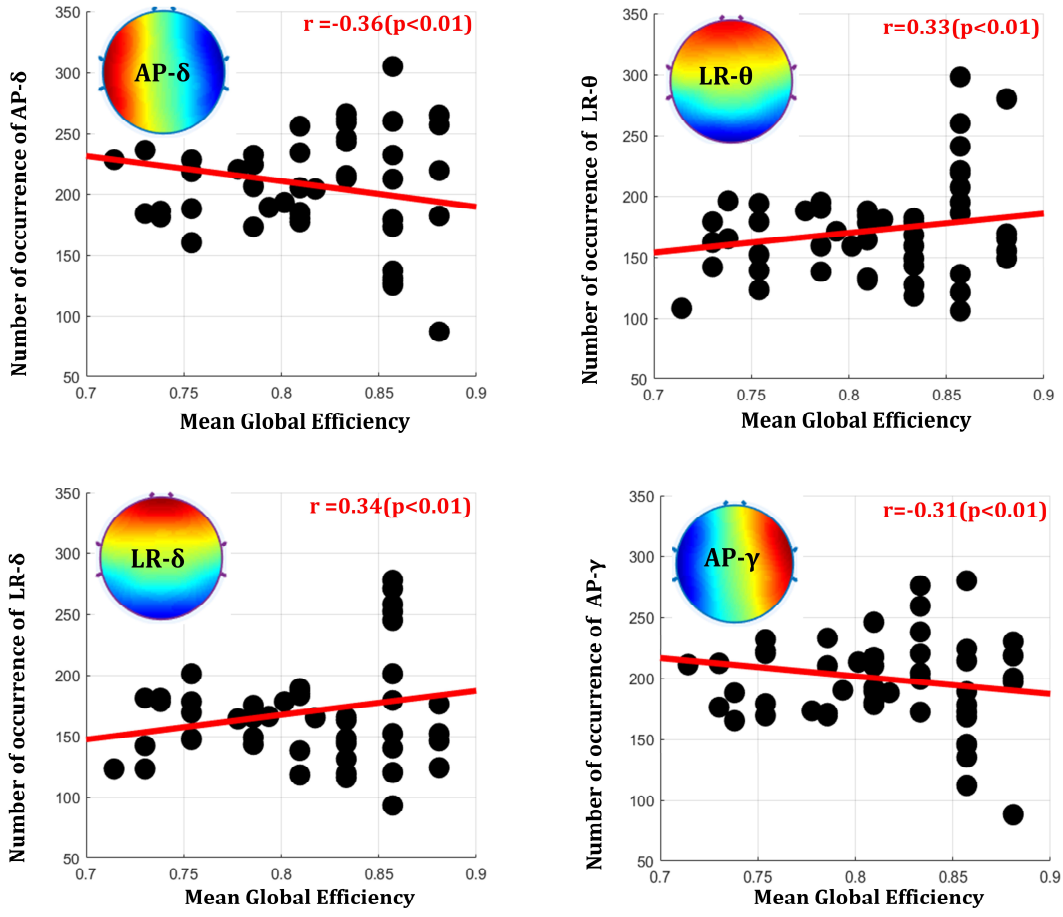

5.6(b): Distractor-engagement

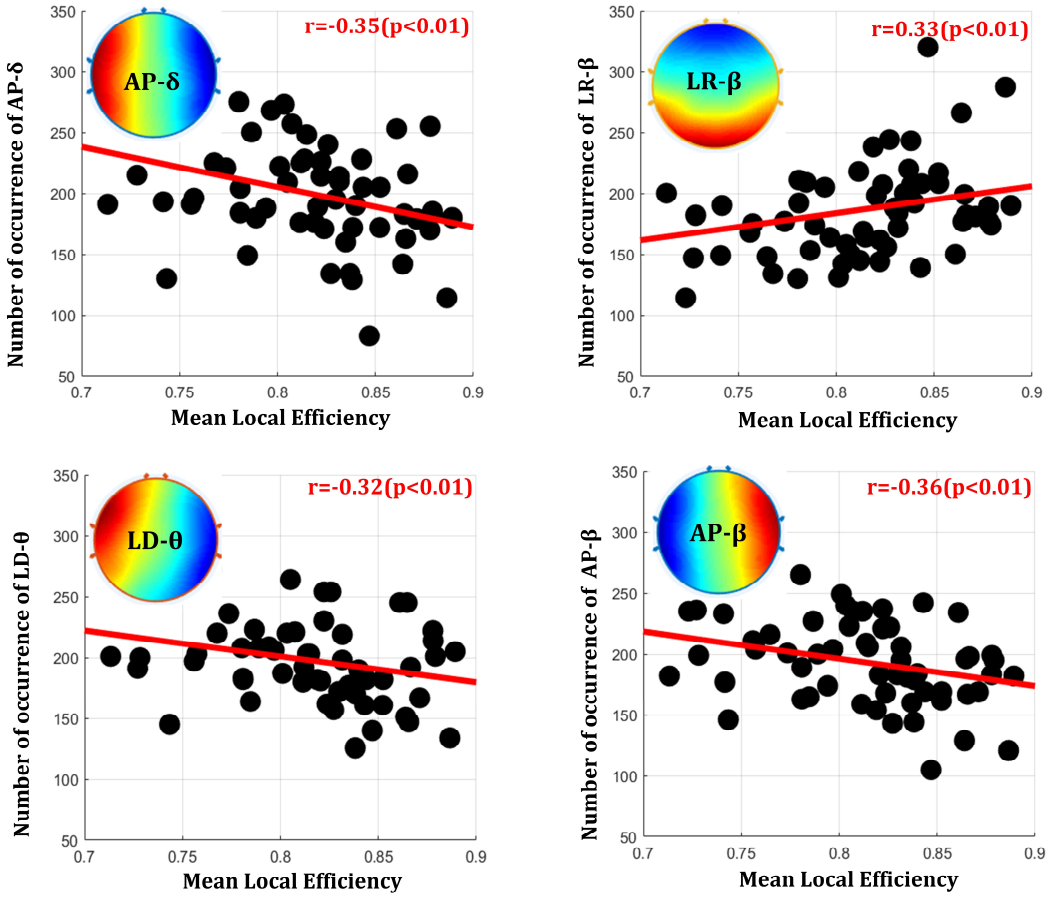

5.6(c): Fixation-engagement

Figure 5.6: Significantly associated, optimized, frequency-microstates with graph-theoretical measures of a) Target, b) Distractor, and c) Fixation task engagement. Frequency microstates are labelled as anterior-posterior (AP), left-right (LR), left diagonal (LD), and right diagonal (RD).

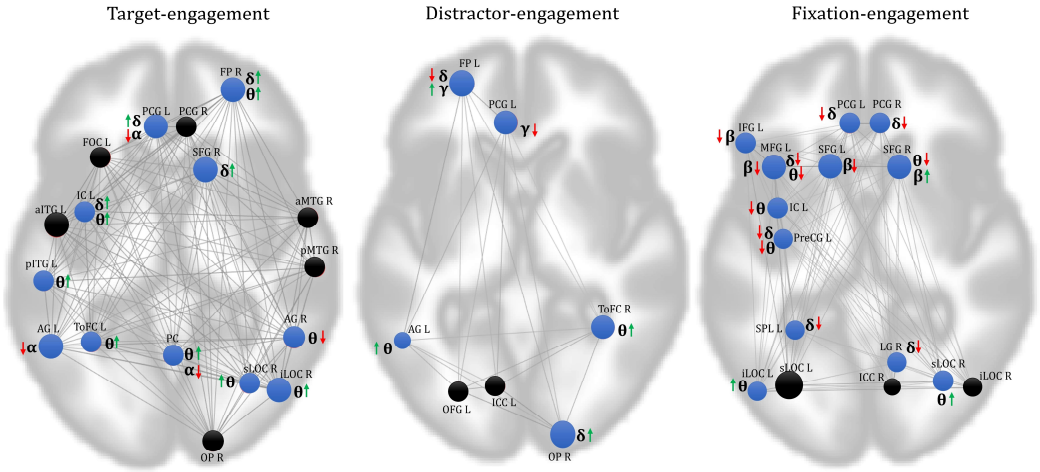

Figure 5.7: Neuro-vascular coupling of each significant, fMRI functional connectivity optimized frequency-microstates of every task. The Regions shown are neural correlates observed for every task. The neuro-vascular association of optimized frequency microstate with each region is drawn through the arrow next to it (Synchronization: Up green arrow, De-synchronization: Down Red arrow). The area coloured black has no neurovascular association with any of the optimized frequency microstates.

5.4.4 Performance of Deep Attentional LSTM Model

Figure 5.8 compares the performance metrics, precision, accuracy, and recall of both deep learning models (LSTM and attention-LSTM). As observed, LSTM combined with attention performed significantly better in all three-performance metrics than the traditional LSTM model. The benefit of choosing different temporal sampling window sizes (180ms/segment to 750ms/segment) of input feature vectors by choosing 16 to 4 LSTM cells in input layers were analyzed within LSTM and attention-LSTM architectures. The results reflected the significant improvement in performance while using ten nodes (300 ms /segment), and a substantial decline in performance metrics is observed for 16 (180 ms/segment) nodes.

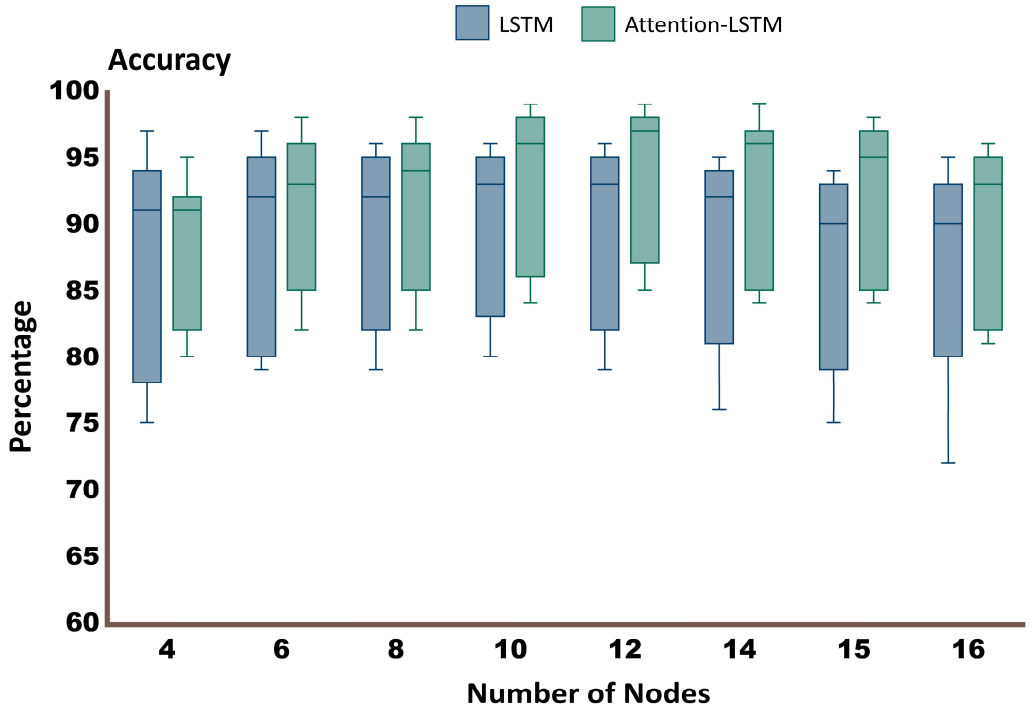

5.8(a): Accuracy

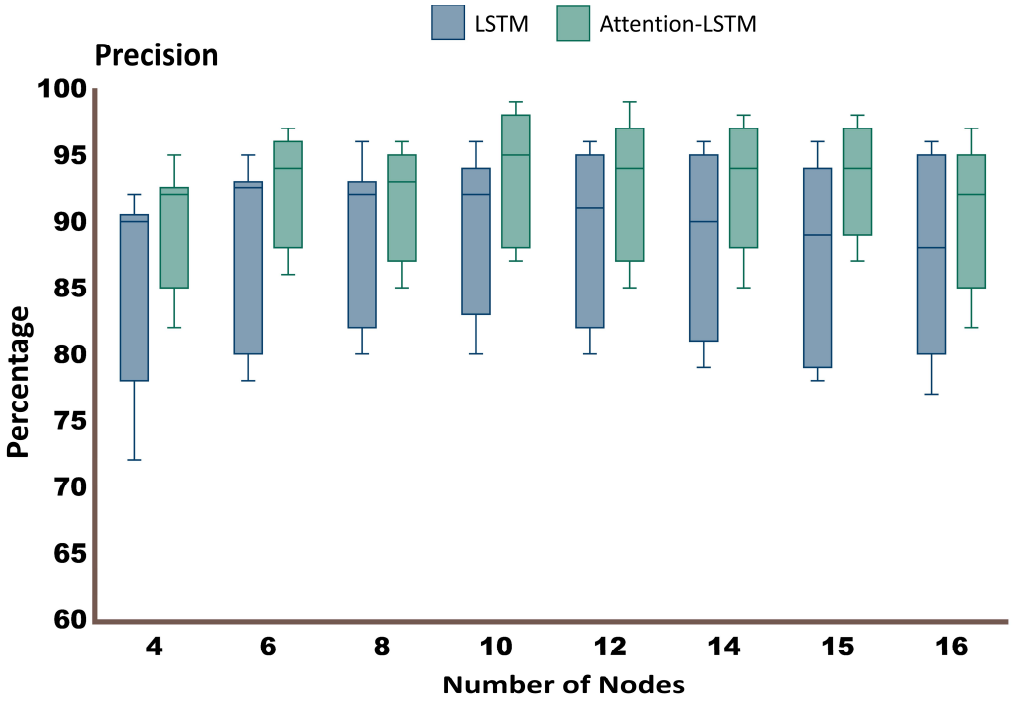

5.8(b): Precision

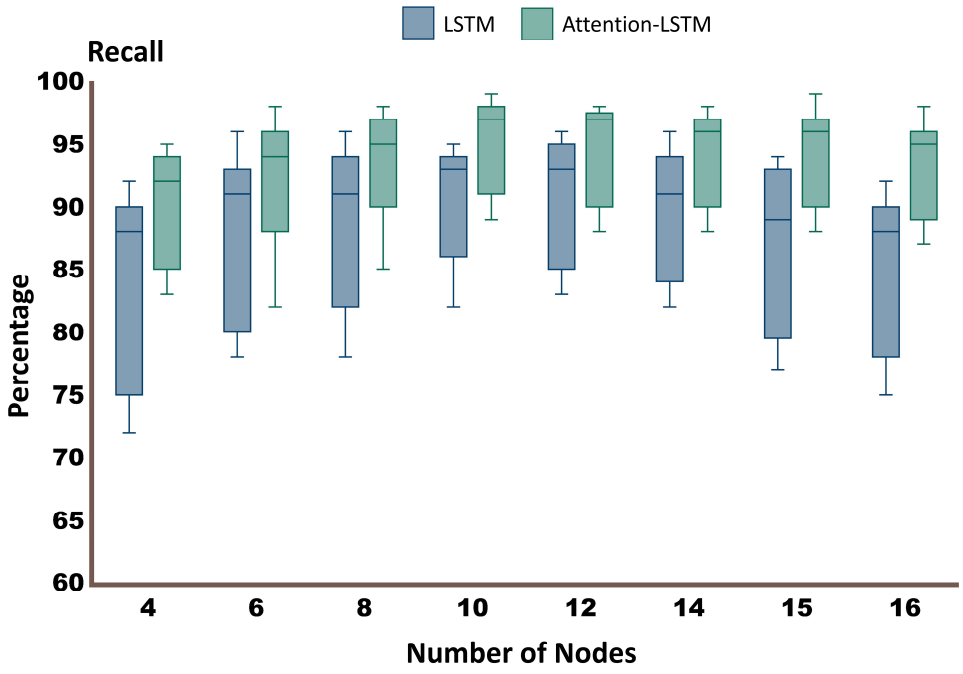

5.8(c): Recall

Figure 5.8: Comparison of performance of the deep learning frameworks. A. Accuracy, B. Precision, C. Recall. Each architecture was independently optimized with 4, 6, 8, 10, 12, 14, 15 and 16 LSTM input cells for temporal EEG sampling of 750, 500, 375, 300, 250, 214, 200 to 180 ms/segment, respectively.

5.5 Discussion

The present study brings more insights into understanding and optimizing frequency microstate information estimated from cortical, coarse EEG information with distant fMRI functional connectivity measures associated with different task engagements. It utilizes them to train a time series of deep learning frameworks. The study employed an attention-based stacked LSTM for effectively remembering and aggregating feature embeddings in the time-series classification of stacked temporal dynamics of the frequency microstate quasi-stable patterns. The results reveal that hemodynamic functional connectivity optimized quasi-stable frequency microstates enable attention-based LSTM algorithm to better classify target engagement, distractors, and fixation. Further, the study employed EEG-informed fMRI to understand the optimized

frequency microstates' neuro-vascular insights and their association mechanisms. The following sections discuss these observations in detail.

5.5.1 Association of distinct frequency microstates with each task's cortical functional connectivity

The study observed four distinct cortical frequency-microstates elicitations for each of three different task engagements (thus, twelve distinct frequency microstates) independently correlated strongly with their hemodynamic functional connectivity measures. Nonoverlap of association of these frequency microstates clearly states the underlying difference in distant cortical communications associated with each task engagement. In addition, the study also has observed a distinct neuro-vascular functional association of slow and faster oscillations in the brain regions involved in each task's cortical communications. Some essential observations of these multi-frequency quasi-stable EEG frequency associations with each task's distant neural interactions are summarized below.

Association of quasi-stable microstates oscillations with global/local neural engagements:

Complex cognitive engagement requires global interactions of different brain regions enabling the large-scale integration of local neural information. The integration of neural engagement of spatially distant areas constituting the large-scale networks is primarily moulded with low-frequency synchronized oscillations due to their long-range communications and integrative roles in various brain functions.

Further, the strength of large-scale networks has also been found to be highest for lower frequencies and seen gradually decreasing with increases in the frequency range. Therefore, the dominance of large-scale networks for the lower range of frequencies confirms their functional significance. The present study's results (Figure 5.6) distinctly revealed synchronization (positive correlation) of the slow frequency oscillations with global, distant brain communication and de-synchronization (negative correlation) with local neural elicitation across all the task engagement. Similarly, the high-frequency quasi-stable oscillation distinctly synchronized with the elicitation of local neural engagement and desynchronized with global

communications across all the task engagements. A similar observation (Figure 5.7) is revealed in the neurovascular coupling from EEG-informed fMRI analysis at the brain regions engaged in all tasks. They demonstrated significant de-synchronization between slow and faster quasi-stable oscillations in most brain regions involved during every task engagement. Further, the region-wise neuro-vascular insights brought slower quasi-stable oscillations associations with large-scale frontoparietal and frontotemporal functional networks. These observations are supported by the proposal of Polich et al [52] and Harper et al, (Harper et al. 2017), explaining the role of delta and theta band activity underlying the frontoparietal and frontotemporal functional networks.

The accumulating literature suggests the association of local neuronal processing with the global cortical communication between neural assemblies by coupling multiple oscillatory frequencies [54] and referred to as cross-frequency coupling. The most well-studied example of cross-frequency coupling is the theta-gamma coupling, which explains the engagement of gamma frequency in certain phases of theta cycles. Further, [55] suggested that low-frequency oscillations may be essential in engaging gamma rhythms during attention. [56] discussed the relationship of alpha and theta frequency oscillations in the cortex and revealed the possibility of the theta-gamma code's contribution to memory and sensory processes. Thus, the functional interaction of more extensive networks oscillating at lower frequencies and local neuronal ensembles oscillating at higher frequencies has been revealed for cortical communication and integration [56–58]. Hence, the studies mentioned above better understand the modulation of faster oscillations from the slow EEG oscillations during cognitive engagements.

The present study's quasi-stable cortical oscillation's neuro-vascular insights and their association with local and global neural information are consistent with these studies and explain the role of multi-frequency interactions in explaining the complex cognitive engagements' neuronal mechanisms.

5.5.2 Performance of attention-based deep learning system in classifying time series quasi-stable cortical frequency EEG information

The proposed deep learning architectures (Figure 5.3) revealed comparable accuracy, precision, and recall rate for classifying target detection task engagements in Figure 5.8. However, two primary aspects distinguished the performance of each proposed deep learning architecture. They are the temporal sampling window and incorporation of the attention mechanism.

5.5.2.1 Temporal sampling window of quasi-stable frequency information optimizes the performance of deep learning architectures

Temporal sampling window size plays a significant role in achieving the best classification accuracy of deep learning architectures. This crucial aspect of time-locked microstates events facilitated a better temporal data handling of multi-frequency interaction in the cognitive task's neural engagements. The present study employed multiple windows of temporal sampling (four nodes: 750 ms, six nodes: 500ms, eight nodes: 375ms, ten nodes: 300 ms, twelve nodes: 250ms, fourteen nodes: 214 ms, fifteen nodes: 200 ms,. and sixteen nodes: 180 ms) to explore optimized, quasi-stable microstate's ability to classify task engagement. The highest classification accuracy, up to 99% for ten and twelve-node attention-based architecture, confirms the temporal dynamics of quasi-stable frequency oscillations optimally with 300ms and 250ms. Several target identification-related EEG studies support this observation [59–63] revealed that the peak of task event-related potentials following the stimulus onset in between 100 ms to 300 ms at multiple. Specifically, a recent EEG study [53] showed event-related synchronization of theta and delta bands occurring around 300 ms after the onset of target stimuli.

5.5.2.2 Effect of attention mechanism with traditional LSTM architectures

The overall better performance of all the deep learning architectures justified the optimization of quasi-stable frequency-microstate information. However, the attention mechanisms further improved this in the deep learning system. The combined effect of attention phenomena and the LSTM architecture allowed the deep learning architecture to dynamically emphasize the task-relevant neural information in the time

series sequence of EEG data and give less attention to other irrelevant information. The improvement in the performance of the attention-based LSTM system can be seen precisely in Figure 5.8. The plots suggest that the attention mechanism is optimum for extracting the most relevant task neural features and improves the LSTM's performance compared to independent LSTM.

5.6. Significance of the study

There is extensive literature (Supplementary Table (ST.2)) on employing a deep learning approach to decode task engagement using EEG elicitations. However, most of those works are restricted to the sensory-motor tasks (hand, leg movements, imagery tasks) whose engagement can be localized in a few cortical regions. However, minimal research is engaged to decode the cognitive task engagement's functional connectivity of distant and distinct cortical engagement using the deep learning framework. Further, despite many research studies that microstates are a promising neural signature, their association with the neural mechanisms of task engagement is still not clearly understood [64–66]. In addition, not many works in the literature explain the quasi-stable nature of the different EEG frequency oscillations either. The present work employs attention-based LSTM architecture to decode the temporal dynamics of cognitive task engagement through fMRI functional connectivity optimized frequency microstates. Recently, [67] investigated the temporal dynamics of traditional microstates using recurrent neural networks. However, their work did not address the quasi-stable frequency microstate's neural mechanism and modulation during task engagement. Our present work further brings more insights into the attention mechanism's ability to improvise the classification of cognitive task engagement based on the optimized neural signatures. To our knowledge, the present study is one of the few works that employs simultaneous EEG-fMRI information to optimize the neural signatures for improvising the performance of deep learning architectures.

5.7. Conclusions

The present study proposes an attention-based deep learning framework that processes temporal dynamics of the twelve distinct, fMRI functional connectivity optimized,

quasi-stable frequency microstates to classify different cognitive task engagement. It further utilizes neurovascular insights of these optimized frequency microstates through EEG-informed fMRI analysis to understand the local and distant cortical interaction revealed by the optimized frequency microstate. This optimized neural information was passed as input at distinct temporal samplings windows to train and validate the attention-based LSTM architecture. The results suggest that the classification accuracies of the attention-based LSTM architectures were better than the traditional LSTM architectures due to the ability of the attention mechanisms in deep learning systems to localize temporal feature information. Notably, the attention-based LSTM model with 250ms per segment and 300ms per segment temporal sampling revealed a higher classification accuracy than other architectures. Hence, the study demonstrates an attention-based deep learning framework to perform a robust classification of complex, distant cortical engagement and communication caused by cognitive task engagements based on the novel, quasi-stable frequency microstates.

Declarations of interest Declarations:

Availability of data and materials: The datasets used and/or analyzed during the current study are available from the corresponding author on reasonable request.

Competing interests: The authors declare that they have no competing interests.

Funding: This research received no specific grant from the public, commercial, or not-for-profit funding agencies.

Authors' contributions: The study was designed by SA, and VC. Data was acquired and processed by SA. Data was interpreted and analyzed by VC, SA, and RS. SA wrote the manuscript with the help of VC. All authors reviewed the manuscript.

Acknowledgements: Not applicable.

References

[1] K.A. Kiehl, P.F. Liddle, Reproducibility of the hemodynamic response to auditory oddball stimuli: A six-week test-retest study, Hum. Brain Mapp. 18 (2003) 42–52. https://doi.org/10.1002/hbm.10074.

[2] H. Laufs, A. Kleinschmidt, A. Beyerle, E. Eger, A. Salek-haddadi, C. Preibisch, K. Krakow, EEG-correlated fMRI of human alpha activity, 19 (2003) 1463–1476. https://doi.org/10.1016/S1053-8119(03)00286-6.

[3] Mantini, Electrophysiological signature of brain resting state networks, Proc. Natl. Acad. Sci. U. S. A. 104 (2007) 13170–13175. papers://40c68295-5659-4035-8dff-71162e06882b/Paper/p3414.

[4] G. Buzsáki, Rhythms of the Brain, 2009. https://doi.org/10.1093/acprof:oso/9780195301069.001.0001.

[5] C. Magri, U. Schridde, Y. Murayama, S. Panzeri, N.K. Logothetis, The amplitude and timing of the BOLD signal reflects the relationship between local field potential power at different frequencies, J. Neurosci. 32 (2012) 1396–1407. https://doi.org/10.1523/JNEUROSCI.3985-11.2012.

[6] T. Murta, U.J. Chaudhary, T.M. Tierney, A. Dias, M. Leite, D.W. Carmichael, P. Figueiredo, L. Lemieux, Phase–amplitude coupling and the BOLD signal: A simultaneous intracranial EEG (icEEG) - fMRI study in humans performing a finger-tapping task, Neuroimage. 146 (2017) 438–451. https://doi.org/10.1016/j.neuroimage.2016.08.036.

[7] S. Agrawal, V. Chinnadurai, A. Kaur, P. Kumar, P. Kaur, R. Sharma, A. Kumar Singh, Estimation of Functional Connectivity Modulations during Task Engagement and Their Neurovascular Underpinnings Through Hemodynamic Reorganization Method, Brain Connect. 9 (2019) 341–355. https://doi.org/10.1089/brain.2018.0656.

[8] A. Kaur, R. Chaujar, V. Chinnadurai, Effects of Neural Mechanisms of Pretask Resting EEG Alpha Information on Situational Awareness: A Functional Connectivity Approach, Hum. Factors. 62 (2020) 1150–1170. https://doi.org/10.1177/0018720819869129.

[9] J.C. Pang, P.A. Robinson, Neural mechanisms of the EEG alpha-BOLD anticorrelation, Neuroimage. 181 (2018) 461–470. https://doi.org/10.1016/j.neuroimage.2018.07.031.

[10] C.M. Michel, T. Koenig, EEG microstates as a tool for studying the temporal dynamics of whole-brain neuronal networks: A review, Neuroimage. 180 (2018) 577–593. https://doi.org/10.1016/j.neuroimage.2017.11.062.

[11] M. Gschwind, M. Hardmeier, D. Van De Ville, M.I. Tomescu, I.K. Penner, Y. Naegelin, P. Fuhr, C.M. Michel, M. Seeck, Fluctuations of spontaneous EEG topographies predict disease state in relapsing-remitting multiple sclerosis, NeuroImage Clin. 12 (2016) 466–477. https://doi.org/10.1016/j.nicl.2016.08.008.

[12] A. Khanna, A. Pascual-Leone, C.M. Michel, F. Farzan, Microstates in resting-state EEG: Current status and future directions, Neurosci. Biobehav. Rev. 49 (2015) 105–113. https://doi.org/10.1016/j.neubiorev.2014.12.010.

[13] H. Yuan, V. Zotev, R. Phillips, W.C. Drevets, J. Bodurka, Spatiotemporal dynamics of the brain at rest - Exploring EEG microstates as electrophysiological signatures of BOLD resting state networks, Neuroimage. 60 (2012) 2062–2072. https://doi.org/10.1016/j.neuroimage.2012.02.031.

[14] P. Croce, A. Quercia, S. Costa, F. Zappasodi, EEG microstates associated with intra- and inter-subject alpha variability, Sci. Rep. 10 (2020) 1–11. https://doi.org/10.1038/s41598-020-58787-w.

[15] A. Kaur, V. Chinnadurai, R. Chaujar, Microstates-based resting frontal alpha asymmetry approach for understanding affect and approach/withdrawal behavior, Sci. Rep. 10 (2020) 1–25. https://doi.org/10.1038/s41598-020-61119-7.

[16] P. Milz, R.D. Pascual-Marqui, P. Achermann, K. Kochi, P.L. Faber, The EEG microstate topography is predominantly determined by intracortical sources in the alpha band, Neuroimage. 162 (2017) 353–361. https://doi.org/10.1016/j.neuroimage.2017.08.058.

[17] F. von Wegner, S. Bauer, F. Rosenow, J. Triesch, H. Laufs, EEG microstate periodicity explained by rotating phase patterns of resting-state alpha oscillations, Neuroimage. 224 (2021) 117372. https://doi.org/10.1016/j.neuroimage.2020.117372.

[18] T. Koenig, L. Prichep, D. Lehmann, P.V. Sosa, E. Braeker, H. Kleinlogel, R. Isenhart, E.R. John, Millisecond by millisecond, year by year: Normative EEG microstates and developmental stages, Neuroimage. 16 (2002) 41–48. https://doi.org/10.1006/nimg.2002.1070.

[19] R.D. Pascual-Marqui, D. Lehmann, P. Faber, P. Milz, K. Kochi, M. Yoshimura, K. Nishida, T. Isotani, T. Kinoshita, The resting microstate networks (RMN): cortical distributions, dynamics, and frequency specific information flow, (2014) 1–14. http://arxiv.org/abs/1411.1949.

[20] P. Milz, P.L. Faber, D. Lehmann, T. Koenig, K. Kochi, R.D. Pascual-Marqui, The functional significance of EEG microstates-Associations with modalities of thinking, Neuroimage. 125 (2016) 643–656. https://doi.org/10.1016/j.neuroimage.2015.08.023.

[21] J.F. Hipp, A.K. Engel, M. Siegel, Oscillatory synchronization in large-scale cortical networks predicts perception, Neuron. 69 (2011) 387–396. https://doi.org/10.1016/j.neuron.2010.12.027.

[22] U. Ribary, S.M. Doesburg, L.M. Ward, Unified principles of thalamo-cortical processing: the neural switch, Biomed. Eng. Lett. 7 (2017) 229–235. https://doi.org/10.1007/s13534-017-0033-4.

[23] T. Akam, D.M. Kullmann, Oscillatory multiplexing of population codes for selective communication in the mammalian brain, Nat. Rev. Neurosci. 15 (2014) 111–122. https://doi.org/10.1038/nrn3668.

[24] N. Ahmadi, Y. Pei, E. Carrette, A.P. Aldenkamp, M. Pechenizkiy, EEG-based classification of epilepsy and PNES: EEG microstate and functional brain network features, Brain Informatics. 7 (2020). https://doi.org/10.1186/s40708-020-00107-z.

[25] et al Vaswani, A., Attention Is All You Need, IEEE Ind. Appl. Mag. 8 (2017) 8–15. https://doi.org/10.1109/2943.974352.

[26] M. Jiang, J. Gu, Y. Li, B. Wei, J. Zhang, Z. Wang, L. Xia, HADLN: Hybrid Attention-Based Deep Learning Network for Automated Arrhythmia Classification, Front. Physiol. 12 (2021). https://doi.org/10.3389/fphys.2021.683025.

[27] Y. Kim, A. Choi, Eeg-based emotion classification using long short-term memory network with attention mechanism, Sensors (Switzerland). 20 (2020) 1–22. https://doi.org/10.3390/s20236727.

[28] M. Rashid, N. Sulaiman, A. P. P. Abdul Majeed, R.M. Musa, A.F. Ahmad, B.S. Bari, S. Khatun, Current Status, Challenges, and Possible Solutions of EEG-Based Brain-Computer Interface: A Comprehensive Review, Front. Neurorobot. 14 (2020) 1–35. https://doi.org/10.3389/fnbot.2020.00025.

[29] X. Yao, X. Li, Q. Ye, Y. Huang, Q. Cheng, G.Q. Zhang, A robust deep learning approach for automatic classification of seizures against non-seizures, Biomed. Signal Process. Control. 64 (2021) 102215. https://doi.org/10.1016/j.bspc.2020.102215.

[30] Z. Zhang, S. Ye, P. Liao, Y. Liu, G. Su, Y. Sun, Enhanced Capsule Network for Medical image classification, Proc. Annu. Int. Conf. IEEE Eng. Med. Biol. Soc. EMBS. 2020-July (2020) 1544–1547. https://doi.org/10.1109/EMBC44109.2020.9175815.

[31] X. Zheng, W. Chen, An Attention-based Bi-LSTM Method for Visual Object Classification via EEG, Biomed. Signal Process. Control. 63 (2021) 102174. https://doi.org/10.1016/j.bspc.2020.102174.

[32] Q. Yao, R. Wang, X. Fan, J. Liu, Y. Li, Multi-class Arrhythmia detection from 12-lead

varied-length ECG using Attention-based Time-Incremental Convolutional Neural Network, Inf. Fusion. 53 (2020) 174–182. https://doi.org/10.1016/j.inffus.2019.06.024.

[33] G.D. Iannetti, R.K. Niazy, R.G. Wise, P. Jezzard, J.C.W. Brooks, L. Zambreanu, W. Vennart, P.M. Matthews, I. Tracey, Simultaneous recording of laser-evoked brain potentials and continuous, high-field functional magnetic resonance imaging in humans, Neuroimage. 28 (2005) 708–719. https://doi.org/10.1016/j.neuroimage.2005.06.060.

[34] R.K. Niazy, C.F. Beckmann, G.D. Iannetti, J.M. Brady, S.M. Smith, Removal of FMRI environment artifacts from EEG data using optimal basis sets, Neuroimage. 28 (2005) 720–737. https://doi.org/10.1016/j.neuroimage.2005.06.067.

[35] P.J. Allen, O. Josephs, R. Turner, A method for removing imaging artifact from continuous EEG recorded during functional MRI, Neuroimage. 12 (2000) 230–239. https://doi.org/10.1006/nimg.2000.0599.

[36] I.I. Christov, Real time electrocardiogram QRS detection using combined adaptive threshold, Biomed. Eng. Online. 3 (2004) 1–9. https://doi.org/10.1186/1475-925X-3-28.

[37] K.H. Kim, H.W. Yoon, H.W. Park, Improved ballistocardiac artifact removal from the electroencephalogram recorded in fMRI, J. Neurosci. Methods. 135 (2004) 193–203. https://doi.org/10.1016/j.jneumeth.2003.12.016.

[38] L.J. Gabard-Durnam, A.S.M. Leal, C.L. Wilkinson, A.R. Levin, The harvard automated processing pipeline for electroencephalography (HAPPE): Standardized processing software for developmental and high-artifact data, Front. Neurosci. 12 (2018) 1–24. https://doi.org/10.3389/fnins.2018.00097.

[39] R.Y. You, Z. Chen, Blind source separation of multichannel electroencephalogram based on wavelet transform and ICA, Chinese Phys. 14 (2005) 2176–2180. https://doi.org/10.1088/1009-1963/14/11/006.

[40] I. Winkler, S. Haufe, M. Tangermann, Automatic Classification of Artifactual ICA-Components for Artifact Removal in EEG Signals, Behav. Brain Funct. 7 (2011) 1–15. https://doi.org/10.1186/1744-9081-7-30.

[41] R.D. Pascual-Marqui, C.M. Michel, D. Lehmann, Segmentation of Brain Electrical Activity into Microstates; Model Estimation and Validation, IEEE Trans. Biomed. Eng. 42 (1995) 658–665. https://doi.org/10.1109/10.391164.

[42] S. Whitfield-gabrieli, A. Nieto-castanon, Conn : A Functional Connectivity Toolbox for Correlated and Anticorrelated Brain Networks, 2 (2012).

https://doi.org/10.1089/brain.2012.0073.

[43] R. Abreu, A. Leal, P. Figueiredo, EEG-informed fMRI: A review of data analysis methods, Front. Hum. Neurosci. 12 (2018) 1–23. https://doi.org/10.3389/fnhum.2018.00029.

[44] R.J. Huster, S. Debener, T. Eichele, C.S. Herrmann, Methods for simultaneous EEG-fMRI: An introductory review, J. Neurosci. 32 (2012) 6053–6060. https://doi.org/10.1523/JNEUROSCI.0447-12.2012.

[45] P. Nagabushanam, S. Thomas George, S. Radha, EEG signal classification using LSTM and improved neural network algorithms, Soft Comput. 24 (2020) 9981–10003. https://doi.org/10.1007/s00500-019-04515-0.

[46] P. Wang, A. Jiang, X. Liu, J. Shang, L. Zhang, LSTM-based EEG classification in motor imagery tasks, IEEE Trans. Neural Syst. Rehabil. Eng. 26 (2018) 2086–2095. https://doi.org/10.1109/TNSRE.2018.2876129.

[47] G. Zhang, V. Davoodnia, A. Sepas-Moghaddam, Y. Zhang, A. Etemad, Classification of Hand Movements from EEG Using a Deep Attention-Based LSTM Network, IEEE Sens. J. 20 (2020) 3113–3122. https://doi.org/10.1109/JSEN.2019.2956998.

[48] V. Mnih, N. Heess, A. Graves, K. Kavukcuoglu, Recurrent models of visual attention, Adv. Neural Inf. Process. Syst. 3 (2014) 2204–2212.

[49] S.R. Gohel, B.B. Biswal, Functional integration between brain regions at rest occurs in multiple-frequency bands, Brain Connect. 5 (2015) 23–34. https://doi.org/10.1089/brain.2013.0210.

[50] X. Li, E.G. Kehoe, T.M. McGinnity, D. Coyle, A.L.W. Bokde, Modulation of Effective Connectivity in the Default Mode Network at Rest and During a Memory Task, Brain Connect. 5 (2015) 60–67. https://doi.org/10.1089/brain.2014.0249.

[51] C.W. Wu, H. Gu, H. Lu, E.A. Stein, J.H. Chen, Y. Yang, Frequency specificity of functional connectivity in brain networks, Neuroimage. 42 (2008) 1047–1055. https://doi.org/10.1016/j.neuroimage.2008.05.035.

[52] J. Polich, Updating P300: An integrative theory of P3a and P3b, Clin. Neurophysiol. 118 (2007). https://doi.org/10.1016/j.clinph.2007.04.019.

[53] J. Harper, S.M. Malone, W.G. Iacono, Theta- and delta-band EEG network dynamics during a novelty oddball task, Psychophysiology. 54 (2017). https://doi.org/10.1111/psyp.12906.

[54] R.T. Canolty, R.T. Knight, The functional role of cross-frequency coupling, Trends Cogn. Sci. 14 (2010) 506–515. https://doi.org/10.1016/j.tics.2010.09.001.

[55] C.E. Schroeder, P. Lakatos, Low-frequency neuronal oscillations as instruments of

sensory selection, Trends Neurosci. 32 (2009) 9–18. https://doi.org/10.1016/j.tins.2008.09.012.

[56] J.E. Lisman, O. Jensen, The Theta-Gamma Neural Code, Neuron. 77 (2013) 1002–1016. https://doi.org/10.1016/j.neuron.2013.03.007.

[57] J. Fell, N. Axmacher, The role of phase synchronization in memory processes, Nat. Rev. Neurosci. 12 (2011) 105–118. https://doi.org/10.1038/nrn2979.

[58] G.G. Knyazev, A.N. Savostyanov, A. V. Bocharov, S.S. Tamozhnikov, E.A. Kozlova, I. V. Leto, H.R. Slobodskaya, Cross-frequency coupling in developmental perspective, Front. Hum. Neurosci. 13 (2019) 1–10. https://doi.org/10.3389/fnhum.2019.00158.

[59] M. Arvaneh, I.H. Robertson, T.E. Ward, A P300-Based Brain-Computer Interface for Improving Attention, Front. Hum. Neurosci. 12 (2019). https://doi.org/10.3389/fnhum.2018.00524.

[60] A.K. Bansal, R. Madhavan, Y. Agam, A. Golby, J.R. Madsen, G. Kreiman, Neural dynamics underlying target detection in the human brain, J. Neurosci. 34 (2014) 3042–3055. https://doi.org/10.1523/JNEUROSCI.3781-13.2014.

[61] C. Bledowski, D. Prvulovic, K. Hoechstetter, M. Scherg, M. Wibral, R. Goebel, D.E.J. Linden, Localizing P300 generators in visual target and distractor processing: A combined event-related potential and functional magnetic resonance imaging study, in: J. Neurosci., 2004. https://doi.org/10.1523/JNEUROSCI.1897-04.2004.

[62] A.K. Pandey, C. Kamarajan, N. Manz, D.B. Chorlian, A. Stimus, B. Porjesz, Delta, theta, and alpha event-related oscillations in alcoholics during Go/NoGo task: Neurocognitive deficits in execution, inhibition, and attention processing, Elsevier B.V., 2016. https://doi.org/10.1016/j.pnpbp.2015.10.002.

[63] R. Sclocco, M.G. Tana, E. Visani, I. Gilioli, F. Panzica, S. Franceschetti, S. Cerutti, A.M. Bianchi, EEG-informed fMRI analysis during a hand grip task: Estimating the relationship between EEG rhythms and the BOLD signal, Front. Hum. Neurosci. 8 (2014) 1–13. https://doi.org/10.3389/fnhum.2014.00186.

[64] K. Kim, N.T. Duc, M. Choi, B. Lee, EEG microstate features according to performance on a mental arithmetic task, Sci. Rep. 11 (2021) 1–14. https://doi.org/10.1038/s41598-020-79423-7.

[65] C.J. Stam, Nonlinear dynamical analysis of EEG and MEG: Review of an emerging field, Clin. Neurophysiol. 116 (2005) 2266–2301. https://doi.org/10.1016/j.clinph.2005.06.011.

[66] E. Tognoli, J.A.S. Kelso, Brain coordination dynamics: True and false faces of phase synchrony and metastability, Prog. Neurobiol. 87 (2009) 31–40.

https://doi.org/10.1016/j.pneurobio.2008.09.014.

[67] A. Sikka, H. Jamalabadi, M. Krylova, S. Alizadeh, J.N. van der Meer, L. Danyeli, M. Deliano, P. Vicheva, T. Hahn, T. Koenig, D.R. Bathula, M. Walter, Investigating the temporal dynamics of electroencephalogram (EEG) microstates using recurrent neural networks, Hum. Brain Mapp. 41 (2020) 2334–2346. https://doi.org/10.1002/hbm.24949.

CHAPTER 6

CONCLUSIONS AND FUTURE DIRECTIONS

6.1 CONCLUSIONS

Decoding of task-engagements has been a prominent area of cognitive science, behavioral science, and neuroscience. Over the last few decades, several remarkable studies advanced the deeper understanding of brain mechanisms from temporal to spatial scale and local to global cortical communications, through the integration of multimodal techniques. This thesis deciphers the mechanisms underlying various cognitive task engagements by designing a system that can integrate human cognitive mechanisms to the vital knowledge of neuroscience. For this, it develops a multimodal approach capable of extracting the information and utilizing them for exploring the inner neurocognitive processes. Since, our approach of using simultaneous EEG-fMRI technique for data acquisition, hemodynamical mechanisms of the task stimulus induce a complex relationship between neural activity measured using electroencephalography (EEG) and associated BOLD response measured using functional MRI. Various voxel level approaches have been used to estimate task as well as resting network such as ICA and DCM in previous studies, they are not capable of facilitating the integrated voxel wise analysis of modulations of functional networks and their associated changes in neurovascular underpinnings. Hence, a novel approach of reorganizing the BOLD information has been proposed in **chapter two** to understand task related modulations through the integrated voxel wise analysis of functional connectivity modulation with their associated changes in neurovascular underpinnings during visual target detection task. The results are further validated through graph theoretical approach at the selected regions. Our BOLD-reorganization approach while exploring the task engagement brings better insight of neuronal dynamics. The findings suggest that the DMN modulations (deactivation and activation) are found task-specific, such as task-negative network (TNN) during target stimulus and not entirely TNN during non-target stimulus. Also, strong association of the deactivations/activation of DMN with its significant neuronal activity is for target stimuli merely. Other networks such as frontal-parietal and visual networks persisted

as TPN during both target and non-target stimulus engagements. Further neurovascular underpinnings of task engagements reflected the task-specific alpha inhibition and its association with significant neuronal activity and synchronization of visual and frontal-parietal network. The DMN was seen de-synchronized with these modulations. The findings also revealed the association of de-synchronized alpha/beta activity with significant neuronal activity during task engagement.

Subsequent to the deeper understanding of neurovascular mechanisms and functional network modulation associated with task engagement, there exist still many questions that require more investigation to appreciate the performance of individuals during task engagement, externally or internally. Feedback-associated learning is a prominent factor affecting the individual's behavior and performance in subsequent task engagements through informative and motivational aspects. Motivation and learning associated with the feedback are observed facilitating the individual to adjust their behavior, improve the performance during subsequent task engagement [1], and behavior adaptations [2]. Further, memory is revealed as a cognitive process that updates with experience, and learning is a process that contributes to the formation of these memories [3]. Specifically, performance feedback can motivate the desire to achieve a goal, such as receiving positive feedback or mastering a task and brings both informative and motivational aspects during task engagement to continue the current approach [4]. Hence, we examined the effect of performance feedback on subsequent task engagement by assessing the role of the frontal-parietal EEG cortical oscillations in the functional interactions of feedback learning with subsequent declarative memory retrieval in **chapter three**. For this, the functional interactions during the feedback learning process and their effect on the subsequent task engagement are analyzed through functional connectivity estimation and the role of EEG oscillations ae explored using neurovascular approach. The findings suggest the association of frontal-parietal regions with MTL-basal ganglia during feedback learning and dissociate in memory retrieval. These modulations are revealed associated with the functioning of the Putamen and the Pallidum (sub-regions of basal ganglia) during task engagements. Also, functional connectivity and neurovascular approaches revealed the major role of frontal-parietal EEG powers in the interactions

of MTL-basal ganglia during feedback and declarative memory task. In specific, enhanced role of frontal-alpha and theta powers in modulating the bold activity of MTL is suggested during memory retrievals. Also, frontal and parietal alpha-beta powers are found desynchronizing and synchronizing with the bold activity of the caudate, respectively. The role of parietal theta power in de-synchronization and frontal higher alpha power in synchronization with the bold activity of right accumbens is found. In such a way, our findings showed critical implication for understanding the major role of frontal and parietal EEG powers in feedback associated declarative memory retrieval.

Another factor is fluid intelligence, which has been revealed as having strong association with individuals' learning abilities in many previous studies [5–7]. It motivates to explore the underlying neural mechanisms of cognitive tasks and their relationship with the individual's fluid intelligence. Neural mechanisms associated with the individual's adaptation to the cognitive tasks can be better explained by deciphering unique cortical EEG oscillations and their mutual interactions in global and local engagements. Hence, we developed a deep learning-based computational model to decode the cortical EEG oscillations that associate individuals' fluid intelligence with their learning mechanisms during performance feedback and subsequent memory retrieval. Also, deciphering the cortical EEG oscillations that associate a person's fluid intelligence with their learning and memory mechanisms will be immensely useful in developing this next-generation, high-order cognitive brain-computer interface. For this, EEG multifrequency interaction, hemodynamic functional connectivity, and EEG informed fMRI measures are analyzed to understand neural mechanisms and distinct cortical oscillations associated with fluid intelligence, learning and memory retrieval in **chapter 4.**

Subsequently, an attention-based LSTM deep-learning model classified the deciphered distinct EEG oscillations that elicit encoded objects' learning and memory retrieval against the engagement of distractors. Our study employs simultaneous EEG-fMRI information to optimize the neural signatures for improvising the performance of deep learning architectures. The results revealed a significantly stronger correlation of fluid intelligence with frontal-alpha, frontal-theta, parietal-

theta, parietal-beta and parietal-delta powers during feedback learning, and frontal-delta and parietal-alpha powers during subsequently engaged memory retrieval phase. Further, the multifrequency interaction revealed a significant influence of frontal-theta, frontal-alpha, parietal-delta, and parietal-beta oscillations elicited during feedback learning on the subsequently engaged memory retrieval's cortical oscillations, particularly on frontal-delta, parietal-alpha elicitations. The neural mechanisms associated with the multifrequency elicitations revealed strong frontal-parietal engagement. In particular, the frontal theta, alpha and a parietal beta of feedback learning synchronize with the BOLD oscillations of frontal-parietal regions. On the other hand, frontal delta and parietal alpha oscillations elicited during the memory retrieval phase desynchronized to the BOLD signal of frontal-parietal regions. The functional connectivity and graph theory approaches validated the association of frontal delta power with frontal-parietal integration, parietal alpha power with the functional dissociation of frontal regions from parietal regions. Further, the study classified the engagement of feedback learning and memory retrieval of encoded objects from distractors based on the deciphered cortical oscillations using attention-based LSTM networks. The performance of the proposed architecture revealed that the integration of LSTM with the attention mechanism significantly improves the performance of our proposed deep learning model.

Following the classification task engagements based on the deciphered cortical oscillations, tasks-elicited cognitive mechanisms measured through electrophysiological and hemodynamic information might be advantageous for categorization purposes with improved performance measures. Many research [8–10] employed simultaneous EEG information acquired with fMRI imaging to understand these functional connectivity, neural origins, and correlated brain states. However, decoding the neural basis of distant cortical region's functional connectivity, mainly involving frontal-parietal and frontal-temporal interactions from spatially coarse-grained cortical EEG information, is still a challenge compared to the hemodynamic approaches based on task fMRI information. Further, multimodal brain mapping, and data integration techniques are strong enough to explore the in-depth neuronal interactions of multiple cognitive mechanisms, associated cortical oscillations, and neurovascular insights. Thus, a hybrid deep learning framework

is designed to classify the task engagement from the cortical EEG signals by utilizing the information extracted from multimodal data integration approach. **Chapter 5** assessed distant cortical interactions that involve frontal-parietal and frontal-temporal functional connectivity elicitation during task engagement through cortical EEG information. It further validates it through the task fMRI functional connectivity, and EEG informed fMRI estimations and finally classified them through deep learning architectures. The study demonstrated a reliable classification of complex cognitive task neural mechanisms using an attention-based deep learning framework utilizing optimized quasi-stable frequency microstates. In addition, optimizing neural signatures using hemodynamical functional connectivity measures estimated from simultaneously acquired fMRI information facilitates better classification results. Fifteen distinct quasi-stable frequency oscillations were observed to be significantly capable of deciphering neural engagement of target detection tasks from distractor and fixation. The association of delta/theta and alpha/beta microstates is established with cortical communications and local neural processing through microstate-informed fMRI analysis. The optimized neural information was passed as input information at three distinct temporal samplings windows (180 to 750 ms/segment) to train and validate the attention-based LSTM architecture. The results suggest that the classification accuracies of the attention-based LSTM architectures were better than the traditional LSTM architectures. This is probably because of the ability of the attention mechanisms in deep learning systems to localize its feature information. Notably, the attention-based LSTM model with 250 to 300 ms temporal sampling revealed a higher classification accuracy than other architectures.

6.2 FUTURE DIRECTIONS

Our thesis showed the possibility of using a multimodal approach for decoding the cognitive task engagements integrating the neurocomputational and data mining techniques. The usage of hemodynamical information were shown to be potentially useful in characterizing and classifying the neural mechanisms during task engagements traditionally probed using EEG merely, thereby increasing their practice for research and clinical applications. The present work incorporates most of the concerned aspects and features from EEG and FMRI techniques for characterizing

and classifying the neural mechanisms during task engagements. However, there are some aspects which can be deepened further for future development of the multimodal integration for understanding task engagements.

The current work studied the characterization of hemodynamic response function for task engagements. There exist several recent studies which reveals that HRF Properties changes for distinct populations such as traumatic brain injury [11], schizophrenia [12] cerebrovascular disease [13], healthy aging [14,15] and cognitive states. Despite seeing modulations of functional networks and associated neurovascular underpinnings for healthy population using EEG and fMRI, their application in the clinical conditions need to be done for future advancements in field.

Further, the deep learning-based framework designed for classification of distinct task engagements, concerning the individual's inherent capabilities such as fluid-intelligence is also capable of extracting multiple features in identifying neural-markers from global and local engagements. The identification of such features from learning from a large data set using deep learning methods will contribute enormously to the medical science in helping human kind.

REFERENCES

[1] T.H. Bailey, L.J. Phillips, The influence of motivation and adaptation on students' subjective well-being, meaning in life and academic performance, High. Educ. Res. Dev. 35 (2016) 201–216. https://doi.org/10.1080/07294360.2015.1087474.

[2] B. Krenn, S. Würth, A. Hergovich, The impact of feedback on goal setting and task performance: Testing the feedback intervention theory, Swiss J. Psychol. 72 (2013) 79–89. https://doi.org/10.1024/1421-0185/a000101.

[3] A.R. Preston, H. Eichenbaum, Interplay of hippocampus and prefrontal cortex in memory, Curr. Biol. 23 (2013) R764–R773. https://doi.org/10.1016/j.cub.2013.05.041.

[4] G. Li, S. Whiteson, W.B. Knox, H. Hung, Using informative behavior to increase engagement while learning from human reward, Auton. Agent. Multi. Agent. Syst. 30 (2016) 826–848. https://doi.org/10.1007/s10458-015-9308-2.

[5] A. Dix, I. Wartenburger, E. van der Meer, The role of fluid intelligence and learning in analogical reasoning: How to become neurally efficient?, Neurobiol. Learn. Mem. 134 (2016) 236–247. https://doi.org/10.1016/j.nlm.2016.07.019.

[6] M. Filičková, I. Ropovik, M. Bobaková, I. Kovalčíková, The relationship between fluid intelligence and learning potential: Is there an interaction with attentional control?, J. Pedagog. 6 (2015) 25–41. https://doi.org/10.1515/jped-2015-0002.

[7] R. Primi, M.E. Ferrão, L.S. Almeida, Fluid intelligence as a predictor of learning: A longitudinal multilevel approach applied to math, Learn. Individ. Differ. 20 (2010) 446–451. https://doi.org/10.1016/j.lindif.2010.05.001.

[8] K.A. Kiehl, P.F. Liddle, Reproducibility of the hemodynamic response to auditory oddball stimuli: A six-week test-retest study, Hum. Brain Mapp. 18 (2003) 42–52. https://doi.org/10.1002/hbm.10074.

[9] H. Laufs, A. Kleinschmidt, A. Beyerle, E. Eger, A. Salek-haddadi, C. Preibisch, K. Krakow, EEG-correlated fMRI of human alpha activity, 19 (2003) 1463–1476. https://doi.org/10.1016/S1053-8119(03)00286-6.

[10] Mantini, Electrophysiological signature of brain resting state networks, Proc. Natl. Acad. Sci. U. S. A. 104 (2007) 13170–13175. papers://40c68295-5659-4035-8dff-71162e06882b/Paper/p3414.

[11] A.R. Mayer, T. Toulouse, S. Klimaj, J.M. Ling, A. Pena, P.S.F. Bellgowan, Investigating the properties of the hemodynamic response function after mild traumatic brain injury, J. Neurotrauma. 31 (2014) 189–197. https://doi.org/10.1089/neu.2013.3069.

[12] F.M. Hanlon, N.A. Shaff, A.B. Dodd, J.M. Ling, J.R. Bustillo, C.C. Abbott, S.F. Stromberg, S. Abrams, D.S. Lin, A.R. Mayer, Hemodynamic response function abnormalities in schizophrenia during a multisensory detection task, Hum. Brain Mapp. 37 (2016) 745–755. https://doi.org/10.1002/hbm.23063.

[13] B. Bonakdarpour, T.B. Parrish, C.K. Thompson, Hemodynamic response function in patients with stroke-induced aphasia: Implications for fMRI data analysis, Neuroimage. 36 (2007) 322–331. https://doi.org/10.1016/J.NEUROIMAGE. 2007.02.035.

[14] M. D'Esposito, E. Zarahn, G.K. Aguirre, B. Rypma, The effect of normal aging on the coupling of neural activity to the bold hemodynamic response, Neuroimage. 10 (1999) 6–14. https://doi.org/10.1006/nimg.1999.0444.

[15] H. Morsheddost, D. Asemani, M.A. Shalchy, Evaluation of hemodynamic response function in vision and motor brain regions for the young and elderly adults, Basic Clin. Neurosci. 6 (2015) 58–69.

APPENDIX 1

SUPPLEMENTARY MATERIAL FOR CHAPTER TWO

Supplementary Table 2.1: Comparison Results Between the Proposed Approach and Graph Theory. The results are summarized as modulations in functional connectivity of brain for visual target detection task from resting state, associated GLM activity with corresponding neurovascular underpinnings, for both stimuli using proposed approach. Every cluster is represented in the following order: [Type of correlation whether Activation (A) or Deactivation (D) (Laterality whether left (L) or right (R)]. Results of graph theory analysis are summarized as variation in measures with respect to resting state, and thus positive values denoted the increment, and negative values denoted the decrement in the variation ratio. BOLD, blood oxygen level dependent; EEG, electroencephalography; GLM, general linear model; LP,lateral parietal; LPFC, lateral

SN	Region of Interest (ROI) (Laterality) (MNI Coordinate)	Modulations in functional connectivity for visual target detection task									
		Proposed Method						Graph Theory			
		Modulation of functional network (Laterality)	Significant GLM (Laterality)	Neurovascular Underpinnings (Reordered-Bold and EEG Power correlation)				Modulation of Graph Theory measures [(Task-Rest)/Rest]			
				Alpha Correlation	Beta Correlation	Gamma (Lower) Correlation	Gamma (Higher) Correlation	Modulation in Global Efficiency	Modulation in Local Efficiency	Modulation in Clustering Coefficient	Modulation in Degree
Stimuli : Target											
Default Mode Network											
1	MPFC (1;55;-3)	D(R,L),A (L)	(R,L)	- (R,L)	- (R,L)	Nil	Nil	0.1698	2.6743	2.4461	1.1875
2	LP (L) (-39;-77;33)	D(L)	Nil	Nil	Nil	- (L)	- (L)	-0.0055	0.1764	0.0652	0.0625
3	LP (R) (47;-67;29)	D(R)	(R)	- (R)	- (R)	- (R)	Nil	0.0078	1.0984	1.1175	0.3636
4	PCC(R) (1;-61;38)	D(R,L)	Nil	Nil	Nil	- (R,L)	- (R,L)	-0.3064	0.6041	0.6453	-0.375
Visual Network											
1	MVC (R)(2;-79;12)	D (R,L)	(R)	+ (R)	Nil	Nil	Nil	0.0222	0.2386	0.2321	0.1261
2	PVC(0;-93;-4)	D(R,L)	(L,R)	+ (R,L)	Nil	- (R)	Nil	0.2137	-0.2274	-0.2971	0.6666
3	LVC (L) (-37;-79;10)	A(L)	(L)	- (L)	Nil	- (L)	- (L)	-0.0471	0.1812	0.1592	0.0416
4	LVC (R) (38;-72;13)	A(R)	(R)	- (R)	- (R)	- (R)	Nil	-0.0506	0.0482	-0.0181	0.0317

SN	Region of Interest (ROI) (Laterality) (MNI Coordinate)	Modulations in functional connectivity for visual target detection task									
		Proposed Method						Graph Theory			
		Modulation of functional network (Laterality)	Significant GLM (Laterality)	Neurovascular Underpinnings (Reordered-Bold and EEG Power correlation)				Modulation of Graph Theory measures [(Task-Rest)/Rest]			
				Alpha Correlation	Beta Correlation	Gamma (Lower) Correlation	Gamma (Higher) Correlation	Modulation in Global Efficiency	Modulation in Local Efficiency	Modulation in Clustering Coefficient	Modulation in Degree
Frontal-Parietal Network											
1	LPFC (L) (-43;33;28)	A(L)	(L)	- (L)	Nil	Nil	- (L)	-0.1484	0.4593	0.3675	0.0585
2	LPFC (R) (41;38;30)	A(R)	(R)	- (R)	- (R)	- (R)	Nil	-0.1430	0.7506	0.8385	-0.2187
3	PPC (L) (-46;-58;49)	A(L)	(L)	Nil	Nil	- (L)	- (L)	-0.2457	0.1715	0.1247	-0.2881
4	PPC (R) (52;-52;45)	A(R)	(R)	- (R)	- (R)	- (R)	Nil	-0.265	0.1587	0.1523	-0.3367
Stimuli : Non-Target											
Default Mode Network											
1	MPFC (1;55;-3)	A(R,L)	(L)	Nil	+ (R,L)	- (L)	Nil	0.4032	2.579	2.43	1.0833
2	LP (L) (-39;-77;33)	Nil	(L)	Nil	+ (L)	Nil	Nil	0.1689	0.5377	0.3873	0.333
3	LP (R) (47;-67;29)	A(R,L)	Nil	- (R)	Nil	- (R), +(R)	Nil	0.1893	1.146	1.1017	0.5909
4	PCC(R) (1;-61;38)	D(L), A(R,L)	Nil	Nil	Nil	+ (R)	Nil	-0.0515	0.389	0.3005	-0.0046
Visual Network											
1	MVC (R)(2;-79;12)	D(R,L)	(R)	Nil	+ (L)	Nil	- (R)	0.1187	-0.1215	-0.1494	0.1711
2	PVC(0;-93;-4)	D(R,L)	(L)	- (L)	+ (R)	- (L)	- (L)	0.2751	-0.1773	-0.2835	0.4942
3	LVC (L) (-37;-79;10)	A(L)	(L)	- (L)	Nil	Nil	- (L)	0.233	0.1381	0.1255	0.4375
4	LVC (R) (38;-72;13)	A(R)	(R)	- (R)	Nil	- (R)	+ (R), - (R)	0.1875	0.2972	0.2616	0.3492
Frontal-Parietal Network											
1	LPFC (L) (-43;33;28)	A(L)	(L)	Nil	+ (L)	Nil	- (L)	-0.348	0.4536	0.3697	-0.2567
2	LPFC (R) (41;38;30)	A(R)	Nil	Nil	Nil	- (R)	Nil	-0.1428	0.417	0.578	-0.2187
3	PPC (L) (-46;-58;49)	A(L)	(L)	Nil	Nil	Nil	Nil	-0.2901	-0.1827	-0.208	-0.427
4	PPC (R) (52;-52;45)	A(R)	Nil	- (R)	Nil	+ (R)	+ (R)	-0.0798	0.2222	0.1247	-0.1326

APPENDIX 2

SUPPLEMENTARY MATERIAL FOR CHAPTER FOUR

Supplementary Table 4.1: Neural Correlates of intelligence-correlated EEG powers for feedback learning phase. R, L and C represent laterality of EEG electrode, right, left and central, respectively. '+' and '-' denote positive and negative correlates of EEG powers.

Feedback Learning phase							
Neural correlates of Frontal Theta power							
Laterality	**Correlate**	**Brain Region**	**Cluster Size**	**MNI Coordinates**			**T-Value**
				x	**y**	**z**	
R	+	Superior Frontal Gyrus	198	-4	56	26	3.76
R	+	Middle Frontal Gyrus	51	-36	26	46	4.1
R	+	Frontal Pole	32	12	58	32	3.02
R	+	Frontal Orbital Cortex	21	-46	34	-14	3.99
L	+	Parietal Operculum Cortex	30	40	-32	24	2.71
L	+	Angular Gyrus	25	42	-50	20	2.94
L	-	Lingual Gyrus	117	-20	-54	-10	-7.16
R	-	Precentral Gyrus	260	-14	-42	72	-4.55
R	-	Postcentral Gyrus	221	12	-26	74	-5.44
R	-	Precuneus Cortex	38	4	-62	60	-3.48
C	-	Superior Parietal Lobule	142	34	-54	64	-3.15
Neural correlates of Frontal Alpha power							
L	+	Middle Frontal Gyrus	229	-50	12	38	5.59
L	+	Superior Frontal Gyrus	67	-20	0	50	3.57
R	+	Frontal Orbital Cortex	65	-40	34	-12	4.49
C	+	Inferior Frontal Gyrus	70	50	32	18	5.02
L	+	Superior Parietal Lobule	38	22	-44	64	2.59
L	+	Angular Gyrus	28	48	-48	38	2.46
R	+	Supramarginal Gyrus	120	48	-24	48	3.6
R	+	Angular Gyrus	65	50	-52	10	3.44
C	-	Frontal Pole	28	8	56	0	-3.18
C	-	Precuneous Cortex	639	-8	-72	44	-7.62
Neural correlates of Parietal Delta power							
R	+	Superior Frontal Gyrus	609	-30	16	60	4.63
R	+	Frontal Pole	86	-4	62	24	3.68
R	+	Frontal Orbital Cortex	83	-26	24	-16	5.17
R	+	Middle Frontal Gyrus	44	-40	6	54	4.28
C	+	Frontal Medial Cortex	67	-2	48	-12	5.49
R	+	Precuneus Cortex	363	-6	-58	26	6.75
R	+	Superior Parietal Lobule	331	14	-56	68	4.18
R	+	Precuneus Cortex	258	6	-46	26	5.22

Feedback Learning phase							
Neural correlates of Frontal Theta power							
Laterality	**Correlate**	**Brain Region**	**Cluster Size**	**MNI Coordinates**			**T-Value**
				x	**y**	**z**	
R	+	Precuneus Cortex	243	-8	-62	68	4.19
R	+	Postcentral Gyrus	191	-2	-40	60	3.31
R	+	Supramarginal Gyrus	30	54	-22	38	2.55
L	-	Inferior Frontal Gyrus	3196	-48	10	-4	7.81
L	-	Frontal Pole	58	32	46	18	2.72
Neural correlates of Parietal Theta power							
L	+	Middle Frontal Gyrus	249	40	28	24	6.3
L	+	Inferior Frontal Gyrus	86	62	10	12	3.5
L	+	Frontal Pole	61	30	30	-14	4.27
L	+	Precentral Gyrus	331	48	-10	46	7.55
L	+	Parietal Operculum Cortex	296	50	-12	20	7.92
L	+	Angular Gyrus	63	-42	-52	52	4.59
L	+	Postcentral Gyrus	34	60	-12	26	3.73
L	+	Superior Parietal Lobule	28	-34	-52	50	4.54
R	-	Frontal Pole	1129	-22	40	34	6.89
R	-	Middle Frontal Gyrus	815	-32	8	60	7.35
R	-	Frontal Orbital Cortex	217	38	24	-6	5.03
C	-	Frontal Operculum Cortex	161	-46	14	2	4.82
C	-	Inferior Frontal Gyrus	40	-50	12	24	4.24
R	-	Lingual Gyrus	7713	-22	-96	0	8.94
R	-	Angular Gyrus	195	50	-52	50	5.34
C	-	Parietal Operculum Cortex	68	-36	-30	22	4.93
C	-	Supramarginal Gyrus	51	-46	-44	26	3.96
C	-	Postcentral Gyrus	39	-46	-28	36	2.66
C	-	Precuneus Cortex	32	12	-54	14	2.64
Neural correlates of Parietal Beta power							
L	+	Middle Frontal Gyrus	220	28	26	40	3.46
L	+	Superior Frontal Gyrus	78	-18	26	42	2.92
R	+	Frontal Pole	36	-34	48	12	2.68
C	+	Frontal Operculum Cortex	110	40	2	4	4.58
L	+	Postcentral Gyrus	137	-24	-34	72	4.41
R	+	Supramarginal Gyrus	61	-50	-40	28	5.26
R	+	Lingual Gyrus	52	-36	-42	-4	4.77
C	+	Precuneus Cortex	52	8	-64	52	4.99

Supplementary Table 4.2: Neural Correlates of intelligence-correlated EEG powers for memory retrieval phase. R, L and C represent laterality of EEG electrode, right, left and central, respectively. '+' and '-' denote positive and negative correlates of EEG powers.

Memory retrieval phase							
Neural correlates of Frontal Delta power							
Laterality	**Correlate**	**Brain Region**	**Cluster Size**	**MNI Coordinates**			**T-Value**
				x	**y**	**Z**	
R	+	Inferior Frontal Gyrus	114	56	32	10	3.93
R	+	Frontal Medial Cortex	32	4	42	-10	3.21
C	+	Frontal Pole	30	26	58	30	4.43
R	+	Postcentral Gyrus	75	44	-24	64	4.73
R	+	Angular Gyrus	63	-62	-50	26	3.4
C	+	Precuneus Cortex	689	-2	-62	24	5.89
R	-	Frontal Pole	502	32	30	34	5.2
R	-	Middle Frontal Gyrus	195	30	10	58	5.75
R	-	Supramarginal Gyrus	262	46	-50	54	11.6
C	-	Postcentral Gyrus	68	54	-18	48	4.03
L	-	Superior Frontal Gyrus	156	16	10	58	3.39
L	-	Frontal Operculum Cortex	59	28	30	4	3.58
L	-	Precentral Gyrus	448	48	10	2	4.28
L	-	Superior Parietal Lobule	301	34	-32	38	4.5
Neural correlates of Parietal Alpha power							
C	+	Frontal Pole	877	-20	66	12	5.2
C	+	Superior Frontal Gyrus	617	-22	24	60	3.78
C	+	Frontal Orbital Cortex	66	-34	30	-18	6.34
C	+	Frontal Operculum Cortex	17	-40	20	8	3.2
C	+	Supramarginal Gyrus	934	-52	-36	52	4.96
L	-	Superior Frontal Gyrus	131	24	14	64	8.88
L	-	Frontal Pole	118	48	36	16	4.72
L	-	Frontal Medial Cortex	86	-12	46	-2	5.69
R	-	Frontal Pole	346	-4	60	16	4.05
R	-	Middle Frontal Gyrus	58	46	28	40	2.96
L	-	Precentral Gyrus	1118	-38	-16	58	5.05
L	-	Precuneus Cortex	33	6	-48	54	3.42

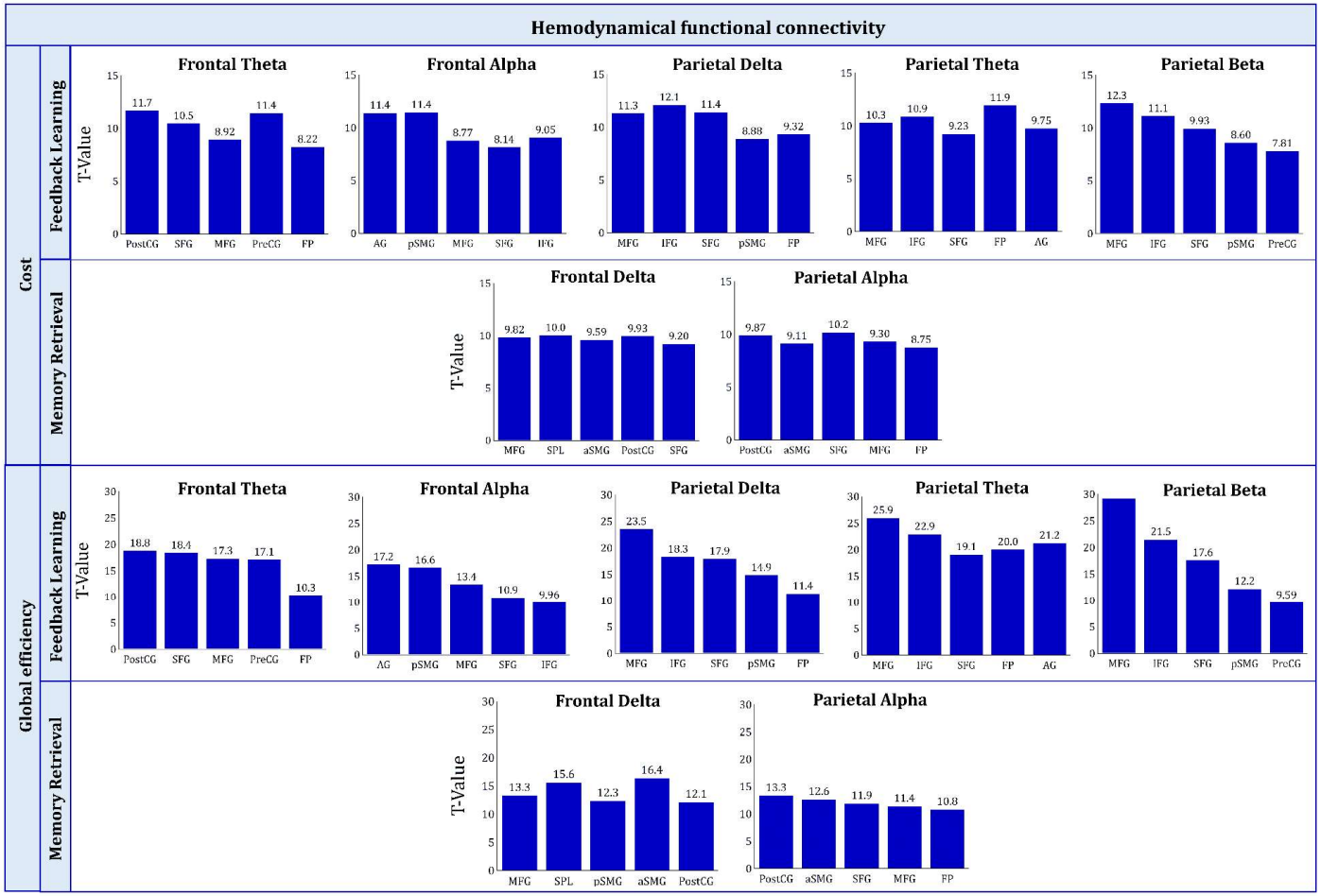

Supplementary Figure 4.1: Bar graphs for graph theory-based functional connectivity during feedback and memory retrieval phases. The bar graph represents the correlation values of significant associations.

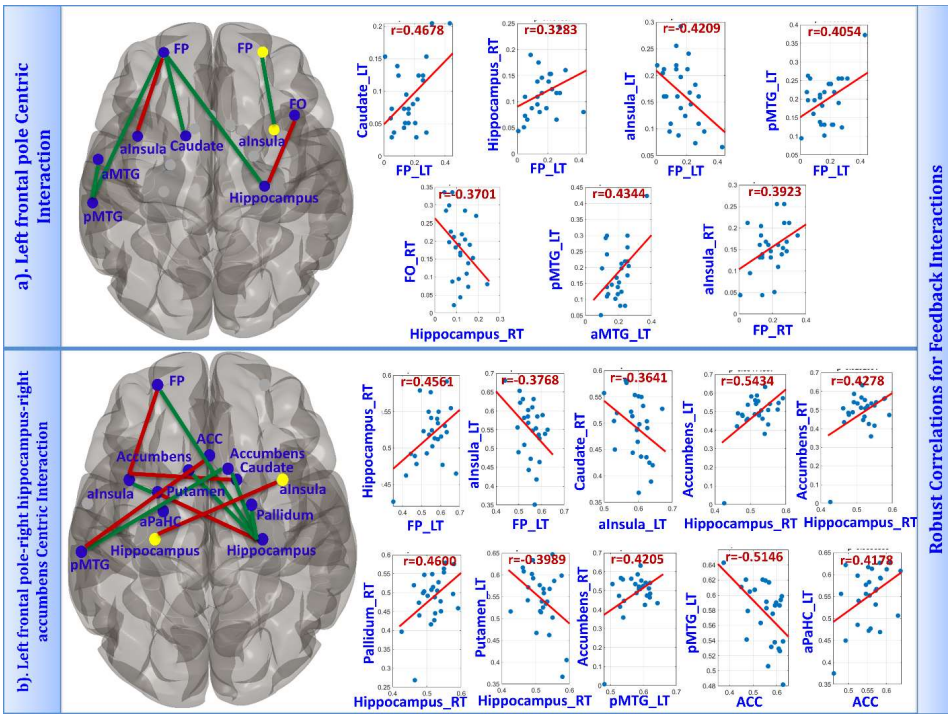

Supplementary Figure 4.2: Robust Pearson correlation of functional connectivity measures during feedback: a). Left frontal pole centric interaction and Right frontal pole-right ventral anterior insula interaction. b). Left frontal pole-right hippocampus-right accumbens centric interaction and Hippocampus-right anterior insula interaction. Green : +ve Correlation, Red: -ve correlation.

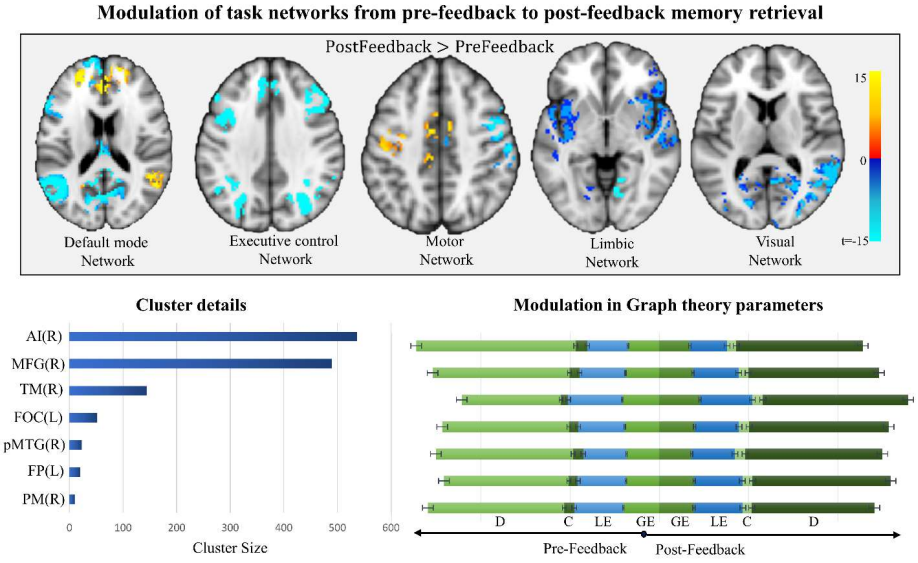

Supplementary Figure 4.3: Functional task network modulation of DMN, ECN, Motor, Limbic, and Visual network in post-feedback declarative memory task compared to pre-feedback. Connectivity shown in red to yellow and blue to aqua indicates activation and deactivation of networks, respectively. Further, modulation of graph theory parameters of post-feedback declarative memory task as compared to pre-feedback task engagement. The figure also illustrates the cluster size of the associated functional network modulations.

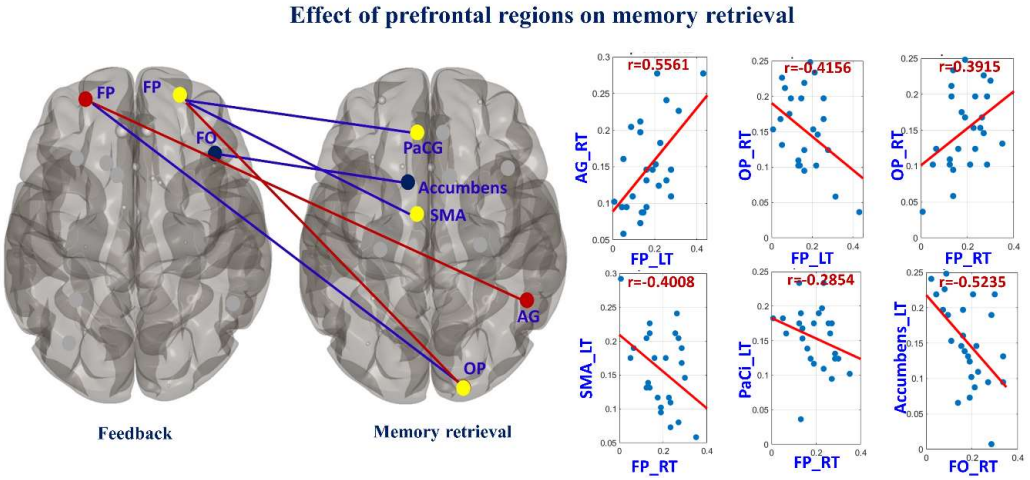

Supplementary Figure 4.4: Effect of prefrontal regions on subsequent task engagement. Nodes illustrated in similar color indicate a significant correlation between them at ($p<0.05$). Red : +ve Correlation , Blue: -ve correlation. Correlation maps illustrate the significant correlation values between the feedback region (x-axis) and the subsequent task-engaged region (y-axis).

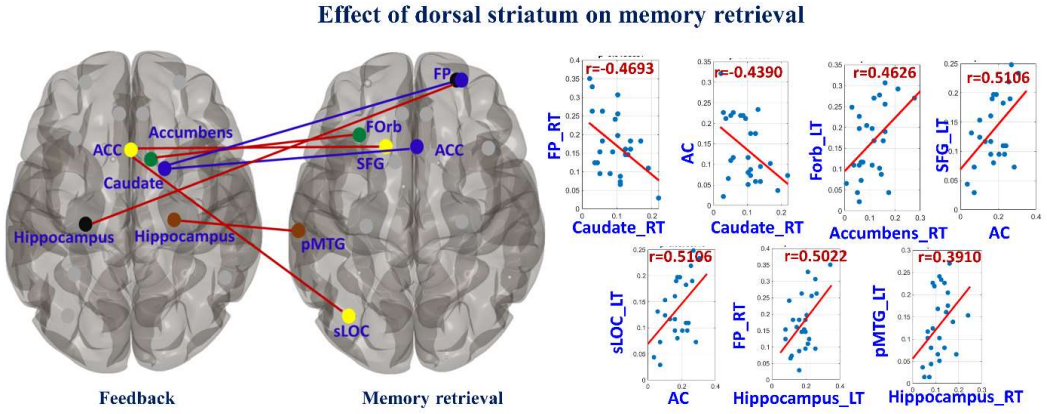

Supplementary Figure 4.5: Effect of Striatum on subsequent task engagement. Nodes illustrated in similar color indicate a significant correlation between them at ($p<0.05$). Red : +ve Correlation , Blue: -ve correlation. Correlation maps illustrate the significant correlation values between the feedback region (x-axis) and the subsequent task-engaged region (y-axis)

BRAIN CONNECTIVITY
Volume 9, Number 4, 2019
© Mary Ann Liebert, Inc.
DOI: 10.1089/brain.2018.0656

Estimation of Functional Connectivity Modulations During Task Engagement and Their Neurovascular Underpinnings Through Hemodynamic Reorganization Method

Swati Agrawal,[1] Vijayakumar Chinnadurai,[1] Ardaman Kaur,[1] Pawan Kumar,[1] Prabhjot Kaur,[1] Rinku Sharma,[2] and Ajay Kumar Singh[1]

Downloaded by Harvard University FRANCIS A COUNTWAY from www.liebertpub.com at 06/27/19. For personal use only.

Abstract

This study proposes an approach to understand the effect of task engagement through integrated analysis of modulations in functional networks and associated changes in their neurovascular underpinnings at every voxel. For this purpose, a novel approach that brings reorganization in acquired task-functional magnetic resonance imaging information based on hemodynamic characteristics of every task stimulus is proposed and validated. At first, modulations in functional networks of visual target detection task were estimated at every voxel through proposed methodology. It revealed task stimulus dependency in the modulation of default mode network (DMN). The DMN modulated as task negative network (TNN) during target stimulus. On the contrary, it was not entirely TNN during nontarget stimulus. The frontal-parietal and visual networks modulated as task positive network during both task stimuli. Further, modulations of neurovascular underpinnings associated with engagement of task were estimated by correlating the hemodynamically reorganized task blood oxygen level dependent information with simultaneously acquired electroencephalography frequency powers. It revealed the strong association of neurovascular underpinnings with their modulation of functional networks and the associated neuronal activity during task engagement. Finally, graph theoretical parameters such as local, global efficiency and clustering coefficient were also measured at the specific regions for validating the results of proposed method. Modulation observed in graph theory measures clearly validated the activation and deactivation of functional networks observed by the proposed method during task engagement. Thus, the voxel-wise estimation of task-related modulation of functional networks and associated neurovascular underpinnings through proposed technique provide better insights into neuronal mechanism involved during engagement in a task.

Keywords: functional connectivity modulation; hemodynamic response function; neurovascular underpinning; target detection

Introduction

Cognitive task and the associated neuronal activity modulate the functional connectivity of resting-state networks. Estimation of the task-induced modulations in resting-state networks and associated neurovascular underpinnings can reveal more insight into the functional dynamics of the brain.

Many researchers have studied the task-related modulations of functional networks using neuroimaging techniques. Raichle and associates (2001) have assessed the nature of intricate modulation in resting-state network caused by the task, and proposed a baseline state for understanding network dynamics. Fox and associates (2005) observed the anticorrelation between default mode network (DMN) and attention network during attention-demanding cognitive task. These anticorrelated networks such as DMN and attention networks were labeled as task negative network (TNN) and task positive network (TPN), respectively. Similarly, the anticorrelation of DMN was also observed with other TPNs such as visual and motor networks (Arbabshirani et al., 2013; Calhoun et al., 2008; Di and Biswal, 2014; Esposito et al., 2018; Gao and Lin, 2012; Manelis and Reder, 2014; Sala-Llonch et al., 2012; Tommasin et al., 2017). Subsequently, volume of research demonstrates the existence of different TPNs during various tasks (Binder et al., 1999; Raichle and Gusnard, 2005) and their modulation from resting state (Calhoun et al., 2008; Gordon et al., 2011; Newton and Morgan, 2011; Spadone et al., 2015).

[1]NMR Research Centre, Institute of Nuclear Medicine and Allied Sciences, Delhi, India.
[2]Delhi Technological University, Shahbad Daulatpur, Delhi, India.

Downloaded by Harvard University FRANCIS A COUNTWAY from www.liebertpub.com at 06/27/19. For personal use only.

On the contrary, many researchers (Andrews-Hanna et al., 2010; Buckner and Carroll, 2007; Bush and Shin, 2006; De Luca et al., 2005; Ino et al., 2011; Xu et al., 2016) observed that the tasks such as autobiographic memory retrieval, self-generated thoughts, mind wandering, and absence of the external goal-directed tasks revealed positive modulation of DMN, which thus makes the DMN as TPN.

However, Nathan Spreng (2012) has cautioned the use of terminology such as TPN and TNN. Furthermore, it is argued that both networks could be simultaneously engaged during tasks. For example, DMN may be coactive as well as functionally coupled with frontal-parietal control network during task. Many studies observed coactivation of these two networks, in particular during problem-solving task (Gerlach et al., 2011), devising the plan to achieve personal goals (Spreng et al., 2010), and working memory encoding and retrieval (Piccoli et al., 2015) tasks. Similarly, several studies have reported the coactivation of DMN with TPNs during many of the cognitive tasks (Beaty et al., 2015; Koshino et al., 2014; Newton et al., 2011; Piccoli et al., 2015; Vaina, 2014; Vatansever et al., 2017; Walz et al., 2014). Hence, the task-related engagement of DMN and its modulation is still poorly understood. These ambiguities motivated us to study the task-related modulation of functional networks.

For this purpose, this study presents the methodology that estimates the modulations of functional networks during task engagement and associated changes in neurovascular underpinnings at voxel level. The neurovascular underpinnings provide better understanding of task-related modulations. Esposito and associates (2006), Klimesch (2012), Kujala and associates (2014), and Uusberg and associates (2013) have revealed that there is a strong interplay between neurovascular underpinnings during task and the hemodynamical changes caused by neuronal activity. Hence, integrated analyses of modulation of functional networks and neurovascular underpinnings are capable of revealing more insight, which will clarify the ambiguities associated with task-related neuronal dynamics. However, the existing functional connectivity measures such as graph theory and dynamic causal model are region of interest (ROI) based techniques, and thus limit the possibility of analyzing task-evoked modulations at the voxel level. This further limits their utility in comparing these observations with neurovascular underpinning modulations at every voxel. Hence, a method that estimates modulation of functional networks during task engagement and compares them with their neurovascular underpinnings at the voxel level would be helpful in addressing the ambiguities of task-associated modulations.

Various voxel-level approaches have been used to estimate task as well as resting network. Shine and associates (2015) have implemented independent component analysis (ICA)-based method by calculating the temporal derivative of each component time course and estimated moment-to-moment functional coupling during visual hallucination tasks. Sambataro and associates (2017) estimated dynamics during rest as well as in the cognitive task by using multivariate analysis and estimated brain voxels with independent component loadings across all intrinsic networks. Arbabshirani and associates (2013) explored the use of spatial ICA in investigating functional connectivity during task to the network level. Schlösser and associates (2008) investigated the task-related effective connectivity using dynamic causal modeling (DCM) analysis, where stroop task was used as event-related paradigm. Rowe and associates (2010) have implemented DCM model and identified the changes in the effective connectivity in Parkinson's disease using finger tapping task. Although these methods reveal voxel-wise modulations of functional networks, they are not capable of facilitating the integrated voxel-wise analysis of modulations of functional networks and their associated changes in neurovascular underpinnings.

Hence, this study aims to understand task-related modulations through the integrated voxel-wise analysis of functional connectivity modulation with their associated changes in neurovascular underpinnings during visual target detection task. A novel approach of reorganizing the blood oxygen level dependent (BOLD) information has been proposed for this purpose, and results are validated through graph theoretical approach at the selected regions. The reordered BOLD information was first subjected to the estimation of voxel-wise modulation of DMN, frontal-parietal and visual networks associated with both target and nontarget task stimuli. Further, these functional network modulations were compared with modulations of neurovascular underpinnings associated with target and nontarget task engagement. The neurovascular underpinnings were estimated by correlating the proposed reorganized BOLD information with simultaneously acquired electroencephalography (EEG) frequency powers. Finally, task functional magnetic resonance imaging (fMRI) data were processed through the conventional general linear model (GLM) to identify the significant neural correlates of both target and nontarget stimuli, and the results are compared with modulations of both functional network and neurovascular underpinnings.

Materials and Methods

Participants

Twenty healthy right-handed volunteers (13 males and 7 females) aged between 20 and 32 years (mean age: 24 years) participated in this study. All participants gave informed consent after the presentation of the study. The exclusion criteria were comprised of any history of psychiatric and neurological disorder, head injury, and use of medication affecting the cognitive performance. The vision of participants was corrected using magnetic resonance (MR)-compatible lenses whenever required. The purpose of the study was explained to the participants before the experiment. The results from two of the volunteers were not considered due to extreme head motion and minimum criteria of corrected answers.

Task paradigm presentation

Participants performed the target detection task by visual search, through collections of colored geometric shapes shown in the slides. The task paradigm used during experiment is described in Figure 1. Volunteers were instructed to respond upon identification of target among the collection of objects by pressing the buttons. The collection of objects was changed every 3 sec. After each object, a slide consisting of single cross in the center was shown as a fixation block for 3 sec. Among the 94 blocks of objects shown, only 32 blocks had target objects embedded. Target and nontarget blocks were mixed in random manner to avoid prediction by volunteers. Stimuli were projected onto MR-compatible lenses fitted on the head coil inside MR.

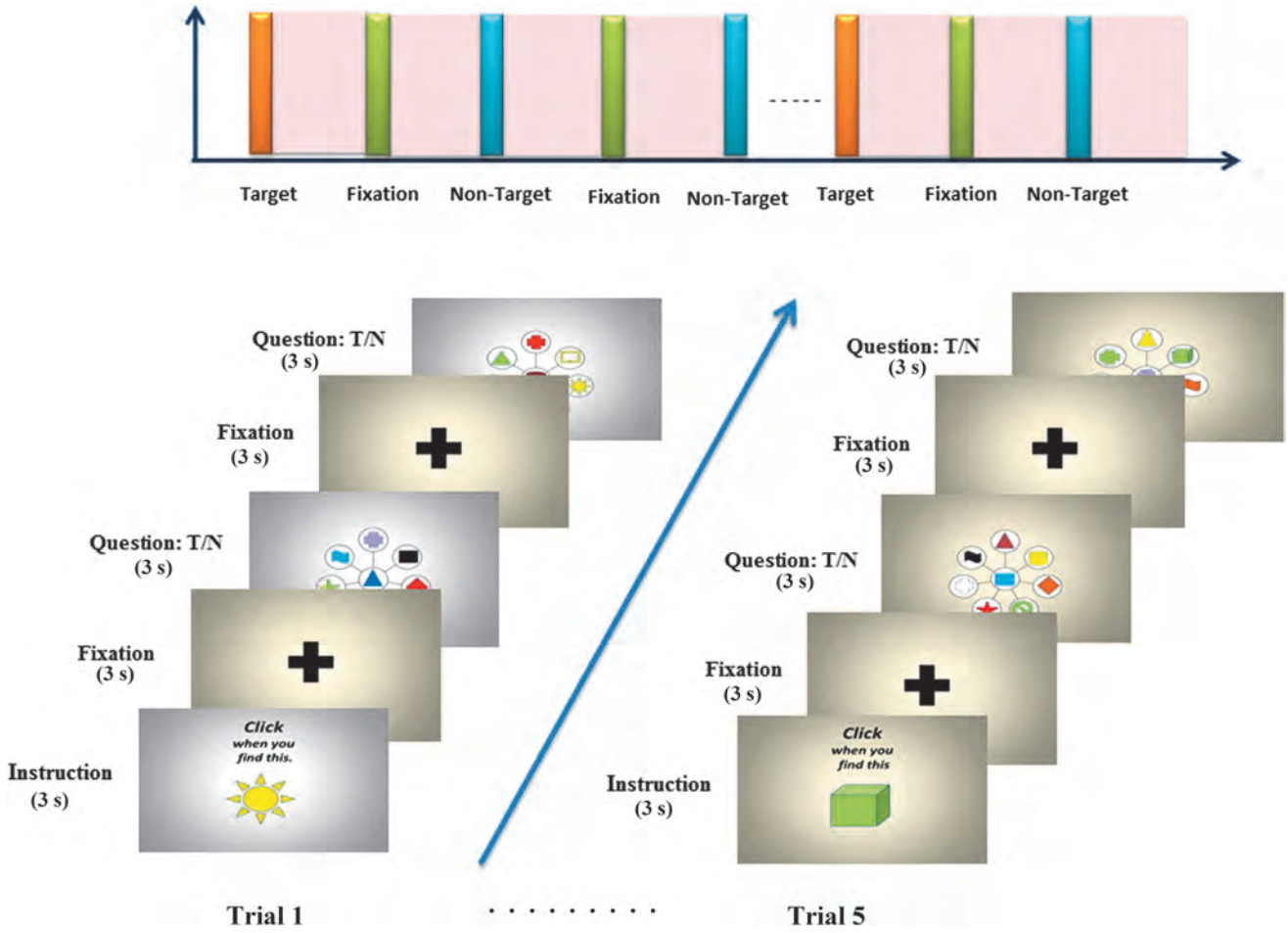

FIG. 1. Schematic illustration of experimental task paradigm: visual target detection task. Five trials with different target objects were used. Each trial consisted of sequence of images, representing collection of objects for 3000 ms followed by subject response. Color images are available online.

Downloaded by Harvard University FRANCIS A COUNTWAY from www.liebertpub.com at 06/27/19. For personal use only.

Data acquisition with simultaneous EEG-fMRI

Data acquisition of both task and resting-state fMRI was performed using a simultaneous EEG-fMRI technique. The MRI acquisition was performed using 3T Siemens Magnetom Skyra scanner. The fMRI data were acquired using Eco Planer Imaging sequence with TR = 3000 ms; TE = 36 ms; voxel size = 3.6 × 3.6 × 3.0 mm; matrix = 64 × 64; FoV read = 230 mm; flip angle = 90°, 36 axial slices. The axial slices were acquired parallel to Anterior-Posterior (AC-PC) line in interleaving manner with slice thickness of 3.0 mm. The high-resolution structural images of the brain were acquired using T1 magnetization prepared rapid acquisition gradient eco sequence with parameters, voxel size = 1.0 × 1.0 × 1.0 mm; TR = 2000 ms; flip angle = 90°; FoV = 240 mm; matrix = 512 × 512; slice thickness = 1.0 mm, 160 axial slices. Before the task fMRI acquisition, resting-state fMRI acquisition was carried out keeping TR = 2000 ms, TE = 30 ms; voxel size = 3.8.0 × 3.8 × 5.0 mm; matrix = 64 × 64; FoV read = 240 mm; flip angle = 90° volumes = 205. The axial slices were acquired parallel to Anterior-Posterior (AC-PC) line in interleaving manner with slice thickness of 5.0 mm. During rest acquisition, volunteers were instructed to close their eyes, but stay awake and remain as still as possible during acquisition.

The EEG data of volunteers were acquired simultaneously during both resting and task fMRI using 32 channel MR-compatible Brain Amp differential amplifier. The Ag/Agcl electrodes integrated in cap were positioned on scalp following 10–20 system with reference electrode in between Fz and Cz. The ground electrode was placed in between Cz and Pz. The electrocardiogram electrode was placed to measure the cardiac effect for the artifact corrections. The impedance of all the scalp electrodes was maintained <5 kOhms. EEG data were acquired at 5 kHz sampling rate.

Reorganization of BOLD information in task fMRI data

In the functional MRI, the task stimulus induces changes in the neuronal activity, which results in variations in the hemodynamic response over space and time. This is observed in the changes of BOLD signals over the time. Although there is no direct relationship between neuronal activities of task stimuli and the hemodynamic response function (HRF) parameters of evoked BOLD responses, Logothetis (2003) showed that these HRF parameters correlate highly with postsynaptic activity. In addition, various researchers (Vazquez et al., 2006; Wager et al., 2005) observed that HRF response of neural activity to be sluggish and spread over the time depends upon the

intensity and duration of neural activity. It typically rises after ~2 sec from the onset of task stimulus and reaches the peak at ~3 to 5 sec, and finally reaches the plateau after ~6 sec (Kwong et al., 1992). However, changes in BOLD activity varies with types of task stimulus and regions of activity. In most of the fMRI connectivity models, this temporal BOLD information is directly used and convolved with standard HRF. But the standard HRF function does not precisely explain the changes caused by the different stimuli and regions where neuronal activity occurs. The time the blood takes to travel from arteries to capillaries and draining veins during neuronal activity is different in different regions. This study quantifies this differential nature of BOLD activity, and then uses it to reorganize the BOLD information (Fig. 2). At first, quantification of changes in BOLD activity at every voxel caused by task stimulus is carried out by assessing their HRF parameters such as amplitude (A), time to peak (TTP), and width (W). Then, this information is used to reorganize the BOLD temporal data. The following section explains these operations in detail for both target and nontarget stimuli at every voxel.

At first, task fMRI data were preprocessed using SPM 12 for artifact removal. Then, the data were corrected for slice timing, realigned, and registered to the MNI template space. The data were first motion corrected by applying rigid body transformation. All the images were then smoothed using Gaussian kernel of 5 mm. The preprocessed task fMRI dataset was subjected to the estimation of characteristics of HRF of every voxel associated with task stimulus. In this study, HRF parameters such as amplitude (A), time to peak (TTP), and width (W) have been estimated as a potential measure of response, latency, and duration of neuronal activity associated with each voxel and stimulus.

A brief methodology used for this purpose is shown in Figure 2. The reconstructed task fMRI data $R(T)$ were measured as follows:

$$R(T) = \{R_{r,c,s}(T)\} = \{\text{Mean}\{Y_{r,c,s}(t)\} \vee t_{\text{earlier}} < t < t_{\text{later}}\}, \quad (1)$$

where r, c, and s represent the row, column, and slice of voxel in the acquired task fMRI dataset $Y(T)$, respectively.

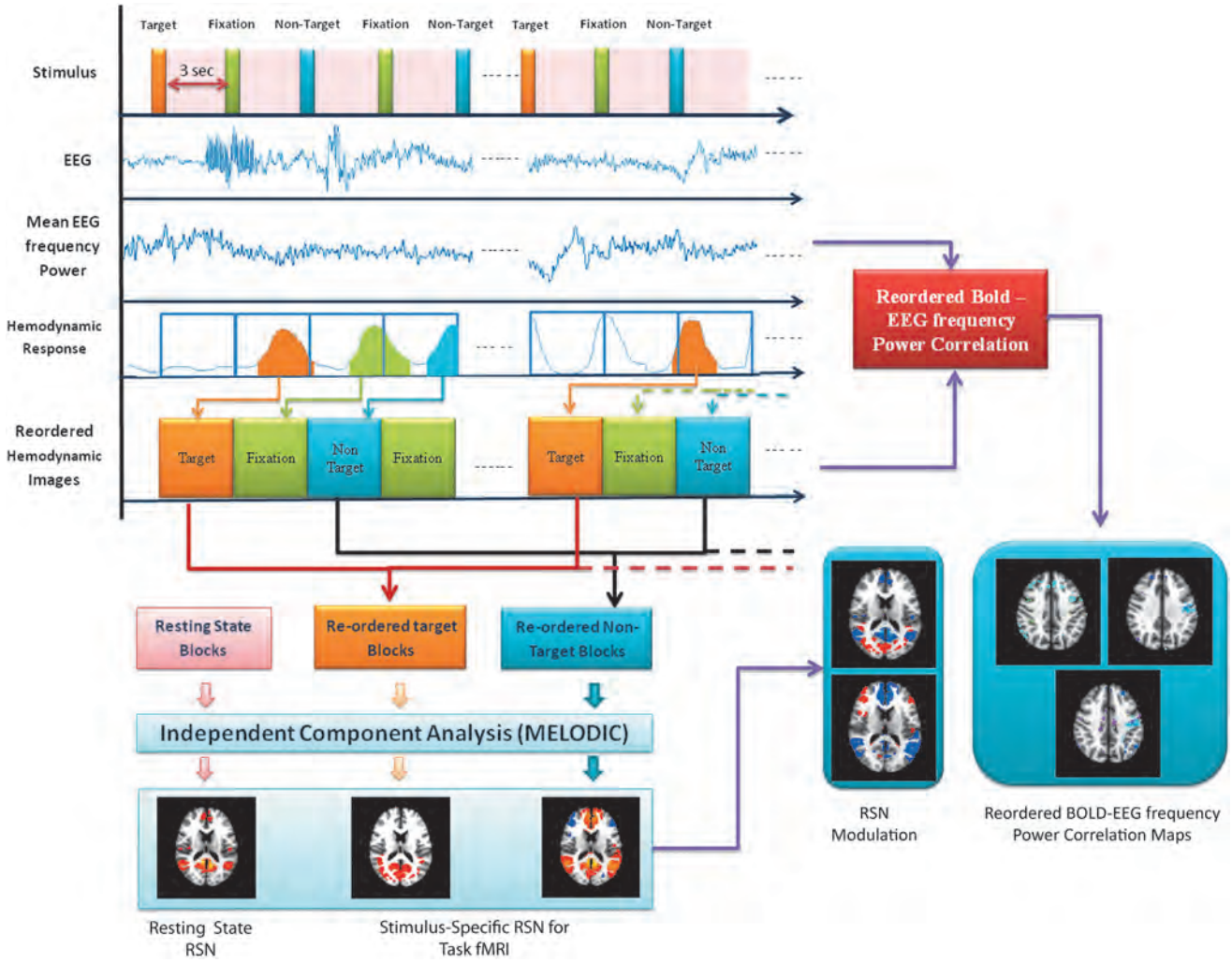

FIG. 2. Hemodynamically reorganized BOLD approach for estimation of modulation in functional networks and their neurovascular underpinnings during task engagement. BOLD, blood oxygen level dependent. Color images are available online.

Downloaded by Harvard University FRANCIS A COUNTWAY from www.liebertpub.com at 06/27/19. For personal use only.

Downloaded by Harvard University FRANCIS A COUNTWAY from www.liebertpub.com at 06/27/19. For personal use only.

t_{earlier} and t_{later} were the earlier and later time points around amplitude (A) of HRF function of the voxel located at given r, c, and s. They were estimated (Lindquist et al., 2009) as follows:

$$t_{\text{earlier}} = \left\{\text{Firstpoint}\{t\} \vee t > \text{TTP}^{\mu}_{r,c,s} \wedge h^{\mu}_{r,c,s}(t) < A^{\mu}_{r,c,s}/2\right\}, \tag{2}$$

$$t_{\text{later}} = \left\{\text{Lastpoint}\{t\} \vee t < \text{TTP}^{\mu}_{r,c,s} \wedge h^{\mu}_{r,c,s}(t) < A^{\mu}_{r,c,s}/2\right\}, \tag{3}$$

where $h^{\mu}_{r,c,s}(t)$is the HRF function estimated for voxel located at (r, c, s) to the given specific stimuli μ. $\text{TTP}^{\mu}_{r,c,s}$ and $A^{\mu}_{r,c,s}$ are the time to peak and amplitude measured from $h^{\mu}_{r,c,s}(t)$. The estimation of $\text{TTP}^{\mu}_{r,c,s}$ and $A^{\mu}_{r,c,s}$ was carried out as follows:

$$\text{TTP}^{\mu}_{r,c,s} = \min\left\{t \vee \frac{dh^{\mu}_{r,c,s}(t)}{dt} = 0 \wedge \frac{d^2h^{\mu}_{r,c,s}(t)}{dt^2} < 0\right\} \tag{4}$$

$$A^{\mu}_{r,c,s} = \text{sign}\left(\beta^{\mu}_{r,c,s}(1)\right) \sqrt{\left(\beta^{\mu}_{r,c,s}(1)\right)^2 + \left(\beta^{\mu}_{r,c,s}(2)\right)^2 + \left(\beta^{\mu}_{r,c,s}(3)\right)^2}. \tag{5}$$

The $\beta^{\mu}_{r,c,s}(1)$,$\beta^{\mu}_{r,c,s}(2)$, and $\beta^{\mu}_{r,c,s}(3)$ are the regression coefficient parameters of the canonical HRF, and its first- and second-order derivative terms. These are obtained by fitting the acquired task fMRI data to the GLM using canonical HRF and its derivatives. The GLM through canonical HRF and its derivatives was carried out in SPM 12. Further, temporal filtering using high pass filtering cutoff of 100s was done to remove the low-frequency artifacts from the data.

Assessment of functional connectivity in task fMRI data

Reconstructed task fMRI data $R_{r,c,s}(T)$ subsequently subjected to MELODIC probabilistic ICA (Beckmann and Smith, 2004) of functional connectivity using FMRIB Software Library (FSL) version 5.0.9. Multisession temporal concatenation ICA using variance-normalized time courses and automatic dimensionality estimation was performed in this process. The thresholds of maps were taken as 0.5 with structural image as a background image. Extraction of resting-state networks across noise was done by masking the task networks for both stimuli with gray matter mask. Masked networks were then labeled and further, modulation in functional networks across DMN, frontal-parietal (FP) and visual networks was carried out.

Besides the functional connectivity approach using ICA, task data were processed using GLM using FSL FEAT with the effect of time and dispersion derivative by considering the different stimuli as conditions with one-sample t-test using the cluster threshold of $z = 2.56$ ($p < 0.05$).

Assessment of functional connectivity in resting fMRI data

The preprocessing of resting fMRI data was performed using FSL version 5.0.9. The data were first motion corrected using MCFLIRT by applying rigid body transformation. Further, slice time-corrected images were imposed for extraction of nonbrain matter using Brain Extraction Tool. Spatial Smoothening was done to remove the noise without affecting the valid activation in data and normalized by grand mean scaling at a value of 5 mm full-width half-maximum Gaussian kernel. Temporal filtering using high pass filtering cutoff of 100s was done to remove the low-frequency artifacts from the data. The preprocessed resting-state data were then analyzed using MELODIC (FSL) for the characterization of resting-state networks by multiple concatenations across group data. Extraction of resting-state networks across noise was done by masking the resting-state networks with gray matter mask. Masked networks were then labeled and further, modulations in functional networks across DMN, FP and visual networks were carried out.

Selection of ROIs

The study primarily focuses on assessing the modulation of functional network during task engagement and the associated changes in neurovascular underpinnings. For this purpose, the method based on reorganization of hemodynamic information is proposed, and the modulations in DMN, frontal-parietal and visual networks were estimated. The DMN revealed modulation in medial prefrontal cortex (MPFC), lateral parietal (LP right and left), and posterior cingulate cortex (PCC). Visual network has revealed high modulations in medial visual cortex (MVC), primary visual cortex (PVC), and lateral visual cortex (LVC right and left). Finally, frontal-parietal network has revealed significant modulations in lateral prefrontal cortex (LPFC right and left) and posterior parietal cortex (PPC right and left). The detailed results are presented in the Results section. To validate these observations of the proposed method, the modulations observed in these regions have been cross-validated through graph theoretical approach. Hence, these regions are considered as ROIs during the analysis of graph theoretical approach.

Graph theory measures

The measures of graph theory were computed using functional connectivity (CONN) toolbox (Whitfield-gabrieli and Nieto-castanon, 2012) implemented in MATLAB. In this ROI-based analysis, temporal correlations for the resting-state and task-specific stimuli's BOLD signal time series were examined for the seed regions of DMN, frontal-parietal and visual networks for each subject. Functional connectivity maps of all the ROIs were further derived from Fisher's r-to-z transformation. For the group-level analysis, one-sample t-test was conducted to detect brain regions showing significant functional connectivity across participants. The group-level functional connectivity maps were further corrected for multiple comparisons using false discovery rate (FDR) correction with a corrected threshold of $p < 0.05$. The graph theory parameters such as global efficiency, local efficiency, clustering coefficient, and degree were then calculated for concerned ROIs.

Preprocessing of EEG data

The simultaneously acquired cortical EEG information of both resting and task was subjected to the following preprocessing procedures before estimations of modulations in neurovascular underpinnings during task engagement. The acquired EEG raw data were processed for MR-related artifact correction using Brain Vision Analyzer, Brain product through adaptive artifact subtraction method. The effect

Downloaded by Harvard University FRANCIS A COUNTWAY from www.liebertpub.com at 06/27/19. For personal use only.

of pulse beats and cardioballistic is removed using CB correction by using peak detection method. Subsequently, data were down sampled to 250 Hz, and digitally filtered between 0.5 and 100 Hz. ICA was used for the attenuation of ocular and the residual imaging artifacts using the filtered EEG recordings. These preprocessed EEG data were subsequently processed through EEGLAB, Mathworks for the estimation of EEG frequency powers.

Estimation of neurovascular underpinnings

The neurovascular underpinning brings better insight into the coupling between task-induced neuronal activity and their hemodynamic information. This hemodynamic information as assessed by BOLD relies on parameters that affect neuronal activities such as cerebral blood flow, cerebral blood volume, and metabolic consumption of oxygen.

In this study, the assessment of these neurovascular underpinnings was carried out in two stages: at first, the mean EEG frequency powers pertaining to every stimulus block (both target and nontarget stimuli) were estimated. For this purpose, artifact-corrected EEG data of every stimulus block were band-pass filtered ranging from 1 to 100 Hz. Then, they were subjected to the estimation of EEG time-locked frequency matrix (Ω) for both target and nontarget stimuli as

$$\Omega = \{\text{median}(\Omega(i,j))|\ i = 1\ to\ N,\ j = 1 : \text{Nf}\ \}, \qquad (6)$$

where $\Omega(i,j)$ is the median of jth EEG frequency component of all the EEG channels pertaining to the ith true positive stimuli block in the paradigm. N and Nf are the total number of true positive stimuli blocks and total number of frequency bands, respectively. In this study, Nf was kept 4, which includes alpha (8–12 Hz), beta (12–30 Hz), lower gamma (30–50 Hz), and upper gamma (50–100 Hz) EEG powers. As mentioned in the Task Paradigm Presentation section, there were 32 target blocks and 62 nontarget blocks in the task paradigm shown to the volunteers. Among these, only those blocks that were identified correctly as target and nontarget by the volunteer were considered to estimate N for this purpose.

Then, hemodynamic parameters associated with every stimulus were quantified and used for reorganization of BOLD information as explained in the Reorganization of BOLD Information in Task fMRI Data section. This reordered BOLD information ($R(i)$) pertaining to both target and nontarget stimuli was correlated with EEG time-locked frequency matrix (Ω) data as follows:

$$\Gamma_{(r,c,s)}(j) = \{\text{Correlation}\ \left(R_{(r,c,s)}(i)\ ,\ \Omega(\text{i},\text{j})\right)||\ i = 1\ to\ N,\ j = 1 : \text{Nf}\ \}, \qquad (7)$$

where $\Gamma_{(r,c,s)}(j)$ is the correlation map pertaining to the jth frequency band. r, c, and s are the row, column, and slice of voxel, respectively. The correlation map (Γ) was estimated by Pearson's correlation for true positive target and nontarget blocks independently for every volunteer. Finally, group analysis of estimated correlation maps of all the volunteers was performed using the one-sample t-test.

Results

This study aims to understand the modulation of functional networks during task engagement and the associated changes in neurovascular underpinnings during visual target detection task. For this purpose, the hemodynamic-based reorganization method is proposed and validated through graph theoretical approach at selected regions. The proposed method revealed task-related network modulations (Figs. 3 and 4) and the associated neurovascular underpinnings (Figs. 5 and 6) at every voxel. Table 1 summarizes the modulations in networks and the corresponding neurovascular underpinnings.

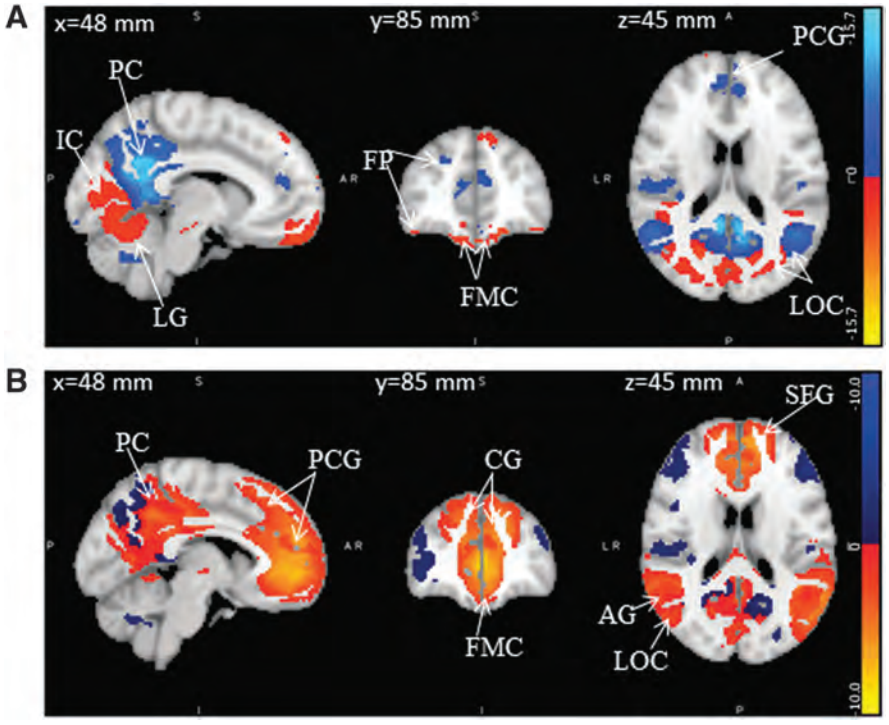

FIG. 3. Illustrations of DMN modulation during task engagement (deactivation: blue, activation: red): **(A)** target stimuli, **(B)** nontarget stimuli. AG, angular gyrus; CG, cingulate gyrus; DMN, default mode network; FMC, frontal medial cortex; FP, frontal pole; IC, intracalcarine cortex; LG, lingual gyrus; LOC, lateral occipital cortex; PC, precuneus cortex; PCG, paracingulate gyrus; SFG, superior frontal gyrus. Color images are available online.

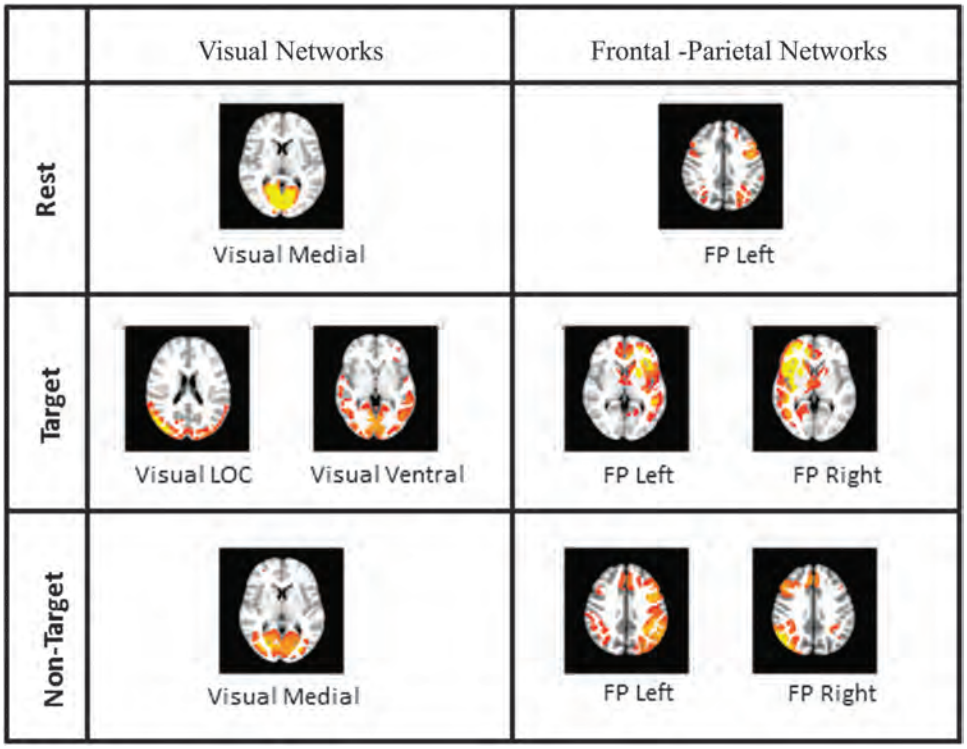

FIG. 4. Illustrations of modulation in visual and frontal-parietal networks. Color images are available online.

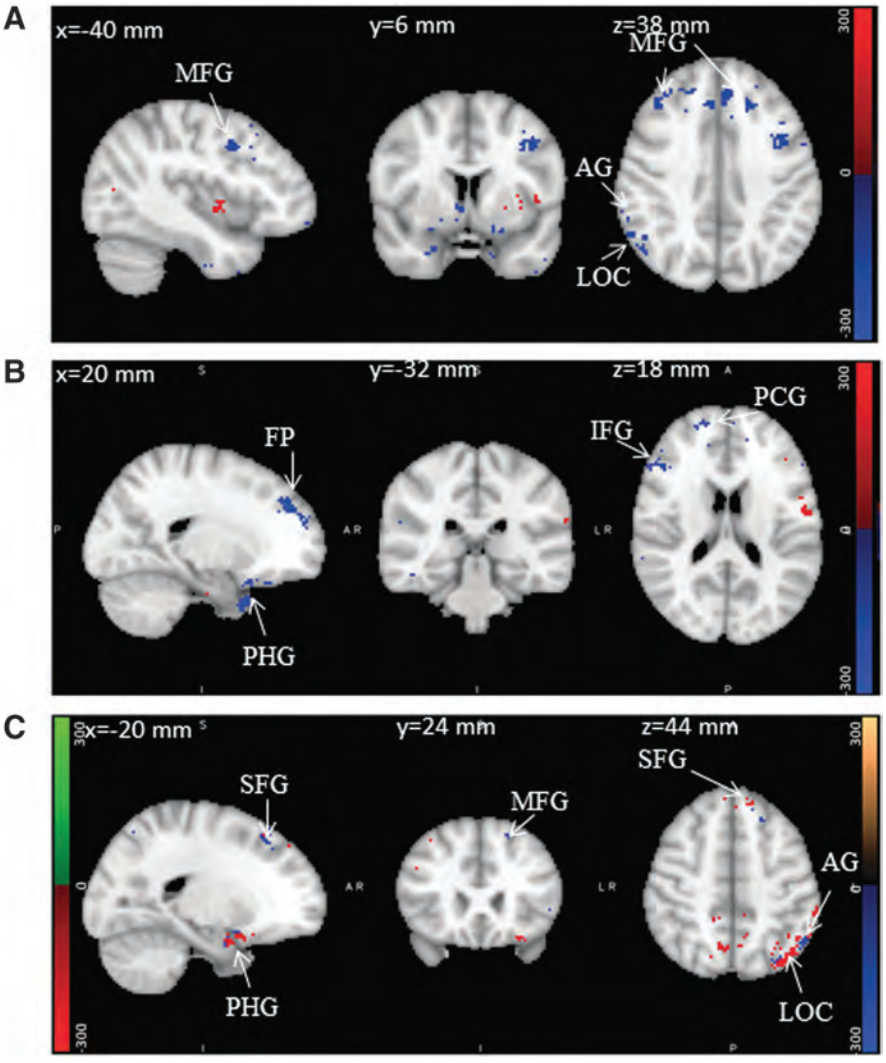

FIG. 5. Neurovascular underpinnings of target stimuli: **(A)** alpha-reordered BOLD correlation (positive: red, negative: blue); **(B)** beta-reordered BOLD correlation (positive: red, negative: blue); and **(C)** gamma-reordered BOLD correlation (positive: green and copper, negative: red and blue). IFG, inferior frontal gyrus; MFG, middle frontal gyrus; PHG, parahippocampal gyrus. Color images are available online.

Downloaded by Harvard University FRANCIS A COUNTWAY from www.liebertpub.com at 06/27/19. For personal use only.

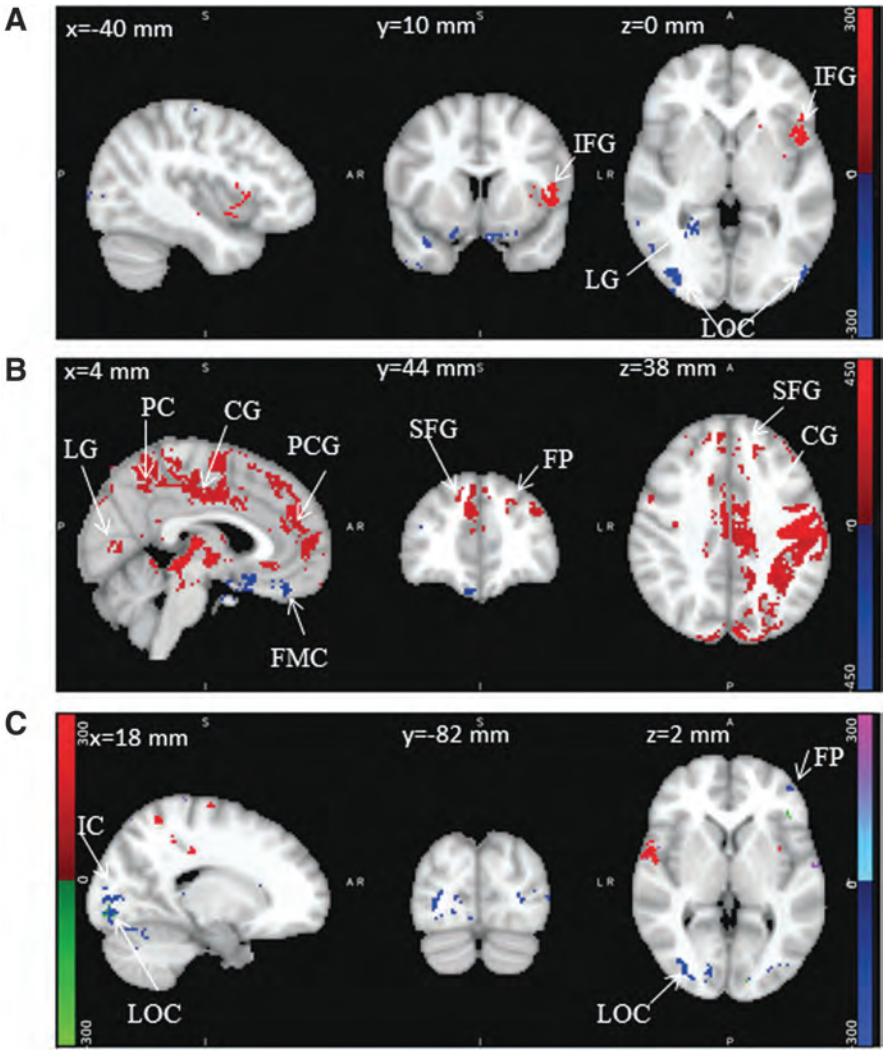

FIG. 6. Neurovascular underpinnings of nontarget stimuli: **(A)** alpha-reordered BOLD correlation (positive: red, negative: blue); **(B)** beta-reordered BOLD correlation (positive: red, negative: blue); and **(C)** gamma-reordered BOLD correlation (positive: red and pink, negative: green and blue). Color images are available online.

Downloaded by Harvard University FRANCIS A COUNTWAY from www.liebertpub.com at 06/27/19. For personal use only.

Task modulations in functional networks and neurovascular underpinnings

Target stimuli. Figure 3A illustrates the modulations in DMN for the true positive target stimuli, and regions are summarized in Table 1. The regions cingulate gyrus, paracingulate gyrus, frontal medial cortex, and parahippocampal gyrus, which are part of MPFC, have revealed negative modulation in both hemispheres during target stimuli. Similarly, angular gyrus and middle temporal cortex that are part of LP cortex and PCC that belongs to precuneus cortex was also deactivated during target stimuli. However, in addition to the deactivation, some portions of frontal medial cortex and parahippocampal gyrus in the left hemisphere, part of MPFC, were seen activated. From neurovascular underpinnings analyses, alpha and beta powers correlated negatively (Fig. 5) with reordered BOLD in MPFC and LP. Similarly, gamma power was correlated negatively in LP and PCC. Hence, these negative modulations of DMN are accompanied by significant neuronal activation observed through GLM in MPFC and LP. These observations explain the established hypothesis that DMN is a TNN during target stimuli. It is also supported by the negative correlation of alpha power with BOLD during target stimuli in this study.

The visual network has also presented (Fig. 4) task-related modulation during target stimuli. The occipital pole, lingual gyrus that are part of PVC, and supracalcarine and intracalcarine cortex, the part of MVC, deactivated during target stimuli. On the contrary, inferior lateral occipital cortex, part of LVC, was modulated positively. These modulations observed in the visual network are supported by significant neuronal activity observed through GLM in visual cortex. Further, it is strengthened by the positive and negative correlations of alpha power observed in the deactivated and activated regions, respectively. This association of negative correlation of alpha power and BOLD with activation in visual network regions justifies the hypothesis that visual network is a TPN during target stimuli.

In frontal-parietal network (Fig. 4), positive modulation was observed in the middle frontal gyrus and inferior frontal gyrus that are part of LPFC. A similar trend was seen in angular gyrus and superior lateral occipital cortex, part of PPC. Both LPFC and PPC revealed significant neuronal activity as seen in GLM. They also revealed negative correlation of alpha, beta, and gamma powers with BOLD. This in turn supports the hypothesis that frontal-parietal network is a TPN during target stimuli.

Downloaded by Harvard University FRANCIS A COUNTWAY from www.liebertpub.com at 06/27/19. For personal use only.

Table 1. Comparison Results Between the Proposed Approach and Graph Theory

		Modulations in functional connectivity for visual target detection task									
		Proposed method						*Graph theory*			
				Neurovascular underpinnings (reordered-BOLD and EEG power correlation)				*Modulation of graph theory measures [(task − rest)/rest]*			
S. No.	*Region of interest (laterality) (MNI coordinate)*	*Modulation of functional network (laterality)*	*Significant GLM (laterality)*	*Alpha correlation*	*Beta correlation*	*Gamma (lower) correlation*	*Gamma (higher) correlation*	*Modulation in global efficiency*	*Modulation in local efficiency*	*Modulation in clustering coefficient*	*Modulation in degree*
Stimuli: target											
Default mode network											
1	MPFC (1;55;−3)	D (R,L), A (L)	(R,L)	−(R,L)	−(R,L)	Nil	Nil	0.1698	2.6743	2.4461	1.1875
2	LP (L) (−39;−77;33)	D (L)	Nil	Nil	Nil	−(L)	−(L)	−0.0055	0.1764	0.0652	0.0625
3	LP (R) (47;−67;29)	D (R)	(R)	−(R)	−(R)	−(R)	Nil	0.0078	1.0984	1.1175	0.3636
4	PCC (R) (1;−61;38)	D (R,L)	Nil	Nil	Nil	−(R,L)	−(R,L)	−0.3064	0.6041	0.6453	−0.375
Visual network											
1	MVC (R) (2;−79;12)	D (R,L)	(R)	+(R)	Nil	Nil	Nil	0.0222	0.2386	0.2321	0.1261
2	PVC (0;−93;−4)	D (R,L)	(L,R)	+(R,L)	Nil	−(R)	Nil	0.2137	−0.2274	−0.2971	0.6666
3	LVC (L) (−37;−79;10)	A (L)	(L)	−(L)	Nil	−(L)	−(L)	−0.0471	0.1812	0.1592	0.0416
4	LVC (R) (38;−72;13)	A (R)	(R)	−(R)	−(R)	−(R)	Nil	−0.0506	0.0482	−0.0181	0.0317
Frontal-parietal network											
1	LPFC (L) (−43;33;28)	A (L)	(L)	−(L)	Nil	Nil	−(L)	−0.1484	0.4593	0.3675	0.0585
2	LPFC (R) (41;38;30)	A (R)	(R)	−(R)	−(R)	−(R)	Nil	−0.1430	0.7506	0.8385	−0.2187
3	PPC (L) (−46;−58;49)	A (L)	(L)	Nil	Nil	−(L)	−(L)	−0.2457	0.1715	0.1247	−0.2881
4	PPC (R) (52;−52;45)	A (R)	(R)	−(R)	−(R)	−(R)	Nil	−0.265	0.1587	0.1523	−0.3367
Stimuli: nontarget											
Default mode network											
1	MPFC (1;55;−3)	A (R,L)	(L)	Nil	+(R,L)	−(L)	Nil	0.4032	2.579	2.43	1.0833
2	LP (L) (−39;−77;33)	Nil	(L)	Nil	+(L)	Nil	Nil	0.1689	0.5377	0.3873	0.333
3	LP (R) (47;−67;29)	A (R,L)	Nil	−(R)	Nil	−(R), +(R)	Nil	0.1893	1.146	1.1017	0.5909
4	PCC (R) (1;−61;38)	D (L), A (R,L)	Nil	Nil	Nil	+(R)	Nil	−0.0515	0.389	0.3005	−0.0046
Visual network											
1	MVC (R) (2;−79;12)	D (R,L)	(R)	Nil	+(L)	Nil	−(R)	0.1187	−0.1215	−0.1494	0.1711
2	PVC (0;−93;−4)	D (R,L)	(L)	−(L)	+(R)	−(L)	−(L)	0.2751	−0.1773	−0.2835	0.4942
3	LVC (L) (−37;−79;10)	A (L)	(L)	−(L)	Nil	Nil	−(L)	0.233	0.1381	0.1255	0.4375
4	LVC (R) (38;−72;13)	A (R)	(R)	−(R)	Nil	−(R)	+(R), −(R)	0.1875	0.2972	0.2616	0.3492
Frontal-parietal network											
1	LPFC (L) (−43;33;28)	A (L)	(L)	Nil	+(L)	Nil	−(L)	−0.348	0.4536	0.3697	−0.2567
2	LPFC (R) (41;38;30)	A (R)	Nil	Nil	Nil	−(R)	Nil	−0.1428	0.417	0.578	−0.2187
3	PPC (L) (−46;−58;49)	A (L)	(L)	Nil	Nil	Nil	Nil	−0.2901	−0.1827	−0.208	−0.427
4	PPC (R) (52;−52;45)	A (R)	Nil	−(R)	Nil	+(R)	+(R)	−0.0798	0.2222	0.1247	−0.1326

The results are summarized as modulations in functional connectivity of brain for visual target detection task from resting state, associated GLM activity with corresponding neurovascular underpinnings, for both stimuli using proposed approach. Every cluster is represented in the following order: [Type of correlation whether Activation (A) or Deactivation (D) (Laterality whether left (L) or right (R)]. Results of graph theory analysis are summarized as variation in measures with respect to resting state, and thus positive values denoted the increment, and negative values denoted the decrement in the variation ratio.

BOLD, blood oxygen level dependent; EEG, electroencephalography; GLM, general linear model; LP, lateral parietal; LPFC, lateral prefrontal cortex; LVC, lateral visual cortex; MPFC, medial prefrontal cortex; MVC, medial visual cortex; PCC, posterior cingulate cortex; PPC, posterior parietal cortex; PVC, primary visual cortex.

Downloaded by Harvard University FRANCIS A COUNTWAY from www.liebertpub.com at 06/27/19. For personal use only.

Nontarget stimuli. Figure 3B illustrates the modulation observed in DMN for the true positive nontarget stimuli, and regions are tabulated in Table 1. Bilateral activation of DMN was observed in MPFC, LP, and PCC. However, some portion of PCC has revealed deactivations in the left hemisphere (Fig. 6). On the contrary, none of the DMN modulations except in MPFC found associated with any statistically significant neuronal activity through GLM. Similarly, no significant alpha correlation with BOLD was observed except in LP. The LP revealed negative correlation of alpha with BOLD. However, positive beta power correlation was seen in MPFC and LP. Gamma power correlated positively with reordered BOLD in PCC and LP and negatively in MPFC. These observations suggest that DMN is not completely manifesting as TNN during nontarget stimuli.

The visual network revealed deactivations in MVC and PVC. On the contrary, bilateral activations were observed in LVC. All these modulations of visual network were accompanied by significant neuronal activity through GLM. However, the deactivation of visual network in MVC and PVC was supported by positive correlation of beta power instead of alpha power. Negative alpha power correlation was found associated with activation observed in LVC. This clearly suggests that visual network is TPN during nontarget stimuli. However, beta power correlated with BOLD during deactivation than alpha power. Further, gamma power correlated negatively with BOLD in MVC, PVC, and LVC.

In frontal-parietal network, bilateral activation was observed in LPFC and PPC. However, left LPFC and PPC have shown significant neuronal activity. In addition, the negative alpha correlation was observed in PPC. These results suggest that frontal-parietal network behaves as TPN during nontarget stimuli. Gamma power showed negative correlation in PPC, and the beta power correlated positively in LPFC.

Graph theory analysis for the validation of modulation in functional networks

As explained in the Graph Theory Measures section, the graph theory was performed on the selected ROIs for resting-state, target, and nontarget stimuli independently, and results are shown in Figure 7. The modulations of graph theory measures during task engagement are tabulated in Table 1. The

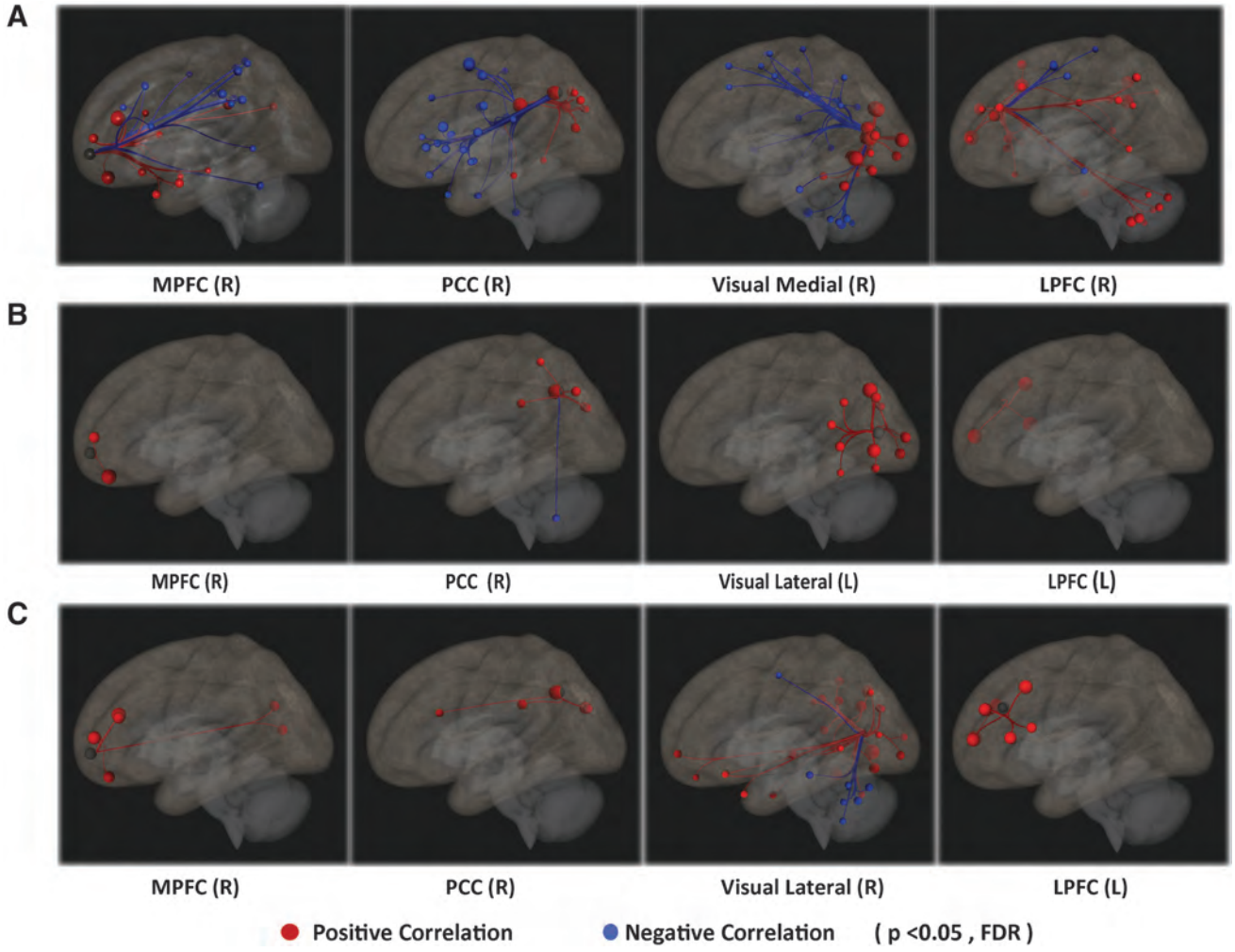

FIG. 7. Graph theory analysis: **(A)** resting state, **(B)** target stimuli, and **(C)** nontarget stimuli (red: positive correlation, blue: negative correlation; for $p < 0.05$, FDR). FDR, false discovery rate; LPFC, lateral prefrontal cortex; MPFC, medial prefrontal cortex; PCC, posterior cingulate cortex. Color images are available online.

Downloaded by Harvard University FRANCIS A COUNTWAY from www.liebertpub.com at 06/27/19. For personal use only.

global efficiency, local efficiency, clustering coefficient, and degree were estimated as graph theory measures in this study.

The local efficiency and clustering coefficient revealed significant increase in all those regions where deactivation of DMN was observed. Similarly, global efficiency and degree have shown significant increase in MPFC and left LP. However, this trend was not seen in PCC. Graph theory measures of nontarget stimuli revealed increase in all DMN regions. In particular, the global efficiency observed in DMN during nontarget stimuli is much higher than target stimuli. This justifies the absence of TNN trend in DMN modulation in nontarget stimuli. Activation of TPN is associated with increase in global efficiency (Hwang et al., 2018; Ma et al., 2018; Voss et al., 2013).

The TPN such as visual and frontal-parietal networks for both task stimuli revealed increase in graph theory measures. Local efficiency and clustering coefficient have shown more sensitivity toward the activation of network. Similarly, the deactivation observed in TPN has revealed decrease in graph theory measures, in particular local efficiency and clustering coefficient.

Discussion

In this study, modulation of functional connectivity during the visual target detection task and their neurovascular underpinnings was estimated through hemodynamically reorganized BOLD method. Further, the results of the proposed method have been validated at specific regions through graph theory.

To date, several studies investigated the functional connectivity to explore the dynamic interaction of brain regions in resting state. Arbabshirani and associates (2013), Desalvo and associates (2014), and Rosazza and associates (2012) have reported the modulation in functional connectivity and reorganization caused by tasks. However, our study presents a simple approach that enables us to visualize task-related modulations of functional connectivity and associated changes in neurovascular underpinnings at the voxel level. The following sections present the observations concluded from this study.

Association of functional network modulation with neural correlates of the task

Task induces the significant activation in engaged brain regions, which causes deactivations in DMN. Hence, DMN has always been referred to as a TNN. However, in this study, DMN revealed dual nature of task-related modulation. During target stimuli, DMN modulated as TNN. On the contrary, it was not entirely TNN during nontarget stimuli. This is possibly due to desynchronization of the task neuronal correlates with the DMN modulation during nontarget stimuli. Specifically, deactivation of DMN was associated with significant neural activity estimated through GLM in most of the regions except PCC during target stimuli. But this association was not observed during nontarget stimuli. Hence, the results revealed the stimuli dependency of DMN modulation during task. Similar results were also observed by many researchers. Newton and associates (2011) and Wenderoth and associates (2005) have reported the correlation between fluctuation in modulation of DMN during distinct cognitive tasks. Simony and associates (2016) have also reported the reconfiguration of DMN during narrative comprehension task. Mayer and associates (2010) have observed DMN deactivation within parts of DMN region, and concluded that they are dependent on specific characteristics of attention and working memory components of the task stimuli. This explains the dual nature of DMN modulation during both target and nontarget stimuli.

Further, the visual and frontal-parietal networks are known as TPN as it reveals positive modulation during task engagement. Hence, TPN associates the activation of networks with significant neuronal activity caused by the task. This trend was clearly evident in modulation of visual and frontal-parietal networks during both target and nontarget stimuli. These observations of the proposed method clearly establish the fundamental interplay between neuronal activity and modulations of TPN and TNN.

Functional inhibition in alpha band reflects the task-relevant neuronal activity

Several studies reported the inhibition of alpha band activity during the task engagement (Esposito et al., 2006; Foxe and Snyder, 2011; Klimesch, 2012; Uusberg et al., 2013). In this study, negative correlation of alpha power with reordered BOLD reflects the inhibition of alpha power during task engagement.

In general, alpha inhibition is associated with significant neuronal activity at the region. Hence, deactivation in TNN as well as activation in TPN will be presenting the inhibition of alpha power at that region. In this study during target stimuli, alpha inhibition was observed in deactivated regions of DMN except in PCC. Similarly, activated regions of frontal-parietal and visual networks also revealed alpha inhibition. Further, significant neuronal activity was found in alpha-inhibited regions of DMN, frontal-parietal and visual networks. This is consistent with the observation of Klimesch and associates (2007) and Min and Park (2010), whose work suggested the active role of alpha band during cognitive task as an inhibitory control. However, during nontarget stimuli alpha inhibition was only associated with activated regions of visual network. No such relationship between alpha inhibition and modulation in DMN and frontal-parietal network was observed during nontarget stimuli.

Hence, the observed dissociation of alpha inhibition in DMN during nontarget stimuli might be connected with its absence of TNN modulation. Moreover, this study is inadequate to strongly conclude on this aspect of observed result. More focus into this dual nature of DMN modulation might bring intricate insight into the neuronal dynamics.

Cross-frequency of alpha/beta neurovascular underpinnings

The decline in alpha/beta activity was found associated with drop in the synchrony of the underlying neural populations suggesting the task-related neuronal activity. The degree of desynchronization is connected with enhanced neuronal activity quantitatively, and found reflected as augmented BOLD signal (Yuan et al., 2010).

Results of proposed method have revealed the desynchronization of alpha and beta powers with their reordered BOLD in addition to their association with significant neuronal activity. For target stimuli, alpha/beta bands correlated

negatively with reordered BOLD in MPFC, LP, LVC, LPFC, and PPC. Further, these regions were associated with significant neuronal activity estimated through GLM. However, no such task-relevant desynchronization was observed in alpha/beta powers with reordered BOLD for nontarget stimuli.

Cross-frequency coupling of alpha/gamma neurovascular underpinnings

Synchronized activity is the resultant of competition (via inhibition) and cooperation (via excitation) of individual or set of neurons or large neuronal assemblies. This results in neuronal oscillations for different frequencies. This brought scientific community to observe the cross-frequency coupling of low and high frequency (Bauer et al., 2014; Bonnefond and Jensen, 2013, 2015; Buffalo et al., 2011; Fries et al., 2001; Osipova et al., 2008; Poch et al., 2014; Roux and Uhlhaas, 2014; van Kerkoerle et al., 2014; Voytek, 2010).

In this study, the proposed method reveals more insight into the synchronization of alpha/gamma bands and their correlation with reordered BOLD. Task-related desynchronization of alpha/gamma power with reordered BOLD was observed for target stimuli in LP, LVC, LPFC, and PPC, in addition to their significant neuronal activation. However, PCC exhibited desynchronization of gamma power with reordered BOLD. For nontarget stimuli, desynchronization of both alpha/gamma powers with reordered BOLD was observed merely in visual regions PVC and LVC. However, synchronization of gamma power with reordered BOLD was observed in LP, PCC, and PPC.

These observations of the proposed method are supported by the observation of Kujala and associates (2014) that BOLD signal not necessarily needs to exhibit positive correlation with high-frequency and negatively with low-frequency neuronal activity. This relationship is also observed to be varying across other cortical areas pertaining to higher cognitive functions as well as based on task stimuli. The results of this study support the same hypothesis.

Validation of proposed approach with graph theory analysis

The modulations observed in graph theory measures clearly support and validate the proposed method's observations. Engagement of task influences both local and distant functional connectivity in the regions that are involved in performing the tasks. This is seen as activation in the TPN during task engagement in the regions where significant neuronal activity is observed (Cole et al., 2016). However, the deactivation is generally associated with significant neuronal activity in the TNN (Takeuchi et al., 2011). Hence, regions that are deactivating in TNN and activating in TPN would increase both local connectivity and interaction with the distant regions (Sepulcre et al., 2010). This is observed through graph theory as positive modulation of local and global efficiency and clustering coefficients (Bolt et al., 2017; Cao et al., 2014; Moussa et al., 2011). This trend is observed in the modulation of functional network as assessed by both proposed method and graph theory measures.

Earlier studies also found that higher global efficiency of the network corresponds to fast global information communication, and local efficiency supports faster local information processing (Sporns, 2011; Wig, 2017).

In this study, increase in local efficiency observed in the regions of task engagement was in line with the present understanding of small worldness. Further, small worldness of functional networks demonstrates the task-related integration of brain regions. Dosenbach and associates (2007) revealed the small-world features of the subnetwork of the task-control system, analogous to the whole-brain network. Wang and associates (2018) highlighted the higher functional connectivity and network efficiencies due to greater cognitive demand. Similarly, the insignificant variation of global efficiency observed in this study in most of the regions is in line with the observation of earlier studies (Buckner et al., 2009). Lin and associates (2017) have observed dynamic alteration in DMN prior, during and post working memory task. In their study, the DMN has revealed high activation in the frontal regions during task, which was in turn observed as lower graph theory measure. This supports our observations of dual nature of DMN and its stimuli dependency. Thus, graph theory observations justify the modulations in functional connectivity as assessed by the proposed method.

Conclusion

In this study, the integrated analysis of modulations in functional networks and the associated changes in neurovascular underpinning were carried out through the proposed method at every voxel. The results of the proposed method were further validated with graph theoretical approach at the selected regions. The integrated analysis brought better insight into neuronal dynamics during task engagement. They are as follows:

1. The deactivation and activation of DMN were specific to nature of task stimuli. In this study, DMN was TNN during target stimulus. However, it was not entirely TNN during nontarget stimulus. On the contrary, frontal-parietal and visual networks remained as TPN during both target and nontarget stimuli.
2. There exists a strong association of the deactivation/activation of DMN with its significant neuronal activity during task engagement. However, this association was not strictly seen for nontarget stimulus.
3. The task-specific alpha inhibition and its association with significant neuronal activity and synchronization of visual and frontal-parietal networks observed throughout this study. However, desynchronization of DMN was seen associated with these variations.
4. The association of desynchronized alpha/beta activity with significant neuronal activity during task engagement is clearly observed in this study.

Thus, the proposed approach of integrated voxel-wise analysis of modulation of functional networks and the associated changes in neurovascular underpinning was found useful and helps us in bringing better understanding of neuronal mechanisms during task engagement.

Author Disclosure Statement

No competing financial interests exist.

Downloaded by Harvard University FRANCIS A COUNTWAY from www.liebertpub.com at 06/27/19. For personal use only.

Downloaded by Harvard University FRANCIS A COUNTWAY from www.liebertpub.com at 06/27/19. For personal use only.

References

Andrews-Hanna JR, Reidler JS, Huang C, Buckner RL. 2010. Evidence for the default network's role in spontaneous cognition. J Neurophysiol 104:322–335.

Arbabshirani MR, Havlicek M, Kiehl KA, Pearlson GD, Calhoun VD. 2013. Functional network connectivity during rest and task conditions: a comparative study. Hum Brain Mapp 34:2959–2971.

Bauer M, Stenner M-P, Friston KJ, Dolan RJ. 2014. Attentional modulation of alpha/beta and gamma oscillations reflect functionally distinct processes. J Neurosci 34:16117–16125.

Beaty RE, Benedek M, Barry Kaufman S, Silvia PJ. 2015. Default and executive network coupling supports creative idea production. Sci Rep 5:1–14.

Beckmann CF, Smith SM. 2004. Probabilistic independent component analysis for functional magnetic resonance imaging. IEEE Trans Med Imaging 23:137–152.

Binder J, Frost J, Hammeke T, Bellgowan PSF, Rao SM, Cox RW. 1999. Conceptual processing during the conscious resting state: a functional MRI study. J Cogn Neurosci 11:80–95.

Bolt T, Nomi JS, Rubinov M, Uddin LQ. 2017. Correspondence between evoked and intrinsic functional brain network configurations. Hum Brain Mapp 38, 1992–2007.

Bonnefond M, Jensen O. 2013. The role of gamma and alpha oscillations for blocking out distraction. Commun Integr Biol 6: 20–22.

Bonnefond M, Jensen O. 2015. Gamma activity coupled to alpha phase as a mechanism for top-down controlled gating. PLoS One 10:1–11.

Buckner RL, Carroll DC. 2007. Self-projection and the brain. Trends Cogn Sci 11:49–57.

Buckner RL, Sepulcre J, Talukdar T, Krienen FM, Liu H, Hedden T, et al. 2009. Cortical hubs revealed by intrinsic functional connectivity: mapping, assessment of stability, and relation to Alzheimer's disease. J Neurosci 29:1860–1873.

Buffalo EA, Fries P, Landman R, Buschman TJ, Desimone R. 2011. Laminar differences in gamma and alpha coherence in the ventral stream. Proc Natl Acad Sci U S A 108: 11262–11267.

Bush G, Shin LM. 2006. The multi-source interference task: an fMRI task that reliably activates the cingulo-frontal-parietal cognitive/attention network. Nat Protoc 1:308–313.

Calhoun VD, Kiehl KA, Pearlson GD. 2008. Modulation of temporally coherent brain networks estimated using ICA at rest and during cognitive tasks. Hum Brain Mapp 29:828–838.

Cao H, Plichta MM, Schäfer A, Haddad L, Grimm O, Schneider M, et al. 2014. Test-retest reliability of fMRI-based graph theoretical properties during working memory, emotion processing, and resting state. Neuroimage 84:888–900.

Cole MW, Ito T, Bassett DS, Schultz DH. 2016. Activity flow over resting-state networks shapes cognitive task activations. Nat Neurosci 19:1718–1726.

De Luca M, Smith S, De Stefano N, Federico A, Matthews PM. 2005. Blood oxygenation level dependent contrast resting state networks are relevant to functional activity in the neocortical sensorimotor system. Exp Brain Res 167:587–594.

Desalvo MN, Douw L, Takaya S, Liu H, Stufflebeam SM. 2014. Task-dependent reorganization of functional connectivity networks during visual semantic decision making. Brain Behav 4:877–885.

Di X, Biswal BB. 2014. Modulatory interactions between the default mode network and task positive networks in resting-state. PeerJ 2:e367.

Dosenbach NUF, Fair DA, Miezin FM, Cohen AL, Wenger KK, Dosenbach RAT, et al. 2007. Distinct brain networks for adaptive and stable task control in humans. Proc Natl Acad Sci U S A 104:11073–11078.

Esposito F, Bertolino A, Scarabino T, Latorre V, Blasi G, Popolizio T, et al. 2006. Independent component model of the default-mode brain function: assessing the impact of active thinking. Brain Res Bull 70:263–269.

Esposito R, Cieri F, Chiacchiaretta P, Cera N, Lauriola M, Di Giannantonio M, et al. 2018. Modifications in resting state functional anticorrelation between default mode network and dorsal attention network: comparison among young adults, healthy elders and mild cognitive impairment patients. Brain Imaging Behav 12:127–141.

Fox MD, Snyder AZ, Vincent JL, Corbetta M, Van Essen DC, Raichle ME. 2005. From the cover: the human brain is intrinsically organized into dynamic, anticorrelated functional networks. Proc Natl Acad Sci U S A 102:9673–9678.

Foxe JJ, Snyder AC. 2011. The role of alpha-band brain oscillations as a sensory suppression mechanism during selective attention. Front Psychol 2:1–13.

Fries P, Reynolds JH, Rorie AE, Desimone R. 2001. Modulation of oscillatory neuronal synchronization by selective visual attention. Science 291:1560–1563.

Gao W, Lin W. 2012. Frontal parietal control network regulates the anti-correlated default and dorsal attention networks. Hum Brain Mapp 33:192–202.

Gerlach KD, Spreng RN, Gilmore AW, Schacter DL. 2011. Solving future problems: default network and executive activity associated with goal-directed mental simulations. Neuroimage 55:1816–1824.

Gordon EM, Stollstorff M, Vaidya CJ. 2011. Using spatial multiple regression to identify intrinsic connectivity networks involved in working memory performance. Hum Brain Mapp 33:10.

Hwang J, Legarreta M, Bueler CE, DiMuzio J, McGlade E, Lyoo IK, Yurgelun-Todd D. 2018. Increased efficiency of brain connectivity networks in veterans with suicide attempts. Neuroimage Clin 20:318–326.

Ino T, Nakai R, Azuma T, Kimura T, Fukuyama H. 2011. Brain activation during autobiographical memory retrieval with special reference to default mode network. Open Neuroimag J 5:14–23.

Klimesch W. 2012. Alpha-band oscillations, attention, and controlled access to stored information. Trends Cogn Sci 16: 606–617.

Klimesch W, Sauseng P, Hanslmayr S. 2007. EEG alpha oscillations: the inhibition-timing hypothesis. Brain Res Rev 53: 63–88.

Koshino H, Minamoto T, Yaoi K, Osaka M, Osaka N. 2014. Coactivation of the default mode network regions and working memory network regions during task preparation. Sci Rep 4:34–39.

Kujala J, Sudre G, Vartiainen J, Liljeström M, Mitchell T, Salmelin R. 2014. Multivariate analysis of correlation between electrophysiological and hemodynamic responses during cognitive processing. Neuroimage 92:207–216.

Kwong KK, Belliveau JW, Chesler DA, Goldberg IE, Weisskoff RM, Poncelet BP, et al. 1992. Dynamic magnetic resonance imaging of human brain activity during primary sensory stimulation. Proc Natl Acad Sci U S A 89:5675–5679.

Lin P, Yang Y, Gao J, De Pisapia N, Ge S, Wang X, et al. 2017. Dynamic default mode network across different brain states. Sci Rep 7:1–13.

Lindquist MA, Meng Loh J, Atlas LY, Wager TD. 2009. Modeling the hemodynamic response function in fMRI: efficiency, bias and mis-modeling. Neuroimage 45:S187–S198.
Logothetis NK. 2003. The underpinnings of the BOLD functional magnetic resonance imaging signal. J Neurosci 23: 3963–3971.
Ma X, Jiang G, Fu S, Fang J, Wu Y, Liu M, et al. 2018. Enhanced network efficiency of functional brain networks in primary insomnia patients. Front Psychiatry 9:1–11.
Manelis A, Reder LM. 2014. Effective connectivity among the working memory regions during preparation for and during performance of the n-back task. Front Hum Neurosci 8:1–11.
Mayer JS, Roebroeck A, Maurer K, Linden DEJ. 2010. Specialization in the default mode: task-induced brain deactivations dissociate between visual working memory and attention. Hum Brain Mapp 31:126–139.
Min BK, Park HJ. 2010. Task-related modulation of anterior theta and posterior alpha EEG reflects top-down preparation. BMC Neurosci 11:79.
Moussa MN, Vechlekar CD, Burdette JH, Steen MR, Hugenschmidt CE, Laurienti PJ. 2011. Changes in cognitive state alter human functional brain networks. Front Hum Neurosci 5:1–15.
Nathan Spreng R. 2012. The fallacy of a ''task-negative'' network. Front Psychol 3:145.
Newton A, Morgan V. 2011. Modulation of steady state functional connectivity in the default mode and working memory networks by cognitive load. Hum Brain Mapp 32:1649–1659.
Newton AT, Morgan VL, Rogers BP, Gore JC. 2011. Modulation of steady state functional connectivity in the default mode and working memory networks by cognitive load. Hum Brain Mapp 32:1649–1659.
Osipova D, Hermes D, Jensen O. 2008. Gamma power is phase-locked to posterior alpha activity. PLoS One 3:e3990.
Piccoli T, Valente G, Linden DEJ, Re M, Esposito F, Sack AT, et al. 2015. The default mode network and the working memory network are not anti-correlated during all phases of a working memory task. PLoS One 10:e0123354.
Poch C, Campo P, Barnes GR. 2014. Modulation of alpha and gamma oscillations related to retrospectively orienting attention within working memory. Eur J Neurosci 40:2399–2405.
Raichle ME, Gusnard DA. 2005. Intrinsic brain activity sets the stage for expression of motivated behavior. J Comp Neurol 493:167–176.
Raichle ME, MacLeod AM, Snyder AZ, Powers WJ, Gusnard DA, Shulman GL. 2001. A default mode of brain function. Proc Natl Acad Sci U S A 98:676–682.
Rosazza C, Minati L, Ghielmetti F, Mandelli ML, Bruzzone MG. 2012. Functional connectivity during resting-state functional MR imaging: study of the correspondence between independent component analysis and region-of-interest-based methods. AJNR Am J Neuroradiol 33:180–187.
Roux F, Uhlhaas PJ. 2014. Working memory and neural oscillations: alpha-gamma versus theta-gamma codes for distinct WM information? Trends Cogn Sci 18:16–25.
Rowe JB, Hughes LE, Barker RA, Owen AM. 2010. Dynamic causal modelling of effective connectivity from fMRI: are results reproducible and sensitive to Parkinson's disease and its treatment? Neuroimage 52:1015–1026.
Sala-Llonch R, Peña-Gómez C, Arenaza-Urquijo EM, Vidal-Piñeiro D, Bargalló N, Junqué C, Bartrés-Faz D. 2012. Brain connectivity during resting state and subsequent working memory task predicts behavioural performance. Cortex 48:1187–1196.
Sambataro F, Visintin E, Doerig N, Brakowski J, Holtforth MG, Seifritz E, Spinelli S. 2017. Altered dynamics of brain connectivity in major depressive disorder at-rest and during task performance. Psychiatry Res Neuroimaging 259:1–9.
Schlösser RGM, Wagner G, Koch K, Dahnke R, Reichenbach JR, Sauer H. 2008. Fronto-cingulate effective connectivity in major depression: a study with fMRI and dynamic causal modeling. Neuroimage 43:645–655.
Sepulcre J, Liu H, Talukdar T, Martincorena I, Thomas Yeo BT, Buckner RL. 2010. The organization of local and distant functional connectivity in the human brain. PLoS Comput Biol 6:1–15.
Shine JM, Muller AJ, O'Callaghan C, Hornberger M, Halliday GM, Lewis SJG. 2015. Abnormal connectivity between the default mode and the visual system underlies the manifestation of visual hallucinations in Parkinson's disease: a task-based fMRI study. Parkinsons Dis 1:15003.
Simony E, Honey CJ, Chen J, Lositsky O, Yeshurun Y, Wiesel A, Hasson U. 2016. Dynamic reconfiguration of the default mode network during narrative comprehension. Nat Commun 7:1–13.
Spadone S, Della Penna S, Sestieri C, Betti V, Tosoni A, Perrucci MG, et al. 2015. Dynamic reorganization of human resting-state networks during visuospatial attention. Proc Natl Acad Sci 112:8112–8117.
Sporns O. 2011. The human connectome: a complex network. Ann N Y Acad Sci 1224:109–125.
Spreng RN, Stevens WD, Chamberlain JP, Gilmore AW, Schacter DL. 2010. NeuroImage default network activity, coupled with the frontoparietal control network, supports goal-directed cognition. Neuroimage 53:303–317.
Takeuchi H, Taki Y, Hashizume H, Sassa Y, Nagase T, Nouchi R, Kawashima R. 2011. Failing to deactivate: the association between brain activity during a working memory task and creativity. Neuroimage 55:681–687.
Tommasin S, Mascali D, Gili T, Eid Assan I, Moraschi M, Fratini M, et al. 2017. Task-related modulations of BOLD low-frequency fluctuations within the default mode network. Front Phys 5:1–8.
Uusberg A, Uibo H, Kreegipuu K, Allik J. 2013. EEG alpha and cortical inhibition in affective attention. Int J Psychophysiol 89:26–36.
Vaina LM. 2014. A computational study of whole-brain connectivity in resting state and task fMRI. Med Sci Monit 20:1024–1042.
van Kerkoerle T, Self MW, Dagnino B, Gariel-Mathis M-A, Poort J, van der Togt C, Roelfsema PR. 2014. Alpha and gamma oscillations characterize feedback and feedforward processing in monkey visual cortex. Proc Natl Acad Sci U S A 111:14332–14341.
Vatansever D, Menon DK, Stamatakis EA. 2017. Default mode contributions to automated information processing. Proc Natl Acad Sci U S A 114:12821–12826.
Vazquez AL, Cohen ER, Gulani V, Hernandez-Garcia L, Zheng Y, Lee GR, et al. 2006. Vascular dynamics and BOLD fMRI: CBF level effects and analysis considerations. Neuroimage 32:1642–1655.
Voss MW, Wong CN, Baniqued PL, Burdette JH, Erickson KI, Prakash RS, et al. 2013. Aging brain from a network science perspective: something to be positive about? PLoS One 8: e78345.
Voytek B. 2010. Shifts in gamma phase-amplitude coupling frequency from theta to alpha over posterior cortex during visual tasks. Front Hum Neurosci 4:1–9.

Downloaded by Harvard University FRANCIS A COUNTWAY from www.liebertpub.com at 06/27/19. For personal use only.

Wager TD, Vazquez A, Hernandez L, Noll DC. 2005. Accounting for nonlinear BOLD effects in fMRI: parameter estimates and a model for prediction in rapid event-related studies. Neuroimage 25:206–218.

Walz JM, Goldman RI, Carapezza M, Muraskin J, Brown TR, Sajda P. 2014. Simultaneous EEG-fMRI reveals a temporal cascade of task-related and default-mode activations during a simple target detection task. Neuroimage 102:229–239.

Wang B, Li P, Li D, Niu Y, Yan T, Li T, et al. 2018. Increased functional brain network efficiency during audiovisual temporal asynchrony integration task in aging. Front Aging Neurosci 10:1–15.

Wenderoth N, Debaere F, Sunaert S, Swinnen SP. 2005. The role of anterior cingulate cortex and precuneus in the coordination of motor behaviour. Eur J Neurosci 22:235–246.

Whitfield-Gabrieli S, Nieto-Castanon A. 2012. Conn: A functional connectivity toolbox for correlated and anticorrelated brain networks. Brain Connect 2:125–41.

Wig GS. 2017. Segregated systems of human brain networks. Trends Cogn Sci 21:981–996.

Xu X, Yuan H, Lei X. 2016. Activation and connectivity within the default mode network contribute independently to future-oriented thought. Sci Rep 6:1–10.

Yuan H, Liu T, Szarkowski R, Rios C, Ashe J, He B. 2010. Negative covariation between task-related responses in alpha/beta-band activity and BOLD in human sensorimotor cortex: an EEG and fMRI study of motor imagery and movements. Neuroimage 49:2596–2606.

Address correspondence to:
Vijayakumar Chinnadurai
NMR Research Centre
Institute of Nuclear Medicine and Allied Sciences
Delhi 110054
India

E-mail: vijayakumar@inmas.drdo.in;
vijayafmc@gmail.com

Downloaded by Harvard University FRANCIS A COUNTWAY from www.liebertpub.com at 06/27/19. For personal use only.

J Biosci (2021)46:75
DOI: 10.1007/s12038-021-00194-y

© Indian Academy of Sciences

Functional connectivity between frontal/parietal regions and MTL–basal ganglia during feedback learning and declarative memory retrieval

Swati Agrawal[1,2], Rinku Sharma[2] and Vijayakumar Chinnadurai[1]*

[1]*NMR Research Centre, Institute of Nuclear Medicine and Allied Sciences, Lucknow Rd, Timarpur, Delhi 110 054, India*

[2]*Delhi Technological University, Shahbad Daulatpur, Main Bawana Road, Delhi 110 042, India*

**Corresponding author (Email, vijayakumar@inmas.drdo.in, vijayafmc@gmail.com)*

MS received 25 September 2020; accepted 21 June 2021

Feedback assists the memory system in preserving the learnings from ongoing activities and updating it for future retrievals. Thus, the feedback coming from an individual's performance affects the behavior and, thereby, the performance. However, little is known regarding the interactions of learning and memory associated regions. Thus, we employ a combination of functional connectivity and neurovascular approach to explore the significance of these interactions. Our study comprises thirty-five volunteers who undergo a feedback declarative memory task using simultaneous EEG-fMRI data acquisition. Functional connectivity analysis showed that medial temporal lobe (MTL) and basal ganglia possess significant connectivity but differential relationships during feedback learning and memory retrieval. Specifically, Putamen and pallidum (sub-regions of basal ganglia) are the central hubs in these mechanisms. The neurovascular analysis reveals the increased correlation of frontal-alpha and theta powers with the bold activity of MTL during memory retrievals. The results also report the role of the frontal (and parietal) alpha-beta powers in de-synchronization (and synchronization) of the bold activity of caudate; and parietal-theta (frontal-higher-alpha) power in de-synchronization (and synchronization) of bold activity of right accumbens. Hence, the study demonstrates the significant role of the frontal-parietal EEG powers in MTL–basal ganglia relationships and neuronal adaptations during declarative memory retrieval.

Keywords. Basal ganglia; declarative memory retrieval; EEG-fMRI; feedback; frontal-parietal; functional connectivity; medial temporal lobe

1. Introduction

Memory is a cognitive process that updates with experience, and learning is a process that contributes to the formation of these memories (Preston and Eichenbaum 2013a). In recent years, several electrophysiological and neuroimaging studies (de Vanssay-Maigne *et al.* 2011; Eichenbaum *et al.* 2007; Fell *et al.* 2011; Tendolkar *et al.* 2008) have emerged to examine long-term memory systems, in particular declarative memory. These studies suggested the prominent role of the medial temporal lobe in declarative memory and revealed its interaction with the feedback learning associated regions, prefrontal cortex and basal ganglia (Brincat and Miller 2015; Cohen *et al.* 2008; Gerraty *et al.* 2014; Seger and Cincotta 2006). Existing literature (Hattie and Timperley 2007; Lee and Reeve 2013; Tricomi and Fiez 2012) explains the electrophysiology of positive-negative feedbacks, the affected regions, and subsequently, the behavior modulations. Several researchers (Chang *et al.* 2013; Ridderinkhof *et al.* 2004; van de Vijver *et al.* 2011; Wagner *et al.* 2005) have also suggested that feedback associated learning and memory retrieval tasks engage frontal and parietal

Supplementary Information: The online version contains supplementary material available at https://doi.org/10.1007/s12038-021-00194-y.

Published online: 04 August 2021

regions, respectively. However, the neuronal mechanisms remain less explored for understanding how frontal-parietal regions contribute to the declarative memory retrieval after feedback learning.

Several previous neuroimaging studies (Maia 2009; Rushworth *et al.* 2011) have outlined a reward-based learning circuit restricted to midbrain dopaminergic structures, the striatum, the orbitofrontal cortex (OFC), and the medial frontal cortex (MFC). Also, the dorsolateral prefrontal cortex is found as a key component in regulating the reward circuit (Haber and Knutson 2010). The EEG based studies (Cohen *et al.* 2007; Doñamayor *et al.* 2011; Marco-Pallares *et al.* 2008) have emphasized the role of beta rhythmic activity and reported it for reward over frontal regions of the brain. A recent study (Knudsen and Wallis 2020) has revealed that the hippocampus also plays a role in reward-guided behavior. The same study suggested that the theta oscillations of OFC are critically important for reward-guided learning, and theta oscillations of the hippocampus drive them. Thus, all these studies indicate a critical role of oscillatory mechanisms in feedback-associated functions of the frontal brain.

Conventionally, the non-declarative memory is associated with the reward-driven mechanisms of the basal ganglia during reward-guided behavior (Cohen *et al.* 1997; Knowlton *et al.* 1996; Packard *et al.* 1989; Daphna Shohamy *et al.* 2004a, b). A few recent studies (Cohn *et al.* 2010; Han *et al.* 2010; Moustafa and Gluck 2011; Daphna Shohamy and Adcock 2010) have highlighted the potential role of the basal ganglia in declarative memory tasks also. Thus, the interactions between MTL and basal ganglia help understand the mechanisms involved in learning and memory. A recent study (Freedberg *et al.* 2020) suggested that the MTL and the striatum (a subregion of basal ganglia) can play a dissociable role during learning. It also indicated that midbrain dopaminergic nuclei and prefrontal cortex might mediate cooperation between the striatum and the MTL for learning. Several studies (Dobbins *et al.* 2002; Euston *et al.* 2012) have also suggested that the prefrontal cortex contributes to memory by cognitive/strategic control over memory retrieval. Another study (Cabeza 2008) has revealed the role of the ventral parietal cortex (VPC) in episodic memory retrieval and showed that the activity of VPC reflects the capture of bottom-up attention by retrieving the relevant memory targets from episodic memory. Some other studies (Ally *et al.* 2008; Wagner *et al.* 2005) also pointed out the role of the parietal cortex during memory retrieval. Thus, the role of frontal and parietal regions is crucial while understanding the relationship between MTL and basal ganglia. To the best of our knowledge, no study explores the role of frontal-parietal regions in this relationship through the neurovascular approach.

Hence, this study examines the association of frontal-parietal EEG powers with MTL and basal ganglia during feedback learning and memory retrieval using functional connectivity and neurovascular approach. First, we test the functional connectivity of frontal-parietal regions with MTL and sub-regions of basal ganglia for feedback learning and memory retrievals. We assess the electrophysiology and estimate the spectral distribution of these time-locked stimuli conditions. The time-locked frontal-parietal powers are then correlated to the bold signal of MTL and basal ganglia. Our research reveals the modulation in the functional connectivity of MTL and basal ganglia from feedback learning to memory retrieval due to the varying roles of basal ganglion sub-regions (putamen and pallidum). It also suggests that frontal-parietal regions dissociate with the MTL and the basal ganglia during memory retrieval. These feedback related modulations are then studied with the neurovascular approach, and results reveal the significant associations of explicit frontal-parietal EEG powers with the bold activity of affected regions.

2. Materials and methods

2.1 *Participants*

Thirty-five healthy right-handed volunteers (17 males and 18 females, aged 20-32 years, mean age: 24 years) participated in this experiment. All participants reported normal or corrected-to-normal vision and no history of psychiatric, neurological disorder, or was using any medication. The participants who took part in the study were not involved in the practice task before the experiment to avoid any prior experiential bias. All participants gave written informed consent for the examination before the experiment. Ethical approval for the study was obtained from the local ethical committee.

2.2 *Experiment design*

During the experiment, we present a collection of simple geometrical figures such as a cube, circle, rectangle, and triangle filled with primary colors, to the participants. For the experiment, a stimulus is assigned

as 'Target' object at the start of each trial for 3 s. During the presentation of 'Target' stimuli in the trial, the volunteer is asked to remember the shape and the color of the article. In the final phase of each trial, we present the volunteer with a collection of different geometric shapes for 3 s, one item at a time, and the volunteer is asked to retrieve the memorized target and respond upon recognition. There are five trials in total; each trial consists of 21 sub-trials. The experiment uses a mixed paradigm design composed of ninety-four stimuli distributed over five trials. Among the ninety-four stimuli slides, there are 32 slides of 'Target' object. We present a fixation block with a single cross in the center of the slide for 3 s after presenting each task stimulus.

The study provides visual feedback after each memory retrieval to assess its effect on their subsequent performance. The use of visual-feedback for 2 s offers the correctness of the volunteer's response after each stimulus and allows the volunteers to learn from their performance feedback. The volunteers were informed to avoid any motor response during feedback presentation. These task stimuli are projected onto MR compatible lenses fitted on the head coil inside MR. A sample task paradigm from the experiments is shown in figure 1.

2.3 *Data acquisition with simultaneous EEG-fMRI*

The study uses a simultaneous EEG-fMRI technique for data acquisition of declarative memory task. All images were acquired using a 3T Siemens Magnetom Skyra scanner. The scanner parameters were identical to those used in our previous study (Agrawal *et al.* 2019). T2× weighted images were acquired using Eco Planar Imaging (EPI) sequence with TR = 3000 ms; TE = 36 ms; voxel size = 3.6×3.6×3.0 mm; matrix = 64×64; FoV read = 230 mm; flip angle =90°, 36 axial slices. The axial slices are acquired parallel to the Anterior-Posterior (AC-PC) line in an interleaving manner with a slice thickness of 3.0 mm. High-resolution T1-weighted structural images were acquired using T1 MPRAGE sequence with parameters, voxel size =1.0×1.0×1.0 mm; TR= 2000 ms; flip angle = 90°; FoV = 240 mm; matrix= 512×512; slice thickness = 1.0 mm, 160 axial slices. The axial slices are acquired parallel to the Anterior-Posterior (AC-PC) line in an interleaving manner with a slice thickness of 5.0 mm.

Simultaneously, EEG data from 32 channel MR compatible Brain Amp differential amplifier is acquired at a 5 kHz sampling rate. EEG data were recorded from 32 Ag/AgCl scalp electrodes, distributed according to

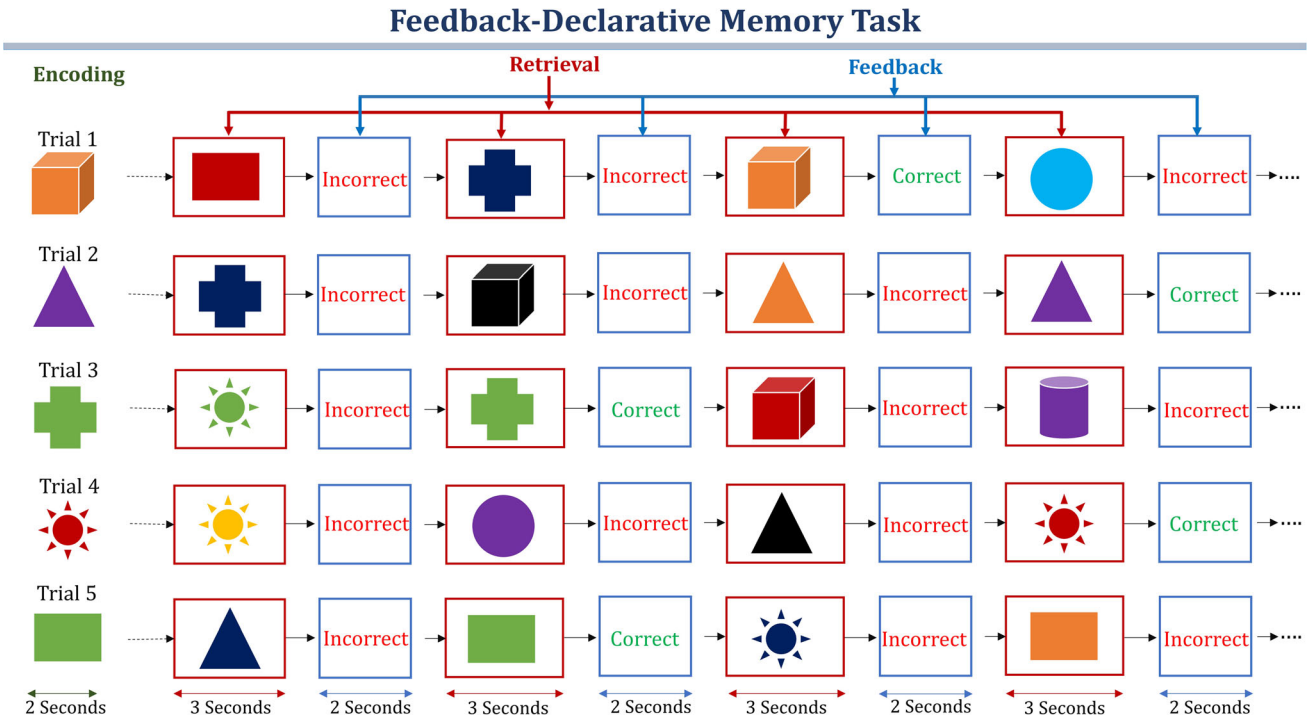

Figure 1. A sample experimental design of the feedback declarative memory task. The participants are asked to retrieve the previously memorized object during the retrieval phase of 3s. The study provides visual feedback after each stimulus for 2s during feedback learning, regarding the correctness of the answer to the volunteer's response. The volunteer's task is to detect, learn, and adjust to these changes.

the 10–20 system with a reference electrode in between Fz and Cz. The ground electrode is placed between Cz and Pz. The ECG electrode is set to measure the cardiac effect for the artifact corrections. The impedance of all the scalp electrodes was maintained below 5 kΩ.

2.4 *Pre-processing*

2.4.1 *Pre-processing of EEG data:* We subject the acquired EEG data to the following pre-processing procedures. First, the EEG data is trimmed to a time-locked dataset. The study then uses the FMRIB (EEGLAB) tool to remove MR related gradient artifacts, detect QRS complexes from an ECG channel, and to remove pulse ballistocardiograph artifacts from our time-locked EEG data. For the removal of MR artifact, FASTR (FMRI Artifact Slice Template Removal) aligns all the slice artifacts with correcting for any slight jitter in the exact location of the slice-timing events. It interpolates the data, and then shift each artifact until the correlation is maximized between data and a reference artifact (the first artifact in the data). The second stage of FASTR (Allen *et al.* 2000), computes an average template for the artifact, and subtract it from the center contaminated data by taking a moving-window average of slice artifacts. QRS detection uses combined adaptive thresholding (Christov 2004) and the Teager energy operator (Kim *et al.* 2004), followed by a correction algorithm. This algorithm aligns all events and corrects for false positives and negatives. The removal of pulse artifacts uses QRS events to subtract an artifact template from the data, and here it is done by using an optimal basis set for the number of PCs 3. For carrying out the time–frequency analyses, the study uses the Harvard Automated Processing Pipeline for EEG (HAPPE) processes (Gabard-Durnam *et al.* 2018) by using filtering, artifact rejection, and re-referencing the contaminated EEG data. We then estimate EEG frequency powers from pre-processed EEG data using EEGLAB (MathWorks).

2.4.2 *Pre-processing of fMRI data:* All the fMRI artifact removal processing is carried out using standard artifact removal pipeline of Statistical Parametric Mapping (version: SPM 12). The following pre-processing is applied: realignment and slice time correction for minimizing the effect of head motion and slice acquisition delays, registration of functional scans to standard MNI template space, spatial smoothing using a Gaussian kernel (5 mm FWHM). Statistical analyses were performed on the smoothed data with a high pass filter to remove low-frequency noise.

2.5 *Data analysis*

The acquired task data is subsequently subjected to the data-analysis procedure, which is as the methodological block diagram of the study shown in figure 2.

2.5.1 *Time–frequency analysis:* Time–frequency analysis is performed by assessing event-related spectral perturbations (ERSP) using a complex-sinusoidal wavelet transform procedure as implemented in EEGLAB (Delorme and Makeig 2004). For this, we have extracted the stimulus-locked EEG data for feedback learning and memory retrievals associated with positive outcomes only for frontal (Fz, F3, F4) and Parietal (Pz, P3, P4) channels. The time–frequency analysis is performed using Morlet wavelets for 2 s epoch (−500 ms to 1500 ms post stimuli or feedback) and then subject the data for baseline correction (−500 to 0 ms) and group the data of all the trials corresponding to the same condition (feedback learning and memory retrievals). For the frequencies from 1 Hz to 35 Hz, the study compute mean-event-related changes in the spectral power for the epoch. The averaged oscillatory activity for the defined period is used to find the power of each frequency following feedback and memory retrieval. The study evaluates time–frequency curves using the data from all the participants and calculates mean ERSP.

2.5.2 *Functional connectivity analysis:* The estimation of functional connectivity is carried out to understand the interactions of frontal-parietal regions with MTL and basal ganglia during feedback and memory retrievals. For this, the areas of interest are selected, and the connectivity is evaluated using graph theory during feedback learning and subsequent memory retrievals. Estimation of graph theory is done based on functional connectivity using the CONN toolbox (Whitfield-Gabrieli and Nieto-Castanon 2012). Functional connectivity maps of all ROI's were further derived using Fisher's r-to-z transformation. The group-level functional connectivity maps were corrected for multiple comparisons using FDR-correction with a corrected threshold of $p < 0.05$.

2.5.3 *Associations of frontal-parietal electrophysiological powers with feedback learning and memory retrieval: The EEG-informed FMRI approach:* We

perform statistical analyses to explore the relationship of EEG powers with the hemodynamics during feedback and subsequent memory retrieval in the GLM framework. For this, we set up a GLM design matrix, consisted of frontal-parietal electrophysiological powers as the parametric modulators. First, we extract the time-locked (200–600 ms) spectral powers from each feedback and memory retrieval block for each volunteer. The estimation is done for frontal (Fz, F3, F4), parietal (Pz, P3, P4) electrodes and bands of interest (i.e., 1–4 Hz for delta, (4–8) Hz for theta, 9–12 Hz for lower-alpha, 12–14 Hz for higher-alpha, 15–21Hz for lower-beta and 22–35 Hz for higher-beta). Each power spectra are then normalized with respect to total power. Normalization of each power spectra in our study is done to minimize the effect of mixing of features associated with multiple volunteers and multiple epochs. We use relative EEG powers as EEG regressors during GLM analyses as parametric modulators in feedback learning and subsequent memory retrieval. For EEG-correlated fMRI analysis, GLMs are applied to the data of each subject at the first level. These EEG regressors are then subjected to a general linear model (GLM) along with the six realignment parameters for each run. We then model the fMRI BOLD responses using a canonical hemodynamic response function with temporal and dispersion derivatives. At the second level, one-sample t-tests are computed for all frequency bands, EEG-BOLD signal correlations are considered significant at a corrected cluster threshold of $p<0.05$. Subsequent analyses are based on the interactions of frontal-parietal powers with MTL and basal ganglia, which correlates outside these brain regions that are not analyzed.

3. Results

Extensive electrophysiological and neuroimaging studies (Anderson *et al.* 2008; Rushworth *et al.* 2011; Thürer *et al.* 2017) have highlighted the association of frontal and parietal regions in learning and task adaptations. Our research explores the role of frontal-parietal EEG powers in a relationship of MTL and basal ganglia during the declarative memory task. The study also uses a functional connectivity approach to understand the relationship of frontal-parietal regions with MTL and basal ganglia. We then explore the role of frontal-parietal EEG powers during the feedback learning and memory retrievals, as shown in supplementary figure 1. Further, we investigate the relationship between neural activity and BOLD signal in simultaneously acquired EEG and fMRI data during a declarative memory task. The results reveal the significant relationships of frontal-parietal EEG powers with the MTL and sub-regions of the basal ganglia. The following sections present these results in detail.

3.1 *Association of frontal-parietal regions with medial temporal lobe and basal ganglia: The functional connectivity analysis*

The functional connectivity analyses explore the interactions of frontal-parietal regions with the MTL and basal ganglia for feedback learning and memory retrieval. Figure 3a and b demonstrate the connectivity patterns of these interactions, and tables 1 and 2 summarize the significant connectivity of these regions.

The study finds a significant connectivity between frontal and parietal regions during feedback learning as well as during memory retrievals. However, there is a significant reduction in the functional connectivity of MFG-SPL, MFG-AG, IFG Oper-AG, IFG Oper-aSMG and IFG Oper-pSMG from feedback learning to memory retrieval at a significant level ($p<0.001$). The study also observes the modulation in the functional connectivity of frontal-parietal regions with the MTL from feedback to memory retrieval. First, there was a significant correlation of the frontal orbital cortex with the rest of the MTL structure during feedback learning (Forb-Amygdala: $r_{Left}=4.74$ and $r_{Right}=6.16$) for both hemispheres. The study observes non-significant correlation values during memory retrieval, indicating that the MTL structure dissociates with the rest of the frontal-parietal regions during memory retrieval.

We find the significant interactions of the frontal cortex with sub-regions of the basal ganglia during feedback learning (Forb-Accumbens; Forb-Putamen). The correlation values (Forb-Accumbens: $r_{Left}=3.95$, $r_{Right}=3.75$; Accumbens-Caudate: $r_{Left}=9.46$, $r_{Right}=6.01$); Accumbens-Putamen: $r_{Left}=4.42$, $r_{Right}=5.11$) of functional connectivity analysis indicate that the accumbens plays a significant role in the relationship of the frontal orbital cortex and the rest of the basal ganglia. The study also finds the significant correlations of inferior frontal gyrus with the sub-regions of the basal ganglia, specifically in the right hemisphere (IFG Oper-Putamen: $r_{Right}=5.43$).

Yet, the study does not observe any correlation and reveals the absence of any connectivity of frontal regions with basal ganglia during memory retrieval, likewise the MTL.

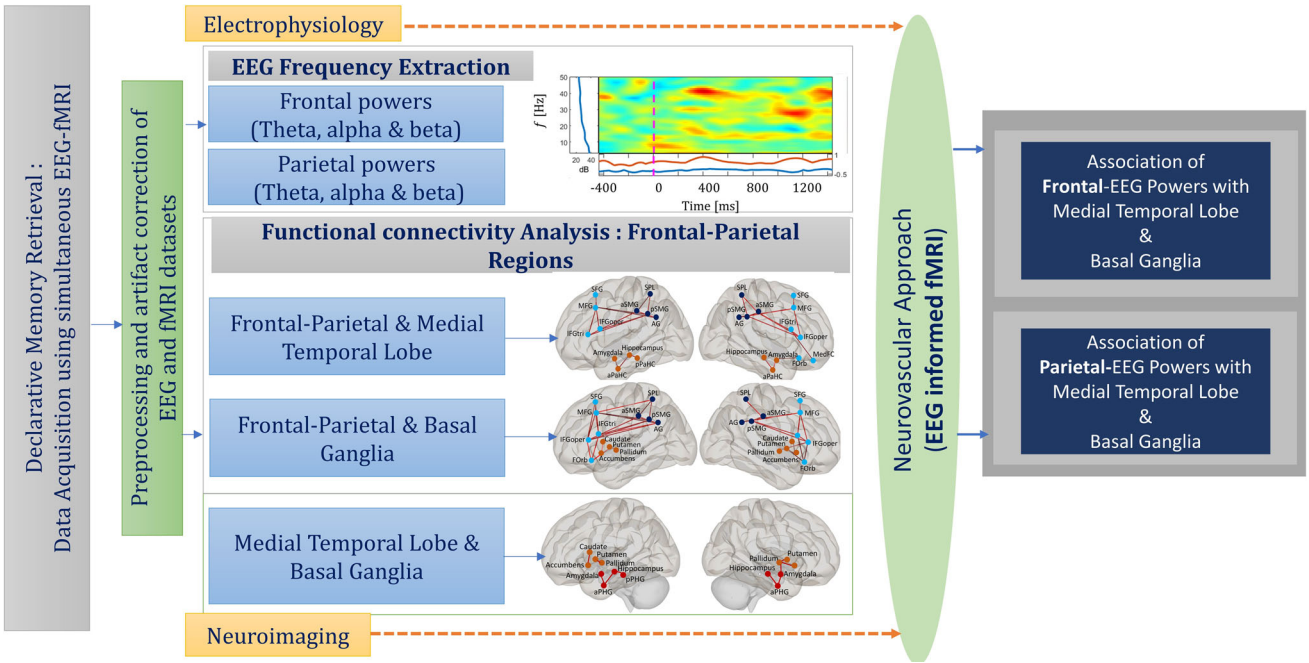

Figure 2. Methodological block diagram of the study. The schematic diagram demonstrates the analyses employed in this study. Using electrophysiology, the frequency extraction of the frontal and parietal EEG channels was done using time–frequency analysis, which was time-locked to the feedback and memory retrievals. Using neuroimaging, we explore the relationship of frontal-parietal regions with medial temporal lobe and subregions of basal ganglia. These interactions are analyzed using functional connectivity analysis for feedback and memory retrievals. Also, the direct relationship of the medial temporal lobe and subregions of basal ganglia associated with the feedback and memory retrievals was analyzed using functional connectivity analysis. Further, the EEG-informed fMRI approach for both feedback and memory retrievals was employed to study the association of frontal-parietal EEG powers with medial temporal lobe and subregions of basal ganglia. For this, the neural correlates of concerned frequencies (delta, theta, lower-alpha, higher-alpha, lower-beta, and higher-beta) and frontal-parietal EEG channels were evaluated using EEG-informed fMRI approach for both feedback and memory retrievals and studied for medial temporal lobe and subregions of basal ganglia.

Thus, results suggest that the introduction of feedback might affect the functional connectivity of these regions.

3.2 *Relationship of the medial temporal lobe and basal ganglia: The functional connectivity analysis*

The results reveal the functional connectivity between MTL and basal ganglia during feedback and memory retrieval (figure 4; table 1) at a significant level ($p<0.001$). The results show the significant correlation for feedback learning (Amygdala- aPHG, $r_{Left}=11.46$, $r_{Right}=13.4$; Putamen-Amygdala: $r_{Left}=5.86$, $r_{Right}=5.26$ and memory retrievals (Amygdala- aPHG, $r_{Left}=5.16$, $r_{Right}=7.21$; Putamen-Amygdala: non-significant). The significant correlation values (Accumbens-Caudate: $r_{Left}=9.46$, $r_{Right}=5.01$; Putamen-Pallidum: $r_{Left}=16.77$, $r_{Right}=10.79$) show the strong relationship of caudate-accumbens and putamen-pallidum throughout the feedback learning. Also, the study observes the modulation in these interactions during memory retrieval and reveals the correlation values (Accumbens-Caudate: $r_{Left}=5.97$; Putamen-Pallidum: $r_{Left}=8.35$, $r_{Right}=5.66$).

Hence, these results suggest that the MTL and the basal ganglia interact during task, and their functional relationship modulates from feedback to memory retrieval.

3.3 *Associations of EEG oscillations and medial temporal lobe: The EEG-informed FMRI approach*

Figure 5 demonstrates the association of frontal EEG powers (delta, theta, lower-alpha, higher-alpha, lower-beta, and higher-beta) in the functioning of the MTL for feedback learning and memory retrievals.

3.3.1 *Feedback learning:* The EEG-informed fMRI results (figure 5) report a positive relationship of

(a) **Frontal-Parietal-Medial Temporal Lobe connectivity**

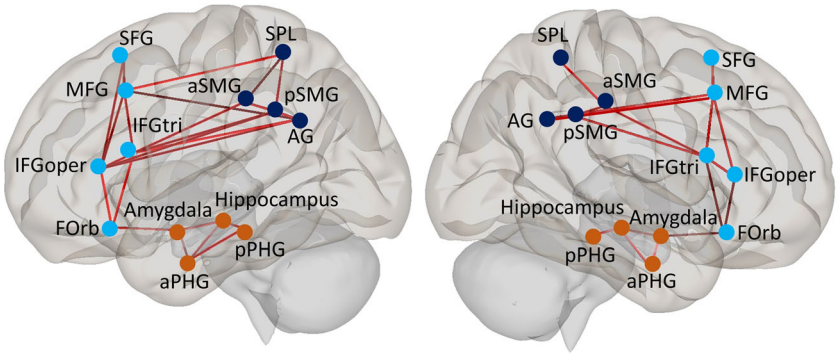

Functional Connectivity maps: Feedback Learning

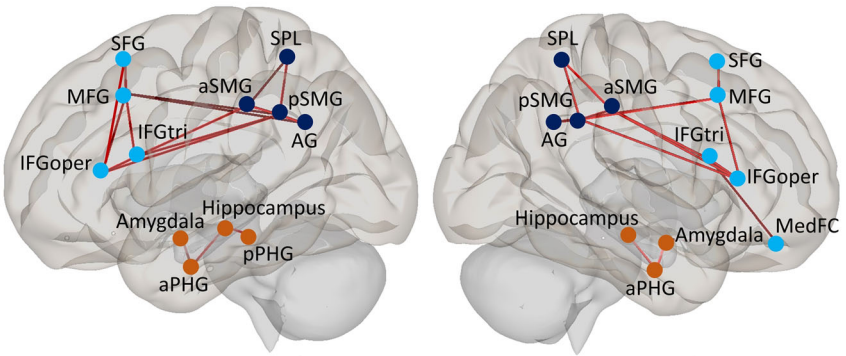

Functional Connectivity maps: Memory Retrieval

(b) **Frontal-Parietal- Basal Ganglia connectivity**

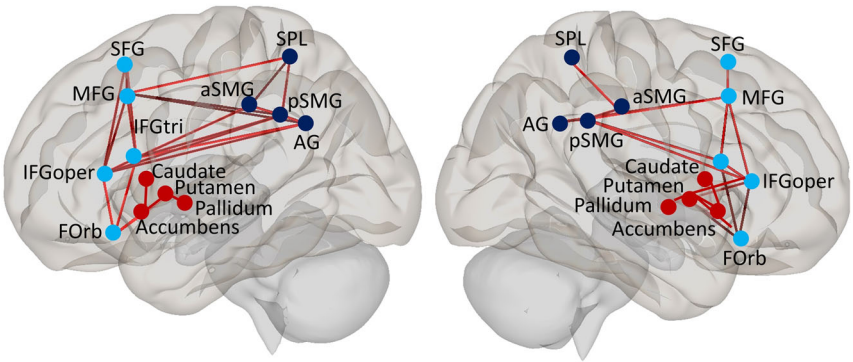

Functional Connectivity maps: Feedback Learning

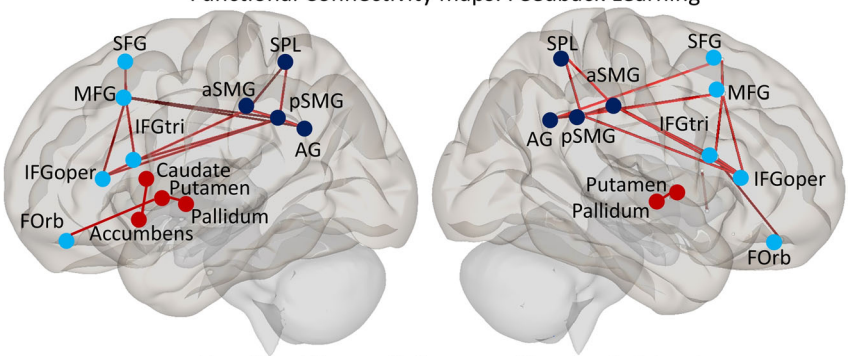

Functional Connectivity maps: Memory Retrieval

◀**Figure 3.** Graphical illustration of functional connectivity of frontal-parietal regions with medial temporal lobe and subregions of basal ganglia. (**a**) Feedback learning. (**b**) Memory retrieval. Azure, indigo, brown and red circles represent frontal, parietal, medial temporal lobe, and basal ganglia, respectively. The significant connectivity among regions is depicted with red lines between nodes. MFG: middle frontal gyrus, IFGOper: inferior frontal gyrus opercular, Forb: frontal orbital cortex, SFG: superior frontal gyrus, IFGtri: inferior frontal gyrus triangular, aSMG: anterior supramarginal gyrus, SPL: superior parietal lobule, pSMG: posterior supramarginal gyrus, AG: angular gyrus, aPHG: anterior parahippocampal gyrus, pPHG: posterior parahippocampal gyrus, MedFC: medial frontal cortex.

frontocentral lower-beta and parietal-delta powers with the bold activity of anterior-para-hippocampal gyrus (aPHG) during feedback learning. We find that the bold activity of the posterior-para-hippocampal gyrus (pPHG) synchronizes with the frontal (lower-alpha, lower-beta) and parietal (theta, delta) EEG powers. The results also observe the pPHG as a negative correlate of parietal higher-beta power. Thus, our study summarizes that frontal lower-beta power enhances the bold activity of aPHG, and combined effect of frontal alpha-beta, parietal theta powers enhances the bold activity of pPHG.

Further, our study finds the enhanced synchronization between frontal powers (lower-beta and delta) and the bold activity of the left amygdala in feedback learning. We also observe that the right amygdala positively associates with frontal-parietal delta power and negatively associates with parietal beta power. Thus, our study reveals that the bold activity of the amygdala enhances due to delta powers and reduce due to beta powers.

3.3.2 *Memory retrieval:* The results (figure 5) reveal that the frontal-theta and parietal-delta powers correlate with the bold activity of aPHG, and the frontocentral higher-beta power anticorrelate with the same. Results suggest that the frontal (higher-beta, delta) and the central-parietal powers (lower-beta, higher-alpha) synchronize with the bold activity of pPHG. Our study also observes the de-synchronization of the bold activity of pPHG, and it is due to the frontal (higher-alpha, lower-alpha, and theta) and parietal-higher-alpha powers. Thus, we suggest that the hemodynamic synchronization of PHG occurs due to frontal EEG powers.

Further, there is a significant association of frontal EEG powers with the bold activity of the left-amygdala. The findings reveal that the bold activity of the left-amygdala synchronizes with lower-beta, theta powers, and de-synchronizes with the higher-alpha power. The study also observes the associations of the frontal-parietal beta powers with the right-amygdala. Thus, we find the enhancement in the bold activity of the amygdala, due to frontal-theta, higher-alpha, and parietal beta powers.

3.4 *Associations of EEG oscillations with basal ganglia*

Figure 6 demonstrates the association of frontal EEG powers (delta, theta, lower-alpha, higher-alpha, lower-beta, and higher-beta) in the functioning of basal ganglia during feedback learning and memory retrievals.

3.4.1 *Feedback learning:* **Caudate:** The study finds a significant role of the caudate in feedback learning such that parietal powers (lower-alpha, higher-alpha, lower-beta, delta) correlate with the left caudate. In specific, parietal-delta power reveal the most significant cluster. The frontal powers (higher-alpha, higher-beta) anti-correlate with the bold activities of the left-caudate. The study also finds the role of the right caudate in feedback learning, and the results report a positive correlation of frontal (theta, delta) and parietal (lower-alpha, delta) powers with its bold activity. Thus, our result highlights the involvement of the caudate in feedback learning and associated EEG powers.

Putamen: The results explain that the frontal theta and parietal delta powers correlate with the bold activity of left putamen and the frontal higher-alpha power anticorrelate with the same. We find the right putamen as a positive correlate of parietal-theta and frontal-parietal lower-alpha powers, and negative correlate of the frontal (higher-alpha, higher-beta) and the parietal lower-beta powers. Thus, our results suggest the involvement of left and right putamen through theta and alpha powers.

Nuclear Accumbens: There is a significant association of frontocentral higher-beta power in the modulation of the bold activity of left accumbens in feedback learning. The study does not find the right accumbens as any of the electrophysiological correlates. Thus, the role of frontocentral higher-beta power suggests an enhancement in the bold activity of left accumbens in feedback learning.

3.4.2 *Memory retrieval:* **Caudate:** Our results emphasize the role of the caudate in declarative

Table 1. Functional connectivity of frontal parietal-MTL–basal ganglia for feedback learning and memory retrieval significant

	Feedback				Memory Retrieval			
Regions	Left Hemisphere		Right Hemisphere		Left Hemisphere		Right Hemisphere	
	T-value	p-value	T-value	p-value	T-value	p-value	T-value	p-value
SFG-IFG Oper	6.03	0.0001	-	-	4.09	0.0083	-	-
SFG-MFG	10.42	<0.0001	10.35	<0.0001	7.2	<0.0001	7.36	<0.0001
MFG-IFG Oper	10.57	<0.0001	8.09	<0.0001	6.73	<0.0001	4.3	0.0054
MFG-SPL	2.94	0.0284	-	-	-	-	-	-
MFG-AG	6	<0.0001	7.21	<0.0001	3.46	0.0293	5.29	0.0008
MFG-IFGTri	9.77	<0.0001	9.64	<0.0001	8.67	<0.0001	-	-
IFG Oper-Forb	6.51	<0.0001	6.14	<0.0001	-	-	-	-
IFG Oper-IFGTri	15.71	<0.0001	13.46	<0.0001	9.54	<0.0001	7.58	<0.0001
IFG Oper-AG	4.2	0.002	-	-	-	-	-	-
IFG Oper-pSMG	5.93	0.0001	3.93	0.0024	5.77	0.0003	3.73	0.0174
IFG Oper-aSMG	6.37	<0.0001	-	-	4.51	0.0036	3.61	0.0223
Forb-Amygdala	4.74	0.0005	6.16	0.0001	-	-	-	-
aSMG-pSMG	13.9	<0.0001	7.52	<0.0001	8.57	<0.0001	7.03	<0.0001
aSMG-SPL	7.49	<0.0001	8.94	<0.0001	6.25	0.0001	6.24	0.0001
pSMG-AG	14.46	<0.0001	15.61	<0.0001	11.17	<0.0001	10.92	<0.0001
Amygdala-Hippocampus	11.45	<0.0001	8.37	<0.0001	4.72	0.0026	4.07	0.0086
Amygdala- aPHG	11.46	<0.0001	13.4	<0.0001	5.16	0.001	7.21	<0.0001
Hippocampus- pPHG	12.41	<0.0001	10.26	<0.0001	5.82	0.0003	3.78	0.016
aPHG-pPHG	7.31	<0.0001	5.53	0.0002	3.34	0.0348	-	-
Forb-Accumbens	3.95	0.0092	3.75	0.0183	-	-	3.44	0.0298
Accumbens-Caudate	9.46	<0.0001	5.01	0.0008	5.97	0.0002	-	-
Accumbens-Putamen	4.42	0.0046	5.11	0.0008	-	-	-	-
Putamen-Pallidum	16.77	<0.0001	10.79	<0.0001	8.35	<0.0001	5.66	0.0003
Forb-Putamen	6.91	<0.0001	6.55	<0.0001	5.48	0.0005	3.32	0.0357
Hippocampus-aPHG	12.17	<0.0001	9.16	<0.0001	7.67	<0.0001	6.17	<0.0001
IFG Oper-Putamen	-	-	5.43	0.0001	-	-	-	-

Non-significant values are highlighted as red. IFG Oper: inferior frontal gyrus pars opercularis, SFG: superior frontal gyrus, MFG: medial frontal gyrus, SPL: superior parietal lobule, AG: angular gyrus, IFGTri: inferior frontal gyrus pars triangularis, FOrb: frontal orbital cortex, pSMG: posterior supramarginal gyrus, aSMG: anterior supramarginal gyrus, aPHG: anterior parahippocampal gyrus, pPHG: posterior parahippocampal gyrus.

Table 2. Functional connectivity of MTL and basal ganglia for feedback learning and memory retrieval

	Feedback				Memory Retrieval			
Regions	Left Hemisphere		Right Hemisphere		Left Hemisphere		Right Hemisphere	
	T-value	p-value	T-value	p-value	T-value	p-value	T-value	p-value
Accumbens-Caudate	9.46	<0.0001	5.01	0.0008	5.97	0.0002	-	-
Putamen-Pallidum	16.77	<0.0001	10.79	<0.0001	8.35	<0.0001	5.66	0.0003
Amygdala- aPHG	11.46	<0.0001	13.4	<0.0001	5.16	0.001	7.21	<0.0001
Hippocampus-aPHG	12.17	<0.0001	9.16	<0.0001	7.67	<0.0001	6.17	<0.0001
Hippocampus- pPHG	12.41	<0.0001	10.26	<0.0001	5.82	0.0003	3.78	0.016
Putamen-Amygdala	5.86	<0.0001	5.26	0.0002	4.44	0.0041	-	-
Amygdala-Hippocampus	11.45	<0.0001	8.37	<0.0001	4.72	0.0026	4.07	0.0086
aPHG-pPHG	7.31	<0.0001	5.53	0.0002	3.34	0.0348	-	-

Non-significant values are highlighted as red.

memory retrieval. In specific, parietal powers (higher-alpha, lower-beta, delta) synchronize and parietal alpha power desynchronizes the bold activity of left caudate. Similarly, we find the associations of parietal powers (higher-alpha, higher-beta, lower-beta) powers in synchronization and frontal powers (lower-alpha, higher-beta) in de-synchronization of the hemodynamic activity of right-caudate. Our study observes that the caudate engages in memory retrieval through an alpha-beta association such that bold activity, enhances through parietal powers and reduces through frontal powers.

Putamen: Our results signify the significant role of the putamen in memory retrieval and reveal the left putamen as a positive correlate of frontal higher-beta and parietal (higher-alpha, beta, delta) powers. The study also observes the negative correlation of frontal (higher-alpha, lower-beta) and parietal (higher-alpha, lower-alpha, and theta) powers with the bold activity of left putamen. Similarly, it finds the engagement of the frontal-parietal higher-beta and parietal lower-beta powers in synchronization with the bold activity of the right putamen. Th study also see a de-synchronization of the bold activity of the same due to frontal-parietal alpha powers. Hence, these results confirm that the frontal-parietal higher-beta power and frontal higher-alpha power enhance the involvement of the putamen in memory retrieval.

Nuclear accumbens: We find that parietal higher-alpha/theta correlates/anticorrelates with the bold activity of the right accumbens. However, the study does not observe any association of EEG powers with the left accumbens during memory retrievals.

4. Discussion

The aim of study is to explore the relationship of frontal-parietal regions with MTL–basal ganglia during feedback learning and declarative memory retrieval. The role of the medial temporal lobe is widely observed in previous studies (Davachi 2006; Squire *et al.* 2004; Tendolkar *et al.* 2008) of declarative memory engagement. The interactions of the MTL with the frontal cortex and the basal ganglia suggest that feedback affects their interaction dynamics and lead towards behavior adjustments (Scimeca and Badre 2012; Preston and Eichenbaum 2013b; Simons and Spiers 2003; Tricomi and Fiez 2008; Walsh and Phillips 2010). In this study, the study investigates the effect of feedback and the role of frontal-parietal EEG spectral powers in the relationship of MTL and basal ganglia for memory retrieval. For this, we first check the functional connectivity of frontal-parietal regions with the MTL and basal ganglia using connectivity analysis. The study then explores the involvement of

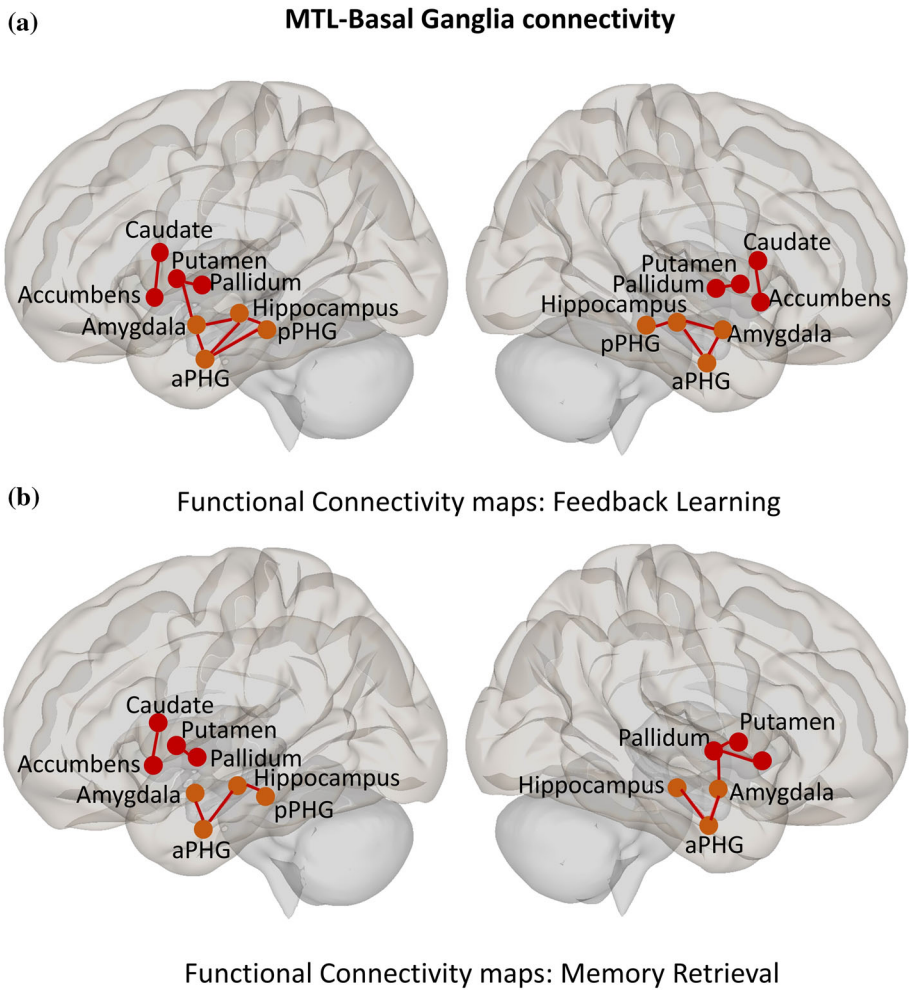

Figure 4. Graphical illustration of functional connectivity of medial temporal lobe with subregions of basal ganglia. (**a**) Feedback learning. (**b**) Memory retrieval. Brown and red circles represent medial temporal and subregions of basal ganglia, respectively. Red lines between nodes depict the significant connectivity among regions.

spectral powers in the feedback related learning and memory retrieval. We discuss all these findings in the following sections in detail.

4.1 *Does the connectivity of MTL, and basal ganglia modulate for memory retrieval from feedback learning?*

The functional interactions analysis reveals the significant functional connectivity of the putamen-pallidum and the caudate-accumbens during the task. In specific, we observe slightly unlike putamen-pallidum dynamics for feedback learning and memory retrievals. The putamen plays a central role during feedback learning and the pallidum in memory retrieval. Our findings are found in line with these earlier neuroimaging studies (Waraczynski and Demco 2006), which suggest the crucial role of pallidum in learning or performing learned responses related to rewards. It has also seen that the reward pathway converges upon ventral pallidum, and this funneling of signals plays a unique role in generating major reward components (Smith *et al.* 2009). However, earlier studies have highlighted the role of putamen in motivational processes (Schultz 2000). Our study finds that the pallidum acknowledges for reward-based responses and interacts with MTL through putamen. There is a vital functional connectivity of the pallidum with the putamen and the MTL for memory retrieval. Yet, the pallidum plays a central role in the interaction between the putamen and MTL, which is different from feedback learning. The modulated dynamics of pallidum and putamen suggest that memory retrieval uses the pallidum as a central hub for performing a declarative memory retrieval by utilizing learned responses and getting motivated.

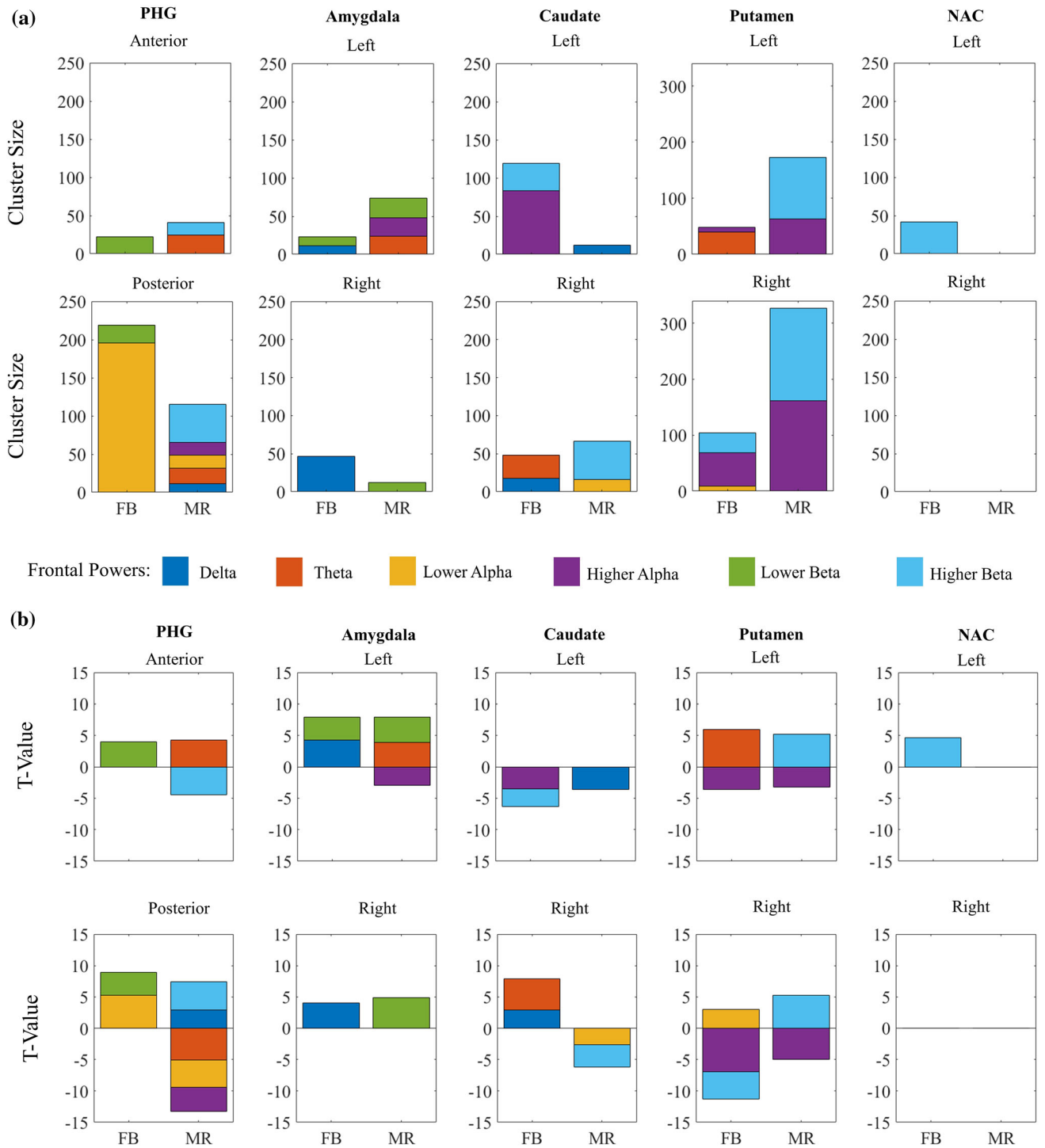

Figure 5. Associations of frontal electrophysiological powers (delta, theta, lower-alpha, higher-alpha, lower-beta, and higher-beta) in the functioning of the medial temporal lobe (Parahippocampal Cortex and Amygdala) and basal ganglia (Caudate, Putamen and Nuclear Accumbens) during feedback learning and memory retrievals. (**a**) Voxel-based distribution. (**b**). Significant T-value based distribution. FB: Feedback learning, MR: Memory retrieval.

Several neuroimaging studies have highlighted the role of the prefrontal cortex in the interaction between MTL and sub-regions of the basal ganglia. It has also been suggested that the prefrontal cortex (PFC) may mediate the functional connectivity between the MTL and the striatum due to the executive control functions of the prefrontal cortex (PFC), which involves the scheduling and optimization of lower-level functions

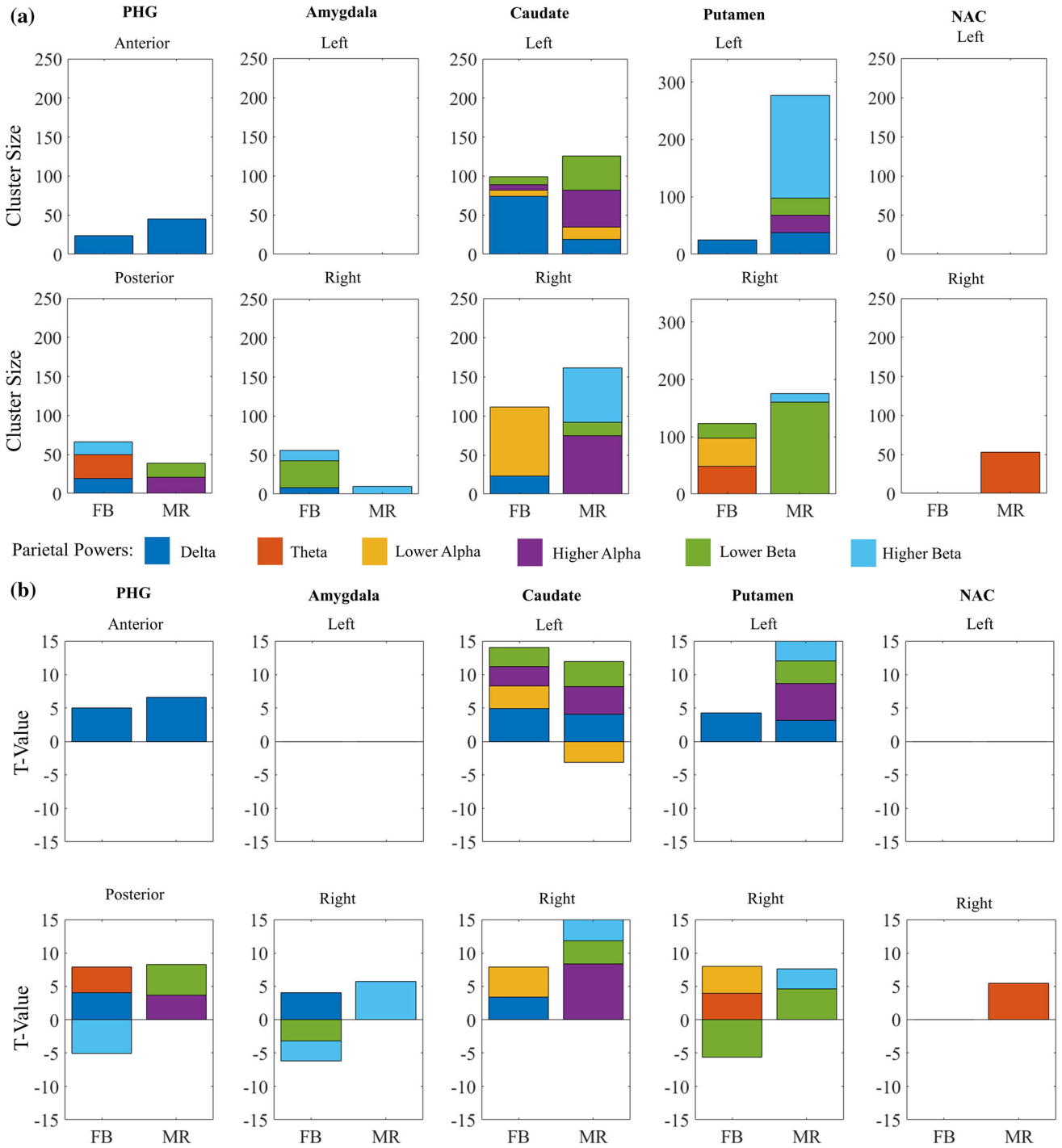

Figure 6. Associations of parietal electrophysiological powers (delta, theta, lower-alpha, higher-alpha, lower-beta, and higher-beta) in the functioning of the medial temporal lobe (Parahippocampal Cortex and Amygdala) and basal ganglia (Caudate, Putamen and Nuclear Accumbens) during feedback learning and memory retrievals. (**a**) Voxel-based distribution. (**b**). Significant T-value based distribution.

implemented in sub-cortical and posterior cortical regions (Miller and Cohen 2001; Poldrack and Rodriguez 2004). We suggest the significant interactions of frontal-parietal EEG powers with MTL and basal ganglia during feedback and memory retrieval.

4.2 *Does memory retrieval dissociate MTL and basal ganglia from frontal-parietal regions?*

Our functional connectivity results demonstrate the significant interactions of frontal-parietal regions with

MTL and basal ganglia during feedback learning. Further, the neurovascular results reveal that the synchronized bold activity of aPHG and pPHG with the frontocentral lower-beta/parietal-delta and frontal alpha-beta/parietal theta powers, respectively. Also, the study finds the bold activity of the left and right amygdala synchronized with the frontal lower-beta/delta and frontal-parietal delta powers. These findings imply the neurovascular relationship of frontal-parietal EEG powers in modulating the bold activity of MTL regions during the learning phase. These results collaborate with the results of several previous electrophysiological studies supporting the role of frontal-beta power in reward-related feedback and successful memory encoding (Cohen *et al.* 2007, 2011; Luft 2014; Marco-Pallares *et al.* 2008; Salari and Rose 2016). Further, the significant increase of theta-power during successful memory encoding is found as a prominent marker of win-associated memory performance (Pu and Yu 2019). The role of the delta band is also revealed during positive mood memory formation (Gärtner and Bajbouj 2013). Thus, our research suggests a significant role of frontal-parietal theta, delta, and lower-beta powers in the modulation of the bold activity of MTL during learning from positive feedback.

Similarly, the interactions of frontal-parietal regions with the basal ganglia during the learning phase reveal the significant functional association of the frontal orbital cortex and inferior frontal gyrus with the sub-regions basal ganglia through accumbens. This finding is consistent with several neuroimaging studies, those have highlighted the role of basal ganglia in learning, such as category learning (D. Shohamy *et al.* 2004a, b, 2008) and habit learning (Ashby *et al.* 2010; Seger and Spiering 2011; Yin and Knowlton 2006). Later, an essential role of the basal ganglia in motivation (Da Cunha *et al.* 2012; Schultz 2016) and decision making (Thibaut 2016) is revealed. Several studies (Camara *et al.* 2009; Frank and Claus 2006; Pasupathy and Miller 2005) have linked the reward-related feedback with the increased functional connectivity of the striatum with the prefrontal cortex. Moreover, a reward study (Hosseini and Holroyd 2015) reported the elicitation of high beta power over the right prefrontal cortex in reward-related feedback stimuli. From our neurovascular results, the bold activity of caudate is found synchronized with the frontal-parietal alpha, parietal beta, parietal delta, and frontal theta powers. Also, the activity of Putamen is found synchronized with the frontal-parietal-theta, frontal-alpha powers, and left accumbens with the frontocentral higher-beta power. Thus, the findings mentioned above reveal the frontal-parietal alpha, beta, and theta powers as a significant cause of frontal-basal ganglia interactions during the learning phase.

However, the interactions between frontal-parietal and MTL regions modulate for memory retrieval from the learning phase. The results affirm the significant functional connectivity between frontal and parietal regions and distinct MTL regions, but no interactions of frontal-parietal with MTL regions. These observations suggest the functional dissociation between MTL and frontal regions. Yet, it is unknown that which mechanism causes the functional dissociation of MTL from frontal-parietal regions. Thus, neurovascular underpinnings are explored, and results show the significant desynchronization of aPHG bold activity due to frontocentral higher-beta and pPHG bold activity due to frontal-alpha-theta and parietal-higher-alpha powers. Also, our study reveals the bold synchronization aPHG due to the combined effect of frontal theta, parietal delta, frontal-higher-beta-delta, and parietal-lower-beta-higher-alpha powers. Further, the bold activity of the left amygdala synchronizes due to frontal-theta, lower-beta powers, and de-synchronizes with frontal-higher-alpha power. Our outcomes highlight the increased role of theta and alpha powers during memory retrieval. Consistent with these observations, a recent study (Herweg *et al.* 2016) provides compelling evidence of binding the hippocampus, PFC, and striatum with the theta and alpha oscillations during successful recollection. However, earlier studies suggest that frontal theta power is a candidate mechanism by which emergent processes such as 'cognitive control' may be biophysically realized (Cavanagh and Frank 2014). Hence, the neurovascular approach demonstrates the essential roles of frontal-alpha-theta powers underlying the functional dissociation of MTL from frontal-parietal regions during memory retrieval from learning phase. Further, memory retrieval reveals a significant dissociation in functional connectivity between basal ganglia and the frontal-parietal regions like the MTL. Yet, the study finds the significant functional connectivity of frontal-parietal regions and the sub-regions of basal ganglia individually. Our findings collaborate with the results of an earlier study (Summerfield and Mangels 2005) that notified the increased frontal-parietal synchrony during recognition memory. The dissociation of basal ganglia with frontal-parietal regions suggests the lack of functional interactions between two during memory retrieval.

5. Conclusion

The study used simultaneous EEG-fMRI to demonstrate the significant associations of frontal-parietal EEG powers with the hemodynamic activity of MTL and basal ganglia to brief feedback learning and declarative memory. The present study provides a novel evidence that frontal-parietal regions associate with MTL–basal ganglia in feedback learning and dissociate in memory retrieval. The modulated relationship highlights the functional role of the Putamen and the pallidum (sub-regions of basal ganglia). The current work converges nicely with the studies implicating the major role of prefrontal cortex in the interactions of MTL–basal ganglia (Guitart-Masip *et al.* 2013; Peters *et al.* 2013; Seger and Miller 2010). Our findings from functional connectivity and neurovascular approach provide evidence that interactions of MTL–basal ganglia during feedback and declarative memory task relies on the mechanism of the frontal-parietal EEG powers. The results reveal the significant modulation in the relationship of frontal-parietal EEG powers with the bold activity of MTL and suggest the enhanced role of frontal-alpha and theta powers during memory retrievals. The frontal-alpha-beta powers desynchronize, and the parietal-alpha-beta powers synchronize the bold activity of the caudate. Also, the parietal theta power significantly de-synchronize and frontal higher-alpha power synchronizes the bold activity of right accumbens. Thus, our findings have important implication for understanding the major role of frontal and parietal EEG powers in feedback associated declarative memory retrieval.

References

Agrawal S, Chinnadurai V, Kaur A, Kumar P, Kaur P, Sharma R and Kumar Singh A 2019 Estimation of functional connectivity modulations during task engagement and their neurovascular underpinnings through hemodynamic reorganization method. *Brain Connect.* **9** 341–355

Allen PJ, Josephs O and Turner R 2000 A method for removing imaging artifact from continuous EEG recorded during functional MRI. *NeuroImage* **12** 230–239

Ally BA, Simons JS, McKeever JD, Peers PV and Budson AE 2008 Parietal contributions to recollection: Electrophysiological evidence from aging and patients with parietal lesions. *Neuropsychologia* **46** 1800–1812

Anderson JR, Byrne D, Fincham JM and Gunn P 2008 Role of prefrontal and parietal cortices in associative learning. *Cereb. Cortex* **18** 904–914

Ashby FG, Turner BO and Horvitz JC 2010 Cortical and basal ganglia contributions to habit learning and automaticity. *Trends Cogn. Sci.* **14** 208–215

Brincat SL and Miller EK 2015 Frequency-specific hippocampal-prefrontal interactions during associative learning. *Nat. Neurosci.* **18** 576–581

Cabeza R 2008 Role of parietal regions in episodic memory retrieval: The dual attentional processes hypothesis. *Neuropsychologia* **46** 1813–1827

Camara E, Rodriguez-Fornells A, Ye Z and Münte TF 2009 Reward networks in the brain as captured by connectivity measures. *Front. Neurosci.* **3** 350–362

Cavanagh JF and Frank MJ 2014 Frontal theta as a mechanism for cognitive control. *Trends Cogn. Sci.* **18** 414–421

Chang LJ, Yarkoni T, Khaw MW and Sanfey AG 2013 Decoding the role of the insula in human cognition: Functional parcellation and large-scale reverse inference. *Cereb. Cortex* **23** 739–749

Christov II 2004 Real time electrocardiogram QRS detection using combined adaptive threshold. *Biomed. Eng. Online* **3** 1–9

Cohen MX, Elger CE and Ranganath C 2007 Reward expectation modulates feedback-related negativity and EEG spectra. *NeuroImage* **35** 968–978

Cohen MX, Elger CE and Weber B 2008 Amygdala tractography predicts functional connectivity and learning during feedback-guided decision-making. *NeuroImage* **39** 1396–1407

Cohen MX, Wilmes K and van de Vijver I 2011 Cortical electrophysiological network dynamics of feedback learning. *Trends Cogn. Sci.* **15** 558–566

Cohen NJ, Poldrack RA and Eichenbaum H 1997 Memory for items and memory for relations in the procedural/declarative memory framework. *Memory* **5** 131–178

Cohn M, Moscovitch M and Davidson PSR 2010 Double dissociation between familiarity and recollection in Parkinson's disease as a function of encoding tasks. *Neuropsychologia* **48** 4142–4147

Da Cunha C, Gomez AA and Blaha CD 2012 The role of the basal ganglia in motivated behaviour. *Rev. Neurosci.* **23** 747–767

Davachi L 2006 Item, context and relational episodic encoding in humans. *Curr. Opin. Neurobiol.* **16** 693–700

de Vanssay-Maigne A, Noulhiane M, Devauchelle AD, Rodrigo S, Baudoin-Chial S, Meder JF, Oppenheim C, Chiron C and Chassoux F 2011 Modulation of encoding and retrieval by recollection and familiarity: Mapping the medial temporal lobe networks. *NeuroImage* **58** 1131–1138

Delorme A and Makeig S 2004 EEGLAB: An open source toolbox for analysis of single-trial EEG dynamics

including independent component analysis. *J. Neurosci. Method.* **134** 9–21

Dobbins IG, Foley H, Schacter DL and Wagner AD 2002 Executive control during episodic retrieval. *Neuron* **35** 989–996

Doñamayor N, Marco-Pallarés J, Heldmann M, Schoenfeld MA and Münte TF 2011 Temporal dynamics of reward processing revealed by magnetoencephalography. *Hum. Brain Map.* **32** 2228–2240

Eichenbaum H, Yonelinas AP and Ranganath C 2007 The medial temporal lobe and recognition memory. *Annu. Rev. Neurosci.* **30** 123–152

Euston DR, Gruber AJ and McNaughton BL 2012 The role of medial prefrontal cortex in memory and decision making. *Neuron* **76** 1057–1070

Fell J, Ludowig E, Staresina BP, Wagner T, Kranz T, Elger CE and Axmacher N 2011 Medial temporal theta/alpha power enhancement precedes successful memory encoding: Evidence based on intracranial EEG. *J. Neurosci.* **31** 5392–5397

Frank MJ and Claus ED 2006 Anatomy of a decision: Striato-orbitofrontal interactions in reinforcement learning, decision making and reversal. *Psychol. Rev.* **113** 300–326

Freedberg M, Toader AC, Wassermann EM and Voss JL 2020 Competitive and cooperative interactions between medial temporal and striatal learning systems. *Neuropsychologia* **136** 107257

Gabard-Durnam LJ, Leal ASM, Wilkinson CL and Levin AR 2018 The harvard automated processing pipeline for electroencephalography (HAPPE): Standardized processing software for developmental and high-artifact data. *Front. Neurosci.* **12** 1–24

Gärtner M and Bajbouj M 2013 Encoding-related EEG oscillations during memory formation are modulated by mood state. *Soc. Cogn. Affect. Neurosci.* **9** 1934–1941

Gerraty RT, Davidow JY, Wimmer GE, Kahn I and Shohamy D 2014 Transfer of learning relates to intrinsic connectivity between hippocampus, ventromedial prefrontal cortex and large-scale networks. *J. Neurosci.* **34** 11297–11303

Guitart-Masip M, Barnes GR, Horner A, Bauer M, Dolan RJ and Duzel E 2013 Synchronization of medial temporal lobe and prefrontal rhythms in human decision making. *J. Neurosci.* **33** 442–451

Haber SN and Knutson B 2010 The reward circuit: Linking primate anatomy and human imaging. *Neuropsychopharmacology* **35** 4–26

Han S, Huettel SA, Raposo A, Adcock RA and Dobbins IG 2010 Functional significance of striatal responses during episodic decisions: Recovery or goal attainment? *J. Neurosci.* **30** 4767–4775

Hattie J and Timperley H 2007 The power of feedback. *Rev. Edu. Res.* **77** 81–112

Herweg NA, Apitz T, Leicht G, Mulert C, Fuentemilla L and Bunzeck N 2016 Theta-alpha oscillations bind the hippocampus, prefrontal cortex and striatum during recollection: Evidence from simultaneous EEG–fMRI. *J. Neurosci.* **36** 3579–3587

Hosseini AH and Holroyd CB 2015 Reward feedback stimuli elicit high-beta EEG oscillations in human dorsolateral prefrontal cortex. *Sci. Rep.* **5** 1–8

Kim KH, Yoon HW and Park HW 2004 Improved ballistocardiac artifact removal from the electroencephalogram recorded in fMRI. *J. Neurosci. Method.* **135** 193–203

Knowlton BJ, Mangels JA and Squire LR 1996 A neostriatal habit learning system in humans. *Science* **273** 1399–1402

Knudsen EB and Wallis JD 2020 Closed-Loop Theta Stimulation in the Orbitofrontal Cortex Prevents Reward-Based Learning. *Neuron* **106** 537-547.e4

Lee W and Reeve J 2013 Self-determined, but not non-self-determined, motivation predicts activations in the anterior insular cortex: An fMRI study of personal agency. *Soc. Cogn. Affect. Neurosci.* **8** 538–545

Luft CDB 2014 Learning from feedback: The neural mechanisms of feedback processing facilitating better performance. *Behav. Brain Res.* **261** 356–368

Maia TV 2009 Fear conditioning and social groups: Statistics, not genetics. *Cog. Sci.* **33** 1232–1251

Marco-Pallares J, Cucurell D, Cunillera T, García R and andrés-Pueyo A, Münte TF and Rodríguez-Fornells A, 2008 Human oscillatory activity associated to reward processing in a gambling task. *Neuropsychologia* **46** 241–248

Miller EK and Cohen JD 2001 An integrate theory of PFC function. *Annu. Rev. Neurosci.* **24** 167–202

Moustafa AA and Gluck MA 2011 Computational cognitive models of prefrontal-striatal-hippocampal interactions in Parkinson's disease and schizophrenia. *Neural Networks* **24** 575–591

Packard MG, White M and Ha Q 1989 Differential effects of fornix and caudate radial maze tasks: evidence for multiple nucleus lesions on two memory systems. *J. Neurosci.* **9** 1465–1472

Pasupathy A and Miller EK 2005 Different time courses of learning-related activity in the prefrontal cortex and striatum. *Nature* **433** 873–876

Peters GJ, David CN, Marcus MD and Smith DM 2013 The medial prefrontal cortex is critical for memory retrieval and resolving interference. *Learn. Mem.* **20** 201–209

Poldrack RA and Rodriguez P 2004 How do memory systems interact? Evidence from human classification learning. *Neurobiol. Learn. Mem.* **82** 324–332

Preston AR and Eichenbaum H 2013a Interplay of hippocampus and prefrontal cortex in memory. *Curr. Biol.* **23** R764–R773

Preston AR and Eichenbaum H 2013b Interplay of hippocampus and prefrontal cortex in memory. *Curr. Biol.* **23** 1–21

Pu M and Yu R 2019 Post-encoding frontal theta activity predicts incidental memory in the reward context. *Neurobiol. Learn. Mem.* **158** 14–23

Ridderinkhof KR, Van Den Wildenberg WPM, Segalowitz SJ and Carter CS 2004 Neurocognitive mechanisms of cognitive control: The role of prefrontal cortex in action selection, response inhibition, performance monitoring and reward-based learning. *Brain Cogn.* **56** 129–140

Rushworth MFS, Noonan MAP, Boorman ED, Walton ME and Behrens TE 2011 Frontal Cortex and Reward-Guided Learning and Decision-Making. *Neuron* **70** 1054–1069

Salari N and Rose M 2016 Dissociation of the functional relevance of different pre-stimulus oscillatory activity for memory formation. *NeuroImage* **125** 1013–1021

Schultz W 2000 Multiple reward signals in the brain. *Nat. Rev. Neurosci.* **1** 199–207

Schultz W 2016 Reward functions of the basal ganglia. *J. Neural Transm.* **123** 679–693

Scimeca JM and Badre D 2012 Striatal contributions to declarative memory retrieval. *Neuron* **75** 380–392

Seger CA and Cincotta CM 2006 Dynamics of frontal, striatal and hippocampal systems during rule learning. *Cereb. Cortex* **16** 1546–1555

Seger CA and Miller EK 2010 Category learning in the brain. *Annu. Rev. Neurosci.* **33** 203–219

Seger CA and Spiering BJ 2011 A critical review of habit learning and the basal ganglia. *Front. Syst. Neurosci.* **5** 1–9

Shohamy D, Myers CE, Kalanithi J and Gluck MA 2008 Basal ganglia and dopamine contributions to probabilistic category learning. *Neurosci. Biobehav. Rev.* **32** 219–236

Shohamy D, Myers CE, Onlaor S and Gluck MA 2004a Role of the basal ganglia in category learning: How do patients with Parkinson's disease learn? *Behav. Neurosci.* **118** 676–686

Shohamy Daphna and Adcock RA 2010 Dopamine and adaptive memory. *Trends Cogn. Sci.* **14** 464–472

Shohamy Daphna, Myers CE, Grossman S, Sage J, Gluck MA and Poldrack RA 2004b Cortico-striatal contributions to feedback-based learning: Converging data from neuroimaging and neuropsychology. *Brain* **127** 851–859

Simons JS and Spiers HJ 2003 Prefrontal and medial temporal lobe interactions in long-term memory. *Nat. Rev. Neurosci.* **4** 637–648

Smith KS, Tindell AJ, Aldridge JW and Berridge KC 2009 Ventral pallidum roles in reward and motivation. *Behav. Brain Res.* **196** 155–167

Squire LR, Stark CEL and Clark RE 2004 the Medial Temporal Lobe. *Annu. Rev. Neurosci.* **27** 279–306

Summerfield C and Mangels JA 2005 Functional coupling between frontal and parietal lobes during recognition memory. *NeuroReport* **16** 117–122

Tendolkar I, Arnold J, Petersson KM, Weis S, Brockhaus-Dumke A, Van Eijndhoven P, Buitelaar J and Fernández G 2008 Contributions of the medial temporal lobe to declarative memory retrieval: Manipulating the amount of contextual retrieval. *Learn. Mem.* **15** 611–617

Thibaut F 2016 Basal ganglia play a crucial role in decision making. *Dialog. Clin. Neurosci.* **18** 3

Thürer B, Stockinger C, Putze F, Schultz T and Stein T 2017 Mechanisms within the parietal cortex correlate with the benefits of random practice in motor adaptation. *Front. Hum. Neurosci.* **11** 1–11

Tricomi E and Fiez JA 2008 Feedback signals in the caudate reflect goal achievement on a declarative memory task. *NeuroImage* **41** 1154–1167

Tricomi E and Fiez JA 2012 Information content and reward processing in the human striatum during performance of a declarative memory task. *Cogn. Affect. Behav. Neurosci.* **12** 361–372

van de Vijver I, Richard Ridderinkhof K and Cohen MX 2011 Frontal oscillatory dynamics predict feedback learning and action adjustment. *J. Cogn. Neurosci.* **23** 4106–4121

Wagner AD, Shannon BJ, Kahn I and Buckner RL 2005 Parietal lobe contributions to episodic memory retrieval. *Trends Cogn. Sci.* **9** 445–453

Walsh ND and Phillips ML 2010 Interacting outcome retrieval, anticipation and feedback processes in the human brain. *Cereb. Cortex* **20** 271–281

Waraczynski M and Demco C 2006 Lidocaine inactivation of the ventral pallidum affects responding for brain stimulation reward more than it affects the stimulation's reward value. *Behav. Brain Res.* **173** 288–298

Whitfield-Gabrieli S and Nieto-Castanon A 2012 Conn: A functional connectivity toolbox for correlated and anti-correlated brain networks. *Brain Connect.* **2** 125–141 Yin HH and Knowlton BJ 2006 The role of the basal ganglia in habit formation. *Nature Rev. Neurosci.* **7** 464–476

Yin HH and Knowlton BJ 2006 The role of the basal ganglia in habit formation. *Nature Rev. Neurosci.* **7** 464–476

corresponding editor: Aurnab Ghose

Agrawal *et al. Brain Informatics* (2022) 9:25
https://doi.org/10.1186/s40708-022-00173-5

Brain Informatics

RESEARCH

Open Access

Hemodynamic functional connectivity optimization of frequency EEG microstates enables attention LSTM framework to classify distinct temporal cortical communications of different cognitive tasks

Swati Agrawal[1,2], Vijayakumar Chinnadurai[1*] and Rinku Sharma[2]

Abstract

Temporal analysis of global cortical communication of cognitive tasks in coarse EEG information is still challenging due to the underlying complex neural mechanisms. This study proposes an attention-based time-series deep learning framework that processes fMRI functional connectivity optimized quasi-stable frequency microstates for classifying distinct temporal cortical communications of the cognitive task. Seventy volunteers were subjected to visual target detection tasks, and their electroencephalogram (EEG) and functional MRI (fMRI) were acquired simultaneously. At first, the acquired EEG information was preprocessed and bandpass to delta, theta, alpha, beta, and gamma bands and then subjected to quasi-stable frequency-microstate estimation. Subsequently, time-series elicitation of each frequency microstates is optimized with graph theory measures of simultaneously eliciting fMRI functional connectivity between frontal, parietal, and temporal cortices. The distinct neural mechanisms associated with each optimized frequency-microstate were analyzed using microstate-informed fMRI. Finally, these optimized, quasi-stable frequency microstates were employed to train and validate the attention-based Long Short-Term Memory (LSTM) time-series architecture for classifying distinct temporal cortical communications of the target from other cognitive tasks. The temporal, sliding input sampling windows were chosen between 180 to 750 ms/segment based on the stability of transition probabilities of the optimized microstates. The results revealed 12 distinct frequency microstates capable of deciphering target detections' temporal cortical communications from other task engagements. Particularly, fMRI functional connectivity measures of target engagement were observed significantly correlated with the right-diagonal delta ($r = 0.31$), anterior–posterior theta ($r = 0.35$), left–right theta ($r = -0.32$), alpha ($r = -0.31$) microstates. Further, neuro-vascular information of microstate-informed fMRI analysis revealed the association of delta/theta and alpha/beta microstates with cortical communications and local neural processing, respectively. The classification accuracies of the attention-based LSTM were higher than the traditional LSTM architectures, particularly the frameworks that sampled the EEG data with a temporal width of 300 ms/segment. In conclusion, the study demonstrates reliable temporal classifications of global cortical communication of distinct tasks using an attention-based LSTM utilizing fMRI functional connectivity optimized quasi-stable frequency microstates.

*Correspondence: vijayakumar.inmas@gov.in; vijayafmc@gmail.com

[1] Institute of Nuclear Medicine and Allied Sciences, Lucknow Road, Timarpur, Delhi 110054, India
Full list of author information is available at the end of the article

Springer Open

© The Author(s) 2022. **Open Access** This article is licensed under a Creative Commons Attribution 4.0 International License, which permits use, sharing, adaptation, distribution and reproduction in any medium or format, as long as you give appropriate credit to the original author(s) and the source, provide a link to the Creative Commons licence, and indicate if changes were made. The images or other third party material in this article are included in the article's Creative Commons licence, unless indicated otherwise in a credit line to the material. If material is not included in the article's Creative Commons licence and your intended use is not permitted by statutory regulation or exceeds the permitted use, you will need to obtain permission directly from the copyright holder. To view a copy of this licence, visit http://creativecommons.org/licenses/by/4.0/.

Keywords: Attention-based deep learning, Frequency-microstates, Hemodynamic functional connectivity, EEG-informed fMRI. Multifrequency coupling, Target detection

1 Introduction

1.1 Decoding distant cortical communications from cortical EEG

The human brain dynamically engages distinct neural populations between distant brain regions, and their spatiotemporal oscillations often modulate systematically with behavioral and cognitive tasks. The synchrony or lack thereof between remote brain regions brings effective global brain communication, functional connectivity for information processing. Many researchers [25, 31, 35] employed simultaneous EEG information acquired with fMRI imaging to understand these functional connectivities, neural origins, and correlated brain states. These researches revealed that the elicitation of local neural systems is observed as high-frequency dynamics in EEG cortical oscillations. Cortical high-frequency gamma oscillation mainly explains local high-level neural information and positively correlates with the fMRI BOLD strength. Further, the distant cortical and long-range coordination emerges as the lower EEG cortical frequency oscillation [9]. The alpha and beta power modulate the BOLD response's latency and strength to gamma power changes [34]. Many researchers [2, 22, 40] have recently observed multi-frequency cortical EEG interaction explaining hemodynamic task elicitation better than single EEG power information. JC Pang et al. [44] revealed that the inverse correlation of alpha and BOLD originates from high- and low-frequency components of the same underlying neural engagement caused by modulation in corticothalamic and intra-thalamic feedback. Despite these clear insights of distinct global and local neural processing associated with every task engagement, decoding their temporal dynamics computationally from spatially coarse-grained cortical times-series EEG information is still challenging.

1.2 Microstates and global cortical communication

Microstates are the cluster centers of EEG information and are unique in every cognitive task engagement in healthy and disease populations. Every microstate topography is associated with a "quasi-stable" functional state [16, 36], explaining the brain's specific neural interaction. These quasi-stable patterns span around 100 ms and are the most robust approach to bringing distant functional communication in cortical EEG information. Many researchers [24, 64] observed that the time course of microstate metrics, when correlated with the fMRI BOLD signal, reveals functional networks similar to the resting-state networks. Further, the microstate dynamics are observed to measure transitions between global cortical communications characterized by specific local neural alpha inhibitions [12, 23, 38, 56]. The traditional microstate estimation employs the EEG frequency range [30, 45] of 2–20 Hz. Hence, their time-series dynamics are primarily influenced by the cortical alpha inhibitory/excitatory modulations [37]. However, the cognitive task engagement's distant and local cortical communication manifests through other EEG rhythms [18, 49]. Thus, the task-induced modulation of cortical communication and associated local neural engagement is manifested as a combination of different frequencies [4]. More recently, the beta-band and the coverage feature of the EEG microstate analysis have been revealed as the essential features for classifying epilepsy and PNES patients with reasonably high accuracy and precision [3].

1.3 Deep learning approaches for temporal EEG analysis

The EEG time-series information is higher-dimensional, and the cognitive information is spread across its timelines. Hence, the feature information derived from a single time point of EEG time-series data is inadequate to explain any cognitive process. Thus, Recurrent Neural networks (RNN) perform better in extracting sequential information embedded in higher dimensional EEG time-series information. However, the traditional RNN system suffers in learning long-term dynamics due to vanishing/exploding gradient problems. Long Short-Term Memory (LSTM) architecture addresses this exploding gradient obstacle by learning both long- and short-term dependencies. Recently, the attention mechanism has been introduced [55] to improve the performance of deep learning models; it highlights the more informative feature and subsequently gives higher weights to the corresponding original feature sequence. It has been embedded with the LSTM architecture in several EEG studies [21, 28, 48, 61, 62, 66, 67] by effectively selecting the feature information and observed with significantly improved efficiency and performance accuracy of deep learning systems.

1.4 Present study

The present study proposes an attention-based LSTM computational model that employs optimized frequency microstates to decipher the distant cortical communication of visual target detection tasks. The temporal dynamics of the frequency microstate metrics are correlated with fMRI hemodynamic functional connectivity

measures to optimize the cortical EEG quasi-stable frequency patterns with the task's local/global brain communication. The hemodynamic functional connectivity is assessed by employing the graph-theoretical analysis on simultaneously acquired fMRI information. The significantly correlated frequency microstates are further subjected to the robust correlation analysis to understand their multi-frequency coupling elicited during intercortical interaction during the task engagement. The local and global neural mechanisms underlying these frequency quasi-stable microstates were further estimated through EEG-informed fMRI analysis. Finally, a hybrid deep learning framework consisting of LSTM with an attention mechanism is employed to classify the target detection task engagement from the temporal dynamics of these optimized frequency microstate quasi-stable patterns. The performance metrics such as precision, accuracy, and recall are estimated for all deep learning architectures and validated using a tenfold cross-validation approach.

2 Methods and materials

2.1 Participants and task design

Seventy healthy right-handed volunteers (30 males and 40 females; mean age: 23 years; age range, 20–32 years) were selected from the academic environment. All participants gave written informed consent and did not have psychiatric or neurological disorders or medication. The experiment was conducted following the World Medical Association (Declaration of Helsinki), and the local ethical committee approved all measurements. The vision of participants was corrected using MR-compatible lenses whenever required.

These participants underwent the task paradigm (Fig. 1) designed to perform three tasks. They are target detection, distractor detection, and fixation identification. For this purpose, the multiple distinct shapes (squares, circles, stars, and triangles) with primary colors (experimental conditions, stimuli) were shown at the beginning (called 'Targets stimulus'). Then volunteers were sequentially shown a single stimulus, one at a time, and asked whether it was part of earlier displayed target stimuli collections. The volunteer must click the right thumb button whenever he identifies the target stimulus. Only 30 percent of stimuli were selected from earlier displayed stimuli, the targets, and randomly distributed among the "Distractor Stimulus". The correct identification of the target stimulus invokes the elicitation of distinct neural mechanisms compared to the identification of distractors. Each sequential stimulus was presented for the duration of 3000 ms. The paradigm consisted of five trials. Each trial started with a different target stimuli collection, and 105 single stimuli were subsequently presented for target/distractor identification. Among 105 stimuli, only 32 were target stimuli and presented randomly. A fixation stimulus followed each stimulus; a single black-colored cross in the slide's center was presented for 3 s. These task

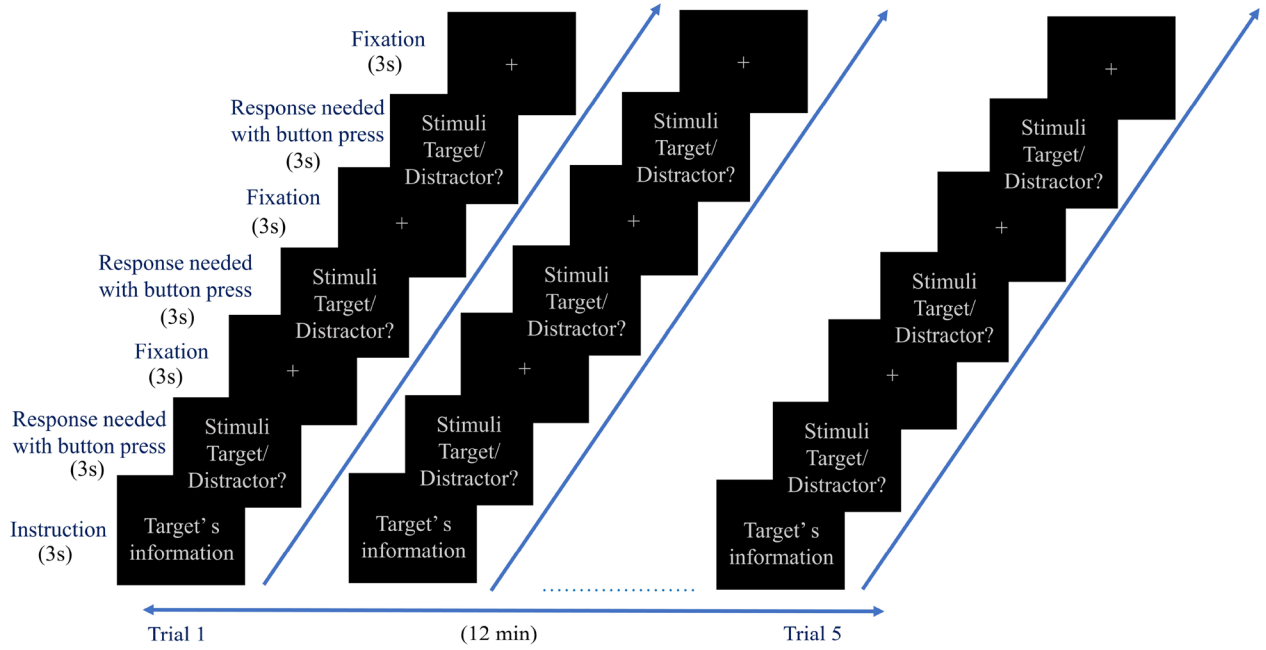

Fig. 1 Schematic of task paradigm design

stimuli are projected onto MR-compatible lenses fitted on the head coil inside MRI.

2.2 Simultaneous EEG–fMRI acquisition and preprocessing

In the present study, simultaneous EEG–fMRI data acquisition is carried out using a 3T Siemens Magnetom Skyra scanner (Siemens, Erlangen) and MR-compatible 32-channel Brain Amp system with an EEG cap. EEG signals are recorded at a sampling rate of 5 kHz, and the impedance of all scalp electrodes is maintained below five kOhms throughout the recording. The fMRI were acquired using Eco Planar Imaging (EPI) sequence with TR = 3000 ms; TE = 36 ms; voxel size = 3.6*3.6*3.0 mm; matrix = 64*64; FoV read = 230 mm; flip angle = 90°, 36 axial slices. The axial slices are acquired parallel to the anterior–posterior (AC–PC) line in an interleaving manner with a slice thickness of 3.0 mm. The high-resolution structural images of the brain are acquired using T1 MPRAGE sequence with parameters, voxel size = 1.0*1.0*1.0 mm; TR = 2000 ms; flip angle = 90°; FoV = 240 mm; matrix = 512*512; slice thickness = 1.0 mm, 160 axial slices. The axial slices are acquired parallel to the anterior–posterior (AC–PC) line in an interleaving manner with a slice thickness of 5.0 mm.

EEG data acquired simultaneously inside the MRI scanner are initially subjected to the FMRIB plugin of EEGLAB to remove the MRI-related artifacts such as gradient switching and cardio ballistic artifacts. The gradient artifact removal process employed FASTR (FMRI Artifact Slice Template Removal) tool [20, 42]. It aligned all the artifact slices to correct any slight jitter in the exact location of the slice-timing events, interpolating and shifting each artifact until the correlation was maximized between data and a reference artifact (the first artifact in the data). The second stage of FASTR [5] computed an average template for the cardio ballistic artifact. It subtracted this template from the center contaminated data by taking a moving window average of slice artifacts. QRS detection utilizes combined adaptive thresholding [11] and the Teager energy operator [27], followed by a correction algorithm to detect heartbeats robustly for false positives and negatives and remove the pulse artifacts by using an optimal basis set for the number of PCs 3.

Further, Harvard Automated Processing Pipeline (HAPPE) [14] is employed for noise-free time–frequency analyses using EEGLAB (MathWorks). MR and CB artifact corrected EEG data are subjected to the 0.1 Hz high-pass and 57 Hz low-pass filtering followed by ICA decomposition using all the EEG channels. The electrical noise is removed using the Clean Line program (Mullen, 2012) through the multi-taper regression approach implemented in EEGLAB. The bad channels are identified by evaluating the normed joint probability of the average log power of all the selected channels and removed for the probability of more than three standard deviations from the mean for further analyses. A wavelet-enhanced ICA (W-ICA) approach removes eye and muscle-generated artifacts, high-amplitude artifacts, and signal discontinuities from EEG data. This approach of W-ICA followed by ICA improves the resulting ICA decomposition of the EEG data [63]. A machine-learning algorithm MARA (Multiple Artifact Rejection Algorithm) [59] evaluates the ICA-derived components for automated component rejection for artifact probabilities greater than 0.5.

Further, artifact rejected data are segmented based on event markers. The artifact-corrected datasets were subsequently downsampled to 250 Hz and re-referenced to the common average reference and bandpass filtered from 1 to 48 Hz ((1–4) Hz for delta, (4–8) Hz for theta, (9–14) Hz for an alpha, (15–35) Hz for beta and (35–48) Hz for gamma)). Finally, all the participants' artifact corrected data are then segregated specific to the target, distractor, and fixation blocks. Further, simultaneously acquired fMRI data are preprocessed using Statistical Parametric Mapping version 12. The information is corrected for slice-timing differences, spatially realigned, and excluded if movement exceeds 3 mm. It follows by registering the functional scans to standard MNI template space. Further, artifact-corrected images are subjected to spatially smoothing with a 5*5*5 mm full-width half-maximum Gaussian kernel.

2.3 Estimation of frequency-microstates and their optimization with task's cortical communications

The present study develops a computational framework that classifies distinct task engagement's temporal global cortical communication through unique temporal EEG quasi-stable information that decodes the neural basis of the distant cortical communications. Figure 2 explains these processes in detail. The following section will elaborate on each one of these steps in detail.

At first, artifact-corrected EEG data are bandpass filtered to segregate it into frequency-band limited data comprising (1–4) Hz for delta, (4–8) Hz for theta, (9–14) Hz for an alpha, (15–35) Hz for beta and (35–48) Hz for gamma. Then, each frequency information's Global Field Power (GFP) is computed and subjected to the modified K-means clustering algorithm [46] to identify every frequency-microstate topographic prototype. A detailed description of this estimation is given in Additional file 1: Section S1. Then, each frequency-microstate prototype is back fitted in every individual's data and estimated re-expressed sequences of microstate classes. Finally, statistics about the sequence of microstate classes, such as

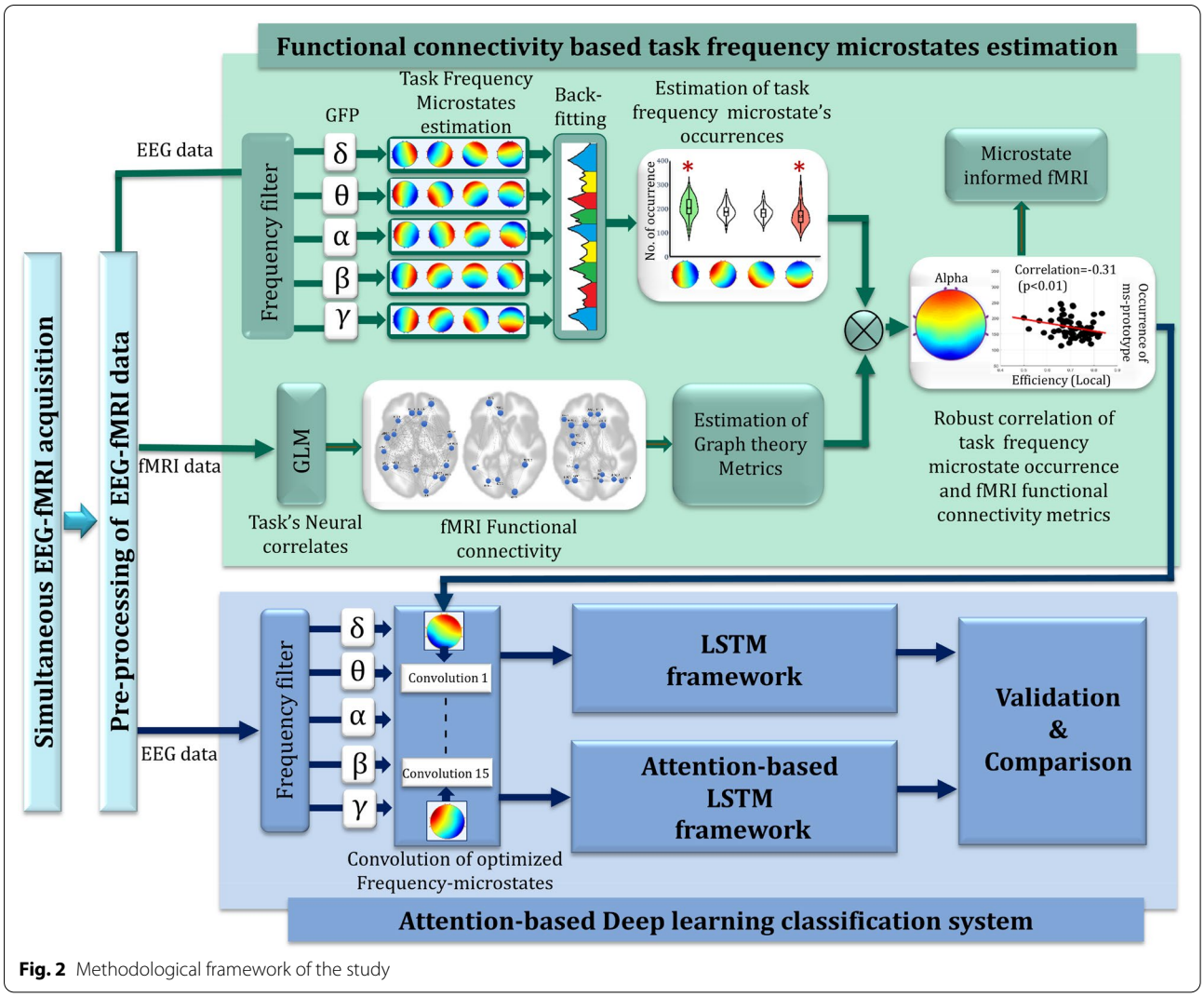

Fig. 2 Methodological framework of the study

their frequency of occurrence or average duration, are calculated. This quasi-stable frequency-microstate patterns elicitation information is subsequently mapped with global functional connectivity of each task engagement assessed from simultaneously acquired fMRI information.

Simultaneously, the task's neural sources are identified from simultaneously acquired fMRI information employing the General Linear Model-based (GLM) analysis. At the subject level analysis, BOLD responses of each task engagement (target, distractor, and fixation) are modeled by a canonical hemodynamic response function with temporal and dispersion derivatives with six realignment parameters for each run. In second-level GLM modeling, group average maps were computed using one-sample t-tests, cluster corrected ($p < 0.05$) across subjects. Subsequently, the second-level GLM model results for every task engagement are passed as regions of interest (ROI) to graph theory analysis to estimate the global/local functional connectivity [58]. A detailed description of this estimation is given in the Additional file 1: Section S2. Finally, the graph theory metrics such as global and local efficiency of the functionally connected regions are estimated for each subject, and the ROI-to-ROI connectivity matrix is thresholded at p-FDR < 0.05 in a two-sided analysis.

Finally, these tasks' global cortical communications information estimated from fMRI graph theoretical measures are utilized to optimize and identify the relevant cortical quasi-stable frequency EEG elicitations that correspond to the task engagement. For this purpose, the number of occurrences of each delta, theta, alpha, beta, and gamma EEG microstates of every individual during task engagements (target, distractor, and fixation) is subjected to the robust correlation with global functional connectivities metrics measured from the simultaneously

measured fMRI information. This study further validated these significantly correlating frequency-microstates by subjecting them to the EEG-informed fMRI analysis [1, 19] and studying their neural mechanisms. Since the frequency microstates that correlate with fMRI functional connectivity metrics are different for target, distractor, and fixation, three separate EEG-informed fMRI models were constructed for every task engagement. A detailed description of this estimation is given in the Additional file 1: Section S3.

2.4 Attention-based LSTM model and validation

This study aims to develop an attention-based LSTM framework to classify the global cortical communication (estimated using fMRI functional connectivity optimized frequency quasi-stable oscillations) associated with global brain communications. For this purpose, each frequency-microstate strongly associated with fMRI functional connectivity measures was correlated with every individual preprocessed EEG information. Then, the feature vector consisting of the correlation value for each quasi-stable frequency microstates belonging to every task engagement is formed and used as a training, testing, and validation dataset for the attention-based LSTM deep learning model. The attention-based LSTM model employed in this study is illustrated in Fig. 3.

LSTM has been a popular recurrent neural network for learning sequential features in time-series data and classifying EEG information [41, 57]. However, the standard LSTM is incapable of detecting important parts for classification. The attention mechanism is recently conceptualized [55] and integrated with the LSTM framework to overcome this issue. The attention mechanism improves the ability of LSTM by concentrating on time fragments with the most discriminative information in EEG time-series. It helps to classify the data that involve remembering and aggregating feature embeddings in time-series information [65]. A detailed description of the LSTM model and attention mechanism is explained below.

The LSTM architecture consists of interconnected cells that hold the memory information through which the input data are processed to evaluate the output results. The cells have a common cell state, keeping long-term dependencies along the entire LSTM chain of cells. In LSTM, input information flow is controlled by the input gate (i_t) and forget gate (f_t) and allows the network to decide whether to forget the previous state (C_{t-1}) or update the current state (C_t) with new information. Further, each cell's result is modulated by an output gate (o_t), which lets the cell compute its output based on the updated information. The function of LSTM cell architecture is calculated as:

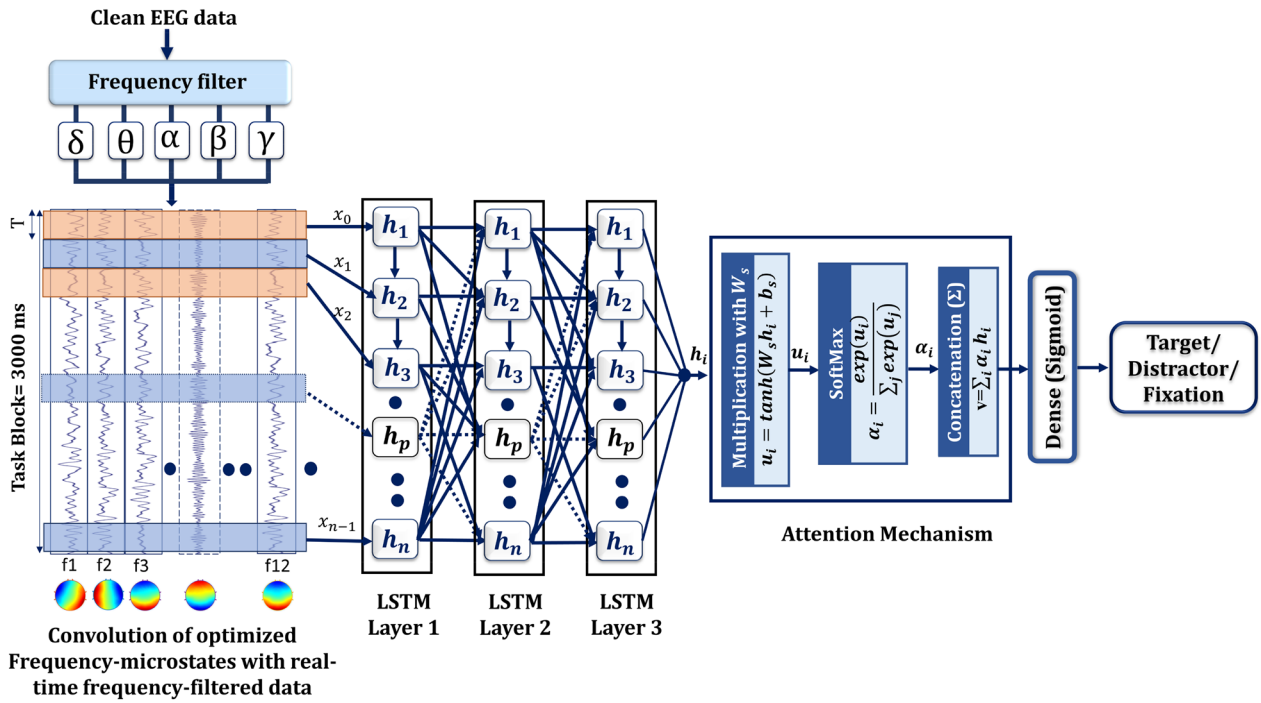

Fig. 3 Schematic diagram of Attention-based LSTM deep learning framework adopted in the study. 'T' represents the temporal, sliding input sampling window size and is chosen between 180 to 750 ms/segment associated with the specific number of cells ranging from 4 to 16, based on the stability of transition probabilities of the optimized microstates

$$i_t = \sigma(W_i.[h_{t-1}, x_t] + b_i), \quad (1)$$

$$f_t = \sigma(W_f.[h_{t-1}, x_t] + b_f), \quad (2)$$

$$C_t = f_t * C_{t-1} + i_t * \tanh(W_c.[h_{t-1}, x_t] + b_c), \quad (3)$$

$$o_t = \sigma(W_o.[h_{t-1}, x_t] + b_o), \quad (4)$$

$$h_t = o_t * \tanh(C_t), \quad (5)$$

where $\sigma(x) = \frac{1}{1+e^{-x}}$,$\tanh(x) = \frac{2}{1+e^{-2x}} - 1$. h_t, C_{t-1} and x_t are the hidden state, cell state and input passed to the architecture at time step t. W_f, W_i, W_c,W_o are the weights, and b_f, b_i, b_c, and b_o are the biases.

2.4.1 Attention mechanism

The core concept of the attention mechanism is to simulate the human attention mechanism to improve the performance of deep learning [39] by utilizing the weighting parameters of the elements in the input sequence to generate the output sequence. It is carried out by multiplying the hidden output states by trainable weights, capturing more discriminative task-related features, and can be expressed as:

$$h_i = \text{LSTM}(s_i), i \in [1, L], \quad (6)$$

where h_i is the output hidden state vector for the ith LSTM cell corresponding to the ith input, and L is the number of cells in each recurrent layer of the LSTM network. To capture the importance of each hidden state, the attention mechanism is defined as follows:

$$u_i = \tanh(W_s h_i + b_s), \quad (7)$$

$$\alpha_i = \frac{exp(u_i)}{\sum_j exp(u_j)}, \quad (8)$$

$$v = \sum_i \alpha_i h_i, \quad (9)$$

where vector v is the attention layer's output, and Ws and bs are trainable parameters.

This study uses all 12 quasi-stable frequency microstates (correlated with task engagement's neural mechanisms) as input information to train attention-based LSTM models. As mentioned in the methods, 70 volunteers participated in the study and performed target identification, distractor identification, and fixation (rest). Each paradigm involved 32 blocks of the target, 62 blocks of the distractor, and 94 blocks of fixation. More distractors and fixation are needed to avoid the expectancy aspect of cognitive engagement. For this, 32-channel EEG is employed to acquire the data with a 5k sampling rate and subsampled to 250 Hz during preprocessing. Each task engagement block was carried out for 3 s; 750 feature vectors were staggered for every task block. The 32nd channel data are ECG, hence not included for processing. Accordingly, each volunteer will have a 750×31 dataset at every block. Equal numbers, 32 blocks from each target, distractor, and fixation are selected for training. Selecting distractor and fixation from many blocks is done randomly to avoid training bias. Hence, each volunteer had selected data with a size of $72{,}000 \times 31$ ($24{,}000 \times 31$ for every task engagement). The preprocessed EEG data of the complete 70 volunteer set ($50{,}40{,}000 \times 31$) are initially subjected to the correlation with all the 12 significant frequency microstates, resulting in feature vectors with the size of $50{,}40{,}000 \times 12$. Each feature vector consists of the correlation value for each one of the quasi-stable frequency microstate information belonging to every task engagement is formed. The feature vectors are combined across task blocks, and distinct segregation of input feature vectors belonging to every task block was explored. For this, the study independently employed different attention-based LSTM architectures in input layers with 4 to 16-LSTM cells. This enabled analyzing the effect of temporal, sliding sampling window width on the performance of deep learning architectures. As every task stimulus last for 3 s, choosing different deep learning architectures with LSTM nodes of 4 to 16 allowed the EEG sliding temporal window to be 750 ms to 180 ms. The final LSTM layer was ensued by an attention layer, which was succeeded by a fully connected layer with a sigmoid activation function to predict the probability of each task engagement. Finally, to estimate the efficacy of attention mechanisms in the original LSTM system, all attention-based LSTM architectures were compared with their attention counterpart. The tuning parameters were applied after each LSTM layer and optimized the weight matrix L2 regularization coefficient of each LSTM layer for optimization. Finally, hyper-parameter such as learning rate was tuned for the stochastic Adam optimizer. The final optimized tuned parameter that performed better is tabulated in Table 1.

2.4.2 Validation

Finally, the attention-based LSTM architecture is validated by employing a tenfold cross-validation approach with no overlap of training and testing segments. True positive (TP), true negative (TN), false negative (FN), and false positive (FP) were used to calculate the performance metrics. They are formulated as Precision = TP/(TP + FP), Accuracy = (TP + TN)/(TP + TN + FP + FN) and Recall = TP/(TP + FN).

Table 1 Final tuning parameter of LSTM model

Hyperparameters	Tuned parameters
Hidden layer size	256
Batch size	64
Training epoch numbers	1000
Rate dropout	Input Layer: 0, 1st LSTM Layer: 0.2, 2nd LSTM Layer: 0.1, 3rd LSTM layer: 0.2
Recurrent depth	3
Learning rate	0.001

3 Results

The present study presents the time-series computational frameworks that classify different task engagement based on temporal modulation of distant brain communications through optimized frequency EEG microstates. The frequency EEG microstates were optimized by associating them with simultaneously eliciting distant hemodynamic functional connectivity measures. Further, the study explored the EEG-informed fMRI approach employed to understand the insights into the neuronal mechanisms related to frequency microstates that correlate with global task communications. The following sections present the results of each of the above steps in detail.

3.1 Frontal–parietal–temporal regions interaction during task engagements

The neural sources associated with each task engagement are assessed through fMRI GLM models with the double-sided *t*-test of $p < 0.5$, FDR corrected. The results suggest that target engagement enhanced the hemodynamic response in the frontal [frontal orbital cortex (FOC), frontal pole (FP), superior frontal gyrus (SFG)], parietal [angular gyrus (AG), Precuneus cortex (PC)], and temporal [Inferior and middle temporal Gyrus (ITG, MTG)] cortices. Further, it involves significant engagement of the cingulate gyrus (CG), lateral occipital cortex, occipital pole (OP), paracingulate gyrus, and insular cortex (IC) regions. The neural correlates of distractor and fixation have also revealed significantly different inter-cortical engagement. The detailed list of neural correlates of each task engagement is tabulated in Additional file 1: Table S1.

This distinct inter-cortical communication during each task engagement is further supported by the graph theoretical functional connectivity metrics such as global (GE) and local efficiency (LE). The target engagement significantly engaged inter and intra-cortical communication at frontal cortex (FP [GE:0.893, LE:0.89], FOC [GE: 0.886, LE:0.89], and SFG [GE:0.886, LE:0.894]), parietal cortex (left AG [GE:0.872, LE:0.893], right AG [GE:0.9, LE:0.887], PC [GE:0.87, LE:0.894]) and temporal cortical regions (ITG [GE: 0.88, LE: 0.889], MTG [GE:0.889, LE: 0.891], temporal occipital fusiform cortex (TOFC) [GE:0.88, LE:0.89]) at $p < 0.05$ with FDR correction. Functional connectivity elicitation remained distinct for the target detection task and had minimal overlap with other task engagement. Notably, frontoparietal and frontotemporal interaction engagement were distinct for target, distractor, and fixation engagement. The detailed information on graph-theoretical measures estimated for each task engagement is given in Additional file 1: Section S2.

3.2 Hemodynamic functional connectivity optimization of quasi-stable frequency-microstates

Frequency microstates estimation revealed four dominant microstates for every EEG frequency band of each task engagement. Figure 4 illustrates spatial topographical patterns of frequency-microstate topography associated with every task engagement.

Further, Fig. 5 presents the mean number of occurrences of all frequency microstates and highlights 12 specific frequency microstates whose number of occurrences is robustly correlated (+ve correlation: green, −ve correlation: red) with the fMRI functional connectivity measures. The detailed correlation information of frequency microstates with graph-theoretical measures of every task engagement is illustrated in Fig. 6. In this study, based on the microstate's green color band direction, they are labeled as anterior–posterior (AP), left–right (LR), left diagonal (LD), and right diagonal (RD) microstate prototypes. For example, the delta microstate with a green band traveling between anterior–posterior is called the "anterior–posterior delta microstate." During target engagement, the number of occurrences of right diagonal delta-microstate positively correlates with the global efficiency of fMRI functional connectivity measures. On the other hand, the local efficiency of fMRI connectivity measures correlates negatively with both left–right theta and alpha microstate occurrences and positively with anterior–posterior theta microstate.

3.3 Neurovascular analysis of optimized frequency microstates: EEG-informed fMRI analysis

Engagement of task generally elicits local neural clustering (high-frequency quasi-stable oscillations) at distinct brain regions, responsible for efficient local information processing, together with distant cortical intercommunication to facilitate global communication (low-frequency quasi-stable oscillations). The neurovascular analysis through EEG-informed fMRI explains these insights through synchronizing neural information

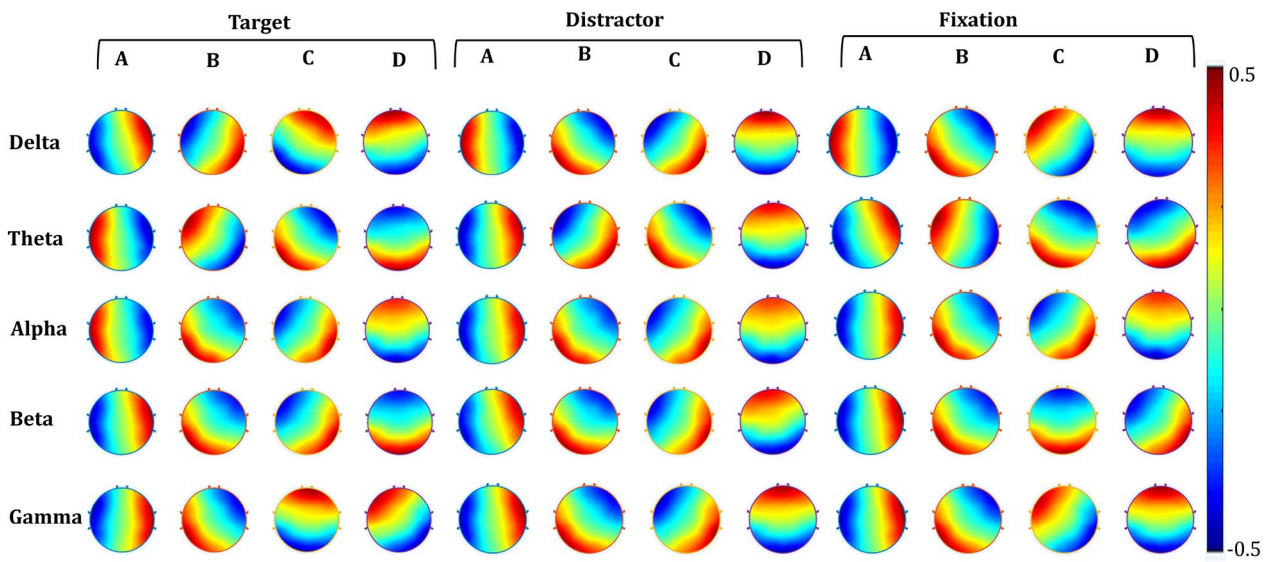

Fig. 4 A topographical representation of frequency-microstates for the target, distractor, and fixation

(optimized quasi-stable EEG oscillations) with hemodynamic information (vascular) elicited from a specific task engagement. For this purpose, each of the 12 optimized frequency microstates is processed in independent EEG-informed fMRI models, which modeled each microstate as separate regressors ($p < 0.01$, FDR corrected) to estimate their neuro-vascular information. Additional file 1: Fig. S1a–c shows neuro-vascular information of each 12 optimized microstates.

Figure 7 shows the neuro-vascular coupling of each significant frequency-microstate at the neural correlates of the respective task engagement and the associated functional connectivity. Target engagement elucidated the right-diagonal delta-microstate synchronously with the BOLD response in the frontal cortex. Further, anterior–posterior and left–right theta-microstates are found to synchronize with the BOLD response of frontal, temporal, parietal, and occipital regions except for right-lateralized SFG and AG. The role of theta-microstate in BOLD-synchronization of these regions characterizes its significant association with target engagement. The alpha-microstate is observed to de-synchronize with the parietal, PCG's BOLD response, and synchronize with the frontal, occipital region during target engagement. Our findings also reveal the effects of multiple frequencies on specific brain regions, such that the BOLD response of FP, PCG, SFG, IC, PC, and AG are modulated with delta, theta, and alpha-microstates. Specifically, the study observes the de-synchronization of alpha-microstate with the delta and theta microstates such as PCG, SFG, PC, and synchronization between delta and theta microstates as IC and FP. Hence, the relationships mentioned above reveal that the multi-frequency interactions modulate the BOLD response of task-engaged brain regions.

3.4 Performance of deep attentional LSTM model

Figure 8 compares the performance metrics, precision, accuracy, and recall of both deep learning models (LSTM and attention-LSTM). As observed, LSTM combined with attention performed significantly better in all three-performance metrics than the traditional LSTM model. The benefit of choosing different temporal sampling window sizes (180 ms/segment to 750 ms/segment) of input feature vectors by choosing 16 to 4 LSTM cells in input layers were analyzed within LSTM and attention-LSTM architectures. The results reflected the significant improvement in performance while using ten nodes (300 ms /segment), and a substantial decline in performance metrics is observed for 16 (180 ms/segment) nodes.

4 Discussion

The present study brings more insights into understanding and optimizing frequency microstate information estimated from cortical, coarse EEG information with distant fMRI functional connectivity measures associated with different task engagements. It utilizes them to train a time-series of deep learning frameworks. The study employed an attention-based stacked LSTM for effectively remembering and aggregating feature embeddings in the time-series classification of stacked temporal dynamics of the frequency microstate quasi-stable patterns. The results reveal that hemodynamic functional

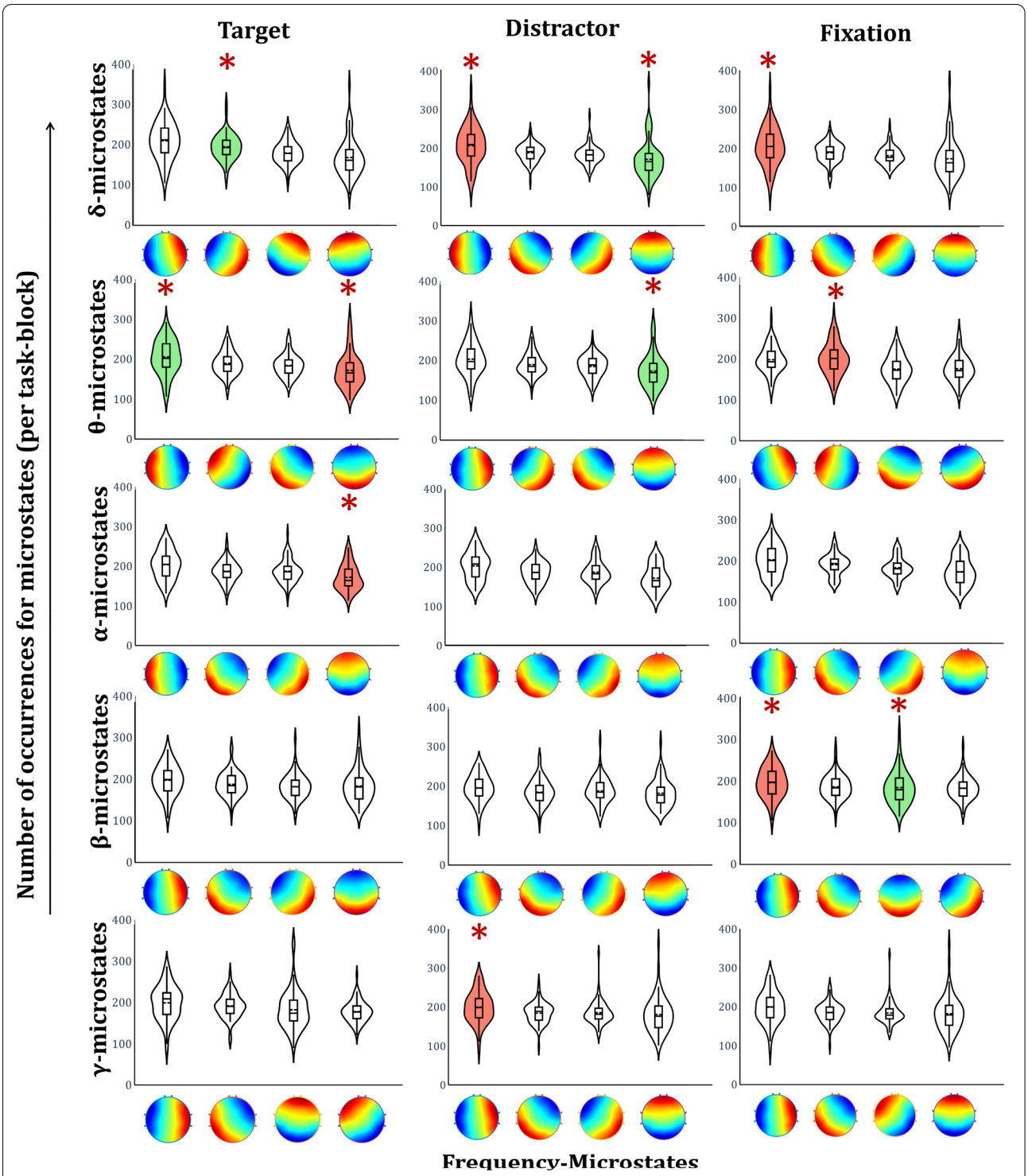

Fig. 5 Estimated metrics of frequency-microstates. The violin graph plots the mean occurrence of each frequency-microstates for each frequency band. The violin plot's green and red color shades reveal the correlation (positive and negative) of the number of occurrences of quasi-stable elicitation with the task's fMRI functional connectivity measures. The red star on violin plots specifies the significance ($p < 0.01$)

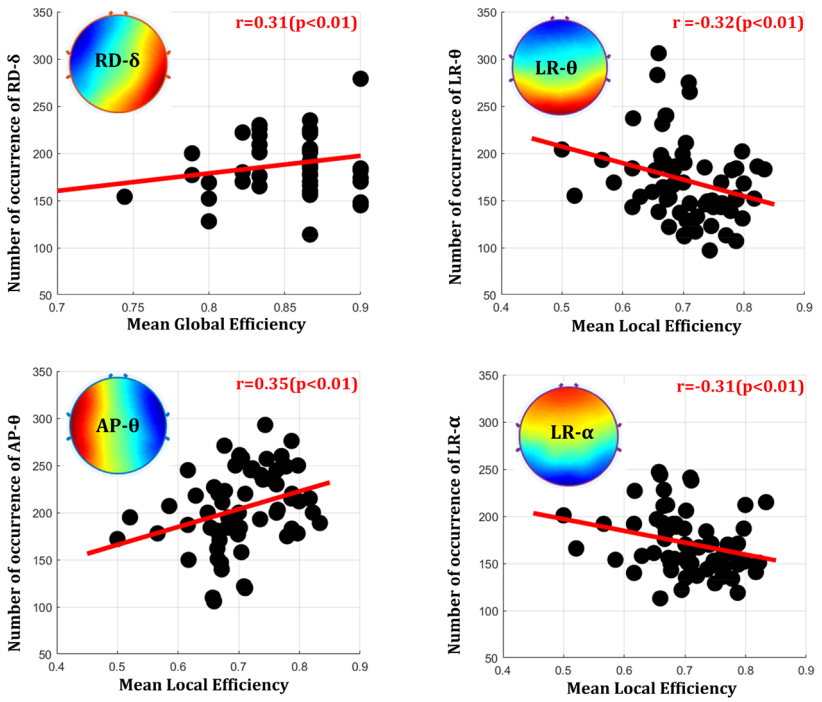

(a): Target-engagement

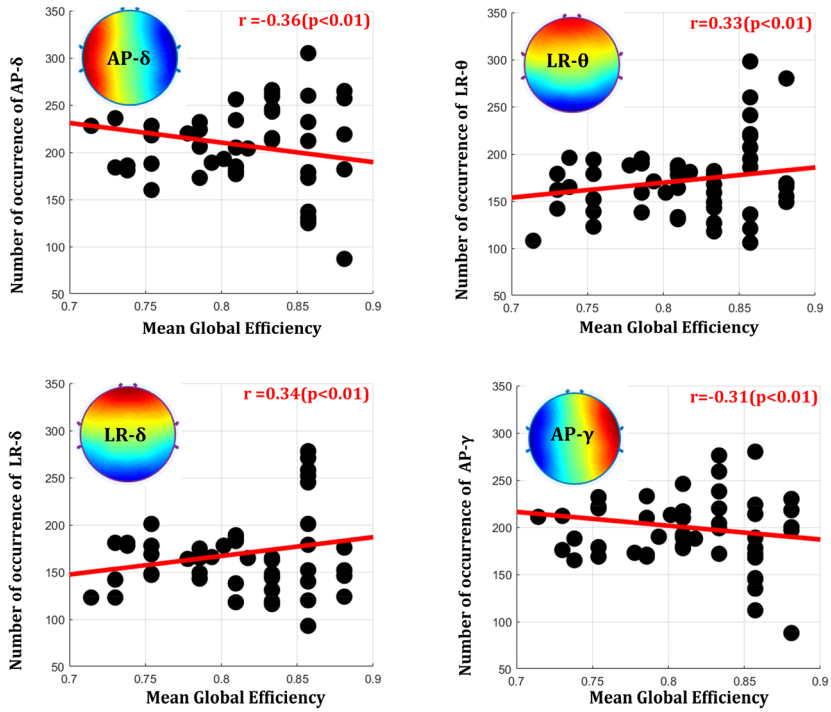

(b): Distractor-engagement

Fig. 6 Significantly associated, optimized, frequency-microstates with graph-theoretical measures of **a** target, **b** distractor, and **c** fixation task engagement. Frequency microstates are labeled as anterior–posterior (AP), left–right (LR), left diagonal (LD), and right diagonal (RD)

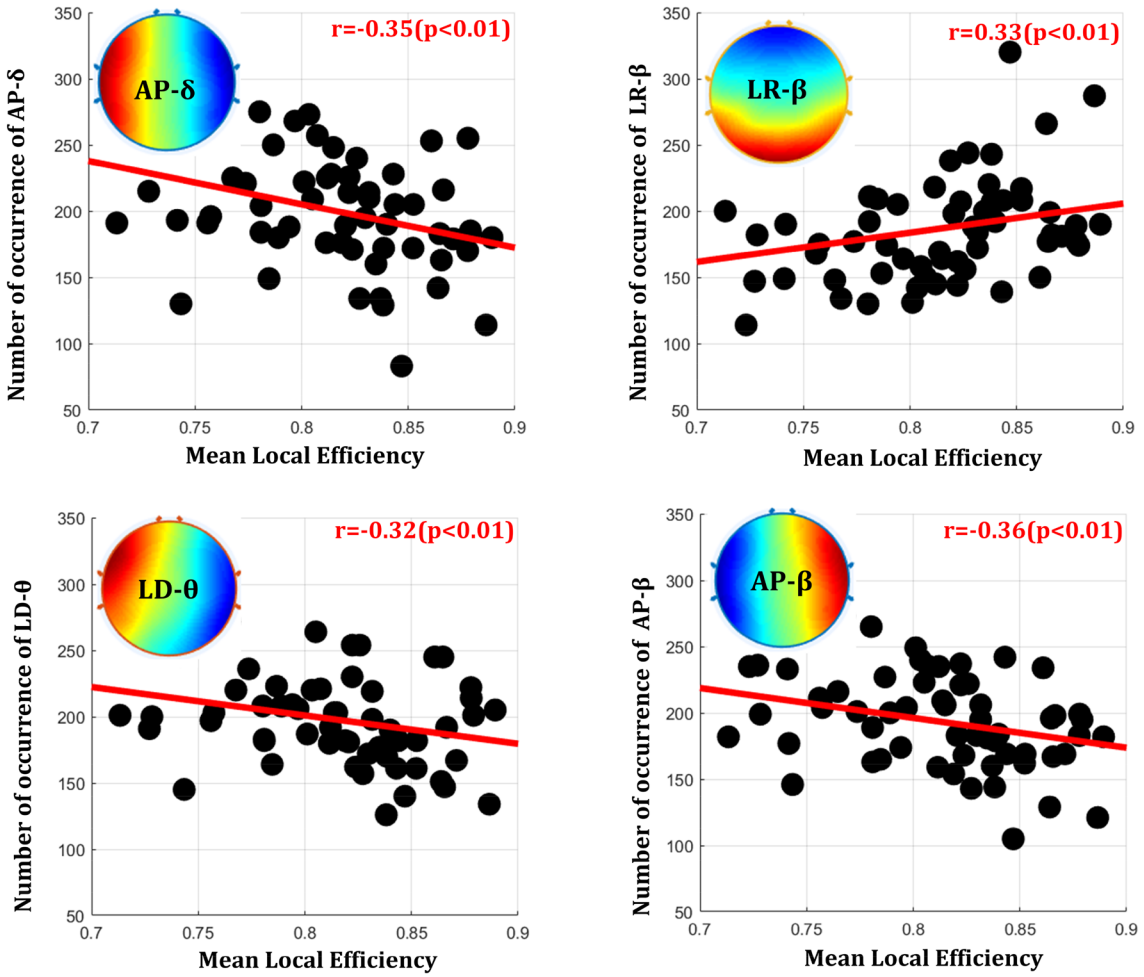

Fig. 6 continued

connectivity optimized quasi-stable frequency microstates enable attention-based LSTM algorithm to better classify target engagement, distractors, and fixation. Further, the study employed EEG-informed fMRI to understand the optimized frequency microstates' neurovascular insights and their association mechanisms. The following sections discuss these observations in detail.

4.1 Association of distinct frequency microstates with each task's cortical functional connectivity

The study observed four distinct cortical frequency-microstates elicitations for each of three different task engagements (thus, 12 distinct frequency microstates) independently correlated strongly with their hemodynamic functional connectivity measures. Non-overlap of association of these frequency microstates clearly states the underlying difference in distant cortical communications associated with each task engagement. In addition, the study also has observed a distinct neuro-vascular functional association of slow and faster oscillations in the brain regions involved in each task's cortical communications. Some essential observations of these multi-frequency quasi-stable EEG frequency associations with each task's distant neural interactions are summarized below.

4.2 Association of quasi-stable microstates oscillations with global/local neural engagements

Complex cognitive engagement requires global interactions of different brain regions enabling the large-scale

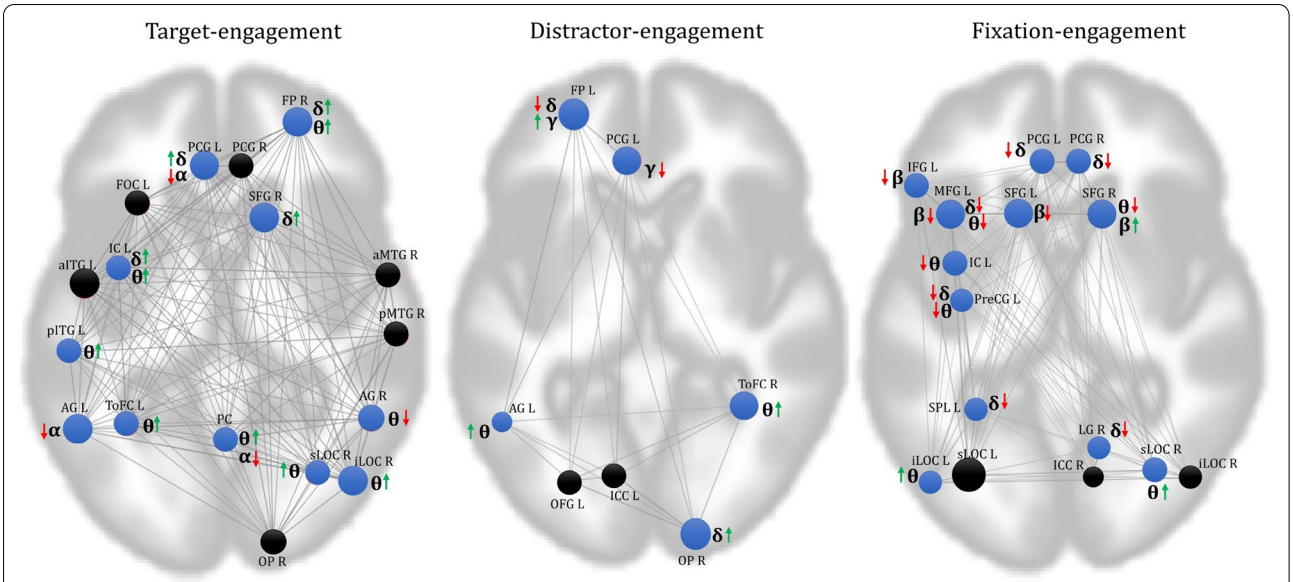

Fig. 7 Neuro-vascular coupling of each significant, fMRI functional connectivity optimized frequency-microstates of every task. The Regions shown are neural correlates observed for every task. The neuro-vascular association of optimized frequency microstate with each region is drawn through the arrow next to it (Synchronization: Up green arrow, De-synchronization: Down Red arrow). The area colored black has no neurovascular association with any of the optimized frequency microstates

integration of local neural information. The integration of neural engagement of spatially distant areas constituting the large-scale networks is primarily molded with low-frequency synchronized oscillations due to their long-range communications and integrative roles in various brain functions.

Further, the strength of large-scale networks has also been found to be highest for lower frequencies and seen gradually decreasing with increases in the frequency range [15, 32, 60]. Therefore, the dominance of large-scale networks for the lower range of frequencies confirms their functional significance. The present study's results (Fig. 6) distinctly revealed synchronization (positive correlation) of the slow frequency oscillations with global, distant brain communication and de-synchronization (negative correlation) with local neural elicitation across all the task engagement. Similarly, the high-frequency quasi-stable oscillation distinctly synchronized with the elicitation of local neural engagement and desynchronized with global communications across all the task engagements. A similar observation (Fig. 7) is revealed in the neurovascular coupling from EEG-informed fMRI analysis at the brain regions engaged in all tasks. They demonstrated significant de-synchronization between slow and faster quasi-stable oscillations in most brain regions involved during every task engagement. Further, the region-wise neuro-vascular insights brought slower quasi-stable oscillations associations with large-scale frontoparietal and frontotemporal functional networks. These observations are supported by the proposal of Polich et al. [47] and Harper et al. [17], explaining the role of delta and theta band activity underlying the frontoparietal and frontotemporal functional networks.

The accumulating literature suggests the association of local neuronal processing with the global cortical communication between neural assemblies by coupling multiple oscillatory frequencies [10] and referred to as cross-frequency coupling. The most well-studied example of cross-frequency coupling is the theta-gamma coupling, which explains the engagement of gamma frequency in certain phases of theta cycles. Further, [50] suggested that low-frequency oscillations may be essential in engaging gamma rhythms during attention. [33] discussed the relationship of alpha and theta frequency oscillations in the cortex and revealed the possibility of the theta-gamma code's contribution to memory and sensory processes. Thus, the functional interaction of more extensive networks oscillating at lower frequencies and local neuronal ensembles oscillating at higher frequencies has been revealed for cortical communication and integration [13, 29, 33]. Hence, the studies mentioned above better understand the modulation of faster oscillations from the slow EEG oscillations during cognitive engagements.

The present study's quasi-stable cortical oscillation's neuro-vascular insights and their association with local and global neural information are consistent with these studies and explain the role of multi-frequency

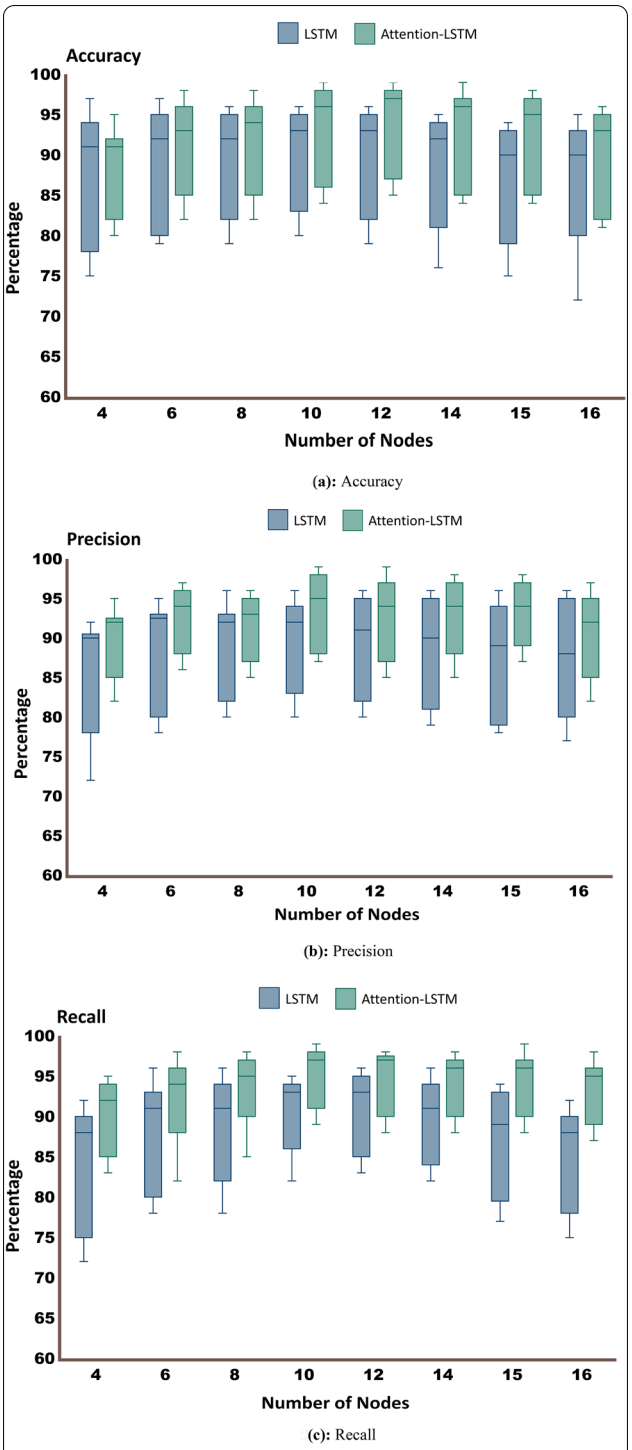

Fig. 8 Comparison of performance of the deep learning frameworks. **A** Accuracy, **B** precision, **C** recall. Each architecture was independently optimized with 4, 6, 8, 10, 12, 14, 15 and 16 LSTM input cells for temporal EEG sampling of 750, 500, 375, 300, 250, 214, 200 to 180 ms/segment, respectively

interactions in explaining the complex cognitive engagements' neuronal mechanisms.

4.3 Performance of attention-based deep learning system in classifying time-series quasi-stable cortical frequency EEG information

The proposed deep learning architectures (Fig. 3) revealed comparable accuracy, precision, and recall rate for classifying target detection task engagements in Fig. 8. However, two primary aspects distinguished the performance of each proposed deep learning architecture. They are the temporal sampling window and incorporation of the attention mechanism.

4.3.1 Temporal sampling window of quasi-stable frequency information optimizes the performance of deep learning architectures

Temporal sampling window size plays a significant role in achieving the best classification accuracy of deep learning architectures. This crucial aspect of time-locked microstates events facilitated a better temporal data handling of multi-frequency interaction in the cognitive task's neural engagements. The present study employed multiple windows of temporal sampling (four nodes: 750 ms, six nodes: 500 ms, eight nodes: 375 ms, 10 nodes: 300 ms, 12 nodes: 250 ms, 14 nodes: 214 ms, 15 nodes: 200 ms, and 16 nodes: 180 ms) to explore optimized, quasi-stable microstate's ability to classify task engagement. The highest classification accuracy, up to 99% for 10- and 12-node attention-based architecture, confirms the temporal dynamics of quasi-stable frequency oscillations optimally with 300 ms and 250 ms. Several target identification-related EEG studies support this observation [6–8, 43, 51] revealed that the peak of task event-related potentials following the stimulus onset in between 100 and 300 ms at multiple. Specifically, a recent EEG study [17] showed event-related synchronization of theta and delta bands occurring around 300 ms after the onset of target stimuli.

4.3.2 Effect of attention mechanism with traditional LSTM architectures

The overall better performance of all the deep learning architectures justified the optimization of quasi-stable frequency-microstate information. However, the attention mechanisms further improved this in the deep learning system. The combined effect of attention phenomena and the LSTM architecture allowed the deep learning architecture to dynamically emphasize the task-relevant neural information in the time-series sequence of EEG data and give less attention to other irrelevant information. The improvement in the performance of the attention-based LSTM system can be seen precisely in Fig. 8. The plots suggest that the attention mechanism is

optimum for extracting the most relevant task neural features and improves the LSTM's performance compared to independent LSTM.

5 Significance of the study

There is extensive literature (Additional file 1: Table S2) on employing a deep learning approach to decode task engagement using EEG elicitations. However, most of those works are restricted to the sensory–motor tasks (hand, leg movements, imagery tasks) whose engagement can be localized in a few cortical regions. However, minimal research is engaged to decode the cognitive task engagement's functional connectivity of distant and distinct cortical engagement using the deep learning framework. Further, despite many research studies that microstates are a promising neural signature, their association with the neural mechanisms of task engagement is still not clearly understood [26, 53, 54]. In addition, not many works in the literature explain the quasi-stable nature of the different EEG frequency oscillations either. The present work employs attention-based LSTM architecture to decode the temporal dynamics of cognitive task engagement through fMRI functional connectivity optimized frequency microstates. Recently, [52] investigated the temporal dynamics of traditional microstates using recurrent neural networks. However, their work did not address the quasi-stable frequency microstate's neural mechanism and modulation during task engagement. Our present work further brings more insights into the attention mechanism's ability to improvise the classification of cognitive task engagement based on the optimized neural signatures. To our knowledge, the present study is one of the few works that employs simultaneous EEG–fMRI information to optimize the neural signatures for improvising the performance of deep learning architectures.

6 Conclusions

The present study proposes an attention-based deep learning framework that processes temporal dynamics of the 12 distinct, fMRI functional connectivity optimized, quasi-stable frequency microstates to classify different cognitive task engagement. It further utilizes neurovascular insights of these optimized frequency microstates through EEG-informed fMRI analysis to understand the local and distant cortical interaction revealed by the optimized frequency microstate. This optimized neural information was passed as input at distinct temporal samplings windows to train and validate the attention-based LSTM architecture. The results suggest that the classification accuracies of the attention-based LSTM architectures were better than the traditional LSTM architectures due to the ability of the attention mechanisms in deep learning systems to localize temporal feature information. Notably, the attention-based LSTM model with 250 ms per segment and 300 ms per segment temporal sampling revealed a higher classification accuracy than other architectures. Hence, the study demonstrates an attention-based deep learning framework to perform a robust classification of complex, distant cortical engagement and communication caused by cognitive task engagements based on the novel, quasi-stable frequency microstates.

Supplementary Information

The online version contains supplementary material available at https://doi.org/10.1186/s40708-022-00173-5.

Additional file 1. Estimation of frequency-microstates. Estimation of global functional connectivity from simultaneously acquired fmri information. Optimizing frequency-microstate elicitations with fmri functional connectivity measures and their validation through microstate informed fmri. Additional figures and tables.

Acknowledgements
Not applicable.

Author contributions
The study was designed by SA, and VC. Data were acquired and processed by SA. Data were interpreted and analyzed by VC, SA, and RS. SA wrote the manuscript with the help of VC. All authors reviewed the manuscript. All authors read and approved the final manuscript.

Funding
This research received no specific grant from the public, commercial, or not-for-profit funding agencies.

Availability of data and materials
The datasets used and/or analyzed during the current study are available from the corresponding author on reasonable request.

Declarations

Competing interests
The authors declare no competing interests.

Author details
[1]Institute of Nuclear Medicine and Allied Sciences, Lucknow Road, Timarpur, Delhi 110054, India. [2]Delhi Technological University, Shahbad Daulatpur, Main Bawana Road, Delhi 110042, India.

Received: 12 April 2022 Accepted: 28 September 2022
Published online: 11 October 2022

References

1. Abreu R, Leal A, Figueiredo P (2018) EEG-informed fMRI: a review of data analysis methods. Front Hum Neurosci 12:1–23. https://doi.org/10.3389/fnhum.2018.00029
2. Agrawal S, Chinnadurai V, Kaur A et al (2019) Estimation of functional connectivity modulations during task engagement and their neurovascular underpinnings through hemodynamic reorganization method. Brain Connect 9:341–355. https://doi.org/10.1089/brain.2018.0656

3. Ahmadi N, Pei Y, Carrette E et al (2020) EEG-based classification of epilepsy and PNES: EEG microstate and functional brain network features. Brain Informatics 7(1):1–22. https://doi.org/10.1186/s40708-020-00107-z
4. Akam T, Kullmann DM (2014) Oscillatory multiplexing of population codes for selective communication in the mammalian brain. Nat Rev Neurosci 15:111–122. https://doi.org/10.1038/nrn3668
5. Allen PJ, Josephs O, Turner R (2000) A method for removing imaging artifact from continuous EEG recorded during functional MRI. Neuroimage 12:230–239. https://doi.org/10.1006/nimg.2000.0599
6. Arvaneh M, Robertson IH, Ward TE (2019) A P300-based brain-computer interface for improving attention. Front Hum Neurosci. https://doi.org/10.3389/fnhum.2018.00524
7. Bansal AK, Madhavan R, Agam Y et al (2014) Neural dynamics underlying target detection in the human brain. J Neurosci 34:3042–3055. https://doi.org/10.1523/JNEUROSCI.3781-13.2014
8. Bledowski C, Prvulovic D, Hoechstetter K et al (2004) Localizing P300 generators in visual target and distractor processing: a combined event-related potential and functional magnetic resonance imaging study. J Neurosci 24(42):9353–9360. https://doi.org/10.1523/JNEUROSCI.1897-04.2004
9. Buzsáki G (2009) Rhythms of the Brain. Oxford University Press, Oxford
10. Canolty RT, Knight RT (2010) The functional role of cross-frequency coupling. Trends Cogn Sci 14:506–515. https://doi.org/10.1016/j.tics.2010.09.001
11. Christov II (2004) Real time electrocardiogram QRS detection using combined adaptive threshold. Biomed Eng Online 3:1–9. https://doi.org/10.1186/1475-925X-3-28
12. Croce P, Quercia A, Costa S, Zappasodi F (2020) EEG microstates associated with intra- and inter-subject alpha variability. Sci Rep 10:1–11. https://doi.org/10.1038/s41598-020-58787-w
13. Fell J, Axmacher N (2011) The role of phase synchronization in memory processes. Nat Rev Neurosci 12:105–118. https://doi.org/10.1038/nrn2979
14. Gabard-Durnam LJ, Leal ASM, Wilkinson CL, Levin AR (2018) The Harvard automated processing pipeline for electroencephalography (HAPPE): Standardized processing software for developmental and high-artifact data. Front Neurosci 12:1–24. https://doi.org/10.3389/fnins.2018.00097
15. Gohel SR, Biswal BB (2015) Functional integration between brain regions at rest occurs in multiple-frequency bands. Brain Connect 5:23–34. https://doi.org/10.1089/brain.2013.0210
16. Gschwind M, Hardmeier M, Van De Ville D et al (2016) Fluctuations of spontaneous EEG topographies predict disease state in relapsing-remitting multiple sclerosis. NeuroImage Clin 12:466–477. https://doi.org/10.1016/j.nicl.2016.08.008
17. Harper J, Malone SM, Iacono WG (2017) Theta- and delta-band EEG network dynamics during a novelty oddball task. Psychophysiology. https://doi.org/10.1111/psyp.12906
18. Hipp JF, Engel AK, Siegel M (2011) Oscillatory synchronization in large-scale cortical networks predicts perception. Neuron 69:387–396. https://doi.org/10.1016/j.neuron.2010.12.027
19. Huster RJ, Debener S, Eichele T, Herrmann CS (2012) Methods for simultaneous EEG-fMRI: An introductory review. J Neurosci 32:6053–6060. https://doi.org/10.1523/JNEUROSCI.0447-12.2012
20. Iannetti GD, Niazy RK, Wise RG et al (2005) Simultaneous recording of laser-evoked brain potentials and continuous, high-field functional magnetic resonance imaging in humans. Neuroimage 28:708–719. https://doi.org/10.1016/j.neuroimage.2005.06.060
21. Jiang M, Gu J, Li Y et al (2021) HADLN: hybrid attention-based deep learning network for automated arrhythmia classification. Front Physiol. https://doi.org/10.3389/fphys.2021.683025
22. Kaur A, Chaujar R, Chinnadurai V (2020) Effects of neural mechanisms of pretask resting EEG alpha information on situational awareness: a functional connectivity approach. Hum Factors 62:1150–1170. https://doi.org/10.1177/0018720819869129
23. Kaur A, Chinnadurai V, Chaujar R (2020) Microstates-based resting frontal alpha asymmetry approach for understanding affect and approach/withdrawal behavior. Sci Rep 10:1–25. https://doi.org/10.1038/s41598-020-61119-7
24. Khanna A, Pascual-Leone A, Michel CM, Farzan F (2015) Microstates in resting-state EEG: current status and future directions. Neurosci Biobehav Rev 49:105–113. https://doi.org/10.1016/j.neubiorev.2014.12.010
25. Kiehl KA, Liddle PF (2003) Reproducibility of the hemodynamic response to auditory oddball stimuli: a six-week test-retest study. Hum Brain Mapp 18:42–52. https://doi.org/10.1002/hbm.10074
26. Kim K, Duc NT, Choi M, Lee B (2021) EEG microstate features according to performance on a mental arithmetic task. Sci Rep 11:1–14. https://doi.org/10.1038/s41598-020-79423-7
27. Kim KH, Yoon HW, Park HW (2004) Improved ballistocardiac artifact removal from the electroencephalogram recorded in fMRI. J Neurosci Methods 135:193–203. https://doi.org/10.1016/j.jneumeth.2003.12.016
28. Kim Y, Choi A (2020) EEG-based emotion classification using long short-term memory network with attention mechanism. Sensors (Switzerland) 20:1–22. https://doi.org/10.3390/s20236727
29. Knyazev GG, Savostyanov AN, Bocharov AV et al (2019) Cross-frequency coupling in developmental perspective. Front Hum Neurosci 13:1–10. https://doi.org/10.3389/fnhum.2019.00158
30. Koenig T, Prichep L, Lehmann D et al (2002) Millisecond by millisecond, year by year: Normative EEG microstates and developmental stages. Neuroimage 16:41–48. https://doi.org/10.1006/nimg.2002.1070
31. Laufs H, Kleinschmidt A, Beyerle A et al (2003) EEG-correlated fMRI of human alpha activity. Neuroimage 19(4):1463–1476. https://doi.org/10.1016/S1053-8119(03)00286-6
32. Li X, Kehoe EG, McGinnity TM et al (2015) Modulation of effective connectivity in the default mode network at rest and during a memory task. Brain Connect 5:60–67. https://doi.org/10.1089/brain.2014.0249
33. Lisman JE, Jensen O (2013) The theta-gamma neural code. Neuron 77:1002–1016. https://doi.org/10.1016/j.neuron.2013.03.007
34. Magri C, Schridde U, Murayama Y et al (2012) The amplitude and timing of the BOLD signal reflects the relationship between local field potential power at different frequencies. J Neurosci 32:1396–1407. https://doi.org/10.1523/JNEUROSCI.3985-11.2012
35. Mantini D (2007) Electrophysiological signature of brain resting state networks. Proc Natl Acad Sci U S A 104:13170–13175. https://doi.org/10.1073/pnas.0700668104
36. Michel CM, Koenig T (2018) EEG microstates as a tool for studying the temporal dynamics of whole-brain neuronal networks: A review. Neuroimage 180:577–593. https://doi.org/10.1016/j.neuroimage.2017.11.062
37. Milz P, Faber PL, Lehmann D et al (2016) The functional significance of EEG microstates-Associations with modalities of thinking. Neuroimage 125:643–656. https://doi.org/10.1016/j.neuroimage.2015.08.023
38. Milz P, Pascual-Marqui RD, Achermann P et al (2017) The EEG microstate topography is predominantly determined by intracortical sources in the alpha band. Neuroimage 162:353–361. https://doi.org/10.1016/j.neuroimage.2017.08.058
39. Mnih V, Heess N, Graves A, Kavukcuoglu K (2014) Recurrent models of visual attention. Adv Neural Inf Process Syst 3:2204–2212
40. Murta T, Chaudhary UJ, Tierney TM et al (2017) Phase–amplitude coupling and the BOLD signal: a simultaneous intracranial EEG (icEEG)—fMRI study in humans performing a finger-tapping task. Neuroimage 146:438–451. https://doi.org/10.1016/j.neuroimage.2016.08.036
41. Nagabushanam P, Thomas George S, Radha S (2020) EEG signal classification using LSTM and improved neural network algorithms. Soft Comput 24:9981–10003. https://doi.org/10.1007/s00500-019-04515-0
42. Niazy RK, Beckmann CF, Iannetti GD et al (2005) Removal of FMRI environment artifacts from EEG data using optimal basis sets. Neuroimage 28:720–737. https://doi.org/10.1016/j.neuroimage.2005.06.067
43. Pandey AK, Kamarajan C, Manz N et al (2016) Delta, theta, and alpha event-related oscillations in alcoholics during Go/NoGo task: Neurocognitive deficits in execution, inhibition, and attention processing. Prog Neuropsychopharmacol Biol Psychiatry 65:158–171. https://doi.org/10.1016/j.pnpbp.2015.10.002
44. Pang JC, Robinson PA (2018) Neural mechanisms of the EEG alpha-BOLD anticorrelation. Neuroimage 181:461–470. https://doi.org/10.1016/j.neuroimage.2018.07.031
45. Pascual-Marqui RD, Lehmann D, Faber P, et al (2014) The resting microstate networks (RMN): cortical distributions, dynamics, and frequency specific information flow. arXiv preprint arXiv:1411.1949. https://doi.org/10.48550/arXiv.1411.1949
46. Pascual-Marqui RD, Michel CM, Lehmann D (1995) Segmentation of brain electrical activity into microstates; model estimation and validation. IEEE Trans Biomed Eng 42:658–665. https://doi.org/10.1109/10.391164

47. Polich J (2007) Updating P300: an integrative theory of P3a and P3b. Clin Neurophysiol 118(10):2128–2148. https://doi.org/10.1016/j.clinph.2007.04.019
48. Rashid M, Sulaiman N, Abdul Majeed PA et al (2020) Current status, challenges, and possible solutions of eeg-based brain-computer interface: a comprehensive review. Front Neurorobot 14:1–35. https://doi.org/10.3389/fnbot.2020.00025
49. Ribary U, Doesburg SM, Ward LM (2017) Unified principles of thalamocortical processing: the neural switch. Biomed Eng Lett 7:229–235. https://doi.org/10.1007/s13534-017-0033-4
50. Schroeder CE, Lakatos P (2009) Low-frequency neuronal oscillations as instruments of sensory selection. Trends Neurosci 32:9–18. https://doi.org/10.1016/j.tins.2008.09.012
51. Sclocco R, Tana MG, Visani E et al (2014) EEG-informed fMRI analysis during a hand grip task: Estimating the relationship between EEG rhythms and the BOLD signal. Front Hum Neurosci 8:1–13. https://doi.org/10.3389/fnhum.2014.00186
52. Sikka A, Jamalabadi H, Krylova M et al (2020) Investigating the temporal dynamics of electroencephalogram (EEG) microstates using recurrent neural networks. Hum Brain Mapp 41:2334–2346. https://doi.org/10.1002/hbm.24949
53. Stam CJ (2005) Nonlinear dynamical analysis of EEG and MEG: review of an emerging field. Clin Neurophysiol 116:2266–2301. https://doi.org/10.1016/j.clinph.2005.06.011
54. Tognoli E, Kelso JAS (2009) Brain coordination dynamics: true and false faces of phase synchrony and metastability. Prog Neurobiol 87:31–40. https://doi.org/10.1016/j.pneurobio.2008.09.014
55. Vaswani A et al (2017) Attention is all you need. IEEE Ind Appl Mag 8:8–15. https://doi.org/10.1109/2943.974352
56. von Wegner F, Bauer S, Rosenow F et al (2021) EEG microstate periodicity explained by rotating phase patterns of resting-state alpha oscillations. Neuroimage 224:117372. https://doi.org/10.1016/j.neuroimage.2020.117372
57. Wang P, Jiang A, Liu X et al (2018) LSTM-based EEG classification in motor imagery tasks. IEEE Trans Neural Syst Rehabil Eng 26:2086–2095. https://doi.org/10.1109/TNSRE.2018.2876129
58. Whitfield-gabrieli S, Nieto-castanon A (2012) Conn: a functional connectivity toolbox for correlated and anticorrelated brain networks. Brain Connect. https://doi.org/10.1089/brain.2012.0073
59. Winkler I, Haufe S, Tangermann M (2011) Automatic classification of artifactual ICA-components for artifact removal in EEG signals. Behav Brain Funct 7:1–15. https://doi.org/10.1186/1744-9081-7-30
60. Wu CW, Gu H, Lu H et al (2008) Frequency specificity of functional connectivity in brain networks. Neuroimage 42:1047–1055. https://doi.org/10.1016/j.neuroimage.2008.05.035
61. Yao Q, Wang R, Fan X et al (2020) Multi-class Arrhythmia detection from 12-lead varied-length ECG using Attention-based time-incremental convolutional neural network. Inf Fusion 53:174–182. https://doi.org/10.1016/j.inffus.2019.06.024
62. Yao X, Li X, Ye Q et al (2021) A robust deep learning approach for automatic classification of seizures against non-seizures. Biomed Signal Process Control 64:102215. https://doi.org/10.1016/j.bspc.2020.102215
63. You RY, Chen Z (2005) Blind source separation of multichannel electroencephalogram based on wavelet transform and ICA. Chinese Phys 14:2176–2180. https://doi.org/10.1088/1009-1963/14/11/006
64. Yuan H, Zotev V, Phillips R et al (2012) Spatiotemporal dynamics of the brain at rest—exploring EEG microstates as electrophysiological signatures of BOLD resting state networks. Neuroimage 60:2062–2072. https://doi.org/10.1016/j.neuroimage.2012.02.031
65. Zhang G, Davoodnia V, Sepas-Moghaddam A et al (2020) Classification of hand movements from EEG using a deep attention-based LSTM network. IEEE Sens J 20:3113–3122. https://doi.org/10.1109/JSEN.2019.2956998
66. Zhang Z, Ye S, Liao P et al (2020) Enhanced Capsule Network for Medical image classification. Proc Annu Int Conf IEEE Eng Med Biol Soc EMBS. https://doi.org/10.1109/EMBC44109.2020.9175815
67. Zheng X, Chen W (2021) An Attention-based Bi-LSTM Method for Visual Object Classification via EEG. Biomed Signal Process Control 63:102174. https://doi.org/10.1016/j.bspc.2020.102174

Publisher's Note

Springer Nature remains neutral with regard to jurisdictional claims in published maps and institutional affiliations.

Submit your manuscript to a SpringerOpen journal and benefit from:

- ► Convenient online submission
- ► Rigorous peer review
- ► Open access: articles freely available online
- ► High visibility within the field
- ► Retaining the copyright to your article

Submit your next manuscript at ► springeropen.com